THEORETICAL AND EXPERIMENTAL STUDY OF CYCLOIDAL PROPELLERS

CENTRE FOR NEWFOUNDLAND STUDIES

TOTAL OF 10 PAGES ONLY
MAY BE XEROXED

(Without Author's Permission)

JIN LI

Theoretical and Experimental Study of Cycloidal Propellers

by

©Jin Li

A thesis submitted to the School of Graduate

Studies in partial fulfillment of the

requirements for the degree of

Master of Engineering

Faculty of Engineering and Applied Science

Memorial University of Newfoundland

May 1991

St. John's Newfoundland Canada

National Library of Canada
Bibliothèque nationale du Canada

Canadian Theses Service
Service des thèses canadiennes

Ottawa, Canada
K1A 0N4

The author has granted an irrevocable non-exclusive licence allowing the National Library of Canada to reproduce, loan, distribute or sell copies of his/her thesis by any means and in any form or format, making this thesis available to interested persons.

L'auteur a accordé une licence irrévocable et non exclusive permettant à la Bibliothèque nationale du Canada de reproduire, prêter, distribuer ou vendre des copies de sa thèse de quelque manière et sous quelque forme que ce soit pour mettre des exemplaires de cette thèse à la disposition des personnes intéressées.

The author retains ownership of the copyright in his/her thesis. Neither the thesis nor substantial extracts from it may be printed or otherwise reproduced without his/her permission.

L'auteur conserve la propriété du droit d'auteur qui protège sa thèse. Ni la thèse ni des extraits substantiels de celle-ci ne doivent être imprimés ou autrement reproduits sans son autorisation.

ISBN 0-315-68239-6

Canada

Abstract

A theoretical and experimental study was made on cycloidal propellers.

Experiments were done on a model trochoidal propeller with a pitch ratio of 2.924π in a cavitation tunnel in the Institute for Marine Dynamics (NRC). Problems which caused unreliable test results from a previous experimental study of the model propeller were examined. A mal-functioned torque transducer was replaced. Problems in the measurement of hydrodynamic torque and in calibration tests were analysed and effective ways to solve those problems were used in the present experimental study. Reliable test results for this model were obtained for propeller revolution speeds of 100,150,200 RPM.

Mendenhall and Spangler's discrete vortex method of studying cycloidal propeller performance was modified so that (a) an angle of attack method was used to calculate effects of wake and other blades; (b) the modeling of dynamic stall effects were included; (c) three-dimensional effects of the blades were included. The theoretical results were compared with the experimental data from the present tests and from published results for cycloidal propellers with different pitch ratios and number of blade. It was found that the three dimensional correction method improved the predicted propeller performance at pitch ratios greater than π. The two dimensional model using the angle of attack method gave better prediction of propeller performance than other models at pitch ratios smaller than π. The effectiveness of these models is discussed.

Acknowledgements

I would like to express my appreciation to my supervisor Dr.N.Bose for providing the opportunity to take part in the research of cycloidal propellers. His guidance and support made this program a memorable experience.

Special thanks are extended to Brian Veitch, Mrs. K. Pawlowska, Tom Hofmann and Dr. Shukai Wu for their constant assistance in the progress of the project.

Thanks are also extended to Dr. C. Williams, C. Harris and A. Wallace for their help at Institute for Marine Dynamics, and to IMD (NRC) for providing the tunnel and other facilities and apparatus for tests of model propellers.

Thanks also for the financial support from the School of Graduate Studies at Memorial University of Newfoundland and from the Natural Sciences and Engineering Research Council of Canada.

The technical support provided by MUN Technical Services and the Center for Computer Aided Engineering was greatly appreciated.

Contents

Abstract ii

Acknowledgement iii

List of Figures v

List of Tables vi

Nomenclature vi

1 Introduction 1

1.1 Description of Cycloidal Propellers 1

1.2 History of Cycloidal Propellers 1

1.3 Advantages of Cycloidal Propellers 2

1.4 Why Study Cycloidal Propellers ? 3

1.5 Geometrical Characteristics of Cycloidal Propellers 4

2 Literature Review 8

2.1 Experimental Studies 8

2.1.1 Tests on Cycloidal Propellers at the Netherlands Ship Model Basin . . . 8
2.1.2 Tests at the David Taylor Research Center . . . 9
2.1.3 Tests at Glasgow University . . . 14
2.1.4 Previous Tests at Memorial University of Newfoundland . . . 16
2.2 Theoretical Studies . . . 19
2.2.1 Theoretical Study of Cycloidal Propellers . . . 19
2.2.2 Taniguchi's Method . . . 20
2.2.3 Zhu's Method . . . 22
2.2.4 Bose's Multiple Stream Tube Method . . . 23
2.2.5 Mendenhall and Spangler's Vortex Model . . . 24

3 Theoretical Study **30**
3.1 Description of the Theoretical Models . . . 30
3.1.1 Modification of Mendenhall and Spangler's Method . . . 30
3.1.2 Formulation of the Theoretical Models . . . 33
3.2 Implementation of the Theoretical Models . . . 43

4 Experimental Study **45**
4.1 Description of the Experimental Set Up . . . 45
4.2 Work Done to Improve the Experimental Technique . . . 48
4.3 Problems and Their Treatment . . . 48
4.4 Test Procedure . . . 56
4.5 Note about the Problems and Their Treatment . . . 57
4.5.1 Choosing the Zero Point for Torque Measurement . . . 57

4.5.2 Friction Test Procedure 58
4.5.3 About the Torque Calibration 58

5 Results and Discussion **60**

5.1 Experimental Results and Discussion 60
5.1.1 Description of the Experimental Results 60
5.1.2 Repeatability of the Experimental Results 60
5.1.3 Differences Between Test Results for Different RPM 64
5.1.4 Comparison of the Cavitation Tunnel Test Results with the Open Water Results 65
5.1.5 Conclusion 66
5.2 Theoretical Results and Discussion 67
5.2.1 Description of the Theoretical Results 67
5.2.2 Naming of the Data Files from Theoretical Models 68
5.2.3 Comparison of the Theoretical Results with Experimental Data - Part I 70
5.2.4 Comparison of the Theoretical Results with Experimental Data - Part II 75
5.2.5 Comparison of the Theoretical Results with Experimental Data - Part III 78
5.2.6 Conclusion 80
5.2.7 Conclusion for Theoretical Study 81
5.2.8 Notes about the Stability of the Computational Method . . . 83

6 Conclusions **86**

6.1 Experimental Study of the Trochoidal Propeller 86
6.2 Theoretical Study 88
6.3 Author's contribution to the study of cycloidal propellers 89
6.3.1 Experimental Study 89
6.3.2 Theoretical Study 89

7 Recommendations **90**
7.1 Experimental Study of the Trochoidal Propeller 90
7.2 Theoretical Study 91

References **93**

A FORTRAN Programs for Theoretical Models **98**

Appendices **98**

B Note About the FORTRAN Programs **144**
B.1 Program Organization 144

C Use of A/D Converter and SOFT500 **145**
C.1 Programs Used in Data Aquisition 145
C.1.1 Program I 145
C.1.2 Program II 146
C.2 Improvement of Signal Resolution 147

D Test Results **148**

E Theoretical Results — Part I **175**

F Theoretical Results — Part II 209

G Theoretical Results — Part III 243

List of Figures

1.1 Cycloidal propeller nomenclature. 6

1.2 Blade paths for cycloidal motions at zero slip. 7

4.1 General arrangement of trochoidal propeller model 47

4.2 Use friction torque as zero to obtain torque test data 51

4.3 Use zeros before each test to obtain torque test data 52

4.4 Efficiency for one test using different calibration data 55

List of Tables

5.1 Pitch Ratios Used in the Calculation 85

List of Symbols

A	aspect ratio of the blade
α	blade angle of attack
α_{ref}	reference angle of attack
b	blade span
c	chord length of blade
C_L	blade section lift coefficient
C_D	blade section drag coefficient
C_T	thrust coefficient
C_Q	torque coefficient
D	diameter of the propeller
J	advance ratio
K_x, K_y	blade axial and normal forces
n	frequency of propeller rotation
N	number of blades
P	pitch ratio
Q	torque
r	distance between the center of the propeller and the steering center
R	radius of the propeller
T	thrust
ω	angular velocity of the propeller
η	efficiency
$\Gamma_{c/4}$	blade bound vortex strength
$\bar{\Gamma}$	wake vortex strength
$\vec{W}$	total flow velocity relative to the blade at the quarter chord point due to the free stream and the rotation of the propeller
ρ	density of the fluid
σ	propeller solidity

Chapter 1

Introduction

1.1 Description of Cycloidal Propellers

A cycloidal propeller consists of a rotating drum and several blades. The blades are mounted near the outer edge of the face of the drum and can be controlled to rotate about their own axes (see Figure 1.1). When a free stream flows through a cycloidal propeller, with drum and blades rotating about their own axes respectively, the trajectory of a single blade is as illustrated in Figure 1.2. Thrust and torque are produced due to the load on each blade. A description and review of the work done on such propellers is given by Lewis (1988).

1.2 History of Cycloidal Propellers

The cycloidal propeller, also called " vertical axis propeller", was first described by Hunter in 1874 (U.S. Patent 150, 956). Its effectiveness was not accepted until Kirsten established the requirements for such a propeller to become competitive

with the conventional screw propeller. Taylor's model tests in 1922 (Kirsten 1928) yielded extremely encouraging results and Kirsten and Boeing built and successfully demonstrated a small boat with this propeller. However, interest subsided completely in the U.S. and did not revive until the close of World War II.

A variable pitch type cycloidal propeller was invented in 1925 in Germany by an Austrian engineer named Schneider. Up to the close of the World War, the J.M. Voith Company had built and installed about 500 propellers with a total of 400,000 hp in commercial vessels and in boats of the German armed forces. The U.S. army and navy became interested in the cycloidal propeller again and restarted the development in 1944.

The first mathematically derived cycloidal propeller was developed in 1920 by F.K. Kirsten. The first comprehensive paper on cycloidal propulsion appeared in 1928 when Kirsten introduced "A New Type of Propeller" to the Society of Automotive Engineer (Kirsten 1928).

1.3 Advantages of Cycloidal Propellers

Although the conventional propeller has a very high degree of effectiveness which has often prevented the development of other types of unconventional propellers with favorable properties, cycloidal propellers are a propeller type with outstanding maneuvering capabilities. The system is best suited for maneuverability, safety, reliability and durability aboard tugs, double ended ferries, buoy tenders, mine hunters/sweepers, oceanographic vessels and other harbor and offshore vessels requiring precise and frequent maneuverability in adverse sea conditions and areas

difficult for navigation.

Ship control in the conventional sense is achieved by a combination of devices consisting principally of those which give control in one degree of freedom (fore and aft) and rudders which provide side forces to generate turning movements. Where sufficient sea room exits, this combination provides adequate control for most underway maneuvers. At low speeds and when the ship is dead in the water, rudders lose their effectiveness.

The advantage of cycloidal propellers lies in the fact that the propeller thrust can be used for steering and stopping the ship without stopping and changing the direction of rotation of the main engine. This makes them eminently suitable for the propulsion of ships that operate in crowded and restricted waters, requiring large steering power at low speeds. The cycloidal propeller is a valuable propulsion device due to its unique maneuvering capability. The direction of the resultant force can be controlled and changed to any desired direction normal to the axis of propeller rotation.

1.4 Why Study Cycloidal Propellers ?

There are three types of cycloidal propellers. Each of them is characterized by its particular blade orbital path in the no-slip condition. These orbital paths are called epicycloidal or curtate cycloidal; cycloidal; trochoidal or prolate cycloid (see Figure 1.2).

The commercial version of the epicycloidal propeller is known as the Voith-Schneider propeller and these have been fitted to many tugs, and vessels where

maneuverability is important. Cycloidal propellers, developed as the Kirsten-Boeing propeller, have been used on some vessels in the United States. Little work has been done on trochoidal propellers and to date the available theoretical methods are inadequate for accurate performance prediction.

"Trochoidal" propellers belong to a commercially unexploited area that specialists in ship propulsion are becoming concerned with especially owing to their high efficiency at very high velocities. There is a lack of systematic experimental data about trochoidal propellers especially for lightly loaded propellers with high aspect ratio blades. This is the main reason why the study of trochoidal propellers has been revived at the Memorial University of Newfoundland to provide propulsion at light loading on vessels over a wide speed range. However in the application, a disadvantage is that they may have to be mounted with their axis in a horizontal plane. If this happens, maneuverability characteristics are lost.

1.5 Geometrical Characteristics of Cycloidal Propellers

The blade angle linkage system is designed so that the blade center of rotation traces a cycloidal path. The blade paths for zero slip are shown in Figure 1.2 for three types of cycloidal motion. The cycloid is generated by a circle of radius r rolling with an angular velocity ω along a surface, where the point of contact is noted S (see Figure 1.1). The cycloidal path is such that a normal to the path at any point passes through the point S. The point S is called the steering center of a cycloidal propeller. In Figure 1.1, the blade is shown perpendicular to the line

connecting the blade rotation axis to the steering center. The pitch ratio of the cycloidal propeller is determined by the radial location of the steering center; thus,

$$P = \frac{r\pi}{R} \tag{1.1}$$

The blade angle is given by

$$tan\beta = \frac{\frac{r}{R}sin\theta}{1 + \frac{r}{R}cos\theta} \tag{1.2}$$

The blade motion at a given instant can be considered the sum of a velocity due to propeller translation and a velocity due to propeller rotation. Consider the propeller to be rotating at a constant angular rate ω in a uniform flow $\vec{V}$. The blade translation velocity is then $\vec{\omega} \times \vec{R}$. Relative to the blade, a velocity $\vec{W}$ occurs which is the vector sum of $\vec{\omega} \times \vec{R}$ and $\vec{V}$. This velocity makes an angle α with the blade chordline.

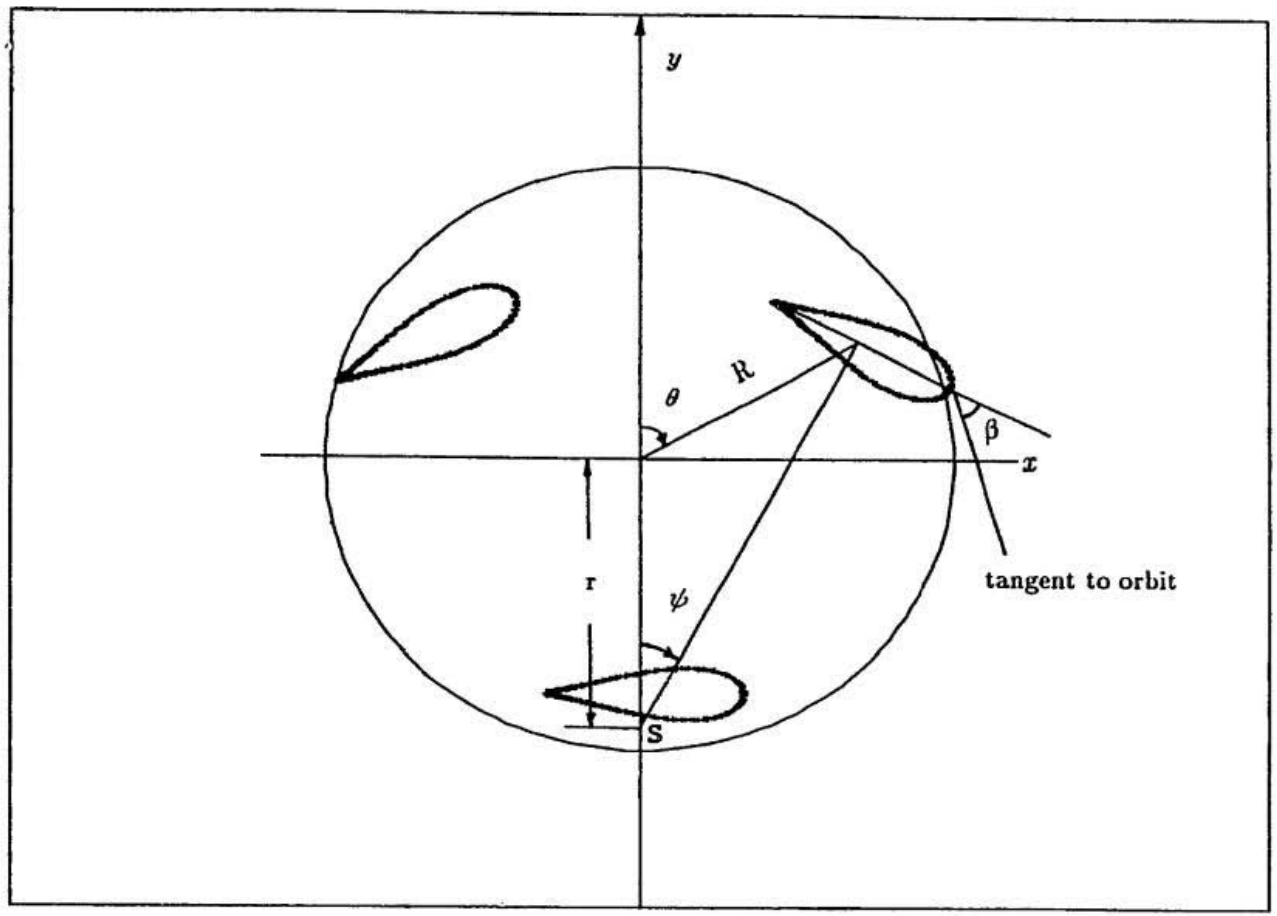


Figure 1.1: Cycloidal propeller nomenclature.

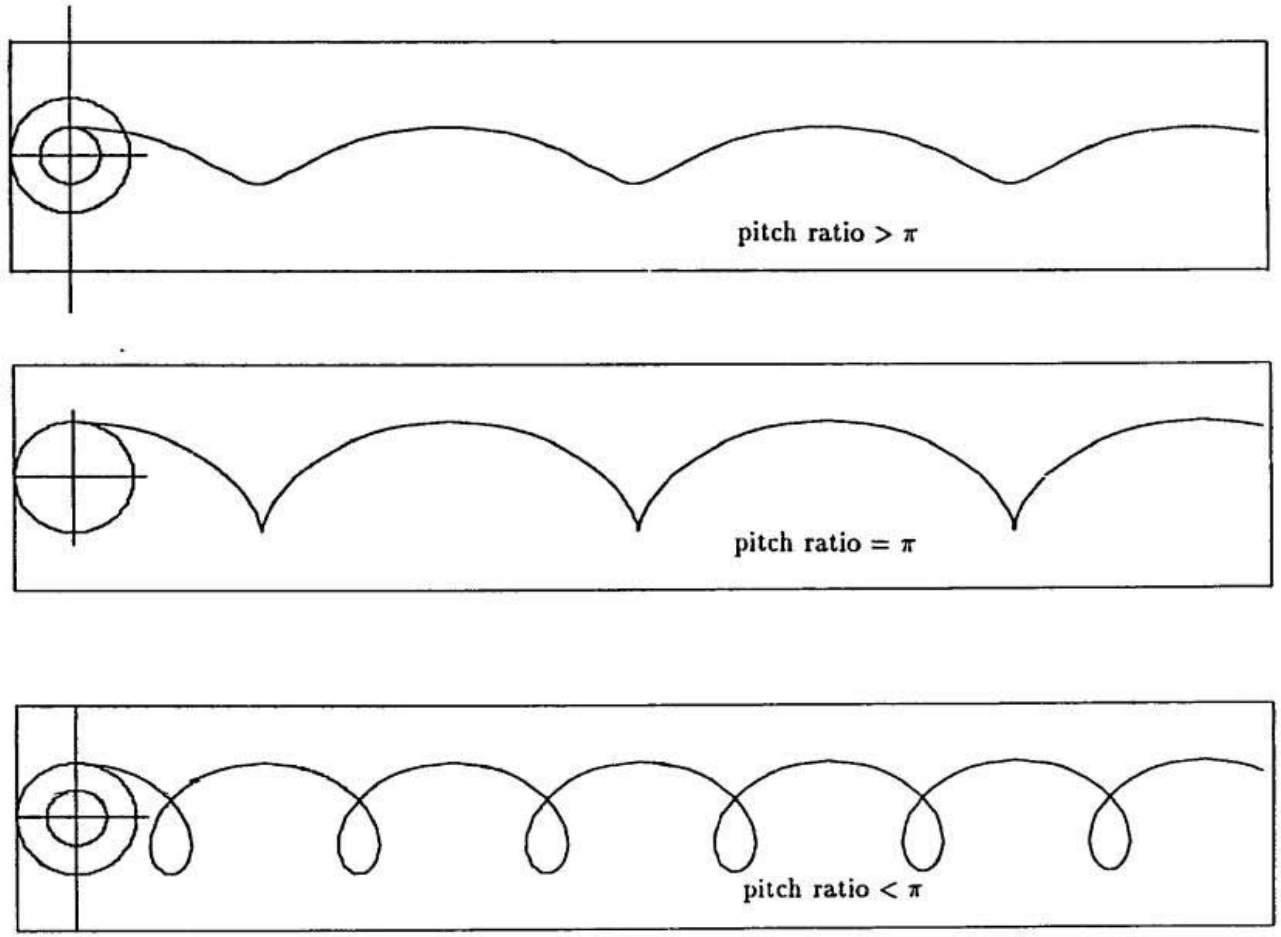


Figure 1.2: Blade paths for cycloidal motions at zero slip.

Chapter 2

Literature Review

2.1 Experimental Studies

2.1.1 Tests on Cycloidal Propellers at the Netherlands Ship Model Basin

Some research was done towards the expansion of knowledge regarding unconventional propeller models in the Netherlands Ship Model Basin (now MARIN) in 1963. Manen (Manen 1963) reported a systematic series of tests done with cycloidal propellers. These tests of low pitch ratio (0.40π, 0.50π, 0.60π, 0.71π, 0.80π) propellers were mainly to investigate (a) the effect of the type of blade movement upon the propeller efficiency; (b) the optimal position of the axis of the blade movement; (c) the effect of blade number and the blade chord length; and (d) cavitation phenomena.

Results show that for the range of propeller pitch ratios smaller than π: (a) in the range of propeller loads that are of significance for existing ships, the optimal

efficiencies of cycloidal propellers are low, around 25-30% lower than the comparable efficiency values for conventional screw propellers; (b) the six-bladed propeller open water efficiency is superior to the four-bladed one; (c) the blade on a four-bladed propeller with a chord length/blade length ratio $c/l = 0.4$ leads to higher efficiencies than do the blades with a chord length/blade length ratio $c/l = 0.3$; and (d) higher blade motion velocities cause serious cavitation.

Some tests were also conducted for a four-bladed trochoidal propeller with pitch ratios of 1.25π, 1.50π, 2.00π, 2.25π. From the test results, it can be inferred that for pitch ratios ranging from 1.50π to 1.75π, a maximum efficiency occurs from 0.69 to 0.70. However this maximum is valid only for the specific propeller geometry tested.

Manen also pointed out that the extent to which these propeller efficiencies are promising for the future applications of this propeller type in the area of high ship speeds, cannot yet be inferred from the results of this first series of tests. An extended investigation is needed of trochoidal propellers, so as to make possible comparisons with other propulsive means for higher velocities in respect both to cavitation and to propeller efficiency. The lack of systematic data for the trochoidal case did not allow one to infer general conclusions from this test.

2.1.2 Tests at the David Taylor Research Center

Tests in Open Water

Ficken and Dickerson(1969) conducted model tests for a series of cycloidal pro-

pellers with pitch ratios ranging from 0.4π to 0.9π to investigate the performance and steering characteristics of these propellers. The major part of the test program was run with six rectangular blades. Each of the six sets of cams, representing the six pitch ratios (0.4π, 0.5π, 0.6π, 0.7π, 0.8π and 0.9π) was tested over a wide range of steering angles and speed coefficient. Test were also run with two and three blades at zero steering angle. Comparative results were obtained for 0.7π and 0.8π pitch ratios.

They found that efficiency is low since the angle of attack of the cycloidal propeller blades varies throughout the cycle between relatively large positive and negative values. Although the blade produces a positive thrust component at negative as well as positive angles of attack, the lift-drag ratios suffer at very high angles of attack. This effect is complicated by the fact that in the downstream quadrants of the orbit, the blades pass through the wake of the blades in the upstream quadrants. The results suggest that this blade interference is considerable since the effect of changing number of blades is much more pronounced than for a screw propeller. With two blades, the peak efficiency with 0.8π pitch ratio was 0.79; this compares favorably with screw propellers.

The effect of blade number was similar to the effect of changing the number of blades of a screw propeller, but it was more pronounced. Specifically, the peak efficiency of the cycloidal propeller with six blades was 10 to 5 points lower than the Troost six-bladed B series (Ficken and Dickerson 1969); with two blades, the cycloidal propeller was very nearly as efficient as the two-bladed B series propeller.

The cycloidal propeller models were found to develop maneuvering and backing forces that are much larger than those available from a screw propeller.

Tests in Water Tunnel

Dobay and Dickerson (1969) conducted tests to investigate cycloidal propeller performance at low cavitation numbers. Their test results show the effects of cavitation on a 9-inch orbital diameter cycloidal propeller in a 24-inch variable-pressure water tunnel. Six blades were used and the blade motion was epicycloidal with pitch ratios of 0.7π and 0.9π.

The effect of cavitation on the force coefficients of a cycloidal propeller is not unlike that for conventional propellers; however, there are differences. At 0.7π pitch ratio a decrease in tunnel cavitation number causes an increase in torque and a decrease in thrust and in side force. This is not the case for the 0.9π pitch ratio. Here, over the significant advance ratio range, efficiency increases with decreasing cavitation number due primarily to the decrease in torque required. The change in forces is minimal.

The conclusions from their tests are as follows. The change in performance characteristics of cycloidal propellers due to cavitation is quite similar to that of conventional screw propellers. In general, the available thrust decreases and the required torque increases with decreasing cavitation number. There is a striking improvement in performance of the 0.9π pitch propeller to that of the 0.7π pitch propeller at the same loading and cavitation number. Dobay and Dickerson suggested that further cavitation tests should explore this trend further, using higher than π pitch ratios. Trochoidal propellers operate at optimum efficiency at high advance ratio values. Thus, they can be thought of as high-speed propulsion de-

vices. If cavitation tests prove them useful at low cavitation numbers, they would be competitive candidates for the propulsion of novel high-speed craft along with the water jet and supercavitating propellers.

The type of cavitation on the propeller blades changes continuously throughout each cycle of revolution. This cyclic loading could cause blade fatigue problems. Dobay and Dickerson pointed out that blade force and fluctuating torque measurements should be made under cavitating conditions.

In the usage of cycloidal propulsion, the propellers may operate in a cavitating environment. Since there was a considerable performance degradation of the low pitch propeller model, Dobay and Dickeson strongly recommended that cavitation tests be conducted of future designs for the better prediction of full-scale performance.

From this first series of tests, the actual test facility appears to have had a strong influence on the test data. It was recommended that the effect of the tunnel facility on propeller performance be further explored, by representing some of these tests in a larger water tunnel or by comparison with open water tests.

Tests in a Towing Tank

The results of towing tank tests of cycloidal propellers of higher than π pitch ratios were reported by Dickerson and Dobay (1975). The test results from Ficken and Dickerson (1969) and from Dickerson and Dobay (1975) represented a systematic (but incomplete) propeller series with cycloidal blade motion. These test data had been obtained through a six year effort, beginning in the year 1964 and continuing

through to 1970. The pitch ratio ranges were from 0.4π to 0.9π for low pitch ratio, and 1.429π, 1.667π, 2.000π and 3.333π for high pitch ratio.

The peak torque values at positive advance ratios increase with pitch ratio quite consistently, up to the 2.000π pitch ratio. There is a large jump in the torque coefficient magnitude when the pitch ratio is increased to 3.333π. This large increase was not expected.

It is noted that thrust coefficient at zero advance ratio decreases with increasing pitch ratio when the pitch ratio is greater than π; there is a wide range of advance ratio values at which high thrust values can be obtained with the high pitch propellers. This relatively flat portion of the thrust coefficient curve enables the high pitch propeller to satisfy a wide range of operating conditions. Also, at close to optimum propeller efficiency the high pitch propellers develop roughly twice the thrust of the low pitch propellers.

The torque coefficients show a trend similar to that of the thrust coefficients. Much higher torque is required to drive a high pitch propeller than to drive a low pitch propeller.

In general, the high pitch propellers behaved in a similar manner to the low pitch propellers. They have excellent maneuvering capabilities and large thrusts are available. Even so, efficiencies proved to be lower than that of the conventional propeller due to the high torque requirement to overcome mechanical friction.

These test results indicated that high pitch cycloidal propellers may offer an alternative propulsion for high speed surface craft. They provide an effective way to control ship-motion in the horizontal plane, at very high advance coefficients. The feasibility for high speed applications could not be completely established from

the results of this report, since they were obtained at low forward speeds. The performance of high-pitch propellers at low cavitation numbers should be evaluated.

2.1.3 Tests at Glasgow University

In 1987, a model of a three-bladed trochoidal propeller was designed and built. Tests were done on this propeller model in the Hydrodynamics Laboratory of the University of Glasgow (Lai and Bose 1988a, 1988b). The object of the experiment was to assess the characteristics and performance of the propeller. A sliding mechanism in the rotary drum controlled the pitch angle of the blades such that the pitch angle followed the slope of a trochoidal curve. The maximum pitching angle of the blades was 20°.

During the experiment, the actual driving torque was much greater than the predicted values. This was because the mechanical friction of the model was high. The net hydromechanical torque was the difference between the driving torque and the frictional torque. The torque to overcome friction was very high in percentage terms. It was very hard to measure the additional torque due to the hydrodynamical action of the blade accurately, which is one of the main values required in an experiment of this type. Therefore the test results of the magnitude of the torque expended on the hydrodynamical effect is open to question.

Later in the same year, Lai and Bose(1988b) did a second set of experimental tests on the performance of the cycloidal propeller. The results included an increase in the overall efficiency values and in the thrust values at low speed. These differences were due to improvements in the measurement of the forces on the propeller,

in particular the torque values, and to the reduction of vibration of the model. The driving torque to overcome the friction obtained from these experiments is approximately 35% less than that which was presented in the results of the first experiment. This reduction of friction was mainly a result of the removal of a supporting bearing.

The propulsive efficiency estimated by using the thrust and torque coefficients data has an unrealistic high peak in the range of advance ratios between 5.5 and 6.0. This peak corresponds to the scatter of the torque coefficient data. In order to eliminate the influence of the torque coefficients on the efficiency, curve-fitted values of torque were used to estimate the efficiency. Although the frictional loss was lowered by removing the supporting bearing, the larger part of the driving torque was still spent to overcome the mechanical friction and this led to difficulty in recording accurate hydrodynamic torque values.

Hydrodynamic propulsive efficiency at forward speed was found to be about 0.8. This is high compared to the normal range of propulsive efficiency of conventional propellers which seldom exceed 0.6 to 0.7. The propulsive efficiency of the cycloidal propeller is much lower when the torque spent to overcome the mechanical friction is included in the analysis. Therefore, effort should be concentrated on lowering the mechanical friction between the moving parts in a commercial design.

2.1.4 Previous Tests at Memorial University of Newfoundland

A trochoidal propeller model was designed by Veitch and Bose (Veitch 1990) specially to fit into the cavitation tunnel at the Institute for Marine Dynamics (IMD - NRC). One of the objectives in the design of the propeller model was to avoid measuring large mechanical friction losses. The results of the friction tests conducted by Veitch did indicate that frictional losses were low throughout the operating range of the propeller compared with the friction losses reported by Lai and Bose (1988a, 1988b) in their experiments.

A preliminary set of tests was done with the model to evaluate its performance in the cavitation tunnel in IMD. Steady state thrust, torque, and side force coefficients were determined for a range of advance ratios for forward operation. A smaller number of tests were done for reverse operations, and a single zero forward speed, or bollard pull test was done. Most of the tests were done under approximately atmospheric conditions, but the propeller was also tested in a cavitating environment at reduced pressure.

Several problems were encountered during these experiments. At the beginning of a test, the three strain gauge transducer channels were zeroed by using their respective bridge balancing potentiometers . It was found that the zero drift was considerable in certain circumstances and the cause of this drift was not clear. It was noticed that at a propeller speed of 275 rpm, the propeller rubbed the casing at higher water speeds. A possible cause of this rubbing was due to the deviation of the model from the center of the casing.

Veitch(1990) also encountered noise in the signals from the transducers. The wires from the transducers were not shielded within the propeller casing. Immediately outside of the casing, the wires were connected to a shielded cable which connected to the analog to digital converter and was approximately 6 meters long. Regardless of the influence of the external noise, there was a voltage drop across this cable.

Four cavitation tests were done by Veitch (1990), but air leakage into the tunnel caused the pressure to slowly increase during the 20 seconds it took for data acquisition at a given propeller speed. The vacuum pump was used briefly between speed steps to reset the test section pressure to its original value. The leakage resulted in a change of test section pressure over the 20 seconds test period of approximately 0.7, 0.5 and 0.1 kPa respectively for the test section pressure of 73.1, 82.5, 91.9 kPa.

Another feature of these test results is that for the thrust coefficient, as the propeller speed increases, the magnitude of the results shift downwards. For example, for the tests at 100, 175, 250 RPM, the average thrust coefficients are approximately 0.265, 0.164, and 0.126.

Also the two tests at each constant propeller speed were done in succession, and as is clear in a number of plots, the repeatability of the test results was not good. The results of each of the two tests, when considered separately, are smooth and show a similar form. However, the two tests are shifted apart by as much as 50% of thrust coefficient at low advance ratio. A possible explanation given by Veitch (1990) for these results is that they are due to drift in the signals from the strain gauge amplifiers.

The results of torque measurement for the forward operation tests showed con-

siderably more scatter than either the thrust or side force measurements. Also, the difference between the two test sets at the same propeller speed were greater than found in either the thrust or side force measurements.

Veitch(1990) indicated that the first 175 RPM test exhibits more scatter than the second, and the two sets of results are separated by large margins. Veitch considered the main reason for the relatively poor torque measurement was due in large part to the noise in the torque transducer signal.

Recommendations for improving the experimental set up for future experiments were given by Veitch. These recommendations are concerned mainly with the collection of data.

It was recommended that the 60 and 120 Hz noise in the torque measurements be eliminated. This noise was caused by the manner in which the motor control unit maintained a constant torque on the motor. In effect, the DC supply voltage was interrupted at a frequency of 120 Hz. In order to eliminate the noise, the motor cannot be operated with the constant torque feature provided by the feedback loop in the motor controller.

It was also recommended that in order to eliminate other noise in the transducer signals, strain gauge transducer signal amplification should be done with amplifiers located nearer to the propeller model and separate from the analog to digital converter. Separate amplifiers would not be influenced by noise from the digital to analog converter, and the signals transmitted from the propeller to the converter would be at a higher voltage.

2.2 Theoretical Studies

2.2.1 Theoretical Study of Cycloidal Propellers

If one knows the blade hydrodynamical characteristics and the flow field around a blade at any instant, then the force experienced by a blade can be obtained. Then the thrust and torque of a cycloidal propeller can be obtained through the sum of the blade forces.

Up till now what is known about hydrodynamic characteristics of sections is confined to certain types of hydrofoil. Even for these only hydrodynamic characteristics in steady flow is known; very little hydrodynamical data exists for hydrofoils in unsteady flow. As for the unsteady flow, especially such flow that the hydrofoil experiences large angles of attack, the so called dynamic stall phenomena is still a problem that needs more understanding. The most developed theory for the hydrodynamic characteristics of foils is steady linear theory for a thin foil with a small angle of attack.

The analytical study of the flow field around each blade of a cycloidal propeller is complicated. Firstly, the blade is in a non-steady movement. Secondly, the uniform incoming flow from infinity is disturbed by the blade in the first and second quarter of the blade trajectory. Blades on the third and fourth quarter of their trajectory are immersed in a disturbed flow field. Analytical simulation of such a flow field is not easily done.

Some work has been done in the analytical study of the cycloidal propeller. Usually the experimental data of the hydrodynamical characteristics of the hydrofoil are used. As for the analytical simulation of the flow field, there are mainly two types of methods. One is the momentum method (Bose 1987). Another is the vortex method (Mendenhall and Spangler 1975).

A brief review of theoretical study of cycloidal propellers is given below.

2.2.2 Taniguchi's Method

Taniguchi developed a method for numerically evaluating the performance characteristics of cycloidal propellers (Taniguchi 1962). This method is based on the assumption that quasi-steady state motion exists at each instant of time at the blade. The total thrust and torque of the propeller is evaluated by integrating the quasi-steady lift and drag forces on each blade section. For this purpose numerical values of lift and drag coefficients of the blade sections are required. In addition, an estimate of the magnitude and direction of the induced velocity at every blade section must be made. Taniguchi assumed (1) that only the longitudinal velocities induced by the trailing vortex system (i.e., those in the direction of propeller advance) contribute to the thrust and torque of the propeller; (2) that they are of constant magnitude over the length of the blade; (3) that the induced velocity is not a function of the orbital position of the blade. The value of the induced velocity is obtained from momentum considerations with modifications based on experimental performance of a six-bladed cycloidal propeller.

Taniguchi (1962) used a momentum relation to obtain an estimate of the induced

velocity. After conducting experiments on a six-bladed propeller, and obtaining a large discrepancy between computed and experimental values of advance coefficient at zero thrust, Taniguchi modified the correction factor in his momentum relation (Taniguchi 1962).

As for the blade section lift force and drag force, Taniguchi used the following values assuming that the angle of attack is small:

$$C_l = 5.34\alpha \tag{2.1}$$

$$C_d = 0.10 + 6\alpha^4 \tag{2.2}$$

where α is in radians.

Good agreement was obtained between the computed and experimental values of propeller performance (Taniguchi 1962). Of particular interest is the good prediction of the effect of changing the number of blades on the propeller.

However the difference between Tanigichi's analytical results and experimental results is large for high pitch ratio cycloidal propellers (Taniguchi 1962).

Taniguchi's method is adequate for evaluating the performance characteristics of cycloidal propellers with cycloidal blade motion and semi-elliptic blades. For this type of propeller, the procedure gives satisfactory prediction of the effect of number of blades on propeller performance. For each blade motion other than cycloidal motion, experimental results are required to obtain new values of the correction factor for calculating induced velocity. In addition, large changes in aspect ratio of the blade will affect the magnitude of the correction factor.

The most serious limitation of this method lies in the way the induced velocities are estimated; in the assumption that only the longitudinal components contribute to propeller performance; in the assumption that the induced velocity is constant over the entire length of the blade; and finally because the induced velocity can not be computed without resorting to determination by experiment.

2.2.3 Zhu's Method

A theoretical computational method to evaluate the performance characteristics of cycloidal propellers was presented by Zhu (1981). Starting from Taniguchi's method (Taniguchi 1962), improvements were made to make it applicable for various pitch ratios in the whole advance ratio region.

Comparing the results calculated by Taniguchi's method with the results of the experiments, some differences were found. In the high pitch ratio region these differences are quite large. Taniguchi's method is adequate only for medium advance ratios (about 0.4 to 0.5).

In order to improve Taniguchi's method, Zhu modified the drag and lift coefficient by considering effects of low Reynolds number and stalling of blades. Zhu considered that it is important to include the effect of curved orbit and blade rotation. Zhu argued that the relative flow velocity on each point of the blade is not constant. So he considered the effect of variation in speed over the blade and also the effect of rotation. Zhu considered the effect of variation in speed over the blade and the effect of blade rotation as to add an induced camber to blade section. Zhu used Taniguchi's relation to obtain the induced velocity factor.

Zhu obtained numerical results for the thrust coefficient, torque coefficient and efficiency by using both his improved method and Taniguchi's method. Comparison between experimental results and computational results of theoretical methods show that better agreement was obtained by using the improved method.

2.2.4 Bose's Multiple Stream Tube Method

A multiple stream tube theoretical model was developed by Bose (Bose 1987) for application to the rotary foil propeller.

The theory assumes that there are two "actuator discs" in tandem at upstream and downstream of a stream tube. This theory is based on momentum considerations. The lift and drag coefficient for the blade is used to calculate the blade forces. The experimental data for the NACA0012 section in the range from 0° to 180° were used in the calculation. Results were obtained for a range of parameter variations and for two types of blade motion: a pure sinusoidal variation of the blade pitch angle relative to the undisturbed flow and a trochoidal motion. A three dimensional correction was added into the theory by assuming an elliptical variation of lift with blade span.

The result showed that higher efficiency was obtained with a trochoidal blade angle variation than with a sinusoidal blade variation. Finite span was found to reduce efficiency and thrust coefficient. A drop of approximately 7% in efficiency and 9% in thrust was estimated for a propeller with blades of aspect ratio 10; 14.5% in efficiency and 16% in thrust respectively for a propeller with blades of aspect ratio 5. The effect of unsteady flow acting around the propeller blades was neglected.

2.2.5 Mendenhall and Spangler's Vortex Model

Description of Mendenhall and Spangler's Model

Mendenhall and Spangler (1973) developed an unsteady discrete vortex model to calculate the performance characteristics of cycloidal propellers. In their approach, the propeller is considered to be initially stationary in uniform onset flow and is brought instantaneously up to speed. The blade loading changes with time, vorticity is shed, and a wake develops for each blade. The wake is characterized by discrete vortex filaments which approximate the real, continuous vorticity distributions shed from the blades. Since the wake vortex filaments move with the local velocity, the wake from each blade can be followed and the wake distortion due to all the vorticity in the flow field can be obtained. The calculation is done for sufficient time such that the initially shed wake vortices are far enough downstream not to affect the flow at the blades, and a periodic solution is obtained. The detailed variation of the blade loading around their orbit is obtained. With this method the average propeller thrust, side force and torque can be obtained from the time averaged values over an orbit.

Mendenhall and Spangler developed their method for two-dimensional flow and programmed it for a digital computer. They reported the results of calculations made over a range of propeller configurations and flow conditions. Systematic variations in configurations and flow conditions were investigated to establish trends in

performance and behaviour. Comparisons were made with three-dimensional data obtained on model propellers at the David Taylor Research Center (Dickerson and Dobay 1969). The comparisons indicate that the two-dimensional theory generally predicts the correct trends and magnitudes of the average propeller forces.

Blade stall, blade frictional drag and wake diffusion were included in the method. Mendenhall and Spangler compared the predicted and measured thrust and torque coefficients for two-, three-, and six-bladed cycloidal propellers.

Some comparisons between theory and experiment for a six-bladed cycloidal propeller are shown in their results for two high pitch ratios 1.429π and 3.333π. For 1.429π pitch, the thrust and torque are in reasonable agreement with the data, whereas the side force is not. At the higher pitch, both thrust and side force are considerably higher than the experimental data, while the torque agrees reasonably well.

Mendenhall and Spangler's method was used to calculate the performance of a three-bladed and a six-bladed cycloidal propeller. The results were compared by Mendenhall and Spangler with the corresponding experimental data, which shows that Mendenhall and Spangler's method does give resonable results in predicting the trends and magnitude of the propeller performance. But the method consistently gives much higher predicted values for thrust coefficient.

In Mendenhall and Spangler's model, the distributed bound and wake vorticity are replaced by discrete vortex filaments. The bound vorticity on the blade is concentrated at the quarter chord point of the blade. The wake vorticity consists of a number of free vortices which are shed at different positions of the blade. The strength of each wake vortex is given by the change in the bound vorticity occurring

Limitations of Mendenhall and Spangler's Method

The Kutta condition comes from the observation that when the blade angle of attack is small, the flow does not separate from the trailing edge of the blade. However, the blades of a cycloidal propeller go through a large variation of angle of attack in one revolution and usually the occurrence of blade stall is inevitable. During the blade stall, the flow separates near the blade trailing edge. Sometimes the separation can extended up to the leading edge. The Kutta condition is obviously irrelevant when stall occurs, so the use of the Kutta condition can not give a good prediction of the flow field around the blades at some positions on their orbit.

Another limitation of the method used by Mendenhall and Spangler is the neglection of dynamic stall phenomena. Dynamic stall is a complex series of events that results in the dynamic delay of the stall, on airfoils and wings experiencing unsteady motion, to angles significantly beyond the static stall angle. In deep dynamic stall, the formation and shedding of a "dynamic stall vortex" from the leading edge region is believed to play a crucial role. Flow near the surface of an airfoil oscillating in pitch has been observed to remain "attached" during the airfoil upstroke to a point well beyond the static stall incidence angle. This delay in incipient separation is followed by the formation of an energetic vortex structure near the airfoil leading edge which grows with time and convects downstream over the suction surface as the airfoil motion proceeds. A strong suction peak in the instantaneous pressure distribution has been observed to remain approximately coincident with the chordwise location of the vortex.

over some time interval Δt. The strengths of these shed vortices remain constant and each moves with the flow.

A time stepping approach was used by Mendenhall and Spangler to solve this problem. At each time step, the flow field and the blade bound vorticities are computed and the motion of all shed vorticity is calculated. Between successive time steps, a shed vortex is generated at each blade trailing edge and is added to the wake vortex system. The calculation continues until steady-state propeller forces are achieved.

The total bound vorticity on a blade is the sum of five components. The first four are due to the kinematics of the blade motion. The fifth component is an induced vorticity due to the presence of the other blades and the wake. Mendenhall and Spangler used the method described by von Kármán and Burgers (1935) to calculate this induced vorticity by computing the circulation on a flat plate due to the interference of an isolated vortex. The total circulation induced on the blade is the sum of the individual circulation components induced by each bound and shed vortex in the flow field. The boundary condition used to determine the induced vorticity on the blade is the specification that the Kutta condition be satisfied at the blade trailing edge at each time step.

Most dynamic stall research has focused on the flow over an airfoil oscillating in pitch. When there are several blades in the flow, interactions between the blades are found to significantly affect the dynamic stall characteristics of each blade and the overall flow field (Sparlart 1985). Studies on rotation stall in a compressor have found that stall is not limited to within a restricted range of angles of attack; the wake vortices from one stalling blade can trigger separated flow over other blades (Sparlart 1985). Although the above mentioned flow phenomena has been observed in the flow through a compressor in an engine (Sparlart 1985), a similar mechanism could exist in the flow through a cycloidal propeller.

Neglection of dynamic stall phenomena in Mendenhall and Spangler's method affects its predictability of propeller performance in two respects. Firstly, dynamic stall can change the flow field around the blade. Secondly, the lift/drag coefficient of the blade under dynamic stall is usually unavailable.

Mendenhall and Spangler's method was developed for a two-dimension cycloidal propeller. The effect of tip vortices are not modeled in their method. The effect of tip vortices on the flow over the blade is not clear under dynamic stall conditions. Three dimensionality in unsteady flow about a finite wing was studied by use of flow visualization by Alder and Luttges (1985). Their results show that far inboard, towards the root of the wing, the flow field was dominated by a leading edge vortex similar in phase of initiation, size, and convection velocity to vortices observed in studies modeling a two-dimensional wing. Flow near the tip is dominated by the induced velocity effect of the wing tip vortex and observation suggests that the wing tip vorticity is fed in part by the increased circulation present in the leading edge vortex. Visualization also showed a transition from flows dominated by the wing tip

vortex to those dominated by the leading edge vortex.

Chapter 3

Theoretical Study

3.1 Description of the Theoretical Models

The theoretical models used in the present study of cycloidal propeller performance were based on Mendenhall and Spangler's method (Mendenhall and Spangler 1973). They are described below.

3.1.1 Modification of Mendenhall and Spangler's Method

Modifications in Calculating Wake and Effects of Other Blades

Mendenhall and Spangler's method (Mendenhall and Spangler 1973) and some of its limitations have been introduced briefly in the previous chapter.

Mendenhall and Spangler used linear potential flow theory with the Kutta condition to evaluate additional forces induced by the wake and the other blades. Since during each propeller revolution, the blades experience large changes of angle of

attack that far exceed the the small angle of attack limitation for potential flow theory, the Kutta condition is no longer a valid description of the real flow around the blade trailing edge since flow separation occurs and friction becomes important.

In order to see how much the wake and other blade effects calculated by the potential flow theory with the Kutta condition contributed to the total flow, Mendenhall and Spangler's model was modified so that the wake and other blade effects were totally cut off. Then the results from this modified model was compared with Mendenhall and Spangler's model results and with the corresponding experimental results. In another modified model, the potential flow theory and the Kutta condition was not used to calculate the wake and the effects of other blades. Instead, the induced velocity due to the wake and the other blades was calculated first. This induced velocity changed the angle of attack of the blade under consideration, which in turn changed the blade forces. This method is called the angle of attack method.

Gormont's Method for Dynamic Stall Calculation

Mendenhall and Spangler's model was also modified to include the dynamic stall effect by using NACA-0012 section characteristic data and Gormont's dynamic stall correction method.

Gormont (1973) developed a method to calculate the dynamic stall effect based on steady airfoil section data in his study of unsteady flow over helicopter rotors. The idea of Gormont's was that a steady state flow needs time to build up, so dynamic stall can be modelled as if there is a time lag in the aerodynamic characteristics of the blade at a certain angle from its steady characteristics at the same angle.

He proposed a formula for calculation of lift and drag of a general type of airfoil oscillating about a mean angle near its static stall angle based on the experimental study of four types of airfoil. As the same flow delay argument holds for the flow through a cycloidal propeller, where the blades oscillate about a zero mean angle with very large amplitude at small advance ratios, Gormont's method was used with Mendenhall and Spangler's theory (1973) to account for dynamic stall. Since the lift coeficient of a foil is not a function of fluid density, Gormont's method can be used for the calculation of forces experienced by hydrofoils during dynamic stall.

Method for Three Dimensional Correction

A three dimensional correction method valid for wings in steady flow with an elliptical distribution of lift was used by Bose (1987) in the calculation of the force characteristics of a cycloidal propeller by multiple stream tube theory. In this method, an estimation of the effect of finite blade span was obtained by assuming that the distribution of circulation along the blade varies elliptically. Bose found that the effect of aspect ratio was to reduce the maximum peak efficiency of the propeller by approximately 7% for propellers with blades aspect ratio 10 and 14.5% for aspect ratio 5 from the two dimensional results. Obviously this method cannot estimate unsteady three dimensional effects.

All the theoretical models described above included the option of including three-dimensional calculation of the blade force.

3.1.2 Formulation of the Theoretical Models

Propeller characteristics

The geometrical characteristics of a cycloidal propeller are given in Figure 1.1. The origin of the coordinate system is chosen at the center of the propeller drum. The angle between the y axis and the radius connecting the pitching point of the blade under consideration and the center of the propeller disc is θ, positive clockwise. The angle between the y axis and the line connecting the pitching point of the blade and the steering center is ψ, measured positive clockwise. The angle between the blade and the tangent to the blade orbit is β, measured positive counterclockwise. A uniform free stream velocity $\vec{V}$ is in the negative x direction. The constant angular velocity of the propeller is ω. The blade is replaced by a point vortex Γ at the $\frac{1}{4}$ chord point from the leading edge in the calculation. The total flow velocity relative to the blade at the $\frac{1}{4}$ chord point due to the free stream and the rotation of the propeller drum is $\vec{W}$. The angle between $\vec{W}$ and the blade chord line is α, which is called the angle of attack. The pitching point of a blade is at x_0 from the leading edge; the chord length of the blade is c; the radius of the propeller disk is R; the distance between the center of the cycloidal propeller and the steering center is r.

The pitch ratio of a cycloidal propeller is defined as

$$P = \frac{r\pi}{R} \tag{3.1}$$

The blade angle is given by

$$tan\beta = \frac{\frac{r}{R}sin\theta}{1 + \frac{r}{R}cos\theta} \tag{3.2}$$

Fig 1.2 gives the different blade positions with pitch ratio greater than π and less than π.

Flow model

(a) Mendenhall and Spangler's Formulation

The formulation started from Mendenhall and Spangler's model (Mendenhall and spangler 1973). The propeller was initially stationary. It was brought up to a constant speed abruptly. The lift and drag produced by each blade changed with time. Vortices were shed from each blade into the flow and were convected downstream. Circulation about each blade due to angle of attack and blade camber, the rotation of the blade, the circulation induced by the wake and other blades were calculated by vortex theory and linear potential thin wing theory. Drag was calculated through experimental section data. Stall was modelled by cutting off the lift coefficient at -1.5 and +1.5 . Diffusion of the discrete vortices in the wake was modeled approximately (Mendenhall and Spangler 1973).

The bound vortex Γ at each blade was placed at the quarter chord point. The wake of each blade was discretised into a number of free vortices $\bar{\Gamma}$. The strength of the blade bound circulation induced by the wake and the other blades was obtained by first mapping the blade into a circle and then calculating the bound vorticity required to impose the Kutta condition on the circle.

The bound vorticity Γ on each blade consisted of 6 parts.

$$\Gamma = \Gamma_1 + \Gamma_2 + \Gamma_3 + \Gamma_4 + \Gamma_w + \Gamma_B \tag{3.3}$$

$$\Gamma_1 = \pi c W \alpha \tag{3.4}$$

$$\Gamma_2 = \pi c W \alpha_0 \tag{3.5}$$

$$\Gamma_3 = -\frac{\pi c^2}{4}\dot{\psi} \tag{3.6}$$

$$\Gamma_4 = \pi c^2 \dot{\psi}(\frac{x_0}{c} - \frac{1}{2}) \tag{3.7}$$

$$\psi = \theta - \beta \tag{3.8}$$

where Γ_1 was the circulation on a flat-plate at an angle of attack of α; and Γ_2 was due to the geometrical camber of the blade. This assumed that a flat-plate must be put at an angle of attack α_0 to produce the same lift as the cambered blade section at zero degrees angle of attack. Γ_3 and Γ_4 were due to angular rotation of the blade about its pivot point, located a distance x_0 from the leading edge. Γ_w and Γ_B were the circulation induced by wake vortices and other blades respectively. The method used in calculating Γ_w and Γ_B was that of von Kármán and Burgers (1935) in computing the circulation on a flat-plate induced by an isolated vortex. W was the relative velocity approaching the blade due to the free incoming flow and

rotation of the propeller (the induced velocity was not included here), which was given by

$$\frac{W}{\omega R} = [1 + (\frac{V}{\omega R})^2 + 2(\frac{V}{\omega R})cos(\theta - \alpha_p)]^2 \tag{3.9}$$

This velocity was broken into normal and axial components W_N and W_A.

$$\frac{W_N}{\omega R} = (\frac{V}{\omega R}sin\alpha_p + sin\theta)cos\psi - (\frac{V}{\omega R}cos\alpha_p + cos\theta)sin\psi \tag{3.10}$$

$$\frac{W_A}{\omega R} = (\frac{V}{\omega R}sin\alpha_p + sin\theta)sin\psi + (\frac{V}{\omega R}cos\alpha_p + cos\theta)cos\psi \tag{3.11}$$

The local blade angle of attack was defined as

$$\alpha = tan^{-1}\frac{W_N}{W_A} \tag{3.12}$$

where α_p was the angle between the free stream and the x axis. In the models used in this study α_p was zero.

The method of calculating the induced circulation Γ_w and Γ_B was as follows. First the blade in its physical plane was mapped into a circle in the ζ-plane by the transformation

$$z = \zeta + \frac{a^2}{\zeta} \tag{3.13}$$

with the location of the vortex in the ζ-plane being r,ϕ. The Kutta condition satisfied at the blade trailing edge in the physical plane corresponds to the condition in the ζ-plane that the velocity be everywhere tangential to the circle on the circle

and zero at the mapped trailing edge on the circle. The circulation on the blade induced by the isolated vortex $\bar{\Gamma}$ (von Kármán and Burgers 1935) was

$$\Gamma_{ind} = \bar{\Gamma}\left(\frac{2ra(cos\phi) - 2a^2}{r^2 - 2ra(cos\phi) + a^2}\right) \tag{3.14}$$

The induced circulation was assumed to act at the quarter chord of the blade.

The circulation on the blade induced by all the discrete wake vortices Γ_w is the sum of the induced circulation due to each vortex. The circulation on the blade induced by all the other blades Γ_B was the sum of the circulation induced by each blade. The total force on a blade consisted of the hydrodynamic force due to the blade circulation, a normal force on the blade due to the acceleration of the blade normal to itself (apparent mass effect) and the viscous drag of the blade.

(b) Mendenhall and Spangler's Model without Wake and the Effects of Other Blades

For some calculations, Mendenhall and Spangler's Model was modified so that the terms Γ_w and Γ_B were not included in the calculation of Γ.

(c) Mendenhall and Spangler's Model with Wake and Other Blade's Effects Modeled as a Change of Angle of Attack

In this model, Γ_w and Γ_B were not included in the calculation of Γ. But velocity induced by wake and other blades were calculated at each blade center point. Then the angle of attack was calculated as:

$$\alpha = \frac{W_N + W_{Nin}}{W_A + W_{Ain}} \tag{3.15}$$

where W_N and W_A are the velocities vertical and parallel to the blade chord line due to the free incoming flow and the rotation of the propeller, W_{Nin} and W_{Ain} were the velocities vertical and parallel to the blade chord line due to the wake and other blades.

The influence of $\bar{\Gamma}$ located at the point $(x_\Gamma,\ y_\Gamma)$ on another point (x_p,y_p) is computed from the velocity induced by $\bar{\Gamma}$. Thus,

$$v_x = \frac{F_x}{2\pi}\bar{\Gamma} \tag{3.16}$$

$$v_y = \frac{F_y}{2\pi}\bar{\Gamma} \tag{3.17}$$

where the influence functions were defined as

$$F_x = \frac{y_p - y_\Gamma}{(y_p - y_\Gamma)^2 + (x_p - x_\Gamma)^2} \tag{3.18}$$

$$F_y = \frac{x_p - x_\Gamma}{(y_p - y_\Gamma)^2 + (x_p - x_\Gamma)^2} \tag{3.19}$$

As written, the above influence functions are for the velocities induced in the x and y directions.

Assume v_x and v_y are the induced velocities at a blade center point. Then the induced velocities vertical and parallel to the blade chord line due to the presence of a discrete vortex located in $(x_\Gamma,\ y_\Gamma)$ are:

$$W_N = v_x sin\Psi + v_y cos\Psi \tag{3.20}$$

$$W_A = -v_x cos\Psi + v_y sin\Psi \tag{3.21}$$

Definition of Ψ is shown in Figure 1.1.

(d) Modification to Include Dynamic Stall Effect

Gormont (1973) used a method of approximating the observed hysteresis loops in lift and drag section data by using two-dimensional static wind tunnel data and an empirically derived stall delay representation developed by Gross and Harris (1969). The accumulated section data for oscillating airfoil tests of four types of airfoil (V23010-1.58,NACA-0012 MOD,V13006-.7 and NACA-0006) were used to obtain a generalized formula for the dynamic stall delay angle:

$$\alpha_{dynamicstall} = \alpha_{staticstall} + \Delta\alpha_{dynamicstall} \tag{3.22}$$

$$\sqrt{|\frac{c\dot{\alpha}}{2V}|}_{break} = 0.06 + 1.5(0.06 - \frac{t}{c}) \tag{3.23}$$

For $\sqrt{|\frac{c\dot{\alpha}}{2V}|} < \sqrt{|\frac{c\dot{\alpha}}{2V}|}_{break}$,

$$\Delta\alpha_{dynamicstall} = \gamma_1(\sqrt{|\frac{c\dot{\alpha}}{2V}|})(sign\dot{\alpha}) \tag{3.24}$$

For $\sqrt{|\frac{c\dot{\alpha}}{2V}|} > \sqrt{|\frac{c\dot{\alpha}}{2V}|}_{break}$,

$$\Delta\alpha_{dynamicstall} = \gamma_1\sqrt{|\frac{c\dot{\alpha}}{2V}|}_{break} + \gamma_2[\sqrt{|\frac{c\dot{\alpha}}{2V}|} - \sqrt{|\frac{c\dot{\alpha}}{2V}|}_{break}](sign\dot{\alpha}) \tag{3.25}$$

where the *sign* function is defined as follows:

if $x > 0$, then $sign(x) = +1$;

if $x < 0$, then $sign(x) = -1$.

$$\alpha_{ref} = \alpha - K_1 \Delta\alpha_{dynamicstall} \tag{3.26}$$

$$C_l = (\frac{C_{l_{Ref}}}{\alpha_{ref} - \alpha_{C_l=0}})\alpha \tag{3.27}$$

$$C_d = C_{d_{Ref}} \tag{3.28}$$

where γ_1,γ_2 are calculated as follows

$$\gamma_2 = 1.4 + 6(0.06 - \frac{t}{c}) \tag{3.29}$$

$$\gamma_1 = 0.5\gamma_2 \tag{3.30}$$

K_1 is chosen as 1.0 in the calculation. Definition of break point is given in Gormont's paper (1973).

Gormont's method was obtained from experimental data for airfoil oscillating sinusoidally about a mean angle of attack α_0 ($0° \sim 15°$) with a relatively low oscillatory pitch amplitude $\Delta\alpha$ ($0° \sim 5°$)

$$\alpha = \alpha_0 + \Delta\alpha sin\omega t \tag{3.31}$$

The range of angle of attack of a blade on a cycloidal propeller can vary from $-180°$ to $180°$ at certain advance ratios and the oscillating motion is not sinusoidal.

Strickland and Graham (1986) tested a NACA-0015 airfoil undergoing a constant pitching rate motion up to 82° of angle of attack. Their results show that Gormont's correlation of dynamic stall delay angle can fit their test data reasonably well. How well Gormont's method can fit the experimental data of an airfoil undergoing a similar *oscillating* motion as that of a cycloidal propeller blade is still to be examined.

(e) Modification to Include Three Dimensional Effects

Three dimensional effects on a blade of finite aspect ratio were obtained by assuming that the distribution of circulation along the blade varied elliptically (Bose 1987). The finite aspect ratio effect based on this method was to reduce the lift due to an assumed elliptical distribution of lift and to increase the total drag by adding an induced drag.

The three dimensional lift slope was

$$(\frac{C_l}{\alpha})_{3d} = (\frac{C_l}{\alpha})_{2d}(\frac{\pi A}{1+\pi A}) \tag{3.32}$$

and the three dimensional drag coefficient was

$$(C_D)_{3d} = (C_D)_{2d} + \frac{(C_D)^2_{2d}}{\pi A} \tag{3.33}$$

where the aspect ratio $A = \frac{b^2}{S}$ (b is blade span; S is blade area).

This method was based on steady flow theory and was not exactly the same as that in unsteady flow over a blade on the cycloidal propeller considered here. In an unsteady flow, it takes time to build up the wake vortex system. Also, this wake vortex system changes with time due to the variation of blade forces after it has

been built up. This can lead to some difference in calculating of three dimensional effects.

(f) Blade and propeller forces

The blade axial and normal forces were

$$K_x = -\rho b\Gamma sin\alpha + \frac{\rho cbC_d}{2}W^2 cos(\alpha) \tag{3.34}$$

$$K_y = -\rho b\Gamma cos\alpha + \frac{\pi\rho c^2 b}{4}[\frac{dv}{dt} - c\ddot{\psi}(\frac{x_0}{c} - \frac{1}{2})] + \frac{\rho cbC_d}{2}W^2 sin\alpha \tag{3.35}$$

where x was along the blade chord line, positive towards the trailing edge, y was normal to the blade chord line in the blade coordinate system; b was blade span; C_d was the section data of viscous drag coefficient; and ρ was the density of the fluid. After conversion into the propeller coordinate system, K_x,K_y of each blade were summed for all the blades to obtain the total propeller thrust T, torque Q and side force S.

The thrust, torque and side force coefficients were defined differently in order to compare the predicted results with the experimental results. Torque and thrust coefficient were defined as follows in Bose and Lai's (1989) experimental results

$$C_T = \frac{T}{\rho\omega^2 R^2 Db} \tag{3.36}$$

$$C_Q = \frac{Q}{\rho\omega^2 R^3 Db} \tag{3.37}$$

$$\eta = \frac{TV}{\omega\pi} \tag{3.38}$$

where b was blade span; D was the propeller diameter. In Dickerson and Dobay's experiments, the thrust and torque coefficients were defined as

$$C_T = \frac{T}{\rho n^2 b D^3} \tag{3.39}$$

$$C_S = \frac{S}{\rho n^2 b D^3} \tag{3.40}$$

$$C_Q = \frac{Q}{\rho n^2 b D^4} \tag{3.41}$$

$$\eta = \frac{CT}{CQ}\frac{J}{2\pi} \tag{3.42}$$

$$J = \frac{V}{nD} \tag{3.43}$$

Both sets of the force coefficients were included as options in the computer programs for the theoretical models above.

3.2 Implementation of the Theoretical Models

A computer program for implementation of Mendenhall and Spangler's theoretical method was given by Mendenhall and Spangler in their report (Mendenhall and Spangler 1973). The implementation of the modified theoretical models is based on

Mendenhall and Spangler's program. In the programs for modified theoretical models, the logic of calculation remains the same as that in Mendenhall and Spangler's program. But the structure of the programs for modified theoretical models have been changed substencially from that of Mendenhall and Spangler's program.

For more detailed description of the computer programs, see Appendix B.

Chapter 4

Experimental Study

4.1 Description of the Experimental Set Up

A cycloidal propeller model was designed by Bose and Veitch(Veitch 1990) specially to fit into the cavitation tunnel in the Institute for Marine Dynamics and constructed by Memorial University of Newfoundland Technical Services. The detailed assembly drawing of the model is given by Veitch (1990). The model is comprised of a casing, a motor and motor seat, three propeller blades, and propeller machinery and transducers. The casing was connected to the top window of the test section. The model propeller was hung inside the casing so that the surface of the propeller drum was flush with the bottom of the top window of the test section. A 2 hp, 175 rpm, 180 volt DC electric motor was seated on top of the model (See Figure 4.1). A motor controller was used to provide variable speed and reversing capabilities.

There were three blades mounted on the rotating disc. The blade sections were NACA 16 series symmetrical sections tapered linearly from root to tip (Veitch 1990 Figure 8). The root section were NACA 16-021, and the tip sections NACA 16-012

basic thickness forms. The rotation axis of the blades were at the quarter-chord length of the sections. The maximum and minimum angles were ±20°. Detailed description of the model propeller was given by Veitch (Veitch 1990).

The strain gauges for thrust measurement was attached on one of two plates on the upper part of the model which were perpendicular to the flow in the test section of the tunnel. The strain gauge for side force measurement was positioned similarly to the thrust gauge, but on one of the two plates which were parallel to the flow in the tunnel. The torque gauge was attached on the surface of a cylindrical part which connected the cam box with the gear box.

The cavitation tunnel at IMD is of the closed circuit type (Veitch and Bose 1989). An impeller circulates the water along a horizontal diffuser which is a 6:1 contraction nozzle. After the nozzle, the water flows through the test section which is fitted with observation windows. The impeller is driven by a 51.5 kW, 1500 RPM motor and can produce water speeds between 0 and approximately 10.5 m/s in the test section.

A multi-channel 2100 system strain gauge conditioner, a 386 SX Unisys microcomputer and a Keithley 570 analog to digital converter were used to transfer and record the signal data from the thrust, side force, and torque transducers on the model propeller.

The flow speed in the tunnel test section was measured by a mercury manometer which measured the pressure drop across the contraction nozzle of the tunnel. An expression for water speed in the test section in terms of pressure was given by Veitch and Bose (1989). The rotation speed of the motor was measured by a tachometer. A vacuum pump was used to lower the pressure in the cavitation tunnel.

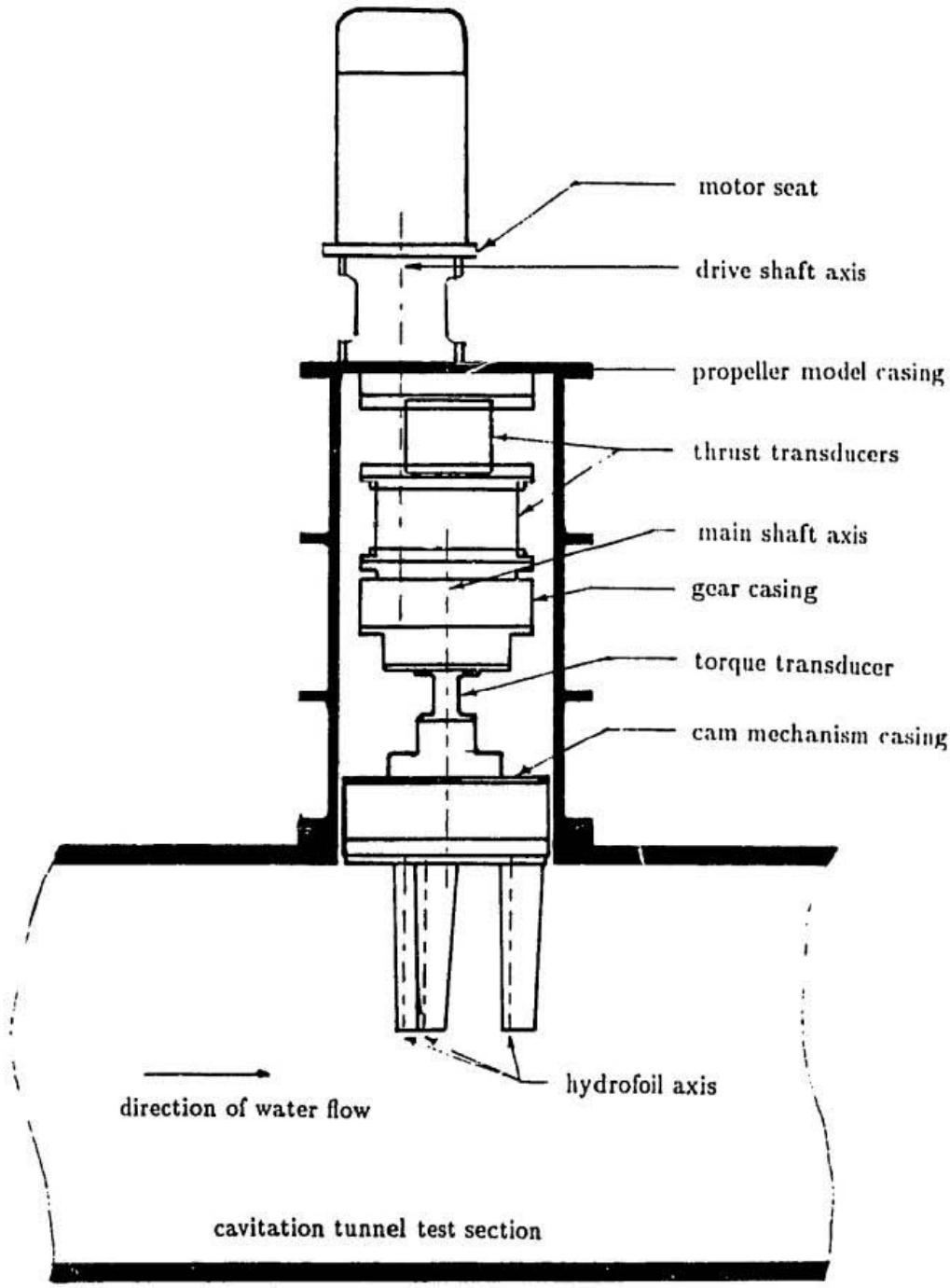


Figure 4.1: General arrangement of trochoidal propeller model

4.2 Work Done to Improve the Experimental Technique

The present experimental study of the cycloidal propeller follows the previous work done by Veitch(1990) at Memorial University. Some of the problems which were encountered previously with the model propeller and the cavitation tunnel were alleviated.

(a) The model was recentered inside the casing to avoid rubbing the casing when the hydrodynamic forces were large during tests.

(b) Strain gauge wires were replaced by new ones and sealed by special rubber tape.

(c) Connections between each part of the casing were redone to improve sealing to avoid water coming out of the tunnel and air leakage into the tunnel during low pressure tests.

(d) Tunnel valves were replaced by new ones to avoid air leakages.

4.3 Problems and Their Treatment

(a) Signal Noise Reduction by Rearranging Experiment Set Up

It was found in the previous experimental study (Veitch 1990) that the noise levels on the strain gauge signals were high during the tests. To avoid electromagnetic interference due to the close arrangement of the equipment, a multi-channel 2100 system strain gauge conditioner was used to amplify the signal from the strain

gauges instead of using the internal amplifier card inside the Keithley 570 A/D converter.

(b) Torque Transducer

During preliminary tests, it was found that the torque gauge used in the previous experimental study was defective. New strain gauges to measure torque were fitted to the transducer element by Inter-technology Inc; heat setting adhesives were used.

(c) Choosing a Zero for Torque Measurement

When testing with the torque gauge, it was expected that every time before turning on the motor and after turning off the motor, the torque reading should be the same. In fact, the torque readings shifted randomly between two considerably different values. In other words, there were two quite different readings from the torque transducer when the model was at rest. This caused a difficulty in choosing a zero for torque measurement. An explanation for this is that each time when the model was stopped after motion, there was still some residual torque applied on the transducer probably caused by friction in bearings and the cams which controlled the blade motion.

To avoid the difficulty in measuring the torque caused by this problem, each time before the test began, the amplifiers were warmed up for approximately 2 hours so that the readings corresponding to the rest state became steady. A friction test was then done. Then the torque channel zero setting on the amplifier was not changed during the entire process of the tests that same day. The friction torque was used as the zero torque reading. All the torque readings collected during the tests on the same day were obtained after subtraction of the friction torque reading, thus the torque caused by hydrodynamic forces was obtained. (Notice that in this way the

real value of the friction torque is never known.)

The above procedure of measuring torque was justified by comparing two sets of data under similar flow conditions and propeller RPM. If the friction torque was used as the torque zero, then the torque coefficients obtained from these two sets of data falls on one curve (allowing for experimental scatter). (See Figure 4.2).

If the torque transducer readings before each of the two tests were used as the corresponding zero torque readings, then the hydrodynamic torque coefficients obtained from those two sets of data were far apart. An example is given in Figure 4.3.

(d) Friction Torque Measurement

Each day before the normal tests, the friction torque at different RPM was measured. After the normal tests, before the end of that day's work, the friction torque was measured again. It was noticed that the friction torque measured at the beginning of the day's work was usually higher than the friction torque measured at the end of the day's work. It implied that a day's tests reduced the friction torque somewhat. This change could also be an actual zero shift throughout the whole day. So the mean of the two friction torques corresponding to different RPM was used as the zero torque in order to get a more reliable torque measurement.

(e) Zero's for Thrust and Side Force Measurement

When comparing the thrust and side force coefficients from two sets of test data under similar flow conditions and propeller revolutions, there were some systematic differences between the two coefficients, especially at lower advance ratios. It was noticed that the zero's of the thrust and side force channels change before and after each test, so during each test, two zero thrust readings were recorded consecutively

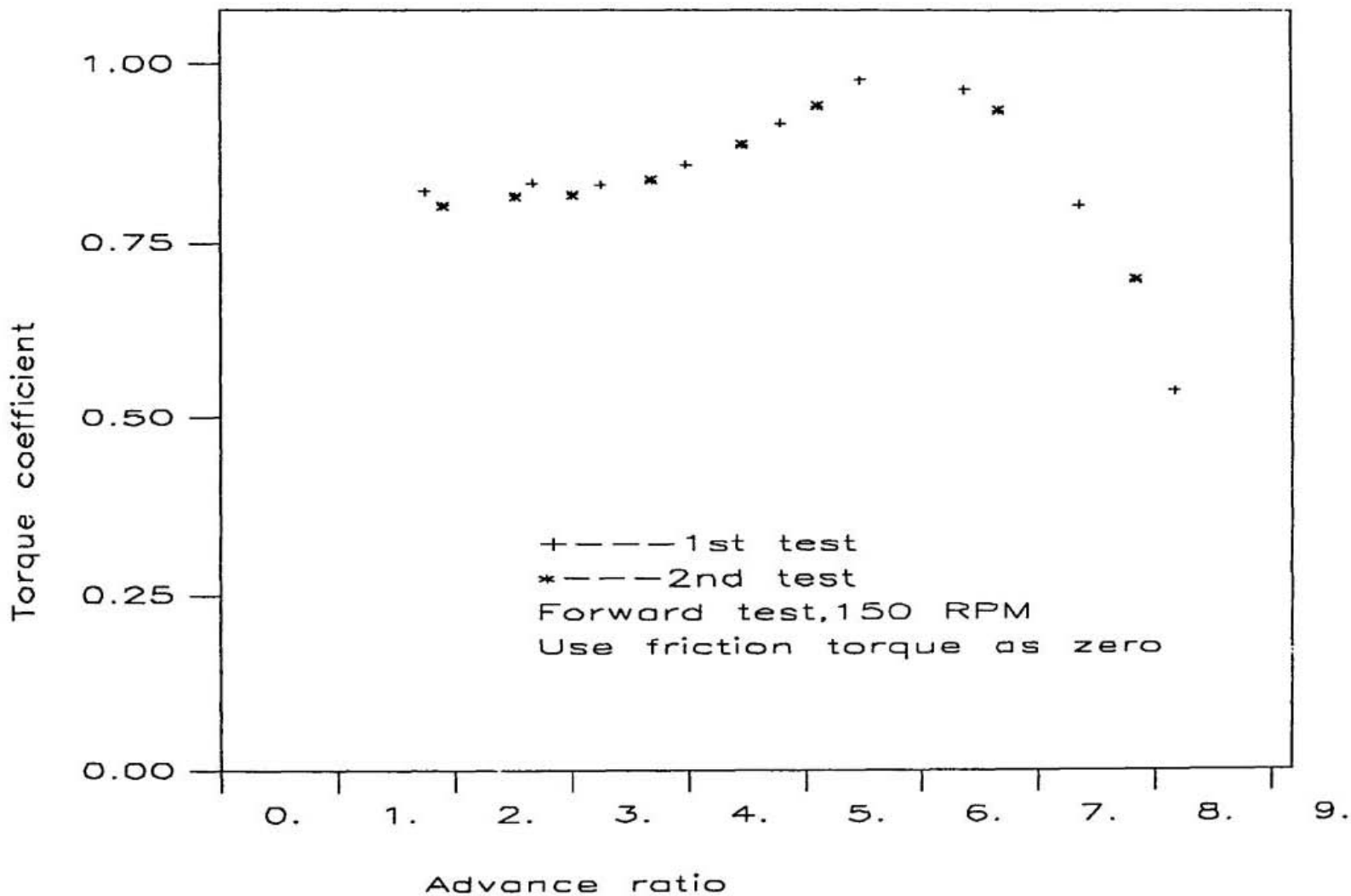


Figure 4.2: Use friction torque as zero to obtain torque test data

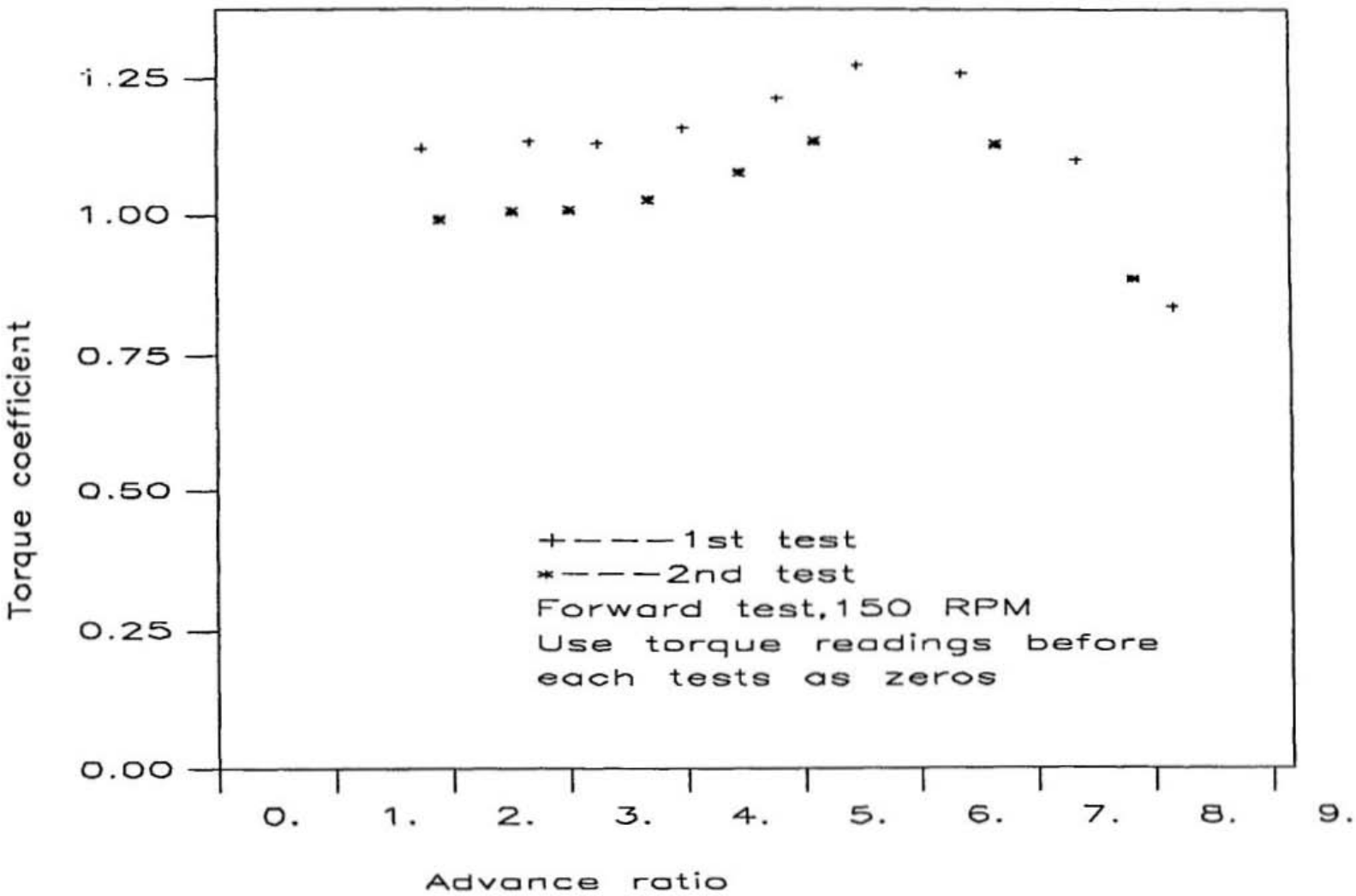


Figure 4.3: Use zeros before each test to obtain torque test data

before and after each test. Then the zero used in calculating the thrust coefficients was the mean of the four recorded zero's. The same method was applied to side force measurement.

(f) Torque Gauge Calibration

When doing the torque gauge calibration, the model propeller was clamped so that the shaft of the model could not turn when torque were applied to the blades of the model propeller. During the calibration, it was found that the torque gauge calibration results were related to the order of the calibration tests. For example, after reverse the applied torque direction, a relatively smaller slope for the torque gauge was obtained from the first test than that from the second test. That means that a relatively larger torque was needed in the first test to twist the shaft to a certain degree than that in the second test.

An explanation for this phenomenon was that when reversing the direction of the applied torque on the model propeller, part of the applied torque was to rearrange the relative position of cams inside the blade control mechanism. After a certain time with the applied torque on the model propeller, the cams which are bathed in oil slide slowly into place. Then all the applied torque was used to rotate the shaft of the model propeller. That is why when torque was applied at the beginning, only a small slope was obtained from the calibration test. After a while, a larger slope was obtained although the applied torque remained the same.

During a normal test of the model propeller, the model propeller was rotating in the water tunnel. The hydrodynamic torque on the model propeller oscillate about zero with time. So the torque measured during a normal test is not the same as the torque applied to the model propeller when doing the calibration test, especially not

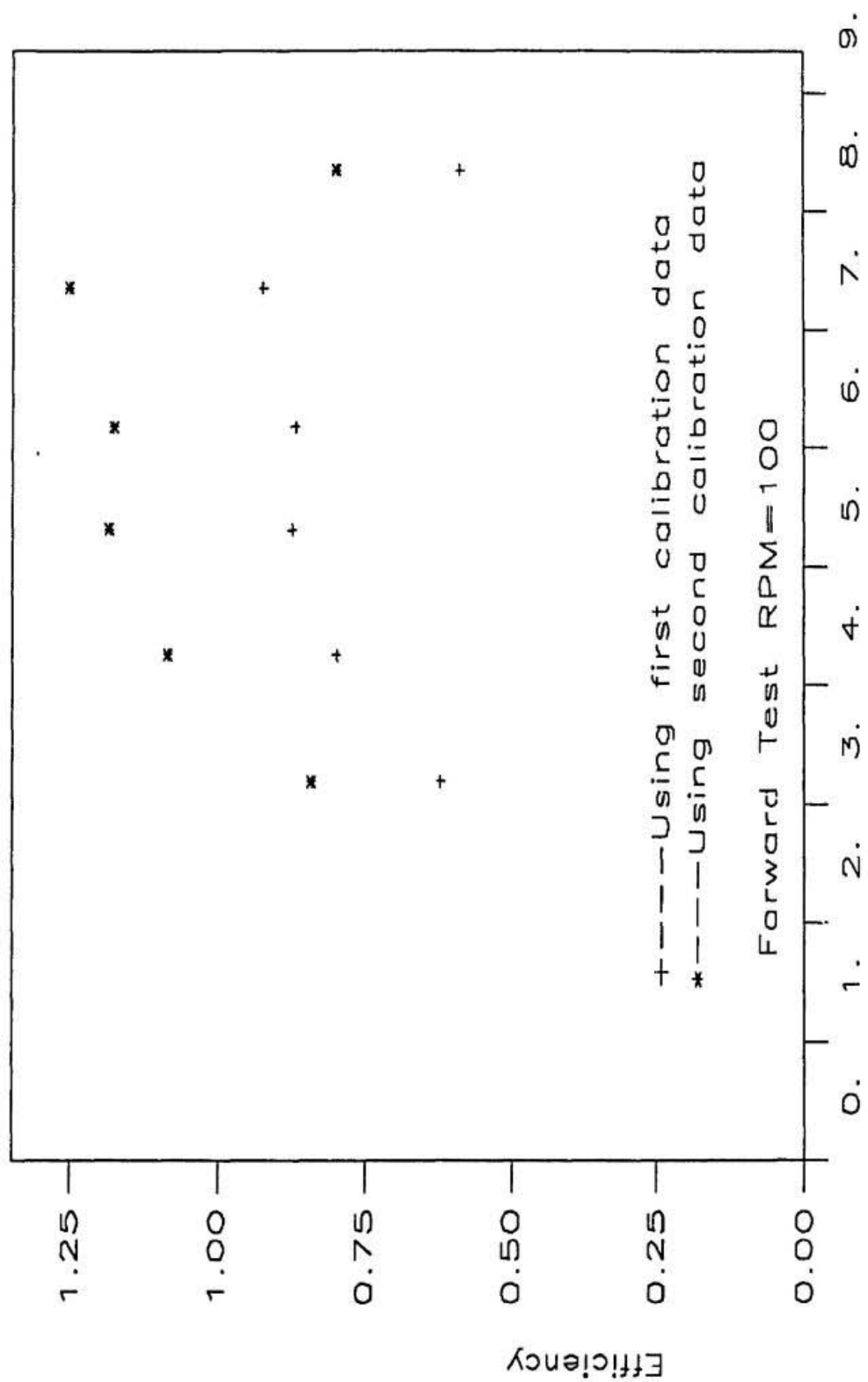


Figure 4.4: Efficiency for one test using different calibration data

the same as the static torque after applying torque for a certain time until the cams inside the blade control mechanism slide into place.

To justify the above explanation, two different slopes for the same amplifier gain from torque calibration tests were used to calculate the torque coefficients from test data. For a single test, when using the slope obtained from the first calibration test after reversing the applied torque direction, the efficiency of the model varies from 0.5 to 0.8. When the slope obtained during the second calibration test after reversing the applied torque direction is used, the efficiency of the model propeller exceeds 1.0, which is not realistic (see Figure 4.4).

(g) Effect of the Water Level in the Tunnel

In the early tests of this experimental study, in order to avoid the wires connecting three gauges and the amplifier to be soaked by the water inside the casing, the water level in the tunnel was only raised just above the top of the diffuser. During the test, it was observed that a lot of air bubbles entrained from the top of the diffuser came into the test section which made the flow in the test section very turbulent. To avoid this problem, in the later tests, the water level in the tunnel was raised approximately 0.2 meters above the top of the diffuser. The observed flow in the test section became uniform and clear.

(h) Increase the Signal Resolution

As the magnitude of the hydrodynamic forces on the propeller model differ significantly during tests at different revolution speeds, two sets of amplifier gains were used to transfer and record the test data. One for tests of propeller RPM less than 200, another for tests of RPM equal to or greater than 200. Still, the torque was so large for a reverse test with propeller RPM equal to 150 that the set of the gain for

high RPM was still not appropriate and the signal was out of range at high advance ratio.

(i) Vertical Force on the Model Propeller

Although the vertical force on the model propeller (force that is along the model shaft) was not measured during tests, it was large enough to move the gear box upwards which caused the electric brushes to fall off the slip ring track and stopped the torque signal transfer. The gear box was therefore reassembled to avoid 'iding up and down due to the vertical forces during tests.

(j) Reduce the Noise from Motor

The problem of noise from the motor was discussed by Veitch (1990). The motor control feed back feature was not used in this experimental study. The 'orque applied by the motor might change with time, so it was necessary to check and record motor RPM from time to time during each test.

4.4 Test Procedure

Test procedure for this experimental study was as follows.

(1) Turn on the strain gauge conditioner. Wait for approximately 2 hours for the signal from the transducers to become steady. Set zero's for each channel. Never change the torque zero during the entire test that day.

(2) Do the friction tests at given propeller revolution speeds.

(3) Raise the water level to approximately 0.2 meter above the diffuser.

(4) Record zero force readings for thrust and side force channels twice.

(5) Turn on the motor and set the propeller at a given propeller RPM.

(6)

(a) Turn on the water speed slowly.

(b) Wait until the flow became steady and observe the flow conditions at the model propeller.

(c) Record the manometer reading (for calculating water speed).

(d) Run SOFT500 program to record data.

(e) Check and take the propeller RPM using the tachometer.

(f) Restart from step (a)

(7) At end of the day, redo friction tests as in step (2).

4.5 Note about the Problems and Their Treatment

Some problems and their treatment are not self-explaining and may cause confusion. The following are some more explanation about those problems.

4.5.1 Choosing the Zero Point for Torque Measurement

In this specific experimental set up and measurement, choosing a zero for torque measurement is only choosing a mark for a certain physical state of the strain gauge. Then measuring the friction is to give another mark for the strain gauge physical state corresponding to the given friction torque. Then measuring the torque when the propeller is rotating in the water is to give a third mark for the strain gauge physical state. Then the difference between the third mark and the second mark is the measure of the hydrodynamic torque on the propeller. The marks can vary

when different zeros are chosen. But the difference between the third and the second mark does not vary with the chosen zeros. That is the whole idea how I solve the problem in measurement of torque when the no strain state of the propeller can not be achieved.

4.5.2 Friction Test Procedure

Detailed procedure for a single friction test is as follws.

(a) Set up all the equipments, wait for them to become stable.

(b) The tunnel test section is empty. So the propeller will be rotating in the air.

(c) Set a zero when the propeller model is at rest.

(d) Turn on the propeller at a given rotation speed.

(e) Wait until the torque reading becomes stable. Take down the reading.

4.5.3 About the Torque Calibration

Theoretically, there is difference between static torque measurement and non-static torque measurement. Since the propeller model is rotating under water, the hydrodynamic torque on the propeller model is changing with time periodically. With the present means of torque measurement,, there is certainly a limit of how accurate one can measure the non-static torque on the propeller model. But by carefully examine the observation during the calibration test, one can choose a calibration factor that gives better accuracy of the measurement than other factors.

In the calibration test, it is observed that the static torque calibration factors are different from factors obtained otherwise. Using this static torque calibration factor in the test data processing lead to higher than 1.0 propeller efficiency, which is

not possible physically. Although the torque calibration factors used in the present experimental study may not be the best one, it can give much more realistic results than the static calibration factors. Better factors are to be obtained in the future in order to get more accurate torque measurement.

Chapter 5

Results and Discussion

5.1 Experimental Results and Discussion

5.1.1 Description of the Experimental Results

Forward tests were conducted for propeller rotational speeds (RPM) equal to 100, 150 and 200. Reverse tests were conducted for 150 RPM. Bollard pull tests were conducted over the RPM range from 100 to 200. Tests for the same RPM were repeated in order to check the repeatability of the experiments.

Torque coefficients, side force coefficients, thrust coefficients, and efficiency were plotted against advance ratio for each test and are shown in Appendix D.

5.1.2 Repeatability of the Experimental Results

Results for Tests at 100 RPM

Four tests were done at 100 RPM. The torque coefficient, side force coefficient, thrust coefficient and efficiency are plotted against advance ratio (see Figures D-1

through D-4).

For the torque coefficient, there is some scatter in the advance ratio range from 2.5 to 6.0. The biggest difference between different test data is about 20% of the averaged test data magnitude (see Figure D-1).

For the side force coefficient, the scatter of the data is more uniform for the entire advance ratio range. The magnitude of the difference between the tests is about 18% of that of the averaged data magnitude (see Figure D-2).

For the thrust coefficient, it is obvious that the first test result is far away from the rest. The scatter of the data between the 2nd, 3rd, and 4th test results are uniform in the entire advance ratio range. The magnitude of that scatter is about 20% that of the data magnitude. The first tests were done in a slightly different way and in different flow conditions from that of the other three tests. When conducting the first test, due to lack of experience, the propeller RPM was not checked and recorded constantly. The water level in the tunnel were only at the top of the diffuser. Air bubbles entrained from the top of the diffuser changed the flow conditions in the test section. The differences between the first and later tests is a result of these changes in test procedure.

As the thrust coefficient of the first test is higher than that of the other tests, it is obvious that the efficiency for the propeller from the first test is also higher than that of the other tests. The efficiencies obtained from the other three tests (range from 0.2 to 0.6) are more realistic than from the first test (range from 0.6 to 0.85) (see Figure D-4).

Results for Tests of 150 RPM

Three tests for 150 RPM were conducted and test repeatability is much better than for test results at 100 RPM (see Figures D-5 through D-8).

For the torque coefficient, the three test data almost all fall on one curve. For the side force coefficient, there is some scatter in the advance ratio range of 1.5 to 2.5. For the thrust coefficient, the magnitude of scatter in the low advance ratio range from 1.5 to 4.5 is about 18% that of the test data. The scatter magnitude in the efficiency is only about 12% that of the test data.

Results for Tests at 200 RPM

Two tests were done at 200 RPM (see Figures D-9 through D-12).

For the torque coefficient, the magnitude of scatter is about 11% that of the test data and the scatter is distributed over the entire advance ratio range. For the side force coefficient, the scatter of the data is so small that it can be neglected. For the thrust coefficient, the scatter occurs mainly in the low advance ratio range from 1.0 to 3.0. This scatter can be as high as 17% that of the test data. The scatter in the efficiency is about 13% that of the test data.

Comparison of Test Results for Different RPM

Test results for different RPM are plotted all in one plot for torque coefficient, side force coefficient, thrust coefficient and efficiency respectively so that the differ-

ence between them can be compared (see Figure D-13 through Figure D-16). More disscusion of this difference will be given later.

Results for Reverse Tests at 150 RPM

Two reverse tests were done for 150 RPM(see Figure D-17 through D-20). The test repeatability is good for torque, thrust, side force, and efficiency. The scatter is so small that it can be discounted. Another reverse test for 150 RPM was done several days later after a signal transmission failure and a computer disk failure were fixed. The results were in good agreement with that from the previous two tests.

In these reverse tests there was no sign of thrust coefficient dropping as the advance ratio increased.

Higher RPM Tests and Low Pressure Tests

During the forward tests at 200 RPM and tests at 150 RPM under low pressure, a model failure occured due to the disconnection of the wiring of the slip ring and the torque transducer. It was observed that the flow during these tests was more turbulent than that of other tests. A lot of bubbles were observed during the low pressure test.

Results for Bollard Pull Tests

Two bollard pull tests were done for the RPM range from 100 to 200. The two results agree well with each other except at 100 RPM (See Figure D-21 through D-23). The thrust coefficient changes little with RPM. The side force coefficient decreases as RPM increases. The torque coefficient increases as RPM increases. Bollard pull tests at higher RPM were not done to avoid the disconnection of the wires to the slip rings that was likely to happen at higher RPM.

5.1.3 Differences Between Test Results for Different RPM

Test results for different RPM are plotted all in one plot for torque coefficient, side force coefficient, thrust coefficient and efficiency respectively so that the difference between them can be compared (see Figure D-13 through Figure D-16). It is noticed that as RPM increases, force coefficients decrease. Veitch also observed such trends in his tests (Veitch 1990). Veitch's explanation of this phenomena is that it is due to Reynolds number effects. The tests covered a range of Reynolds number, as defined in Veitch's thesis (1990 equation 10), from 4.0×10^4 to 2.2×10^5. For all the tests, at an advance ratio of 1.0, the Reynolds number was less than 10^5. At these Reynolds numbers, the boundary layer is in either a laminar regime, or making the transition from laminar to turbulent flow. The change of the Reynolds number not only changes the lift slope of the blade section, but also changes the maximum lift coefficient.

Another explanation for this difference is because of the tunnel wall effect on the flow around the propeller. When the propeller is rotating, it is an obstacle for the free incoming flow. Without the wall, the free incoming flow would deflect and go around

the propeller. With the wall, the incoming flow has to pass the propeller without much room to adjust itself. So the resultant relative flow around the propeller would not be the same for the flow with propeller rotating under different RPM. The higher the rotation speed, the greater the wall effect on the propeller performance. The wall effect is discussed in Pankhurst and Holder's book "Wind tunnel technique" (Pankhurst and Holder 1965). The presence of the wall changes two things in flow field in test section. Firstly, since the test section has rigid boundaries the velocity component normal to the walls must be zero. The imposition of the rigid boundaries in the test section causes the flow around a body placed in the test section to differ from that around the same body placed in an unlimited stream. Secondly, since the lateral expansion of the streamlines in the region of the model will be restricted, the influence of the wall constraint implies that the model is being tested at a higher velocity than the tunnel speed. Quantitative correction methods are also given by Pankhurst and Holder (1965). However, these corrections were not made to the results presented.

5.1.4 Comparison of the Cavitation Tunnel Test Results with the Open Water Results

When comparing the tunnel test results with the open water test results by Bose and Lai (Bose and Lai 1989), it was found that the trends for torque and thrust coefficient from both tests are similar (see Figure D-24 through D-26). The torque and thrust coefficient from open water tests are lower than that from tunnel test results.

The thrust and torque coefficients are both lower for the open water tests than for the tunnel tests, so the efficiency of the both tests are close except near the advance ratio of 6.0 where the open water test result has a higher peak than that of the tunnel test result.

Bose developed a multiple stream tube theoretical model for application to cycloidal propellers (Bose 1987). With this model he studied the effect of changing propeller solidity ($\sigma = Nc/R$) on the calculated thrust coefficient, torque coefficient and efficiency for a propeller with varied solidity (from 0.3 to 1.8) and for a maximum pitch angle of 20 degrees. He found that variation in solidity causes only a small variation in efficiency at the peak of the efficiency curve. However, his theoretical results show that the thrust and torque coefficient increase more or less linearly with solidity at any given value of advance ratio (Bose 1987 Figure 9).

The above comparison of the test results in the open water ($\sigma = 1.2$) and in the cavitation tunnel ($\sigma = 1.6$) showed a similar trend to that predicted by Bose (1987).

5.1.5 Conclusion

Problems encountered in a previous set of experiments with a trochoidal propeller model were addressed here before a set of experiments on this model were done. Reliable results for a propeller RPM range from 100 to 200 were obtained. At higher RPM's, it was found that the transducer wires to the slip rings became disconnected and this stopped tests at these speeds. Replacement of these connections involved strip down of the model.

5.2 Theoretical Results and Discussion

5.2.1 Description of the Theoretical Results

There are two groups of computational models used in the present theoretical study. The first group included three computational models which are Mendenhall and Spangler's model, the modified M&S's model without considering wake and other blade effects, and the modified M&S's model using an angle of attack method to account for the wake and other blade effects. In this first group of models, the method of modelling the induced flow field was of major concern. The second group of computational models included three modified M&S's models where the blade force characteristics were calculated by using NACA-0012 section data and Gormont's dynamic stall correction method. In this group of computational models, the modelling of blade force characteristics was of major concern. In all the computational models the three-dimensional correction method was included as an option.

The thrust coefficients, torque coefficients and the efficiency are plotted against advance ratio for data from each theoretical method (see Figure E-1 though E-33). The theoretical results are compared with experimental data by Dickerson and Dobay (1969, 1970) and by Bose and Lai (1989).

In the following sections, theoretical results are compared with experimental results. In Part I, results from the two dimensional Mendenhall and Spangler's model, results from the two dimensional model using the angle of attack method and results from the two dimensional model without wake and other blade effects

are compared with experimental results by Dickerson and Dobay (1969, 1970) and by Bose and Lai (1989). In Part II, results from the three dimensional model using the angle of attack method and results from the two dimensional model using the angle of attack method are compared with experimental results by Dickerson and Dobay (1969, 1970) and by Bose and Lai (1989). In part III, results from the two dimensional Mendenhall and Spangler's model with dynamic stall correction, results from the two dimensional model the using angle of attack method and dynamic stall correction, and results from the two dimensional model with dynamic stall correction but without wake and other blade effects are compared with experimental results by Dickerson and Dobay (1969,1970) and by Bose and Lai (1989).

5.2.2 Naming of the Data Files from Theoretical Models

Naming of the data files from Mendenhall and Spangler's model and its modified models is explained in following examples.

m211a.dat is a data file containing data obtained from Mendenhall and Spangler's model. The potential flow theory and the Kutta condition was used to calculate the wake effect and blade-blade interaction.

m211b.dat is a data file containing data obtained from a modified M&S model. Wake effect and the effect of other blades are NOT included. Change of angle of attack due to wake and effects of other blades is NOT included.

m211cd.dat is a data file containing data obtained from a modified M&S model. The potential flow theory and the Kutta condition is NOT used to calculate

the wake and effects of other blade. Such effects are calculated by the change of the angle of attack caused by the induced velocity around the blade due to the presence of the wake and other blades.

d211a.dat is a data file containing data obtained from a modified M&S model. Dynamic stall effects are included. The potential flow theory and the Kutta condition is used to calculate the wake effect and blade-blade interaction.

d211b.dat is a data file containing data obtained from a modified M&S model. Dynamic stall effects are included. Wake effect and effects of other blades are NOT included. Change of angle of attack due to wake and effects of other blades are NOT included.

d211cd.dat is a data file containing data obtained from a modified M&S model. Dynamic stall effects are included. The potential flow theory and the Kutta condition is NOT used to calculate the wake and effects of other blades. Such effects are calculated by the change of the angle of attack caused by the induced velocity around the blades due to the presence of the wake and other blades.

The first integer 2 in a filename indicate that this is a data file from a two-dimensional model (3 for a three dimensional model). The second integer 1 indicates that the geometry characteristics are that of the propeller used by Bose and Lai (Bose and Lai 1989) in their tests (2 for that by Dickerson and Dobay, 3 for that by Veitch). The third integer 1 indicates the pitch ratio of the propeller (see table below).

5.2.3 Comparison of the Theoretical Results with Experimental Data - Part I

The theoretical results from the two dimensional Mendenhall and Spangler's model, results from the two dimensional model using the angle of attack method and results from the two dimensional model without wake and other blade effects are compared with experimental results by Dickerson and Dobay (1969, 1970) and by Bose and Lai (1989).

Before comparing theoretical results with experimental results, it is helpful to indicate the difference between the angle of attack method and the method used by Mendenhall and Spangler to calculate wake and effects of other blades.

Difference Between the Angle of Attack Method and M&S's Method in Calculating Wake and Effects of Other Blades

Mendenhall and Spangler used a linear potential flow theory to calculate effects of wake and other blades. First the blade was mapped into a transformed plane where the blade contour becomes a circle. The discrete vortices and other blades (represented by point vortices) were mapped into the transformed plane outside the circle. It was assumed that the flow is not separated along the surface of the blade in the physical plane. So in the transformed plane, the circle should be one of the streamlines. In order to make the circle a streamline, for every point vortex, there is a image vortex inside the circle at some point on the line connecting the origin of the circle and the point vortex outside the circle. Since a point vortex of any strength

can be added at the origin of the circle which does not violate the condition that the circle should be a streamline, the solution that can make the circle a streamline is not unique. In order to make the solution unique, another assumption is made that the trailing edge of the blade in the physical plane is a stagnation point (the Kutta condition). So for every point vortex in the transformed plane outside the circle, there is an image vortex inside the circle and a point vortex at the origin of the circle to make the circle not only a streamline, but also the trailing edge of the blade in the physical plane a stagnation point. These two assumptions are strict. In many of the flows, the blade contour is not a streamline. The flow can become separated along some portion of the blade surface. The trailing edge is not always a stagnation point.

In order to avoid these strict assumptions, an angle of attack method was used. In this method there were no assumptions about the flow condition. As in Mendenhall and Spangler's method, wake was represented by discrete vortices and other blades as point vortices. These vortices produce an induced velocity around the blade under consideration. This induced velocity changes the angle of attack calculated by the free incoming flow and the propeller rotation.

Comparison of Thrust Coefficient

For pitch ratios of 0.4π, 0.5π, 0.6π, 0.7π, 0.8π, and 0.9π, the thrust coefficients obtained from the model using the angle of attack method agree not only with the trend of Dickerson and Dobay's experimental data, but also are close to the experimental data in magnitude (see Figure E-12 through E-17).

The thrust coefficients obtained from Mendenhall and Spangler's model and the modified M&S's model without wake and other blade effects are far away from the experimental data both in trends and in magnitude (see Figure E-12 through E-17).

For pitch ratios of 1.43π, 1.667π and 2.000π, the results from the model using the angle of attack method are still in better agreement with the experimental data than that from the other two models (see Figure E-18 through E-20), but for a pitch ratio of 3.333π, the model with the angle of attack method and Mendenhall and Spangler's method gives similar results while the model without wake and other blade effects gives a higher peak value at an advance ratio of about 5 than the other two models (see Figure E-21). The angle of attack method has lost its advantage in modelling the induced flow field at high pitch ratio numbers for six-bladed cycloidal propellers.

When comparing the theoretical results with Bose and Lai's 3-bladed cycloidal propeller test data, it was found that all three models give higher predicted thrust coefficient than the experimental data (see Figure E-22). The model without wake and other blade effects gives higher peak values at an advance ratio of about 5.0. The difference between the results from Mendenhall and Spangler' model and the model using the angle of attack method is small, especially at high advance ratios above 4.5. The model using the angle of attack method gives a little larger prediction of thrust coefficient than that from Mendenhall and Spangler's model at advance ratios below 4.5. This implies that for this pitch ratio, the difference between the two methods of modelling the wake and other blade effects is not significant. That is probably because flow remains attached for these high pitch ratio, high aspect ratio propellers.

Comparison of Torque Coefficient

For pitch ratios of 0.4π, 0.5π, 0.6π, 0.7π, 0.8π, and 0.9π, the torque coefficients obtained from the model using the angle of attack method agrees more than the other two methods both in trends and in magnitude with Dickerson and Dobay's experimental data, especially for low advance ratio range (see Figure E-1 through E-6).

For pitch ratios of 1.43π, 1.67π, and 2.00π, the angle of attack method does not give better predictions in magnitude than the other two methods, but does give a better shape than the other two methods when compared with the experimental data (see Figure E-7 through E-9).

For a pitch ratio of 3.333π, the modified model without wake and other blade effects gives worse predicted results compared with the other two methods (see E-10). At this pitch ratio, the difference between the results from Mendenhall and Spangler's model and the model using the angle of attack method is very small.

When compared with the predicted torque results from Bose and Lai's 3-bladed cycloidal propeller test results (pitch ratio = 2.924π), it was also found that the modified model without wake and other blade effects gave a larger prediction of torque in the advance ratio range from 4.5 to 6, while Mendenhall and Spangler's model and the model using the angle of attack method gave better prediction at this pitch ratio range (see Figure E-11). The difference between Mendenhall and Spangler's model and the model using the angle of attack method was small. All three models predicted lower torque coefficients than the experimental data in the

low advance ratio range from 0.5 to 4.0. The model using the angle of attack method predicts higher torque coefficient than that of Mendenhall and Spangler's method.

The above comparison for a 6-bladed propeller of 3.333π pitch ratio and a 3-bladed propeller of 2.924π pitch ratio implies that the method of calculating wake and other blade effects used in Mendenhall and Spangler's method differs little from the angle of attack method when torque coefficient is considered for pitch ratios of 2.924π and 3.333π.

Comparison of Efficiency

For pitch ratios of 0.4π, 0.5π, 0.6π, 0.7π, 0.8π, and 0.9π, a higher prediction of thrust coefficient and lower prediction of torque coefficient from the model using the angle of attack method gave higher predicted efficiency when compared with the experimental data (see Figure E-23 through E-28). The other two models gave much higher efficiency than the model using the angle of attack method.

For pitch ratios of 1.429π, 1.667π, 2.000π, and 3.333π and for the 3-bladed propeller of pitch ratio 2.924π, the model using the angle of attack method still gives better predicted efficiency than the other two, but the difference between the predicted efficiency from all three models was smaller than that at lower pitch ratios (see Figure E-29 through E-33).

Conclusion

From the above comparisons, it is seen that the angle of attack method gives

better prediction of blade forces induced by the wake and other blade effects than that by the method used in Mendenhall and Spangler's model when pitch ratios are less than π. At higher pitch ratios (greater than π), the difference between the two methods is not significant. At high pitch ratios, the flow condition is more close to that of a linear potential flow which allows the Kutta condition to describe the flow condition near the blade trailing edge more accurately.

The wake and other blade effects always decrease the predicted thrust and torque coefficients no matter which method is used.

5.2.4 Comparison of the Theoretical Results with Experimental Data - Part II

Results from the three dimensional model using the angle of attack method and results from the two dimensional model using the angle of attack method are compared with experimental results by Dickerson and Dobay (1969, 1970) and by Bose and Lai (1989).

Comparison of Thrust Coefficient

For pitch ratios of 0.4π, 0.5π, 0.6π, 0.7π, 0.8π and 0.9π, the three dimensional correction made the predicted results of thrust coefficient move further away from the experimental data than the predicted results from the model without a three dimensional correction (see Figure F-12 through F-17).

For pitch ratios of 1.429π and 1.667π, the discrepancies between the predicted

results and the experimental results are of the same order for both the models with and without three dimensional correction, but the predicted results from the model with three dimensional correction are in a better agreement with trends of the experimental results (See Figures F-18 and F-19).

For pitch ratios of 2.000π, 2.924π and 3.333π, the predicted results from the model with three dimensional correction are not only in good agreement with trends, but also in magnitude with the experimental results, while the predicted results from the model without three dimensional correction are much higher than the experimental results throughout most of the advance ratio range (see Figure F-20 through F-22).

Comparison of Torque Coefficient

For pitch ratios of 0.4π and 0.5π, the three dimensional correction method made the predicted results move further away from the experimental results than the model without a three dimensional correction (see Figure F-1 1nd F-2).

For pitch ratios of 0.6π, 0.7π, 0.8π, 0.9π, 1.429π, 1.667π, 2.000π, 2.924π, and 3.333π, the results from the models with and without the three dimensional correction differ little from each other in predicting the magnitude of the experimental data, but for large pitch ratios such as 2.000π, 2.924π and 3.333π, the predicted results from the model with three dimensional correction give better trends than that without the three dimensional correction (see Figure F-3 through F-11).

Comparison of Efficiency

Since the model with the three dimensional correction gives much higher torque predictions and lower thrust predictions for pitch ratios of 0.4π, 0.5π, 0.6π, 0.7π and 0.8π, the predicted efficiencies from the model with the three dimensional correction are much lower than the experimental data (see Figure F-23 through F-27).

For pitch ratios of 0.9π, 1.429π, 1.667π, 2.000π, 2.924π and 3.333π, the model with three dimensional correction gives much better prediction of the efficiency than the model without the three dimensional correction when compared with the experimental data (see Figure F-28 through F-33).

Conclusion

From the above comparisons, it is seen that the model with the three dimensional correction gives better prediction of propeller characteristics than the model without a three dimensional correction for high pitch ratios (1.667π, 2.000π, 2.924π, 3.333π). For low pitch ratios, the model without three dimensional correction gives better prediction of the propeller characteristics. This implies that for low pitch ratios, the elliptical assumption used in the three dimensional correction method is not appropriate. For high pitch ratios, the flow is more steady (lower frequencies of oscillation), so the three dimensional correction method based on a steady elliptical lift distribution is a good approximation of the blade lift force.

5.2.5 Comparison of the Theoretical Results with Experimental Data - Part III

The predicted results analyzed in this section are from three models which use NACA-0012 sectional characteristics data and Gormont's method to include the dynamic stall effect. They differ only in the way they model the change of the flow field around a blade caused by the wake and other blades.

Comparison of Thrust Coefficient

For pitch ratios of 0.4π, 0.5π, and 0.6π, the three models did not give good prediction of the thrust coefficient either in trend or in magnitude (see Figure G-12 through G-14).

For pitch ratios of 0.7π, 0.8π, and 0.9π, the model using Mendenhall and Spangler's original method to calculate the wake and the effect of other blades and the model without calculating the wake and the effects of other blades gave better predicted thrust coefficients compared with the model using the angle of attack method (see Figure G-15 through G-17).

For pitch ratios of 1.429π, 1.667π, 2.000π, 2.924π, and 3.333π, the three models did not give good prediction of the trend of the thrust coefficient versus advance ratio (see Figure G-18 through G-22). All three models predicted too high thrust coefficients at high advance ratios.

Comparison of Torque Coefficient

For pitch ratios of 0.4π, 0.5π and 0.6π, the three models did not give good prediction either in magnitude or in trend (see Figure G-1 through G-3). The predicted values were too high compared with the experimental results especially at low advance ratios.

For pitch ratios of 0.7π, 0.8π nd 0.9π, the models with Mendenhall and Spangler's method to calculate wake and effect of other blades and the model without wake and other blade effects gave a better prediction both in trend and in magnitude compared with the results from the model using the angle of attack method and with the predicted results at other pitch ratios (see Figure G-4 through G-6).

For pitch ratios of 1.429π, 1.667π, 2.000π, 2.924π and 3.333π, the three models did not give good prediction of torque coefficients. The model results are too low in the low advance ratio range (around 1.0 to 3.0) and too high at high advance ratios compared with the experimental data from Dobay and Dickerson(1973). For the three-bladed propeller with pitch ratio of 2.924π, the predicted results are in good agreement with Bose and Lai's (1989) experimental results at advance ratios above 5.0 (see Figure G-7 through G-11).

Comparison of Efficiency

As the predictability of the thrust and torque coefficients is poor by the three models with dynamic stall correction, the predicted efficiencies are not in good

agreement with the experimental results either (see Figure G-23 through G-33).

5.2.6 Conclusion

It is seen that the three models using Gormont's dynamic stall correction method were not successful in predicting the propeller characteristics. The possible reasons for this are as follows.

(1) Gormont's method uses the steady force characteristics of a blade to predict its unsteady force characteristics when the blade is in oscillating motion in and out of the stall region. During the oscillation, vortices are generated on the blade and are carried away by the flow. So the force characteristics predicted by Gormont's method already includes the blade's own wake effects. Therefore, it is not surprising that the model with the angle of attack method gives the worst predicted results. This computational model adds an additional angle of attack by calculating the wake and the effect of other blades to the original angle of attack obtained from the rotational speed of the blade and the free incoming flow. Then this resultant angle of attack is used in Gormont's method. This way of calculating the dynamic stall effect is not consistent with the requirement by Gormont's method.

The computational model using Mendenhall and Spangler's original method with the dynamic stall correction included gave better prediction of all propeller characteristics than the other two models with dynamic stall correction. This model uses the rotation speed of the propeller and the free incoming flow to obtain the angle of attack, then uses Gormont's method to obtain the blade characteristics, and then use the Kutta condition to determine the wake and the effect of other blades. So there is less inconsistency between the original method and Gormont's method ex-

cept that the blade's own wake effects should not be calculated and included in the same way as the other blades, since it is already included in Gormont's method.

The computational model with dynamic stall correction but without wake and other blade effects gives predicted results similar to Mendenhall and Spangler's model with dynamic stall correction except that the former gives larger predicted forces as the wake and blade effect is always to reduce the forces on the blade. The computational model with dynamic stall correction but without wake and other blade effects is not inconsistent with Gormont's dynamic stall correction method, but it does not include the effect of the other blades and the wake from the other blades.

(2) Another possible reason for the poor predictability of the three dynamic stall models lies in the use of NACA-0012 section data instead of the force characteristic data for this specific type of blade. The experimental data for the NACA 16 seriers blades used in the propeller was not available.

5.2.7 Conclusion for Theoretical Study

In the above discussion, results from theoretical methods were compared with experimental results. These computational models were, the two dimensional models, one without wake and other blade effects, one with Mendenhall and Spangler's original method to calculate wake and other blade effects, and one with an angle of attack method to calculate the wake and other blade effects. Then the results from models using the angle of attack method with three dimensional corrections were discussed. Finally, the results from two dimensional computational models using

5.2.8 Notes about the Stability of the Computational Method

Instability problem was not encountered by Mendenhall and Spangler. It was not a problem when I was doing the computation. That is due to the nature of this simplified computational method. The vortices are shed from blades at each time step. They are carried away from the blades by the incomming flow at a constant speed. The strength of each vortex decays with time due to turbulent diffusion. The interractions between vortices are neglected in this method. The neglection of this interraction was justified by Mendenhall and Spangler through their computational test (Mendenhall and Spangler 1973). Their computational test results showed that the contribution of the interraction between the vortices to the propeller forces are small and can be neglected. So there is no deformation of the vortex sheet or combination of several vortices into a single vortex with a larger vortex strength. The induced velocity due to a single vortex near each blade is finite unless the distance between the vortex and the blade becomes too small. This distance is checked at every time step. If any vortex happens to be too close to a blade, the induced velocity on the blade by the vortex is set to zero. This is to say that the interraction between the blade and the vortex when they collide with each other is neglected. Also the number of wake vortices behind each blade is limited to 200. When a vortex is too far behind the blade it shed from, its induced velocities on all the blades are so small that can be neglected. This was justified by Mendenhall and Spangler's computational tests. When I was testing the programs for modified theoretical methods, I got the same conclusion as Mendenhall and Spangler got in

Gormont's dynamic stall correction method were discussed.

The unsuccessful nature of the computational models with dynamic stall corrections was mainly due to the inconsistency of using the method in conjunction with the calculation for wake and other blade effects. Improvement of the predicted results is expected if this inconsistency is removed.

The good predictability of the computational model using the angle of attack method with a three dimensional correction at high pitch ratios (greater than π) and of the two dimensional computational model with the angle of attack method at low pitch ratios (smaller than π) is very likely related to the geometrical characteristics of the blade trajectory (see Figure 2). At high pitch ratios (greater than π), the blade trajectory is of wavy shape. When the advance ratio is large, this wavy trajectory becomes flat (see Figure 2), so the blade angle of attack does not change abruptly. Linear potential flow theory is a good approximation of such a flow. Since the three dimensional method used here is also based on linear steady potential flow theory, it is not surprising that the model using the angle of attack method with a three dimensional correction gave good predicted results.

At low pitch ratios (smaller than π), the blade trajectory is quite different from that at high pitch ratios (see Figure 2). The blade angle of attack goes through abrupt changes, especially at low advance ratios. So the Kutta condition and the three dimensional correction method based on linear steady potential flow theory is not a good approximation of the flow around a blade anymore. That explains why the two dimensional computational model with the angle of attack method gives better prediction than other models when pitch ratios are smaller than π.

their computational tests that after four propeller rotation cycles, the forces on the propeller becomes stable and converge to a periodical solution.

The flow image at each time step is not given here because in this simplified computational method, the calculation of the propeller forces are not directly related to the flow field. Usually in a numerical method, the flow field is calculated first. Then the pressure field is obtained. By integrating the pressure field, the total forces on the immersed body is obtained. But in this simplified method, a quite different approach is used. This model is a combination of a theoretical model of calculating velocity induced by a single vortex and the lifting line theory of an airfoil section or experimental results of the section's dynamic characteristics. The velocity induced by the vortex sheet at each blade is calculate by the theoretical method. Then the angle of attack or the induced blade vortex is calculated. From here, the blade forces are obtained. So there is no need to calculate the flow field at every point. Also, the blade is modeled as a point vortex, the physical boundary condition is not imposed on the blade. So, the flow field obtained from this simplified method can not give a detailed and accurate description of the flow field around the blade.

Pitch ratio number	Pitch ratio
1	2.924π
2	3.333π
3	2.000π
4	1.667π
5	1.429π
6	0.9π
7	0.8π
8	0.7π
9	0.6π
10	0.5π
11	0.4π

Table 5.1: Pitch Ratios Used in the Calculation

Chapter 6

Conclusions

Theoretical and experimental studies have been done on cycloidal propellers. Conclusions from the theoretical and experimental studies are as follows.

6.1 Experimental Study of the Trochoidal Propeller

A trochoidal propeller model was tested in a cavitation tunnel in the Institute for Marine Dynamics (NRC).

Some work was done to obtain more reliable results than obtained in a previous set of tests (Veitch 1990). A mal-functioning torque transducer was replaced on the model propeller, and the zero drift problem was solved. A multi-channel strain gauge conditioner was used to replace the internal amplifier inside the Keithley 570 A/D converter in order to reduce electromagnetic interference. This strain gauge conditioner was placed near the model propeller to avoid voltage drops through the wires before the signal was amplified. A new test procedure was developed in order

to avoid the uncertainty of the zero torque reading due to the presence of the residue torque when the model propeller was at rest. The friction tests were done before and after each day's tests, and the hydrodynamic torque was obtained by subtracting the friction torque of that day from the measured total torque of the same day. The torque calibration results were analysed carefully to choose the proper calibration data to be used in the test data manipulation.

The model propeller parts were reconnected and the cavitation tunnel was repaired to avoid air and water leakage.

Tests in forward motion under atmospheric pressure were conducted for 100, 150, and 200 RPM. Reverse tests for 150 RPM under atmospheric pressure and bollard pull tests were done. The test repeatability was good in most cases and the reliability of the test results was very much improved. The torque coefficients, side force coefficients, thrust coefficients and efficiencies of all tests at the same propeller RPM were compared with each other. The maximum scatter of the test results never exceeded 20% of the test data magnitude. In most cases, the scatter was about 11-18%. This is a much better repeatability compared with more than 50% scatter in the previous experimental results (Veitch 1990). The force coefficients and efficiencies of tests at different propeller RPM's were compared with each other. It was found that all force coefficients decreased as propeller RPM increased. This trend is similar to that obtained in the previous experimental study (Veitch 1990). The Reynolds number effect and the blockage effect are believed to be responsible for the difference between results at different propeller RPM's.

The test results were also compared with Bose and Lai's open water test results on a trochoidal propeller model with a smaller solidity (Bose and Lai 1989). The

torque coefficients and the thrust coefficients from this tests are both higher that that from Bose and Lai's tests. This difference is consistent with the prediction by Bose (1987) about the effect of propeller solidity on propeller force coefficients based on a multiple stream tube theory.

6.2 Theoretical Study

Mendenhall and Spangler developed a discrete vortex theory for predicting cycloidal propeller performance. The limitations of Mendenhall and Spangler's method were analysed. Modified models were developed based on Mendenhall and Spangler's method to improve the calculation for the effects of wake and other blades, to include three dimensional correction and to include dynamic stall correction.

The results from the modified models show the following.

(1) The angle of attack method used in modelling the wake and the effects of other blades improved the prediction from Mendenhall and Spangler's method for low pitch ratio (smaller than π) propeller performance.

(2) For high pitch ratio (greater than π) propellers, the Kutta condition used in Mendenhall and Spangler's original method is still a good approximation of the flow.

(3) The three dimensional method improved the prediction from Mendenhall and Spangler's method for high pitch ratio (greater than π) propeller performance. For low pitch ratio (smaller than π) propellers, this method is not a good approximation for the three dimensional effects of the blades in the flow.

(4) The modified models with a dynamic stall correction did not give improve-

ments in predicting the propeller performance. This is thought to be due to the inconsistency of the original method and Gormont's dynamic stall correction method. Gorment's method were developed from the comparison of experimental results of blade characteristics when the blade was in steady motion and when in unsteady oscillation. So the wake effect is already included in this method. The calculation of the wake effect in the theoretical models using Gormont's dynamic stall correction method made the effect of each blade's own wake to be considered twice.

6.3 Author's contribution to the study of cycloidal propellers

6.3.1 Experimental Study

Problems in the previous experimental work have been examined carefully. Major problems that affected the reliability and repeatibility of test results in equipments, experimental set up, and test procedures have been solved and the test results are very much improved in reliability and repeatibility compared with the previous experimental work (Veitch 1990).

6.3.2 Theoretical Study

Limitations of Mendenhall and Spangler's method have been examined. Modified computational models were developed based on Mendenhall and Spangler's method. Improved agreement between the experimental results and the results from the modified computational models has been achieved.

Chapter 7

Recommendations

7.1 Experimental Study of the Trochoidal Propeller

Further work to improve the experimental study of the model propeller characteristics is suggested as follows.

(1) Make the connection point in the torque signal transmission line at the slip rings more flexible to avoid break down due to the model oscillation at high RPM and during turbulent flow conditions.

(2) A wall effect or blockage correction method should be developed to get more accurate test data.

(3) A more accurate water speed measurement method should be adopted in the low speed range (0-2.0m/s) as the mercury manometer for measuring water speed has a very low resolution when the water speed is below 2.0m/s.

(4) Reverse tests of 150 RPM should be repeated to eliminate the problem of

unrealistically high efficiency values at high advance ratios.

(5) Better accuracy of torque measurement may be obtained if a new way of torque calibration test is invented and more accurate torque calibration factors for non-static torque measurement is obtained.

7.2 Theoretical Study

More work could be done to improve the predictability of the modified models with a dynamic stall correction method.

(1) In order to eliminate the inconsistency discussed in Chapter 6, the effect of the blade's own wake should not be calculated in models with a dynamic stall correction included, since Gormont's method has already included the effect of the blade's own wake to some extent.

(2) Interractions between the vortices can be added into the computational methods to include the effect of deformation of the vortex sheets.

(3) Interraction between the wake and the blades when the blades cut through the wake vortex sheets can be included into the computational methods.

(4) Reynolds number can be changed in the present computational methods to examine its effect on the vortex diffusion and the effect on propeller forces.

(5) If the section data of the specific blade type used in experimental study can be obtained,, it can be used in the present computational methods to predict the propeller performance.

(6) Variations of angle of attack along a blade chord line can be calculated instead of only calculating the angle of attack at one point on the blade to improve

the accuracy of the blade forces calculation.

References

Adler, J.N., and Luttges, M.W. (1985). *Three dimensionality in unsteady Flow About a Wing.* AIAA-85-0132. AIAA 23rd Aerospace Sciences Meeting, Reno, Nevada., American Institute of Aeronautics, 1633 Broadway, New York, NY 10019.

Bose, N. (1987). *Rotary Foil Propellers.* Papers of the Ship Research Institute, Ministry of Transport, Tokyo. Vol.24, No.5, pp.45-67.

Bose, N., and Lai, P.S.K. (1989). *The Experimental Performance of a Rotary Foil Propeller.* Marine Technology, Vol.26, No.3, pp.192-201.

Bose, N. and Lai, P.S.K. (1989). *Experimental performance of a Trochoidal Propeller with High-Aspect-Ratio Blades.* Marine Technology, Vol.26, No.3, pp. 192-200.

Bose, N. and Lai, P.S.K, Veitch, B.J. and Li, J. (1990). *Is There a Future for the Trochoidal Propeller?* CSME Mechanical Engineering Forum.

Critzos, C.C.,Heyson, H.H. and Boswinkle, R.W. (1955). *Aerodynamic Characteristics of NACA 0012 Airfoil Section*, NACA Technical Note 3361. National Advisory Committee for Aeronautics. 21 pages.

Dickerson, M.C. and Dobay, G.F. (1975). *Experimental Performance of Some High-Pitch Cycloidal Propellers.* Report SPD-399-01. David W. Taylor Naval Ship Research and Development Center, Bethesda, Maryland 20084. 45 pages.

Dobay, G.F. and Dickerson, M.C. (1969). *Performance of Cycloidal Propellers in Cavitation Environment.* Report SPD-363-01. David W. Taylor Naval Ship Research and Development Center, Bethesda, Maryland 20084. 52 pages.

Ficken, N.L. and Dickerson, C. (1969). *Experimental Performance and Steering Characteristics of Cycloidal Propellers.* Report 2983. Hydrodynamics Laboratory Research and Development Report. Naval Ship Research and Development Center, Washington, D.C. 20007. 69 pages.

Gormont, R.E. (1973). *A Mathematical Model of Unsteady Aerodynamics and Radial Flow for Application to Helicopter Rotors.* USAAMRDL Technical Report 72-67. Eustis Directorate, U.S. Army Air Mobility Research and Development Laboratory, Fort Eustis, Virginia. 131 pages.

Gross, D.W. and Harris, F.D. (1969). *Prediction of Inflight Stalled Airloads from Oscillating Airfoil Data.* Presented at the 25th Annual national forum of the American Helicopter Society. Washington, D.C.

Haberman, W.L., and Harley E.E. (1961). *Performance of Vertical Axis (Cycloidal) Propellers Calculated by Taniguchi's Method.* DTMB Report 1564, David Taylor Model Basin, Bethesda, MD., 39 pages.

Harvald, S.A. (1983). *Resistance and Propulsion of Ships.* John Wiley and Sons, Inc., New York, 353 pages.

Jones, H.E. and Caradonna, F.X. (1988). *Full Potential Modeling of Blade-Vortex Interactions.* Vertica, Vol.12, No.1/2, pp.129-145.

Kirsten, F.K. (1928). *A New Type Propeller.* Journal of the Society of Automotive Engineers.

von Kármán, T. and Burgers, J.M. (1935). *General Aerodynamic theory-Perfect Fluids*, Aerodynamic Theory - A General Review of Progress, Volume II, Division E, edited by Durand, W.F. 363 pages.

Lai, P.S.K., and Bose, N. (1988a). *Experimental Studies of Rotary Foil Propeller - Part I.* Report NAOE Report No. 88-06, Department of Naval Architecture and Ocean Engineering, University of Glasgow, Glasgow, 34 pages.

Lai, P.S.K., and Bose, N. (1988b). *Experimental Studies of Rotary Foil Propeller - Part II.* Report NAOE Report No. 88-22, Department of Naval Architecture and Ocean Engineering, University of Glasgow, Glasgow, 49 pages.

Lewis, Edward V. (1988). *Principles of Naval Architecture. Volume II Resistance, Propulsion and Vibration.* Published by The Society of Naval Architects and Marine engineers.

van Manen, I.J. (1966). *Results of Systematic Tests with Vertical Axis Propellers.* International Shipbuilding Progress, Vol. 13, No. 148, pp. 382-398

van Manen, I.J. (1973). *Non-Conventional Propulsion Devices.* International Shipbuilding Progress, Vol. 20, No. 226, pp. 173-193.

McCrosky, W.J. (1981). *The Phenomenon of Dynamic Stall.* NACA Technical Memorandum 81264, USAAVRADCOM TR81-A-6. Aeromechanics Laboratory, AVRADCOM Research and Technology Laboratories, Ames Research

Center, Moffett Field, California.

Mendenhall, M.R. and Spangler, S.B. (1973a). *Theoretical Analysis of Cycloidal Propellers*, NEAR Report TR53, Neilsen Engineering and Research Inc. for Naval Ship Research and Development Center, Bethesda, MD., 85 pages.

Mendenhall, M.R. and Spangler, S.B. (1973b). *Theoretical Analysis of Cycloidal Propellers - Part II - Program Manual*, NEAR Report TR53, Neilsen Engineering and Research Inc. for Naval Ship Research and Development Center, Bethesda, MD., 49 pages.

Pankhurst, R.C, and Holder, D.W . (1965). *Wind Tunnel Technique — An Account of Experimental Methods in Low- and High-Speed Wind Tunnels* . Sir Isaac Pitman&Sons, LTD.

Paraschivoiu, I.Dáesy, P. and Masson, C. (1988). *Blade Tip,Finite Aspect Ratio, and Dynamic Stall Effects on the Darrieus Rotor.* J.propulsion, Vol.4, No.1, pp 73-80.

Spalart, P.R. (1985). *Simulating of Rotating Stall by the Vortex Method.* J. Propulsion, Vol.1, No.3, pp 235-241.

Strickland, J.H. and Graham, G.M. (1986). *Dynamic Stall Inception Correlation for Airfoil Undergoing Constant Pitch Rate Motions.* AIAA J. Vol.24, No.4, pp 678-680.

Taniguchi, K. (1962). *Sea Analysis of the Vertical Axis Propeller*, 4th Symposium on Naval Hydrodynamics, Office of Naval Research, Washington, p.429-446

Veitch, B.J., and Bose, N. (1989). *Cavitation Tunnel Model Propeller Tests*,EAST Report No. 89-009, Faculty of Engineering and Applied Science, Memorial University of Newfoundland, St. John's, NF., 31 pages.

Veitch, B.J. (1990). *Experimental Results and Theoretical Predictions of Trochoidal Propeller Performance*, M.Eng Thesis, Faculty of Engineering and Applied Science, Memorial University of Newfoundland, St. John's, NF.

Zhu, D.M. (1981). *A Computational Method for Cycloidal Propellers*, International Shipbuilding Progress, Vol. 28, No.321, pp. 102-111.

Appendix A

FORTRAN Programs for Theoretical Models

```
C     ------------------------------------------------------
C                    A PROGRAM FOR PREDICTING THE
C       TWO-DIMENSIONAL CYCLOIDAL PROPELLER PERFORMANCE
C              USING M&S'S MODEL AND ITS MODIFIED MODELS
C     ------------------------------------------------------
      INCLUDE 'MENDENHALL.INC'
      character*1         jobname
      character*3         j1
      character*4         j2
      character*4         job
      integer             jobnumber

      write(6,*) 'restart? yes(1),no(0)'
      read(5,*) krst    ! 0_th parameter
      if(krst.eq.0) write(6,*) 'new start'
      if(krst.eq.1) write(6,*) 'restart'

      write(6,*) '3-D(3) or 2-D(2)?'
      read(5,*)   k3       !first parameter
      write(6,*) 'k3',k3

      write(6,*) 'count for the wake and blade effects?'
      read(5,*)   kwake
      write(6,*) 'kwake',kwake

      write(6,*) 'count for induced velocity effects?'
      read(5,*)   kinduce
      write(6,*) 'kinduce',kinduce

      write(6,*) 'Reduce the drag coefficient?'
      read(5,*)   kdrag
      write(6,*) 'kdrag',kdrag

      write(6,*) 'Enter the drag reduce coefficient?'
```

```
      read(5,*)   dragcoef
      write(6,*) 'dragcoef',dragcoef
write(6,*) 'INPUT DATA---BOSE(1)'
write(6,*) 'INPUT DATA---DICKSON(2)'
write(6,*) 'INPUT DATA---VEITCH(3)'
READ(5,*) KINPUT
      write(6,*) 'kinput=',kinput
IF(KINPUT.EQ.1) WRITE(6,*) 'INPUT DATA---BOSE'
IF(KINPUT.EQ.2) WRITE(6,*) 'INPUT DATA---DICKERSON'
IF(KINPUT.EQ.3) WRITE(6,*) 'INPUT DATA---VEITCH'
      write(6,*) 'enter Pitch ratio number'
      read(5,*)   kpitch
      if(kpitch.eq.1) pitch=2.924
      if(kpitch.eq.2) pitch=3.333
      if(kpitch.eq.3) pitch=2.000
      if(kpitch.eq.4) pitch=1.667
      if(kpitch.eq.5) pitch=1.429
      if(kpitch.eq.6) pitch=0.9
      if(kpitch.eq.7) pitch=0.8
      if(kpitch.eq.8) pitch=0.7
      if(kpitch.eq.9) pitch=0.6
      if(kpitch.eq.10) pitch=0.5
      if(kpitch.eq.11) pitch=0.4
      write(6,*) 'kpitch=',kpitch
      write(6,*) 'pitch',pitch
      if(kpitch.le.9) then
        jobnumber=k3*100+kinput*10+kpitch
        write(6,*) 'jobnumer=',jobnumber
        write(j1,'(i3)') jobnumber
           job=j1
        write(6,*) 'jobnumer=',job
      end if
      if(kpitch.ge.10) then
        jobnumber=k3*1000+kinput*100+kpitch
        write(6,*) 'jobnumer=',jobnumber
        write(j2,'(i4)') jobnumber
        job=j2
        write(6,*) 'jobnumer=',job
      end if
      jobname='m'
      write(6,*) 'jobname=',jobname
      if(kwake.eq.1) then
                open(17,file=jobname//job//'a',status='new')
      end if
      if(kwake.eq.0.and.kinduce.eq.0) then
         open(17,file=jobname//job//'b',status='new')
```

```
      end if
      if(kwake.eq.0.and.kinduce.eq.1) then
          if(kdrag.eq.0) then
                open(17,file=jobname//job//'c',status='new')
 end if
          if(kdrag.eq.1) then
                open(17,file=jobname//job//'cd',status='new')
 end if
      end if

DO MI=1,50
        write(6,*) 'ENTER ADVJ'
read(5,*) advj
WRITE(6,*) 'ADVJ=',ADVJ
IF(ADVJ.LT.0.) GOTO 123
CALL CONST
CALL INPUT
CALL INITIAL
CALL START    !calculte starting vortex
          DO NI=1,4                !calculate 4 revolutions
            CALL INITIALCT
                  DO NJ=1,NCYCLE
               CALL NEWSTEP      !calculate circulation at newstep
                     CALL BFORCE     !calculate blade forces
                 IF(NI.EQ.4) CALL AFORCE     !calculate averaged force
            END DO
END DO
CALL OUTAVGJ   !output CTG,CQG,ETA---ADVJ
END DO

CLOSE(17)
CLOSE(18)
CLOSE(19)
CLOSE(22)
CLOSE(23)
CLOSE(24)
close(21)
STOP
123 END

C
C ******************
C         SUBROUTINE   CONST
C ******************
C
INCLUDE 'MENDENHALL.INC'
C
    PI=3.1415926
        TPI=2.*PI
        RAD=180./PI
        MMAX=200   ! max number of wake vorticities.
  NMAX=6     ! max number of blades
RETURN
END
C
C ******************
C         SUBROUTINE   INPUT
C ******************
C
INCLUDE 'MENDENHALL.INC'
```

```
CHARACTER*6   INPUTFILE
CHARACTER*30  directory

directory='disk$user06:[grad.jinli.data]'

IF(KINPUT.EQ.1) INPUTFILE='INPUT1'
IF(KINPUT.EQ.2) INPUTFILE='INPUT2'
IF(KINPUT.EQ.3) INPUTFILE='INPUT3'
C
open(20,file=directory//INPUTFILE,
     *                              status='old')
read(20,*) nbld
read(20,*) c
read(20,*) bbld
read(20,*) alpz
read(20,*) xzc
read(20,*) d
READ(20,*) KCOEF      !FLAG FOR CHOICE OF COEFFICIENT OF FORCES
close(20)
write(21,*) '**********'
write(21,*) 'INPUT DATA'
WRITE(21,*) '**********'
IF(KINPUT.EQ.1) WRITE(21,*) 'BOSE'
IF(KINPUT.EQ.2) WRITE(21,*) 'DICKERSON'
IF(KINPUT.EQ.3) WRITE(21,*) 'VEITCH'
write(21,*) 'advj',advj
write(21,*) 'nbld',nbld
write(21,*) 'pitch',pitch
write(21,*) 'c',c
write(21,*) 'bbld',bbld
write(21,*) 'alpz',alpz
write(21,*) 'xzc',xzc
write(21,*) 'd',d
write(21,*) 'k3',k3
write(21,*) 'kcoef',kcoef
C
C         ------parameters for the blade-----
C
AC4=C/4.0
RNBLD=NBLD
A2=AC4**2
ASPT=2.0*BBLD/C! aspect ratio.(not used except for output)
AZTST=10.0     ! (alpha)i-----induced camber limit(due to the
      ! rotation of blade about their orbit)
CLMAX=1.5       ! clmax for a zero camber airfoilCLMAX=1.5
CLMAX=2.0       ! clmax for a zero camber airfoil
C         ------parameters for the propeller-----
R=D/2.0
ALPHAP=0.0     ! flow angle
DTHP=10.       !delta(theta)-----increment of theta
THPF=1800.     !maxmum theta
THOUT=1800.    !for output
THPI=0.0       !only for restart run---theta(initial)
C         ------parameters for the fluid-------
```

```
RENL=1.074E+05 ! Reynold's number
ENU=6.30E+04   ! effective eddy viscosity (for diffusion
               ! of wake vortex)
C        ------parameters for choices-----
MBETA=0         ! 0---blade motion is cycloidal
MDRAG=1         ! mdrag=1----including drag
MWAKE=0         ! 0--- wake-wake interaction is not included
             ! 1--- all kinds of interaction is accounted
       ! 2--- no wake-wake interaction,blade-wake
       ! interaction are only accounted if they are
       ! near(MINFL).
MINFL=0         ! radius(in C)of a circle of influence
                ! centred at mid-chord(to get the influence
       ! effect of blade on wake)
RINFL=MINFL
MDWAKE=0        ! when wake vortex is more than MDWAKE disk
                ! diameters away from the propeller,they move
                       ! only with free stream
MRWAKE=0        ! radius(in C) of a circle of influence centred
                       ! at each wake vortex(to account for wake-wake
         ! interaction)

C        ---SPECIFY BLADE MOTION---
BETAMX=0.
IF(MBETA.LE.1) GOTO 4
    4   IF(MBETA.EQ.1) BETAMX=ATAN(PITCH/SQRT(1.-PITCH**2))
! comes from tan(BETA)=PITCH*sin(THETA)/(1.+PITCH*cos(THETA))
ST=BETAMX*RAD
C        ---check the the type of interaction---
IF(MWAKE.GT.0.AND.MINFL.EQ.0) MINFL=1
IF(ENU.EQ.0.0) ENU=1.0
IF(MWAKE.EQ.1.AND.MRWAKE.LE.0) MRWAKE=2
RWAKE=MRWAKE
RWAKE=(RWAKE*C)**2     !why do this?
C        ---SPECIFY CLMAX,CLMIN---
CLCAM=2.*PI*ALPZ/RAD
DUM=CLMAX
CLMAX=DUM+CLCAM
CLMIN=-DUM+CLCAM
IF(DUM.GT.0.) GOTO 6
CLMAX=10.
CLMIN=-10.
    6   CONTINUE
C ------output parameters-----
IF(AZTST.LE.90.) AZTST=SIN(AZTST/RAD)  !why?
IF(MBETA.LE.1) GOTO 3          !cycloidal blade motion
    3 RENL=RENL/ENU                 !effective Reynolds number
DRENL=RENL*PI/(4.0*R*C*ADVJ)   !see eq(27) in M&S's paper
DELTH=360.0/RNBLD  !DELTH is angle between two consecutive blades
CYCLE=360./DTHP + 0.05
NCYCLE=CYCLE
    9   CYCLE=NCYCLE  !NCYCLE is number of steps in a cycle.
NCY=0          !NCY---counting number of steps
CT=0.0
CS=0.0
CQ=0.0
```

```
CTG=0.0
CSG=0.0
CQG=0.0
DELTA=0.0    !angle of the total force
CRG=0.0
CTAVG=0.0
CSAVG=0.0
CQAVG=0.0
    5   CONTINUE
ALPZ=ALPZ/RAD
DTHP=DTHP/RAD      !change into radians
THPF=THPF/RAD + DTHP/4.0
THOUT=THOUT/RAD + DTHP/4.0
THPRT=THOUT
ALPHAR=ALPHAP/RAD
CSALPH=COS(ALPHAR)
SNALPH=SIN(ALPHAR)
DXI=ADVJ/PI*R*DTHP/2.0          !DXI=V*delta(T)/2
DXG=-ADVJ/PI*R*CSALPH*DTHP/2.0  !DXG=V*delta(T)*cos(ALPHA)/2
DYG= ADVJ/PI*R*SNALPH*DTHP/2.0  !DYG=V*delta(T)*sin(ALPHA)/2
C ------coefficient used in BFORCE and AFORCE------------------
IF(KCOEF.EQ.0) THEN   !FOR DICKSON'S COEFFICIENT
  CFFT=PI*PI/(2.*BBLD*R)
  CFFQ=PI*PI/(2.*BBLD*R)/2.
  CFFE=1./2.                    !coefficient to convert T,S,Q to
       ELSE                           !Dickson's  CT,CS,CQ
  CFFT=1.0/(2.*BBLD*R)   !COEFF FOR BOSE'CASE
  CFFQ=1.0/(2.*BBLD*R)
  CFFE=1.0
END IF
C ---------------------------------------------------------------
RETURN
END

C
C ******************
      SUBROUTINE  INITIAL
C ******************
C
INCLUDE 'MENDENHALL.INC'
C
DO 11  J=1,NMAX
IBLADE(J)=0         !number of the blade
XBD(J)=0.0          !axial force the blade
YBD(J)=0.0     !normal force of the blade
QBD(J)=0.0          !torque of the blade
XC4(J)=0.0          !POSITION OF THE BLADES
YC4(J)=0.0
UC4(J)=0.0          !total velocity approaching a blade made
VC4(J)=0.0          !up of W and induced velocities
GAMC4(J,1)=0.0      !GAMA at c/4 at last time step
GAMC4(J,2)=0.0      !GAMA at c/4 at present
DO 11 K=1,MMAX
      GAMB(J,K)=0.0       !GAMA of the wake vortex
XGAMB(J,K)=0.0      !position of the wake vortex
YGAMB(J,K)=0.0
      DXGAMB(J,K)=0.0    !displacement of the wake vortex during
```

```
DYGAMB(J,K)=0.0    !a time step
        FVTX(J,K)=1.0       !FVTX=?
   11   CONTINUE
RETURN
END
C
C       ****************
SUBROUTINE START
C      ****************
C
INCLUDE 'MENDENHALL.INC'
C
C       ***  SET UP STARTING CONDITIONS   (T=0)  ***
C
MM=1
M=1
        XCNTR=0.0               !position of centre of prropeller.
        YCNTR=0.0
        THP(1)=0.0              !theta'=0.0
DO 14 N=2,NBLD          !starting angle position of each blade
   14   THP(N)=THP(N-1)+DELTH
DO 15 N=1,NBLD
IBLADE(N)=N
THETAP=THP(N)/RAD       !change into radians from degrees
c ------calculate beta,d(beta)/dt,d2(beta)/dt2-------
CALL BLADE(THETAP,PITCH,1.0,B,DBDT,DB2DT)
PSIDT(N)=1.0-DBDT
   15   BETA(N)=B
C
CC          COMPUTE STRENTH AND LOCATION OF STARTING VORTIES
C
  DO 16 N=1,NBLD
 IBLADE(N)=N
 THP(N)=THP(N)/RAD
 XTE(N)=R*SIN(THP(N))+C*(XZC-1.0)*COS(THP(N)-BETA(N))
 YTE(N)=R*COS(THP(N))-C*(XZC-1.0)*SIN(THP(N)-BETA(N))
C         Xte=R*sin(theta')+c*(x0/c-1)*cos(theta'-beta)
C         Yte=R*cos(theta')-c*(x0/c-1)*sin(theta'-beta)
 XGAMB(N,M)=XTE(N)  !starting vortex is at the trailing edge
 YGAMB(N,M)=YTE(N)
C         ---calculation of alpha(eq.5,6,7 in the paper)---
 SNTH=SIN(THP(N))
 CSTH=COS(THP(N))
 PSI=THP(N)-BETA(N)
         SNPSI=SIN(PSI)
         CSPSI=COS(PSI)
 WX=-(ADVJ/PI*CSALPH + CSTH)
 WY=ADVJ/PI*SNALPH + SNTH
 WN=WX*SNPSI + WY*CSPSI
 WA=-WX*CSPSI + WY*SNPSI
 TA=WN/WA
 ALPHA(N)=ATAN(TA)          !local blade angle of attack
 W(N)=SQRT(WX**2+WY**2)   !local vel approaching blade

C
CC         CALCULATE BLADE ALPHA*DOT AND EFFECTIVE BLADE ALPHA
C          (definition of effective blade angle---see part2 of the
C           M&S's paper,p.14----alphae is effective blade angle at which
```

```
C     a flat-plate must be placed to have the same circulation
C     as the blade.)
C
 DWN=-WA*PSIDT(N)+CSTH*CSPSI+SNTH*SNPSI
 DWA=WN*PSIDT(N)+CSTH*SNPSI-SNTH*CSPSI
 ALPDT(N)=1./(1.+TA**2)*(WA*DWN*D*A)/(WA**2)
 GAMC4(N,2)=PI*C*(W(N)*(N) - C/R*(XZC-.5)*PSIDT(N))
     1             + PI*C*(W(N)*ALPZ + C/R/4.0*PSIDT(N))
 CL(N)=2.0*(GAMC4(N,2))/C/W(N)
 SF=1.0      !stall correct facter
 IF(CL(N).GT.CLMAX) SF=CLMAX/CL(N)
 IF(CL(N).LT.CLMIN) SF=CLMIN/CL(N)
 IF(SF.GE.1.0) GOTO 215
 GAMC4(N,2)=GAMC4(N,2)*SF
 215     CONTINUE
 ALPHAE(N)=GAMC4(N,2)/(PI*C*W(N))  !effective blade angle
 GAMB(N,M)= -GAMC4(N,2)            !starting vortex
 ALPE(N)=ALPHAE(N)*RAD                !effective blade angle in
 CL(N)=CL(N)*SF                    !degrees
 THPD(N)=THP(N)*RAD                   !theta in degrees
 ALP=ALPHA(N)*RAD
 CALL DRAG(N,ALP,DUM)
 CD(N)=DUM*dragcoef
 BETAD(N)=BETA(N)*RAD
 IBLADE(N)=N
   16    CONTINUE
IME=1        !transfer control in GOTO statement
        CTSAV(1)=CT
CSSAV(1)=CS
CQSAV(1)=CQ
RETURN
END
C

C ******************
SUBROUTINE NEWSTEP
C ******************
C
INCLUDE 'MENDENHALL.INC'
C
C devide NEWSTEP into 4 steps in order to calculate deformation
C of wake vortices due to mutual interference
C
C         ***   CALCULATE CONDITIONS AT TIME=DT/4 ***
C        CALCULATE LOCATION OF BOUND VORTICITY AT C/4
C
       DO 18 N=1,NBLD
F(N)=1.0
THP(N)=THP(N)+DTHP/4.0
THETAP=THP(N)
CALL BLADE(THETAP,PITCH,1.0,B,DBDT,DB2DT)
BETA(N)=B
XC2(N)=R*SIN(THETAP)+(XZC*C-C/2.)*COS(THETAP-B)
YC2(N)=R*COS(THETAP)-(XZC*C-C/2.)*SIN(THETAP-B)
   18   CONTINUE
   27   IF(MWAKE.EQ.0) GOTO 128  !wake moves at free stream velocity
  327   IF(MWAKE.GT.1) GOTO 319  !only blade-vortex interaction is
```

```
                                    !counted
C
C -----calculate new locations of shed vorticity------
  127 CALL INTRVV                !calculate  displacement due to
                                    !vortex-vortex interactions
  319 CALL INTRBV           !calculate new location due to
                                    !blade-vortex interactions
DO 322 N=1,NBLD
DO 322 I=1,M
XGAMB(N,I)=XGAMB(N,I) + DXGAMB(N,I) +DXG*FVTX(N,I)
YGAMB(N,I)=YGAMB(N,I) + DYGAMB(N,I) +DYG*FVTX(N,I)
  322   FVTX(N,I)=1.
  128   CONTINUE
   28   CONTINUE
C
C       ***   CALCULATE CONDITIONS AT TIME=DT/2  ***
C
MM=M    !number of vorticities already shed off blades
M=M+1
DO 22 N=1,NBLD
THP(N)=THP(N) + DTHP/4.
THETAP=THP(N)
CALL BLADE(THETAP,PITCH,1.0,B,DBDT,DB2DT)
XTE(N)=R*SIN(THETAP) + C*(XZC-1.0)*COS(THETAP-B) !blade tail
YTE(N)=R*COS(THETAP) - C*(XZC-1.0)*SIN(THETAP-B) !position
XGAMB(N,M)=XTE(N)   !assume that at t/2 the new wake vorticities
                    !have moved to the trailing edges of each
YGAMB(N,M)=YTE(N)   !blade.
   22   CONTINUE
C
C
C   ***  CALCULATE CONDITIONS AT TIME=3*DT/4  ***
C
C            COMPUTE LOCATIONS OF BOUND VORTICITY AT C/4
C
C
DO 23 N=1,NBLD
THP(N)=THP(N)+DTHP/4.
THETAP=THP(N)
CALL BLADE(THETAP,PITCH,1.0,B,DBDT,DB2DT)
BETA(N)=B
XC2(N)=R*SIN(THETAP) + (XZC*C-C/2.0)*COS(THETAP-B)
YC2(N)=R*COS(THETAP) - (XZC*C-C/2.0)*SIN(THETAP-B)
   23   CONTINUE
IME=2
IF(MWAKE) 327,29,327    !calculate new locations of shed
!voticity
C
C ---calculate locations of shed vorticity assuming no
C                                   mutual interference---
C
C ------calculate displacement of wake vorticities-----
   29   XGAM=-ADVJ/PI*R*CSALPH*DTHP !XGAM=V*delta(T)*cos(ALPHA)
        YGAM=ADVJ/PI*R*SNALPH*DTHP !YGAM=V*delta(T)*sin(ALPHA)
C -----calculate position of the already-shed wake vorticities------
DO 229 N=1,NBLD
DO 129 I=1,MM
XGAMB(N,I)=XGAMB(N,I) + XGAM
```

```
YGAMB(N,I)=YGAMB(N,I) + YGAM
  129   CONTINUE
C -----calculation of new-born wake vorticity positions-----
C -----assume they only move during last half of delta(T)---
XGAMB(N,M)=XGAMB(N,M) + XGAM/2.0
  229   YGAMB(N,M)=YGAMB(N,M) + YGAM/2.0
   24   IME=1
C

C
CC
C       ***  CALCULATE CONDITION AT TIME=DT ***
C
C            COMPUTE LOCATIONS OF BOUND VORTICITY AT C/4
C
CC
DO 25 N=1,NBLD
THP(N)=THP(N)+DTHP/4.
THETAP=THP(N)
CALL BLADE(THETAP,PITCH,1.0,B,DBDT,DB2DT)
BETA(N)=B
XC2(N)=R*SIN(THETAP) + (XZC*C-C/2.0)*COS(THETAP-B)
YC2(N)=R*COS(THETAP) - (XZC*C-C/2.0)*SIN(THETAP-B)
   25   CONTINUE
C
C -------calculate angle of attack
DO N=1,NBLD
VC4(N)=0.0
UC4(N)=0.0
END DO

IF(KINDUCE.EQ.1) THEN
CALL VELCAL         ! calculate induced velocity.
END IF

CALL ALPHACAL     !calculate alpha(n),fk(n)
CALL STEADYCL     !MENDENHALL's method of calculating steady cl(n)

C -------calculate drag coefficient(no dynamic stall correction)--------
DO N=1,NBLD
  ALPD=ALPHA1(N)*RAD
  CALL DRAG(N,ALPD,DUM)
  CD(N)=DUM*dragcoef
END DO
CC
CALL FWCAL   !calculate influence coefficient for shed
                    !voticity. use TRANSF to calculate wake positions
       !in transformed plane.
CALL FBCAL   !calculate influence coefficient for
     !bound vorticity.use TRANSF to calculate wake positions
       !in transformed plane.
CALL COEFCAL !calculate coefficient matrix Q
   53   CALL INV(Q,QA,QC,NBLD,NBLD) !solve for unknown circulation
DO  N=1,NBLD
       GAMC4(N,2)=QC(N)           ! new blade bound vortex strength
 GAMB(N,M)=GAMC4(N,2)-GAMC4(N,1)
END DO
```

```
DUM=0.0
CALL STALLCR        !accound for stall correction
CALL GAMWB          !calculate wake induced cl and other
  !blade induced cl.
! CALL CPCALC         !calculate CPU,CPL for cavitition #
CALL OUTRAN         !transform radians into degrees for
C   !output
C
RETURN
END

C
C ***************************************************
SUBROUTINE BLADE(THETAP,RRAT,OMEGA,FBETA,FDBDT,FDB2DT)
C ***************************************************
C
INCLUDE 'MENDENHALL.INC'
C
C   CALCULATION OF BLADE ANGLE(FBETA),ANGULAR VELOCITY(FDBDT),
C            AND ANGULAR ACCELERATION(FDB2DT)
C
SNTP=SIN(THETAP)
CSTP=COS(THETAP)
IF(MBETA.GT.0) GOTO 10
C
C CYCLOIDAL BLADE MOTION
C
C COMPUTE BETA(RADIANS)
C
CB=RRAT*SNTP
DB=1.0+RRAT*CSTP
FBETA=ATAN2(CB,DB)
C
C         COMPUTE DBDT
C
DEN=RRAT**2+2.*RRAT*CSTP+1.0
FDBDT=OMEGA*RRAT*(RRAT+CSTP)/DEN
C
C   COMPUTE DB2DT
C
FDB2DT=(OMEGA**2)*RRAT*(RRAT**2-1.)*SNTP/(DEN**2)
RETURN
   10   IF(MBETA.GT.1) GOTO 20
C
C    SINUSOIDAL BLADE MOTION
C
FBETA=BETAMX*SNTP
FDBDT=BETAMX*CSTP
FDB2DT=-FBETA
RETURN
C
C   TABULAR SPECIFICATION OF BLADE MOTION
C
   20   T=ATAN2(SNTP,CSTP)
IF (T.LT.0.) T=T+6.28318531
DO 21 J=1,MBETA
JJ=J
IF(T-TTHT(J)) 25,26,21
   21   CONTINUE
   25   DELTA=(TTHT(JJ)-T)/(TTHT(JJ)-TTHT(JJ-1))
FBETA=TBTA(JJ)-DELTA*(TBTA(JJ)-TBTA(JJ-1))
FDBDT=TBTD(JJ)-DELTA*(TBD2(JJ)-TBD2(JJ-1))
```

```
FDB2DT=TBD2(JJ)-DELTA*(TBD2(JJ)-TBD2(JJ-1))
RETURN
   26   FBETA=TBTA(JJ)
FDBDT=TBTD(JJ)
FDB2DT=TBD2(JJ)
RETURN
END
C
C
C

C ****************************
SUBROUTINE  DRAG(N,ALPHA,CD)
C ****************************
C
C          CALCULATE UNCAMBERED AIRFOIL DRAG COEFFICIENT
C
IF(ALPHA.GT.180.) ALP=360.-ALPHA
IF(ALPHA.LE.180.) ALP=ALPHA
ALP=ABS(ALP)
   11   IF(ALP.LE.14.0) GOTO 20
IF(ALP.GT.14.0.AND.ALP.LE.16.0) GOTO 30
IF(ALP.GT.16.0.AND.ALP.LT.30.0) GOTO 40
IF(ALP.GE.30.0.AND.ALP.LE.150.0) GOTO 50
ALP=180.-ALP
GOTO 11
   20   CD=(ALP**2)/17071.4 + 0.006
GOTO 60
   30   CD=0.08*ALP - 1.1
GOTO 60
   40   CD=(ALP**2)/1406.2
GOTO 60
   50   ALP=ALP-(90.-ALP)/5.
CD=2.08*SIN(ALP/57.29578)
   60   CONTINUE
RETURN
END
C
C
C

C ******************
subroutine outavgJ
C ******************
C
include 'mendenhall.inc'
C
! output  CTAVG,CSAVG,CQAVG-ADVJ for plotting
C
DIFT=CTG-CTLG-CTDG-CTMG
DFQ=CQG-CQLG-CQDG-CQMG
write(17,'(4E12.5)') ADVJ,CTG,CQG,ETAG
return
end

C ******************
subroutine outwake
C ******************
C
include 'mendenhall.inc'
C
! output positions of all the wake vortices
open(14,file='wake',status='new')
write(14,'(i3)') m
```

```
do i=1,m
write(14,'(4E12.5)')
     *      XGAMB(1,I),YGAMB(1,I),XGAMB(2,I),YGAMB(2,I)
end do
return
end

C
C ****************
SUBROUTINE INTRVV
C ****************
C
C (1) CONSIDER VORTEX-VORTEX INTERACTIONS (MWAKE=1)
C
INCLUDE 'MENDENHALL.INC'
  127   DO 21 N=1,NBLD
DO 21 I=1,M
XP=XGAMB(N,I)
IF(XP.LT.DWAKE) GOTO 21
YP=YGAMB(N,I)
SUMU=0.
SUMV=0.
DO 19 NG=1,NBLD
DO 19 IG=1,MM
IF(NG.EQ.N.AND.IG.EQ.I) GOTO 19   !no interaction on itself
XGAM=XGAMB(NG,IG)
YGAM=YGAMB(NG,IG)
R2=(XP-XGAM)**2 + (YP*YGAM)**2
IF (R2.GT.RWAKE) GOTO 19     !no intercation if too far apart
FX=(YP-YGAM)/R2
FY=(XP-XGAM)/R2
DIFF=1.0
IF(RENL.LE.0.0) GOTO 219
DUM=M-IG
DUM=(DUM+0.75)*DTHP
IF(IME.EQ.2) DUM=DUM-DTHP/2. !ime=2-----t=dt*3/4
DUM=-R2*DRENL/DUM
DIFF=1.-EXP(DUM)
  219   SUMU=SUMU+FX/TPI*GAMB(NG,IG)*DIFF
SUMY=SUMY+FY/TPI*GAMB(NG,IG)*DIFF
   19   CONTINUE
DXGAMB(N,I)=-SUMU*R*DTHP/2.
DYGAMB(N,I)= SUMV*R*DTHP/2.
   21   CONTINUE
RETURN
END
C

C
C ****************
SUBROUTINE INTRBV
C ****************
C
INCLUDE 'MENDENHALL.INC'
C  (2)  CONSIDER BLADE-VORTEX INTERACTIONS
C
       DO 20 N=1,NBLD
XP=XC2(N)
YP=YC2(N)
PSI=THP(N)-BETA(N)
```

```
CSPSI=COS(PSI)
SNPSI=SIN(PSI)
DO 320 NG=1,NBLD
DO 320 IG=1,M
XGAM=XGAMB(NG,IG)
YGAM=YGAMB(NG,IG)
XG=(XP-XGAM)*CSPSI + (YGAM-YP)*SNPSI
YG=(XGAM-XP)*SNPSI + (YGAM-YP)*CSPSI
RG=SQRT(XG**2 + YG**2)/C
PHI=ATAN2(YG,XG)
IF(RG.GT.RINFL) GOTO 320
XG=XG/C
YG=YG/C
CALL TRANSF(XG,YG,SR,TH)
SR=SR*C
DEL=(GAMC4(N,2)+GAMB(NG,IG))/SR-GAMB(NG,IG)/(SR-A2/SR)
DEL=DEL*R/TPI*DTHP*0.5/SR
TH=TH*DEL
IF(FVTX(NG,IG).LT.1.0) GOTO 321
ALPV=ALPHAR+BETA(N)-THP(N)
AMT=3.0*ALPV-2.0*THP(N)
XI=SR*COS(TH) + DXI*(COS(ALPV)-A2/(SR*SR)*COS(AMT))
ETA=SR*SIN(TH) + DXI*(SIN(ALPV)-A2/(SR*SR)*SIN(AMT))
SRP=SQRT(XI*XI + ETA*ETA)
IF (SRP.GT.AC4) SR=SRP
TH=ATAN2(ETA,XI)
FVTX(NG,IG)=0.0
  321   XG=(SR+A2/SR)*COS(TH)
YG=(SR+A2/SR)*SIN(TH)
XGAMB(NG,IG)=XC2(N) + XG*CSPSI + YG*SNPSI
YGAMB(NG,IG)=YC2(N) + XG*SNPSI + YG*CSPSI
  320   CONTINUE
   20   CONTINUE
RETURN
END
C

C ******************
SUBROUTINE VELCAL
C ******************
C         COMPUTE VELOCITY INDUCED AT BLADE C/4 BY SHED VORTICITY
C
INCLUDE 'MENDENHALL.INC'

DO 31 N=1,NBLD
XP=XC2(N)
YP=YC2(N)
SUMV=0.0
SUMU=0.0
PSI=THP(N)-BETA(N)
CSPSI=COS(PSI)
SNPSI=SIN(PSI)
DO 32 NG=1,NBLD
DO 32 IG=1,MM
XGAM=XGAMB(NG,IG)
YGAM=YGAMB(NG,IG)
        R2=(XP-XGAM)**2 + (YP-YGAM)**2
```

```
FX=(YP-YGAM)/R2
FY=(XP-XGAM)/R2
DIFF=1.0
FDIFF(NG,IG)=1.0
IF(RENL.LE.0.0) GOTO 232
DUM=M-IG
DUM=(DUM+0.5)*DTHP
DUM=-R2*DRENL/DUM
DIFF=1.0-EXP(DUM)
FDIFF(NG,IG)=DIFF
  232   FX=FX*DIFF
FY=FY*DIFF
FN=FY*CSPSI - FX*SNPSI
FA=FX*CSPSI + FY*SNPSI
SUMV=SUMV + FN*GAMB(NG,IG)/TPI
SUMU=SUMU + FA*GAMB(NG,IG)/TPI
   32   CONTINUE
C
C    UC4 AND VC4 ARE VELOCITIES INDUCED AT BLADE C/4 BY SHED
C                VORTICITY
C
UC4(N)=SUMU + UC4(N)
VC4(N)=SUMV + VC4(N)
   31   CONTINUE
C
DO 30 N=1,NBLD
XP=XC2(N)
YP=YC2(N)
SUMV=0.0
SUMU=0.0
PSI=THP(N)-BETA(N)
CSPSI=COS(PSI)
SNPSI=SIN(PSI)
DO 33 kN=1,NBLD
IF(kN.EQ.N) GOTO 33
XGAM=XC2(kN)
YGAM=YC2(kN)
        R2=(XP-XGAM)**2 + (YP-YGAM)**2
FX=(YP-YGAM)/R2
FY=(XP-XGAM)/R2
FN=FY*CSPSI - FX*SNPSI
FA=FX*CSPSI + FY*SNPSI
SUMV=SUMV + FN*GAMC4(kN,2)/TPI
SUMU=SUMU + FA*GAMC4(kN,2)/TPI
   33   CONTINUE
C
C
UC4(N)=SUMU + UC4(N)
VC4(N)=SUMV + VC4(N)
   30   CONTINUE
C
C    UC4 AND VC4 ARE VELOCITIES INDUCED AT BLADE C/4 BY SHED
C                VORTICITY AND BLADE BOUND VORTICITY
C
RETURN
END

C ******************
SUBROUTINE ALPHACAL
C ******************
```

```
C calculate angle of attack
C calculate leading edge and trailing edge positions
INCLUDE  'MENDENHALL.INC'
DO 30 N=1,NBLD
THP(N)=THP(N) + DTHP/4.0
THPD(N)=THP(N)*RAD
THETAP=THP(N)
CALL BLADE(THETAP,PITCH,1.0,B,DBDT,DB2DT)
BETA(N)=B
BETADT(N)=DBDT
PSIDT(N)=1.0-DBDT
PSIDT2(N)=-DB2DT
C -----calculate angle of attack due to free stream and rotation
C            of the propeller(alpha)
CSTH=COS(THP(N))
SNTH=SIN(THP(N))
PSI=THP(N)-BETA(N)
CSPSI=COS(PSI)
SNPSI=SIN(PSI)
WX=-(ADVJ/PI*CSALPH + CSTH)
WY=ADVJ/PI*SNALPH + SNTH
WN=WX*SNPSI + WY*CSPSI + VC4(N)
WA=-WX*CSPSI + WY*SNPSI + UC4(N)
WN1=WX*SNPSI + WY*CSPSI + xzc*c*psidt(n)/r + VC4(N)
TA=WN/WA
W(N)=SQRT(WA**2 + WN**2)
ALPHA(N)=ATAN(TA)
ALPH=ATAN2(WN,WA)
IF(ALPH.LT.0.0) ALPHA1(N)=ALPH+2.*3.14159265
IF(ALPH.GE.0.0) ALPHA1(N)=ALPH
C ----calculate L.E and T.E positions-----
C
RS=R*SIN(THETAP)
RC=R*COS(THETAP)
CTB=COS(THETAP-B)
STB=SIN(THETAP-B)
XLE(N)=RS+XZC*C*CTB
YLE(N)=RC-XZC*C*STB
XTE(N)=RS+(XZC*C-C)*CTB
YTE(N)=RC-(XZC*C-C)*STB
XC4(N)=RS+(XZC*C-C/4.0)*CTB
YC4(N)=RC-(XZC*C-C/4.0)*STB
XC2(N)=RS+(XZC*C-C/2.0)*CTB
YC2(N)=RC-(XZC*C-C/2.0)*STB
   30   CONTINUE
return
end
C

C ***************
SUBROUTINE FWCAL
C ***************
CC
CC    COMPUTE INFLUENCE COEFFICIENTS FOR SHED VORTICITY
C
INCLUDE 'MENDENHALL.INC'
```

```
A=C/4.
DO 33 N=1,NBLD
XP=XC2(N)
YP=YC2(N)
PSI=THP(N)-BETA(N)
CSPSI=COS(PSI)
SNPSI=SIN(PSI)
DO 34 NG=1,NBLD
DO 34 IG=1,M
XGAM=XGAMB(NG,IG)
YGAM=YGAMB(NG,IG)
XG=(XP-XGAM)*CSPSI+(YGAM-YP)*SNPSI
YG=(XGAM-XP)*SNPSI+(YGAM-YP)*CSPSI
RG=SQRT(XG**2+YG**2)/C
PHI=ATAN2(YG,XG)
XG=XG/C
YG=YG/C
SR=RG
TH=PHI
IF(RG.LT.4.0) CALL TRANSF(XG,YG,SR,TH)
RG=SR*C
CSP=COS(TH)
FW(N,NG,IG)=(2.*RG*A*CSP-2.*A*A)/(RG*RG-2.*RG*A*CSP+A*A)
!N---the blade on which the wake vortex was shed
!NG---the blade from which the wake vortex was shed
!IG---the particular wake vortex under consideration
   34   CONTINUE
   33   CONTINUE
RETURN
END

C ****************
SUBROUTINE FBCAL
C ****************
C   COMPUTE INFLUENCE COEFFICIENT FOR BOUND VORTICITY
C
INCLUDE 'MENDENHALL.INC'
A=C/4.
DO 35 N=1,NBLD
XP=XC2(N)
YP=YC2(N)
PSI=THP(N)-BETA(N)
CSPSI=COS(PSI)
SNPSI=SIN(PSI)
DO 36 NG=1,NBLD
IF(NG.EQ.N) GOTO 45
   38   XGAM=XC4(NG)
YGAM=YC4(NG)
   40   R2=(XP-XGAM)**2 + (YP-YGAM)**2
FX=(YP-YGAM)/R2
FY=(XP-XGAM)/R2
FN=FY*CSPSI-FX*SNPSI      !for the completion of calculation of
FA=FX*CSPSI+FY*SNPSI      !induced velocity at blade c/4 after
FBN(N,NG)=FN              !solve for unknown vorticity
FBA(N,NG)=FA
XG=(XP-XGAM)*CSPSI+(YGAM-YP)*SNPSI
YG=(XGAM-XP)*SNPSI+(YGAM-YP)*CSPSI
```

```
RG=SQRT(XG**2 + YG**2)/C
PHI=ATAN2(YG,XG)
XG=XG/C
YG=YG/C
CALL TRANSF(XG,YG,SR,TH)
RG=SR*C
CSP=COS(TH)
FB(N,NG)=(2.*RG*A*CSP-2.*A*A)/(RG*RG-2.*RG*A*CSP+A*A)
GOTO 36
   45   FB(N,NG)=-1.
FBN(N,NG)=0.0
FBA(N,NG)=0.0
   36   CONTINUE
   35   CONTINUE
RETURN
END


C ******************
SUBROUTINE STEADYCL
C ******************
INCLUDE 'MENDENHALL.INC'
DO N=1,NBLD
AXTST=PSIDT(N)*C/(4.*R*W(N))/AZTST  !AZTST=(ALPHA)i---put
!limit on rotation effect.(see p.10 in M&S'spaper 2)
IF(AXTST.GT.1.) PSIDT(N)=PSIDT(N)/AXTST
BETADT(N)=1.0-PSIDT(N)              !used in BFORCE
GAM1=PI*C*W(N)*ALPHA(N)             !angle of attack effect
GAM4=PI*C*C*(XZC-.5)*PSIDT(N)/R  !rotation effect(translation)
GAM2=PI*C*W(N)*ALPZ                 !camber effect.(ALPZ=(ALPHA)0.)
GAM3=-PI*C*C*PSIDT(N)/4./R            ! rotation effect(rotation)
ccl1(N)=2.*gam1/w(n)/c
ccl2(N)=2.*gam2/w(n)/c
ccl3(N)=2.*gam3/w(n)/c
ccl4(N)=2.*gam4/w(n)/c
CL1(N)=2.*(gam1+gam2+gam3+gam4)/w(n)/c
END DO
C
RETURN
END
C ******************
SUBROUTINE COEFCAL
C ******************
CC
C   CALCULATE THE COEFFICIENT MATRIX Q(N,I) AND
C    THE CORRESPONDING RIGHT HAND SIDE RHS(N)
C
INCLUDE 'MENDENHALL.INC'
DO 52 N=1,NBLD
GAMC4(N,1)=GAMC4(N,2)
   52   CONTINUE
NG=0
   50   DO 60 N=1,NBLD
GAMC4(N,2)=0.   !this is to be solved unknown
C
DO 57 I=1,NBLD
Q(N,I)=0.0
IF(N.EQ.I) Q(N,I)=1.0
```

```
   57   CONTINUE
C
if(kwake.eq.0) goto 58
C
DO 55 I=1,NBLD
Q(N,I)=FW(N,I,M)-FB(N,I)
   55   CONTINUE
C
   58 RHS(N)=CL1(N)*C*W(N)/2.    ! RHS(N)=GAM1+GAM2+GAM3+GAM4
if(kwake.eq.0) goto 59    ! don't count for the wake and other
C   ! blade's effect
DO 56 I=1,NBLD
RHS(N)=RHS(N)+GAMC4(I,1)*FW(N,I,M)  !other blade's effect
DO 56 J=1,MM
RHS(N)=RHS(N)+FW(N,I,J)*GAMB(I,J)*FDIFF(I,J)  !wake effect
   56   CONTINUE
   59 QA(N)=RHS(N)
   60   CONTINUE
C
RETURN
END
C

C ******************
SUBROUTINE STALLCR
C ******************
C       APPLY APPROXIMATE STALL CORRECTION TO BLADE LOADING
C     COMPUTE STRENTH OF LAST ELEMENTS OF SHED VORTICITY
C
INCLUDE 'MENDENHALL.INC'
DO 63 N=1,NBLD
IBLADE(N)=N
F(N)=1.     !F(N) is a scale factor
CL(N)=2.*GAMC4(N,2)/(C*W(N))
SF=1.0
IF(CL(N).GT.CLMAX) SF=CLMAX/CL(N)
IF(CL(N).LT.CLMIN) SF=CLMIN/CL(N)
IF(SF.GE.1.) GOTO 63
IBLADE(N)=IBLADE(N)+10
F(N)=SF
DUM=DUM+1.
   63   CONTINUE
DO 263 N=1,NBLD
GAMC4(N,2)=GAMC4(N,2)*F(N)      !new blade bound vortex
!strength
CL(N)=CL(N)*F(N)
ALPHAE(N)=GAMC4(N,2)/(PI*C*W(N))
  263   GAMB(N,M)=GAMC4(N,1)-GAMC4(N,2) !new shed wake vortex strength
C
RETURN
END
C
C ****************
SUBROUTINE GAMWB
C ****************
C calculate vorticity induced by wake and other blades
INCLUDE 'MENDENHALL.INC'
DO N=1,NBLD
! calculate induced voticity due to old wakes
```

```
 S2=0.
 S1=0.
 DO IG=1,NBLD
  DO JG=1,M-1
    S1=S1+GAMB(IG,JG)*FW(N,IG,JG)*FDIFF(IG,JG)     !due to wakes
  END DO
     IF(IG.EQ.N) FB(N,IG)=0.0   !no effect on it's self
     S2=S2+GAMC4(IG,2)*FB(N,IG)
 END DO
 GAMW=S1              !induced vortivity due to wakes
 GAMBB=S2         !induced vorticity due to other blades
 CLW(N)=2.*S1/W(N)/C
 CLB(N)=2.*S2/W(N)/C
END DO
IF(NI.EQ.4) THEN
END IF
         !CL---CL FROM STALLCR
        !CL1----STEADY CL BEFORE SOLVE THE LINEAR EQN.
        !CLW---CL DUE TO WAKE
        !CLB---CL DUE TO OTHER BLADES
RETURN
END

C
C *****************
SUBROUTINE CPCALC
C *****************
INCLUDE 'MENDENHALL.INC'
DO N=1,NBLD
        CZ=GAMC4(N,2)*2.0/(C*PI)
DUM=1.2*U(N)*COS(ALPHAD(N))    !WHY?
UU=DUM+3.56*CZ
UL=DUM-3.56*CZ
CPU(N)=1.-(UU/W(N))**2
CPL(N)=1.-(UL/W(N))**2
DUM=(W(N)*PI/ADVJ)**2
CPU(N)=-CPU(N)*DUM   !only calculate CPU,CP at one point for
CPL(N)=-CPL(N)*DUM   !test of cavitition.
END DO
RETURN
END
C
C ***************************
SUBROUTINE TRANSF(XQ,YQ,RB,TH)
C ***************************
integer    ndeg
parameter (ndeg=2)
real rb,th,xq,yq
complex   coeff(ndeg+1),zero(ndeg)
external  zpocc
coeff(1)=(0.0625,0.0)
coeff(2)=cmplx(-xq,-yq)
coeff(3)=(1.0,0.0)
call zpocc(ndeg,coeff,zero)
do i=1,ndeg
rr=(real(zero(i)))**2+(aimag(zero(i)))**2
rr=rr**0.5
if(rr.lt.0.25) goto 1
```

```
rx=real(zero(i))
ry=aimag(zero(i))
tn=atan2(ry,rx)
rb=rr
th=tn
    1   end do
return
end
C
C ***********************
SUBROUTINE INV(A,B,X,LDA,N)
C ***********************
C
REAL A(LDA,LDA),B(N),X(N)
IPATH=1
CALL LSLRG(N,A,LDA,B,IPATH,X)
RETURN
END
C

C
C ********************
SUBROUTINE INITIALCT
C ********************
INCLUDE 'MENDENHALL.INC'
NCY=0          !NCY---counting number of steps
CT=0.0
CS=0.0
CQ=0.0
CTG=0.0
CSG=0.0
CQG=0.0
CTLG=0.0
CQLG=0.0
CTDG=0.0
CQDG=0.0
CTMG=0.0
CQMG=0.0
CRG=0.0
CTAVG=0.0
CSAVG=0.0
CQAVG=0.0
CTLAVG=0.0
CQLAVG=0.0
CTDAVG=0.0
CQDAVG=0.0
CTMAVG=0.0
CQMAVG=0.0
RETURN
END

C *****************
SUBROUTINE BFORCE
C *****************
C
C
C    COMPUTE FORCES ON INDIVIDUAL BLADES
C
INCLUDE 'MENDENHALL.INC'
CT=0.0
CS=0.0
CQ=0.0
CTL=0.0
```

```
CQL=0.0
CTD=0.0
CQD=0.0
CTM=0.0
CQM=0.0
C
C -----3-d correction or not------
IF(K3.EQ.3) THEN
  DO N=1,NBLD
   GAMC4(N,3)=GAMC4(N,2)*PI/4.
   CD(N)=CD(N)+CL(N)**2/PI/BBLD*C
  END DO
End if
if(k3.eq.2) then
  DO N=1,NBLD
    GAMC4(N,3)=GAMC4(N,2)
  END DO
END IF
C
DO 70 N=1,NBLD
C
SNA=SIN(ALPHA1(N))
CSA=COS(ALPHA1(N))
SNTB=SIN(THP(N)-BETA(N))
CSTB=COS(THP(N)-BETA(N))
CSBTA=COS(BETA(N))
SNBTA=SIN(BETA(N))
C ----(1).calculate force due to circulation-----
C        ! lift is pependicular to the coming flow
XBC4(N)=-GAMC4(N,3)*W(N)*SNA*BBLD !along the blade chord
YBC4(N)= GAMC4(N,3)*W(N)*CSA*BBLD !perpendicular to chord
C
C -----(2).calculate force due to apparent mass effect------
C -----      (see eq.30,31,32 in M&S's paper)   -----
SUM=BETADT(N)*CSBTA+ADVJ/PI*(BETADT(N)-1.0)*(SNALPH*SNTB
     1    +CSALPH*CSTB)        !eq.(32)--------dv/dt
ZB(N)=-PI*C*C*SUM/(4.*R)-PI*(C**3)*PSIDT2(N)*(XZC-.5)/(4.*R*R)
ZB(N)=ZB(N)*BBLD   !eq.(30)-------apparent mass effect
C       -----(3).calculate force due to viscous drag----
C (along the coming flow)
IF(MDRAG.LE.0) GOTO 69
XBD(N)=.5*C*BBLD*(W(N)**2)*CD(N)*CSA   !along the blade chord
YBD(N)=.5*C*BBLD*(W(N)**2)*CD(N)*SNA   !perpendicular to chord
   69   CONTINUE
TB(N)=((YBC4(N)+YBD(N)+ZB(N))*SNTB -
     *                          (XBC4(N)+XBD(N))*CSTB)*CFFT
     !along x-dir in
                      !propeller co-ordinate
SB(N)=((YBC4(N)+YBD(N)+ZB(N))*CSTB +
     *                          (XBC4(N)+XBD(N))*SNTB)*CFFT
     !along y-dir in
     !propeller co-ordinate
QB(N)=((XBC4(N)+XBD(N))*CSBTA+
     *                         (YBC4(N)+YBD(N)+ZB(N))*SNBTA)*CFFQ
TL=(YBC4(N)*SNTB-XBC4(N)*CSTB)*CFFT
```

```
TD=(YBD(N)*SNTB-XBD(N)*CSTB)*CFFT
TM=(ZB(N)*SNTB)*CFFT
QL=(XBC4(N)*CSBTA+YBC4(N)*SNBTA)*CFFQ
QD=(XBD(N)*CSBTA+YBD(N)*SNBTA)*CFFQ
QM=ZB(N)*SNBTA*CFFQ
C ---CALCULATE FORCE ON THE PROPELLER
CT=CT+TB(N)
CS=CS+SB(N)
CQ=CQ+QB(N)
CTL=CTL+TL
CQL=CQL+QL
CTD=CTD+TD
CQD=CQD+QD
CTM=CTM+TM
CQM=CQM+QM
  70 CONTINUE
ETA=CT/CQ*ADVJ/PI*CFFE      !efficiency
RETURN
END

C *****************
SUBROUTINE AFORCE
C *****************
C
C   COMPUTE AVERAGE THRUST,SIDEFORCE,TORQUE,EFFICIENCY
C          (definition of AVERAGE---see part2 of the paper,p.15)
INCLUDE 'MENDENHALL.INC'
IF(NCYCLE.GT.91) GOTO 73 !ncycle is number of steps in a cycle.
NCY=NCY+1
CTAVG=CTAVG+CT      !CTAVG---sum of the force calculated before
CSAVG=CSAVG+CS      !in this cycly.
CQAVG=CQAVG+CQ
CTLAVG=CTLAVG+CTL
CQLAVG=CQLAVG+CQL
CTDAVG=CTDAVG+CTD
CQDAVG=CQDAVG+CQD
CTMAVG=CTMAVG+CTM
CQMAVG=CQMAVG+CQM
C
  IF(NCY.LT.NCYCLE) GOTO 73
CTG=CTAVG/CYCLE     !calculate average force coefficient after
CSG=CSAVG/CYCLE     !complete a cycle(ncy=ncycle).
CQG=CQAVG/CYCLE
ETAG=CTG/CQG*ADVJ/PI*CFFE
CTLG=CTLAVG/CYCLE
CQLG=CQLAVG/CYCLE
CTDG=CTDAVG/CYCLE
CQDG=CQDAVG/CYCLE
CTMG=CTMAVG/CYCLE
CQMG=CQMAVG/CYCLE
DIFT=CTG-CTLG-CTDG-CTMG
DIFQ=CQG-CQLG-CQDG-CQMG
CRG=SQRT(CTG**2+CSG**2)  !average resultant force coefficient
   73   CONTINUE
RETURN
END
C
```

```
C     ------------------------------------------------------
CCCCC  DYNAMIC STALL EFFECT IS INCLUDED IN M&S'S MODEL
CCCCC        USING GOMONT'S METHOD TO PREDICT A
CCCCC     CYCLOIDAL PROPELLER PERFORMANCE
C     ------------------------------------------------------
INCLUDE 'MENDENHALL.INC'
C
character*1        jobname
character*3        j1
character*4        j2
character*4        job
integer            jobnumber
     write(6,*) 'restart? yes(1),no(0)'
     read(5,*) krst
     if(krst.eq.1) write(6,*) 'restart'
     if(krst.eq.0) write(6,*) 'new start'
C
     write(6,*) '3-D(3) or 2-D(2)?'
     read(5,*)   k3
     write(6,*) 'k3',k3
     write(6,*) 'include wake effect? no(0),yes(1)'
         read(5,*) kwake
     write(6,*) 'include induced velocity  effect? no(0),yes(1)'
         read(5,*) kinduce
write(6,*) 'INPUT DATA---BOSE(1)'
write(6,*) 'INPUT DATA---DICKSON(2)'
write(6,*) 'INPUT DATA---MENDENHALL(3)'
READ(5,*) KINPUT
     write(6,*) 'kinput=',kinput
IF(KINPUT.EQ.1) WRITE(6,*) 'INPUT DATA---BOSE'
IF(KINPUT.EQ.2) WRITE(6,*) 'INPUT DATA---DICKERSON'
IF(KINPUT.EQ.3) WRITE(6,*) 'INPUT DATA---MENDENHALL'
C
     write(6,*) 'enter Pitch ratio number'
     read(5,*)   kpitch
     if(kpitch.eq.1) pitch=2.924
     if(kpitch.eq.2) pitch=3.333
     if(kpitch.eq.3) pitch=2.000
     if(kpitch.eq.4) pitch=1.667
     if(kpitch.eq.5) pitch=1.429
     if(kpitch.eq.6) pitch=0.9
     if(kpitch.eq.7) pitch=0.8
     if(kpitch.eq.8) pitch=0.7
     if(kpitch.eq.9) pitch=0.6
     if(kpitch.eq.10) pitch=0.5
     if(kpitch.eq.11) pitch=0.4
     write(6,*) 'kpitch=',kpitch
     write(6,*) 'pitch',pitch
```

```
C
   if(kpitch.le.9) then
     jobnumber=k3*100+kinput*10+kpitch
     write(6,*) 'jobnumer=',jobnumber
     write(j1,'(i3)') jobnumber
     job=j1
     write(6,*) 'jobnumer=',job
    end if
  if(kpitch.ge.10) then
     jobnumber=k3*1000+kinput*100+kpitch
     write(6,*) 'jobnumer=',jobnumber
     write(j2,'(i4)') jobnumber
     job=j2
     write(6,*) 'jobnumer=',job
    end if
  jobname='d'
     write(6,*) 'jobname=',jobname

     if(kwake.eq.1) then
             open(17,file=jobname//job//'a',status='new')
     end if
C
     if(kwake.eq.0.and.kinduce.eq.0) then
     open(17,file=jobname//job//'b',status='new')
     end if
C
     if(kwake.eq.0.and.kinduce.eq.1) then
     open(17,file=jobname//job//'c',status='new')
     end if
C
DO MI=1,50
write(6,*) 'ENTER ADVJ'
read(5,*) advj
WRITE(6,*) 'ADVJ=',ADVJ
IF(ADVJ.LT.0.) GOTO 123
CALL CONST
CALL INPUT
CALL INITIAL
CALL START    !calculte starting vortex
CALL OUTDATA  !output data of t=0
         DO NI=1,4                !calculate 4 revolutions
           CALL INITIALCT
         DO NJ=1,NCYCLE
              CALL NEWSTEP      !calculate circulation at newstep
                        CALL BFORCE     !calculate blade forces
                   IF(NI.EQ.4) CALL AFORCE     !calculate averaged force
           END DO
END DO
CALL OUTAVGJ   !output CTG,CQG,ETA---ADVJ
END DO
C
CLOSE(17)
STOP
```

```
C
AC4=C/4.0
RNBLD=NBLD
A2=AC4**2
ASPT=2.0*BBLD/C! aspect ratio.(not used except for output)
AZTST=10.0     ! (alpha)i-----induced camber limit(due to the
      ! rotation of blade about their orbit)
CLMAX=1.5       ! clmax for a zero camber airfoil
C        ------parameters for the propeller-----
R=D/2.0
C       ADVJ=2.0       !advance ratio. if PITCH>1.,then ADVJ>1.
                  ! if PITCH<1.,then ADVJ<1.
ALPHAP=0.0     ! flow angle
DTHP=10.       !delta(theta)-----increment of theta
THPF=1800.     !maxmum theta
THOUT=1800.    !for output
THPI=0.0       !only for restart run---theta(initial)
C         ------parameters for the fluid-------
RENL=1.074E+05 ! Reynold's number
ENU=6.30E+04  ! effective eddy viscosity (for diffusion
              ! of wake vortex)
C        ------parameters for choices-----
MBETA=0        ! 0---blade motion is cycloidal
              ! 1---blade motion is sinusoidal
         ! 2---tabular input blade motion
MDRAG=1        ! mdrag=1----including drag
MWAKE=0        ! 0--- wake-wake interaction is not included
          ! 1--- all kinds of interaction is accounted
       ! 2--- no wake-wake interaction,blade-wake
       ! interaction are only accounted if they are
       ! near(MINFL).
MINFL=0        ! radius(in C)of a circle of influence
               ! centred at mid-chord(to get the influence
       ! effect of blade on wake)
RINFL=MINFL
MDWAKE=0       ! when wake vortex is more than MDWAKE disk
               ! diameters away from the propeller,they move
                     ! only with free stream
MRWAKE=0       ! radius(in C) of a circle of influence centred
                     ! at each wake vortex(to account for wake-wake
         ! interaction)


C       ---SPECIFY BLADE MOTION---
BETAMX=0.
IF(MBETA.LE.1) GOTO 4
    4   IF(MBETA.EQ.1) BETAMX=ATAN(PITCH/SQRT(1.-PITCH**2))
! comes from tan(BETA)=PITCH*sin(THETA)/(1.+PITCH*cos(THETA))
ST=BETAMX*RAD
C       ---check the the type of interaction---
IF(MWAKE.GT.0.AND.MINFL.EQ.0) MINFL=1
IF(ENU.EQ.0.0) ENU=1.0
IF(MWAKE.EQ.1.AND.MRWAKE.LE.0) MRWAKE=2
RWAKE=MRWAKE
RWAKE=(RWAKE*C)**2
C       ---SPECIFY CLMAX,CLMIN---
```

```
123 END
C
C ******************
      SUBROUTINE   CONST
C ******************
C
INCLUDE 'MENDENHALL.INC'
C
    PI=3.1415926
      TPI=2.*PI
      RAD=180./PI
      MMAX=200    ! max number of wake vorticities.
  NMAX=6      ! max number of blades
RETURN
END


C
C ******************
      SUBROUTINE   INPUT
C ******************
C
INCLUDE 'MENDENHALL.INC'
CHARACTER*6   INPUTFILE
CHARACTER*30  directory

directory='disk$user06:[grad.jinli.data]'

IF(KINPUT.EQ.1) INPUTFILE='INPUT1'
IF(KINPUT.EQ.2) INPUTFILE='INPUT2'
IF(KINPUT.EQ.3) INPUTFILE='INPUT3'
C
open(20,file=directory//INPUTFILE,
     *                                    status='old')
read(20,*) nbld
read(20,*) c
read(20,*) bbld
read(20,*) alpz
read(20,*) xzc
read(20,*) d
READ(20,*) KCOEF      !FLAG FOR CHOICE OF COEFFICIENT OF FORCES
close(20)
write(21,*) '**********'
WRITE(21,*) 'INPUT DATA'
write(21,*) '**********'
if(KINPUT.eq.1) write(21,*) 'INPUT DATA___BOSE'
if(KINPUT.eq.2) write(21,*) 'INPUT DATA___Dickerson'
if(KINPUT.eq.3) write(21,*) 'INPUT DATA___VEITCH'
write(21,*) 'advj',advj
write(21,*) 'nbld',nbld
write(21,*) 'pitch',pitch
write(21,*) 'c',c
write(21,*) 'bbld',bbld
write(21,*) 'alpz',alpz
write(21,*) 'xzc',xzc
write(21,*) 'd',d
write(21,*) 'k3',k3
write(21,*) 'kcoef',kcoef
```

```
CLCAM=2.*PI*ALPZ/RAD
DUM=CLMAX
CLMAX=DUM+CLCAM
CLMIN=-DUM+CLCAM
IF(DUM.GT.0.) GOTO 6
CLMAX=10.
CLMIN=-10.
    6   CONTINUE
C ------output parameters-----
IF(AZTST.LE.90.) AZTST=SIN(AZTST/RAD)
IF(MBETA.LE.1) GOTO 3           !cycloidal blade motion
    3 RENL=RENL/ENU                 !effective Reynolds number
DRENL=RENL*PI/(4.0*R*C*ADVJ)    !see eq(27) in the paper
DELTH=360.0/RNBLD  !DELTH is angle between two consecutive blades
CYCLE=360./DTHP + 0.05
NCYCLE=CYCLE
    9   CYCLE=NCYCLE  !NCYCLE is number of steps in a cycle.
NCY=0          !NCY---counting number of steps
CT=0.0
CS=0.0
CQ=0.0
CTG=0.0
CSG=0.0
CQG=0.0
DELTA=0.0    !angle of the total force
CRG=0.0
CTAVG=0.0
CSAVG=0.0
CQAVG=0.0
    5   CONTINUE
ALPZ=ALPZ/RAD
DTHP=DTHP/RAD      !chage into radians
THPF=THPF/RAD + DTHP/4.0
THOUT=THOUT/RAD + DTHP/4.0
THPRT=THOUT
ALPHAR=ALPHAP/RAD
CSALPH=COS(ALPHAR)
SNALPH=SIN(ALPHAR)
DXI=ADVJ/PI*R*DTHP/2.0          !DXI=V*delta(T)/2
DXG=-ADVJ/PI*R*CSALPH*DTHP/2.0  !DXG=V*delta(T)*cos(ALPHA)/2
DYG= ADVJ/PI*R*SNALPH*DTHP/2.0  !DYG=V*delta(T)*sin(ALPHA)/2
C ------coefficient used in BFORCE and AFORCE------------------
IF(KCOEF.EQ.0) THEN   !FOR DICKSON'S COEFFICIENT
  CFFT=PI*PI/(2.*BBLD*R)
  CFFQ=PI*PI/(2.*BBLD*R)/2.   !coefficient to convert T,S,Q to
  CFFE=1./2.                !coefficient to convert T,S,Q to
       ELSE                       !Dickson's  CT,CS,CQ
  CFFT=1.0/(2.*BBLD*R)    !COEFF FOR BOSE'CASE
  CFFQ=1.0/(2.*BBLD*R)    !coefficient to convert T,S,Q to
  CFFE=1.0                !coefficient to convert T,S,Q to
END IF
C
C ------------------------------------------------------------
RETURN
END
C


C
```

```
C ******************
      SUBROUTINE  INITIAL
C *. ****************
C
INCLUDE 'MENDENHALL.INC'
C
DO 11  J=1,NMAX
IBLADE(J)=0          !number of the blade
XBD(J)=0.0           !axial force the blade
YBD(J)=0.0     !normal force of the blade
QBD(J)=0.0           !torque of the blade
UC4(J)=0.0           !total velocity approaching a blade made
VC4(J)=0.0           !up of W and induced velocities
GAMC4(J,1)=0.0       !GAMA at c/4 at last time step
GAMC4(J,2)=0.0       !GAMA at c/4 at present
DO 11 K=1,MMAX
        GAMB(J,K)=0.0       !GAMA of the wake vortex
XGAMB(J,K)=0.0       !position of the wake vortex
YGAMB(J,K)=0.0
        DXGAMB(J,K)=0.0     !displacement of the wake vortex during
DYGAMB(J,K)=0.0     !a time step
        FVTX(J,K)=1.0       !FVTX=?
   11   CONTINUE
RETURN
END


C
C       ****************
SUBROUTINE START
C     ****************
C
INCLUDE 'MENDENHALL.INC'

C       ***  SET UP STARTING CONDITIONS   (T=0)  ***
C
MM=1
M=1
        XCNTR=0.0               !position of centre of prropeller.
        YCNTR=0.0
        THP(1)=0.0              !theta'=0.0
DO 14 N=2,NBLD          !starting angle position of each blade
   14   THP(N)=THP(N-1)+DELTH
DO 15 N=1,NBLD
IBLADE(N)=N
THETAP=THP(N)/RAD       !change into radians from degrees
c ------calculate beta,d(beta)/dt,d2(beta)/dt2-------
CALL BLADE(THETAP,PITCH,1.0,B,DBDT,DB2DT)
PSIDT(N)=1.0-DBDT
   15   BETA(N)=B
C
C          COMPUTE STRENTH AND LOCATION OF STARTING VORTIES
C
  DO 16 N=1,NBLD
 IBLADE(N)=N
 THP(N)=THP(N)/RAD
 XTE(N)=R*SIN(THP(N))+C*(XZC-1.0)*COS(THP(N)-BETA(N))
 YTE(N)=R*COS(THP(N))-C*(XZC-1.0)*SIN(THP(N)-BETA(N))
```

```
C        Xte=R*sin(theta')+c*(x0/c-1)*cos(theta'-beta)
C        Yte=R*cos(theta')-c*(x0/c-1)*sin(theta'-beta)
 XGAMB(N,M)=XTE(N)  !starting vortex is at the trailing edge
 YGAMB(N,M)=YTE(N)
C        ---calculation of alpha(eq.5,6,7 in the paper)---
 SNTH=SIN(THP(N))
 CSTH=COS(THP(N))
 PSI=THP(N)-BETA(N)
         SNPSI=SIN(PSI)
         CSPSI=COS(PSI)
 WX=-(ADVJ/PI*CSALPH + CSTH)
 WY=ADVJ/PI*SNALPH + SNTH
 WN=WX*SNPSI + WY*CSPSI
 WA=-WX*CSPSI + WY*SNPSI
 TA=WN/WA
 ALPHA(N)=ATAN2(WN,WA)        !local blade angle of attack
 W(N)=SQRT(WX**2+WY**2)   !local vel approaching blade
C
C         CALCULATE BLADE ALPHA*DOT AND EFFECTIVE BLADE ALPHA
C         (definition of effective blade angle---see part2 of M&S's
C          paper,p.14----alphae is effective blade angle at which
C    a flat-plate must be placed to have the same circulation
C    as the blade.)
C
 DWN=-WA*PSIDT(N)+CSTH*CSPSI+SNTH*SNPSI
 DWA=WN*PSIDT(N)+CSTH*SNPSI-SNTH*CSPSI
 ALPDT(N)=1./(1.+TA**2)*(WA*DWN*D*A)/(WA**2)   !seems no use
 GAMC4(N,2)=PI*C*(W(N)*(N) - C/R*(XZC-.5)*PSIDT(N))
     1            + PI*C*(W(N)*ALPZ + C/R/4.0*PSIDT(N))
C        The above eq should be compared with eq(20) in M&S's paper.
 CL(N)=2.0*(GAMC4(N,2))/C/W(N)
 SF=1.0     !stall correct facter
 IF(CL(N).GT.CLMAX) SF=CLMAX/CL(N)
 IF(CL(N).LT.CLMIN) SF=CLMIN/CL(N)
 IF(SF.GE.1.0) GOTO 215
 GAMC4(N,2)=GAMC4(N,2)*SF
 215     CONTINUE
 ALPHAE(N)=GAMC4(N,2)/(PI*C*W(N))  !effective blade angle
 GAMB(N,M)= -GAMC4(N,2)            !starting vortex
 ALPE(N)=ALPHAE(N)*RAD                !effective blade angle in
 CL(N)=CL(N)*SF                    !degrees
 THPD(N)=THP(N)*RAD                   !theta in degrees
 ALP=ALPHA(N)*RAD
 CALL DRAG(N,ALP,DUM) !dum is output
 CD(N)=DUM
 BETAD(N)=BETA(N)*RAD
 IBLADE(N)=N
  16     CONTINUE
IME=1        !transfer control in GOTO statement
        CTSAV(1)=CT    !no use
CSSAV(1)=CS
CQSAV(1)=CQ
RETURN
END
```

```
C
C  ******************
      SUBROUTINE NEWSTEP
C  ******************
C
      INCLUDE 'MENDENHALL.INC'
C
C devide NEWSTEP into 4 steps in order to calculate deformation
C of wake vortices due to mutual interference
CC
C         ***   CALCULATE CONDITIONS AT TIME=DT/4 ***
C        CALCULATE LOCATION OF BOUND VORTICITY AT C/4
C
        DO 18 N=1,NBLD
      F(N)=1.0
      THP(N)=THP(N)+DTHP/4.0
      IF(MWAKE.EQ.0) GOTO 18    !wake moves at free stream velocity
      THETAP=THP(N)
      CALL BLADE(THETAP,PITCH,1.0,B,DBDT,DB2DT)
      BETA(N)=B
      XC2(N)=R*SIN(THETAP)+(XZC*C-C/2.)*COS(THETAP-B)
      YC2(N)=R*COS(THETAP)-(XZC*C-C/2.)*SIN(THETAP-B)
   18   CONTINUE
   27   IF(MWAKE.EQ.0) GOTO 128  !wake moves at free stream velocity
  327   IF(MWAKE.GT.1) GOTO 319  !only blade-vortex interaction is
                                 !counted
C
C -----calculate new locations of shed vorticity------
  127 CALL INTRVV                !calculate  displacement due to
                                 !vortex-vortex interactions
  319 CALL INTRBV          !calculate new location due to
                                 !blade-vortex interactions
      DO 322 N=1,NBLD
      DO 322 I=1,M
      XGAMB(N,I)=XGAMB(N,I) + DXGAMB(N,I) +DXG*FVTX(N,I)
      YGAMB(N,I)=YGAMB(N,I) + DYGAMB(N,I) +DYG*FVTX(N,I)
  322   FVTX(N,I)=1.
  128   GOTO (28,24),IME
   28   CONTINUE
C
C        ***   CALCULATE CONDITIONS AT TIME=DT/2  ***
C
      MM=M    !number of vorticities already shed off blades
      M=M+1
      DO 22 N=1,NBLD
      THP(N)=THP(N) + DTHP/4.
      THETAP=THP(N)
      CALL BLADE(THETAP,PITCH,1.0,B,DBDT,DB2DT)
      XTE(N)=R*SIN(THETAP) + C*(XZC-1.0)*COS(THETAP-B) !blade tail
      YTE(N)=R*COS(THETAP) - C*(XZC-1.0)*SIN(THETAP-B) !position
      XGAMB(N,M)=XTE(N)   !assume that at t/2 the new wake vorticities
                          !have moved to the trailing edges of each
      YGAMB(N,M)=YTE(N)   !blade.
   22   CONTINUE
C
```

```
C
C    ***  CALCULATE CONDITIONS AT TIME=3*DT/4  ***
C
C             COMPUTE LOCATIONS OF BOUND VORTICITY AT C/4
C
C
DO 23 N=1,NBLD
THP(N)=THP(N)+DTHP/4.
IF(MWAKE.EQ.0) GOTO 23  !wake moves with free stream velocity
THETAP=THP(N)
CALL BLADE(THETAP,PITCH,1.0,B,DBDT,DB2DT)
BETA(N)=B
XC2(N)=R*SIN(THETAP) + (XZC*C-C/2.0)*COS(THETAP-B)
YC2(N)=R*COS(THETAP) - (XZC*C-C/2.0)*SIN(THETAP-B)
   23   CONTINUE
IME=2
IF(MWAKE) 327,29,327    !calculate new locations of shed
!voticity
C
C ---calculate locations of shed vorticity assuming no
C                                    mutual interference---
C
C ------calculate displacement of wake vorticities-----
   29   XGAM=-ADVJ/PI*R*CSALPH*DTHP !XGAM=V*delta(T)*cos(ALPHA)
        YGAM=ADVJ/PI*R*SNALPH*DTHP !YGAM=V*delta(T)*sin(ALPHA)
C -----calculate position of the already-shed wake vorticities------
DO 229 N=1,NBLD
DO 129 I=1,MM
XGAMB(N,I)=XGAMB(N,I) + XGAM
YGAMB(N,I)=YGAMB(N,I) + YGAM
  129   CONTINUE
C -----calculation of new-born wake vorticity positions-----
C -----assume they only move during last half of delta(T)---
XGAMB(N,M)=XGAMB(N,M) + XGAM/2.0
  229   YGAMB(N,M)=YGAMB(N,M) + YGAM/2.0
   24   IME=1
C
C
C       ***  CALCULATE CONDITION AT TIME=DT ***
C
C -------calculate angle of attack and reduced frequency
DO N=1,NBLD
VC4(N)=0.0
UC4(N)=0.0
END DO

IF(KINDUCE.EQ.1) THEN
CALL VELCAL    ! calculate induced velocity
END IF

CALL ALPHACAL    !calculate alpha(n),fk(n)
CALL ALPHAREF    !calculate alpha(ref)---for dynamic stall
 !correction
DO N=1,NBLD
  CALL LIFT(ALPREF(N),CL0)      !alpref in degrees
  CLREF=CL0
  CLL=CLREF*(ALPHAN(N)*RAD)/(ALPREF(N)-0.0)
```

```
  CL1(N)=CLL
C -------calculate drag coefficient(with dynamic stall correction)--------
  IF(KCD.EQ.1)  ALPD=ALPREF(N) !REMEMBER:ALPREF IS IN DEGREE!
  IF(KCD.EQ.0)  ALPD=ALPHA(N)*RAD
  CALL DRAG(N,ALPD,DUM)
  CD(N)=DUM
END DO
C
   78 CALL FWCAL    !calculate influence coefficient for shed
                     !voticity. use TRANSF to calculate wake positions
       !in transformed plane.
CALL FBCAL   !calculate influence coefficient for
     !bound vorticity.use TRANSF to calculate wake positions
       !in transformed plane.
CALL COEFCAL !calculate coefficient matrix Q
   53   CALL INV(Q,QA,QC,NBLD,NBLD) !solve for unknown circulation
DO  N=1,NBLD
        GAMC4(N,2)=QC(N)            ! new blade bound vortex strength
 GAMB(N,M)=GAMC4(N,2)-GAMC4(N,1)
END DO
DUM=0.0
CALL STALLCR      !accound for stall correction
  !blade induced cl.
C
RETURN
END
C


C
C
C ****************************************************
SUBROUTINE BLADE(THETAP,RRAT,OMEGA,FBETA,FDBDT,FDB2DT)
C ****************************************************
C
INCLUDE 'MENDENHALL.INC'
C
C   CALCULATION OF BLADE ANGLE(FBETA),ANGULAR VELOCITY(FDBDT),
C             AND ANGULAR ACCELERATION(FDB2DT)
C
PI=3.14159265
SNTP=SIN(THETAP)
CSTP=COS(THETAP)
IF(MBETA.GT.0) GOTO 10
C
CC CYCLOIDAL BLADE MOTION
C
C COMPUTE BETA(RADIANS)
C
CB=RRAT*SNTP
DB=1.0+RRAT*CSTP
FBETA=ATAN2(CB,DB)
IF(FBETA.LT.0..and.rrat.lt.1.) FBETA=FBETA+2.*PI
C
CC        COMPUTE DBDT
C
DEN=RRAT**2+2.*RRAT*CSTP+1.0
FDBDT=OMEGA*RRAT*(RRAT+CSTP)/DEN
C
C   COMPUTE DB2DT
```

```
C
FDB2DT=(OMEGA**2)*RRAT*(RRAT**2-1.)*SNTP/(DEN**2)
RETURN
   10   IF(MBETA.GT.1) GOTO 20
C
C     SINUSOIDAL BLADE MOTION
C
FBETA=BETAMX*SNTP
FDBDT=BETAMX*CSTP
FDB2DT=-FBETA
RETURN
C
C    TABULAR SPECIFICATION OF BLADE MOTION
C
   20   T=ATAN2(SNTP,CSTP)
IF (T.LT.0.) T=T+6.28318531
DO 21 J=1,MBETA
JJ=J
IF(T-TTHT(J)) 25,26,21
   21   CONTINUE
   25   DELTA=(TTHT(JJ)-T)/(TTHT(JJ)-TTHT(JJ-1))
FBETA=TBTA(JJ)-DELTA*(TBTA(JJ)-TBTA(JJ-1))
FDBDT=TBTD(JJ)-DELTA*(TBD2(JJ)-TBD2(JJ-1))
FDB2DT=TBD2(JJ)-DELTA*(TBD2(JJ)-TBD2(JJ-1))
RETURN
   26   FBETA=TBTA(JJ)
FDBDT=TBTD(JJ)
FDB2DT=TBD2(JJ)
RETURN
END
C


C
C ************************
SUBROUTINE LIFT(ALPHA,CL)
C ************************
C calculate cl for NACA0012 airfoil
IF(ALPHA.GT.180.AND.ALPHA.LE.360.) THEN
BETA=360-ALPHA
CALL NACA0012(BETA,CLA)
CL=-CLA
END IF
IF(ALPHA.LE.180..AND.ALPHA.GT.0.0) THEN
CALL NACA0012(ALPHA,CLA)
CL=CLA
END IF
IF(ALPHA.LT.0.0.AND.ALPHA.GT.-180.) THEN
BETA=-ALPHA
CALL NACA0012(BETA,CLA)
CL=-CLA
END IF
IF(ALPHA.LT.-180..AND.ALPHA.GT.-360.) THEN
BETA=ALPHA+360.
CALL NACA0012(BETA,CLA)
CL=CLA
END IF
C
RETURN
END
C
C ****************************
```

```
SUBROUTINE NACA0012(ALPHA,CL)
C ****************************
C approximate formular for cl data of naca0012
IF(ALPHA.LE.13.) THEN
CL=1.35/13.*ALPHA
END IF
IF(ALPHA.GT.13..AND.ALPHA.LE.20.) THEN
CL=0.7+(1.35-0.7)/(13.-20.)*(ALPHA-20.)
END IF
IF(ALPHA.GT.20..AND.ALPHA.LE.70.) THEN
CL=0.7+0.4*(1.-(ALPHA-45.)**2/(25*25))
END IF
IF(ALPHA.GT.70..AND.ALPHA.LE.115.) THEN
CL=1.4/45.*(115.-ALPHA)-0.7
END IF
IF(ALPHA.GT.115..AND.ALPHA.LE.160.) THEN
CL=-0.7-0.4*(1.-(ALPHA-137.5)**2/(22.5*22.5))
END IF
IF(ALPHA.GT.160..AND.ALPHA.LE.173.) THEN
CL=-0.8+(0.8-0.7)/(160.-173.)*(ALPHA-173.)
END IF
IF(ALPHA.GT.173..AND.ALPHA.LE.180.) THEN
CL=-0.8/(173.-180.)*(ALPHA-180.)
END IF
C
RETURN
END


C
C ****************************
SUBROUTINE  DRAG(N,ALPHA,CD)
C ****************************
C
C         CALCULATE UNCAMBERED AIRFOIL DRAG COEFFICIENT
C
ALPHA1=ABS(ALPHA)
    1 IF(ALPHA1.GT.360.) GOTO 2
GOTO 5
    2 ALPHA1=ALPHA1-360.
GOTO 1
    5 IF(ALPHA1.GT.180.) ALP=360.-ALPHA1
IF(ALPHA1.LE.180.) ALP=ALPHA1
! ALP=ABS(ALP)
   11   IF(ALP.LE.14.0) GOTO 20
IF(ALP.GT.14.0.AND.ALP.LE.16.0) GOTO 30
IF(ALP.GT.16.0.AND.ALP.LT.30.0) GOTO 40
IF(ALP.GE.30.0.AND.ALP.LE.150.0) GOTO 50
ALP=180.-ALP
GOTO 11
   20   CD=(ALP**2)/17071.4 + 0.006
GOTO 60
   30   CD=0.08*ALP - 1.1
GOTO 60
   40   CD=(ALP**2)/1406.25
GOTO 60
   50   ALP=ALP-(90.-ALP)/5.
CD=2.08*SIN(ALP/57.29578)
   60   CONTINUE
RETURN
```

```
      END
C
C
C ******************
      SUBROUTINE VELCAL
C ******************
C          COMPUTE VELOCITY INDUCED AT BLADE C/4 BY SHED VORTICITY
C
      INCLUDE 'MENDENHALL.INC'
C
      DO 31 N=1,NBLD
      XP=XC4(N)
      YP=YC4(N)
      SUMV=0.0
      SUMU=0.0
      PSI=THP(N)-BETA(N)
      CSPSI=COS(PSI)
      SNPSI=SIN(PSI)
      DO 32 NG=1,NBLD
      DO 32 IG=1,M
      XGAM=XGAMB(NG,IG)
      YGAM=YGAMB(NG,IG)
            R2=(XP-XGAM)**2 + (YP-YGAM)**2
      FX=(YP-YGAM)/R2
      FY=(XP-XGAM)/R2
      DIFF=1.0
      FDIFF(NG,IG)=1.0
      IF(RENL.LE.0.0) GOTO 232
      DUM=M-IG
      DUM=(DUM+0.5)*DTHP
      DUM=-R2*DRENL/DUM
      DIFF=1.0-EXP(DUM)
      FDIFF(NG,IG)=DIFF
        232   FX=FX*DIFF
      FY=FY*DIFF
      FN=FY*CSPSI - FX*SNPSI
      FA=FX*CSPSI + FY*SNPSI
      IF(IG.EQ.M) GOTO 132
      SUMV=SUMV + FN*GAMB(NG,IG)/TPI
      SUMU=SUMU + FA*GAMB(NG,IG)/TPI
      GOTO 32
        132   UC4(N)=FA*GAMB(NG,M)/TPI
      VC4(N)=FN*GAMB(NG,M)/TPI
       32   CONTINUE          !vorticity.
C
C     UC4 AND VC4 ARE VELOCITIES INDUCED AT BLADE C/4 BY SHED
C                 VORTICITY AND BLADE INDUCED VELOCITY
C
      UC4(N)=SUMU + UC4(N)
      VC4(N)=SUMV + VC4(N)
       31   CONTINUE
      RETURN
      END


C
C ******************
      SUBROUTINE DIFFUSE
C ******************
C CALCULATE DIFFUSION COEFFICIENT FDIFF(N,M)
```

```
INCLUDE 'MENDENHALL.INC'
C
DO 32 NG=1,NBLD
DO 32 IG=1,M
DIFF=1.0
FDIFF(NG,IG)=1.0
IF(RENL.LE.0.0) GOTO 32
DUM=M-IG
DUM=(DUM+0.5)*DTHP
DUM=-R2*DRENL/DUM
DIFF=1.0-EXP(DUM)
FDIFF(NG,IG)=DIFF
  32    CONTINUE
RETURN
END
C
C ********************
SUBROUTINE ALPHACAL
C ********************
C calculate angle of attack and reduced frequency
C calculate leading edge and trailing edge positions
INCLUDE  'MENDENHALL.INC'
DO 30 N=1,NBLD
THP(N)=THP(N) + DTHP/4.0
THPD(N)=THP(N)*RAD
THETAP=THP(N)
CALL BLADE(THETAP,PITCH,1.0,B,DBDT,DB2DT)
BETA(N)=B
BETADT(N)=DBDT
PSIDT(N)=1.0-DBDT
PSIDT2(N)=-DB2DT
C -----calculate angle of attack due to free stream and rotation
C            of the propeller(alpha)
CSTH=COS(THP(N))
SNTH=SIN(THP(N))
PSI=THP(N)-BETA(N)
CSPSI=COS(PSI)
SNPSI=SIN(PSI)
WX=-(ADVJ/PI*CSALPH + CSTH)
WY=ADVJ/PI*SNALPH + SNTH
WN=WX*SNPSI + WY*CSPSI + VC4(N)
WA=-WX*CSPSI + WY*SNPSI + UC4(N)
WN1=WX*SNPSI + WY*CSPSI + xzc*c*psidt(n)/r
TA=WN/WA
W(N)=SQRT(WA**2 + WN**2)
AL=ATAN2(WN,WA)  !atan can give angle only in (-90,90)
   !atan2 can give angle in (-180,180)
if(pitch.gt.1) then
IF(AL.LT.0.0.AND.ADVJ.LT.PI) AL=AL+2.*PI
end if
ALPHA(N)=AL
ta1=wn1/wa
al=atan2(wn1,wa)      ! nose angle of attack(including
                                ! pithing effect of blade at nose)
if(pitch.gt.1) then
IF(AL.LT.0.00000001.AND.ADVJ.LT.PI) AL=AL+2.*PI
```

```
end if
ALPHAN(N)=AL
C
    DWN=-WA*PSIDT(N)+CSTH*CSPSI+SNTH*SNPSI
DWA=WN*PSIDT(N)+CSTH*SNPSI-SNTH*CSPSI
ALPDT(N)=1./(1.+TA**2)*(WA*DWN-WN*DWA)/(WA**2)
C
PSIDS(N)=(1.+PITCH*CSTH)/(1.+2.*PITCH*CSTH+PITCH**2)
DWN=-WA*PSIDS(N)+CSTH*CSPSI+SNTH*SNPSI
DWA=WN*PSIDS(N)+CSTH*SNPSI-SNTH*CSPSI
ALPDS(N)=1./(1.+TA**2)*(WA*DWN-WN*DWA)/(WA**2)
ALPDS2=ALPDS(N)                ! d(alpha)/d(theta)
FK(N)=ALPDS2*C/(W(N)*R*2.)     ! [d(alpht)/dt]*c/(2.*W)
       ! reduced frequency
C ----calculate L.E and T.E positions-----
C
RS=R*SIN(THETAP)
RC=R*COS(THETAP)
CTB=COS(THETAP-B)
STB=SIN(THETAP-B)
XLE(N)=RS+XZC*C*CTB
YLE(N)=RC-XZC*C*STB
XTE(N)=RS+(XZC*C-C)*CTB
YTE(N)=RC-(XZC*C-C)*STB
XC4(N)=RS+(XZC*C-C/4.0)*CTB
YC4(N)=RC-(XZC*C-C/4.0)*STB
XC2(N)=RS+(XZC*C-C/2.0)*CTB
YC2(N)=RC-(XZC*C-C/2.0)*STB
   30   CONTINUE
C
return
end


C
C ****************
SUBROUTINE FWCAL
C ****************
CCC
CC    COMPUTE INFLUENCE COEFFICIENTS FOR SHED VORTICITY
C
INCLUDE 'MENDENHALL.INC'
A=C/4.
DO 33 N=1,NBLD
XP=XC2(N)
YP=YC2(N)
PSI=THP(N)-BETA(N)
CSPSI=COS(PSI)
SNPSI=SIN(PSI)
DO 34 NG=1,NBLD
DO 34 IG=1,M
XGAM=XGAMB(NG,IG)
YGAM=YGAMB(NG,IG)
XG=(XP-XGAM)*CSPSI+(YGAM-YP)*SNPSI
YG=(XGAM-XP)*SNPSI+(YGAM-YP)*CSPSI
RG=SQRT(XG**2+YG**2)/C
PHI=ATAN2(YG,XG)
```

```
XG=XG/C
YG=YG/C
SR=RG
TH=PHI
IF(RG.LT.4.0) CALL TRANSF(XG,YG,SR,TH)
RG=SR*C
CSP=COS(TH)
fww=(2.*RG*A*CSP-2.*A*A)/(RG*RG-2.*RG*A*CSP+A*A)
     1  FW(N,NG,IG)=fww
!N---the blade on which the wake vortex was shed
!NG---the blade from which the wake vortex was shed
!IG---the particular wake vortex under consideration
   34   CONTINUE
   33   CONTINUE
RETURN
END
C
C ****************
SUBROUTINE FBCAL
C ****************
C    COMPUTE INFLUENCE COEFFICIENT FOR BOUND VORTICITY
C
INCLUDE 'MENDENHALL.INC'
A=C/4.
DO 35 N=1,NBLD
XP=XC2(N)
YP=YC2(N)
PSI=THP(N)-BETA(N)
CSPSI=COS(PSI)
SNPSI=SIN(PSI)
DO 36 NG=1,NBLD
IF(NG.EQ.N) GOTO 45  !no effect on itself
   38   XGAM=XC4(NG)
YGAM=YC4(NG)
   40   R2=(XP-XGAM)**2 + (YP-YGAM)**2
FX=(YP-YGAM)/R2
FY=(XP-XGAM)/R2
FN=FY*CSPSI-FX*SNPSI     !for the completion of calculation of
FA=FX*CSPSI+FY*SNPSI     !induced velocity at blade c/4 after
FBN(N,NG)=FN             !solve for unknown vorticity
FBA(N,NG)=FA
XG=(XP-XGAM)*CSPSI+(YGAM-YP)*SNPSI
YG=(XGAM-XP)*SNPSI+(YGAM-YP)*CSPSI
RG=SQRT(XG**2 + YG**2)/C
PHI=ATAN2(YG,XG)
XG=XG/C
YG=YG/C
CALL TRANSF(XG,YG,SR,TH)
RG=SR*C
CSP=COS(TH)
FB(N,NG)=(2.*RG*A*CSP-2.*A*A)/(RG*RG-2.*RG*A*CSP+A*A)
GOTO 36
   45   FB(N,NG)=-1.    !no effect on itself
FBN(N,NG)=0.0
FBA(N,NG)=0.0
   36   CONTINUE
   35   CONTINUE
RETURN
```

```
END


C
C ******************
SUBROUTINE COEFCAL
C ******************
C
C    CALCULATE THE COEFFICIENT MATRIX Q(N,I) AND
C     THE CORRESPONDING RIGHT HAND SIDE RHS(N)
C
INCLUDE 'MENDENHALL.INC'
DO 52 N=1,NBLD
GAMC4(N,1)=GAMC4(N,2)
   52   CONTINUE
NG=0

   50   DO 60 N=1,NBLD
GAMC4(N,2)=0.   !this is to be solved unknown

do 57 I=1,nbld
Q(N,I)=0.0
   57 if(N.eq.I) Q(N,I)=1.

if(kwake.eq.0) goto 58

DO 55 I=1,NBLD
Q(N,I)=FW(N,I,M)-FB(N,I)
   55   CONTINUE

   58 RHS(N)=CL1(N)*C*W(N)/2.   ! for dynamic stall case
if(kwake.eq.0) goto 59

DO 56 I=1,NBLD
RHS(N)=RHS(N)+GAMC4(I,1)*FW(N,I,M)    ! other blade effect
DO 56 J=1,MM
RHS(N)=RHS(N)+FW(N,I,J)*GAMB(I,J)*FDIFF(I,J)   !wake effect
   56   CONTINUE
   59 QA(N)=RHS(N)
   60   CONTINUE
C
RETURN
END
C
C ****************
SUBROUTINE GAMWB
C ****************
C calculate vorticity induced by wake and other blades
INCLUDE 'MENDENHALL.INC'
DO N=1,NBLD
! calculate induced voticity due to old wakes
 S2=0.
 S1=0.0
 DO IG=1,NBLD
  DO JG=1,M
    S1=S1+GAMB(IG,JG)*FW(N,IG,JG)*FDIFF(IG,JG)      !due to wakes
  END DO
     IF(IG.EQ.N) FB(N,IG)=0.0   !no effect on it's self
     S2=S2+GAMC4(IG,2)*FB(N,IG)
 GAMW=S1              !induced vortivity due to wakes
 GAMBB=S2        !induced vorticity due to other blades
```

```
 clww=2.*S1/W(N)/C
 CLW(N)=clww
 CLB(N)=2.*S2/W(N)/C
 END DO
END DO
!CL---DYNAMIC STALL CORRECT LIFT WITH WAKE EFFECT AND OTHER
!BLADE EFFECT
!CL1----DYNAMIC STALL CORRECT LIFT WITHOUT OTHER EFFECT
!CLW---CL DUE TO WAKE
!CLB---CL DUE TO OTHER BLADES
C
RETURN
END


C
C ******************
SUBROUTINE STALLCR
C ******************
C        APPLY APPROXIMATE STALL CORRECTION TO BLADE LOADING
C     COMPUTE STRENTH OF LAST ELEMENTS OF SHED VORTICITY
C
INCLUDE 'MENDENHALL.INC'
DO 63 N=1,NBLD
IBLADE(N)=N
F(N)=1.     !F(N) is a scale factor
CL(N)=2.*GAMC4(N,2)/(C*W(N))
SF=1.0
C ----- no such limit here---------
! IF(CL(N).GT.CLMAX) SF=CLMAX/CL(N)
! IF(CL(N).LT.CLMIN) SF=CLMIN/CL(N)
! IF(SF.GE.1.) GOTO 63
C --------------------------------
IBLADE(N)=IBLADE(N)+10
F(N)=SF
DUM=DUM+1.
   63   CONTINUE
DO 263 N=1,NBLD
GAMC4(N,2)=GAMC4(N,2)*F(N)      !new blade bound vortex
!strength
CL(N)=CL(N)*F(N)
ALPHAE(N)=GAMC4(N,2)/(PI*C*W(N))
        GAMBB=GAMC4(N,1)-GAMC4(N,2) !new shed wake vortex strength
  263   GAMB(N,M)=GAMBB             !new shed wake vortex strength
C
RETURN
END
C
C ***************************
SUBROUTINE TRANSF(XQ,YQ,RB,TH)
C ***************************
integer    ndeg
parameter (ndeg=2)
real rb,th,xq,yq
complex   coeff(ndeg+1),zero(ndeg)
external  zpocc
coeff(1)=(0.0625,0.0)
coeff(2)=cmplx(-xq,-yq)
coeff(3)=(1.0,0.0)
```

```
call zpocc(ndeg,coeff,zero)
do i=1,ndeg
rr=(real(zero(i)))**2+(aimag(zero(i)))**2
rr=rr**0.5
if(rr.lt.0.25) goto 1
rx=real(zero(i))
ry=aimag(zero(i))
tn=atan2(ry,rx)
rb=rr
th=tn
    1   end do
return
end


C
C ***********************
SUBROUTINE INV(A,B,X,LDA,N)
C ***********************
C
REAL A(LDA,LDA),B(N),X(N)
IPATH=1
CALL LSLRG(N,A,LDA,B,IPATH,X)
RETURN
END
C
C ********************
SUBROUTINE ALPHAREF
C ********************
C for dynamic stall correction
INCLUDE 'MENDENHALL.INC'
!     FK----reduced frequency
ALPO=0.     !alpha(cl=0.)
TOC=0.12      !for naca0012 foil (t/c)
QD=0.06+1.5*(0.06-TOC)
GA2=1.4-6.*(0.06-TOC)
GA1=0.5*GA2
C
DO N=1,NBLD
  QQ=FK(N)*RAD    ![d(alpht)/dt]*c/(2.*W)
  IF(QQ.GE.0.) SING=1.
  IF(QQ.LT.0.) SING=-1.
  QQ=SQRT(ABS(QQ))
  IF(QQ.GT.QD) THEN
  DTALP=GA1*QD+GA2*(QQ-QD)*SING
  ELSE
  DTALP=GA1*QQ*SING
  END IF
  ALPREF(N)=ALPHAN(N)*RAD-DTALP
END DO
C
RETURN
END
C
C ********************
SUBROUTINE INITIALCT
C ********************
INCLUDE 'MENDENHALL.INC'
NCY=0          !NCY---counting number of steps
```

```
CT=0.0
CS=0.0
CQ=0.0
CTG=0.0
CSG=0.0
CQG=0.0
CTLG=0.0
CQLG=0.0
CTDG=0.0
CQDG=0.0
CTMG=0.0
CQMG=0.0
CRG=0.0
CTAVG=0.0
CSAVG=0.0
CQAVG=0.0
CTLAVG=0.0
CQLAVG=0.0
CTDAVG=0.0
CQDAVG=0.0
CTMAVG=0.0
CQMAVG=0.0
RETURN
END


C
C ******************
subroutine outavgJ
C ******************
C
include 'mendenhall.inc'
C
! output  CTAVG,CSAVG,CQAVG-ADVJ for plotting
C
write(17,'(5e12.5)') ADVJ,CTG,CQG,ETAG
return
end
C
C ******************
SUBROUTINE BFORCE
C ******************
C
C     COMPUTE FORCES ON INDIVIDUAL BLADES
C
INCLUDE 'MENDENHALL.INC'
CT=0.0
CS=0.0
CQ=0.0
CTL=0.0
CQL=0.0
CTD=0.0
CQD=0.0
CTM=0.0
CQM=0.0
C
C -----3-d correction or not------
IF(K3.EQ.3) THEN
  DO N=1,NBLD
   GAMC4(N,3)=GAMC4(N,2)*PI/4.
   CD(N)=CD(N)+CL(N)**2/PI/BBLD*C
  END DO
ELSE
  DO N=1,NBLD
```

```
    GAMC4(N,3)=GAMC4(N,2)
  END DO
END IF
C
DO 70 N=1,NBLD
C
SNA=SIN(ALPHAN(N))
CSA=COS(ALPHAN(N))
SNTB=SIN(THP(N)-BETA(N))
CSTB=COS(THP(N)-BETA(N))
CSBTA=COS(BETA(N))
SNBTA=SIN(BETA(N))
C ----(1).calculate force due to circulation-----
C        ! lift is pependicular to the coming flow
IF(ALPHAN(N).LT.PI/2.) THEN
XBC4(N)=- GAMC4(N,3)*W(N)*SNA*BBLD !along the blade chord
YBC4(N)=GAMC4(N,3)*W(N)*CSA*BBLD !perpendicular to chord
END IF
IF(ALPHAN(N).GE.PI/2.AND.ALPHAN(N).LT.PI) THEN
XBC4(N)=- GAMC4(N,3)*W(N)*SNA*BBLD !along the blade chord
YBC4(N)=-GAMC4(N,3)*W(N)*CSA*BBLD !perpendicular to chord
END IF
IF(ALPHAN(N).GE.PI.AND.ALPHAN(N).LT.3.*PI/2.) THEN
XBC4(N)= GAMC4(N,3)*W(N)*SNA*BBLD !along the blade chord
YBC4(N)=-GAMC4(N,3)*W(N)*CSA*BBLD !perpendicular to chord
END IF
IF(ALPHAN(N).LT.2.*PI.AND.ALPHA(N).GT.3.*PI/2.) THEN
XBC4(N)=- GAMC4(N,3)*W(N)*SNA*BBLD !along the blade chord
YBC4(N)=GAMC4(N,3)*W(N)*CSA*BBLD !perpendicular to chord
END IF
C
C -----(2).calculate force due to apparent mass effect------
C -----      (see eq.30,31,32 in paper)   -----
SUM=BETADT(N)*CSBTA+ADVJ/PI*(BETADT(N)-1.0)*(SNALPH*SNTB
     1    +CSALPH*CSTB)        !eq.(32)--------dv/dt
ZB(N)=-PI*C*C*SUM/(4.*R)-PI*(C**3)*PSIDT2(N)*(XZC-.5)/(4.*R*R)
ZB(N)=ZB(N)*BBLD   !eq.(30)-------apparent mass effect
C       -----(3).calculate force due to viscous drag----
C (along the coming flow)
IF(MDRAG.LE.0) GOTO 69
XBD(N)=.5*C*BBLD*(W(N)**2)*CD(N)*CSA    !along the blade chord
YBD(N)=.5*C*BBLD*(W(N)**2)*CD(N)*SNA    !perpendicular to chord
   69   CONTINUE
TB(N)=((YBC4(N)+YBD(N)+ZB(N))*SNTB -
     *                          (XBC4(N)+XBD(N))*CSTB)*CFFT
     !along x-dir in
                        !propeller co-ordinate
SB(N)=((YBC4(N)+YBD(N)+ZB(N))*CSTB +
     *                          (XBC4(N)+XBD(N))*SNTB)*CFFT
     !along y-dir in
     !propeller co-ordinate
QB(N)=((XBC4(N)+XBD(N))*CSBTA+
     *                  (YBC4(N)+YBD(N)+ZB(N))*SNBTA)*CFFQ
TL=(YBC4(N)*SNTB-XBC4(N)*CSTB)*CFFT
```

```
TD=(YBD(N)*SNTB-XBD(N)*CSTB)*CFFT
TM=(ZB(N)*SNTB)*CFFT
QL=(XBC4(N)*CSBTA+YBC4(N)*SNBTA)*CFFQ
QD=(XBD(N)*CSBTA+YBD(N)*SNBTA)*CFFQ
QM=ZB(N)*SNBTA*CFFQ
C ---CALCULATE FORCE ON THE PROPELLER
CT=CT+TB(N)
CS=CS+SB(N)
CQ=CQ+QB(N)
CTL=CTL+TL
CQL=CQL+QL
CTD=CTD+TD
CQD=CQD+QD
CTM=CTM+TM
CQM=CQM+QM
  70 CONTINUE
ETA=CT/CQ*ADVJ/PI*CFFE       !efficiency
RETURN
END


C
C *****************
SUBROUTINE AFORCE
C *****************
C
C    COMPUTE AVERAGE THRUST,SIDEFORCE,TORQUE,EFFICIENCY
C           (definition of AVERAGE---see part2 of the paper,p.15)
INCLUDE 'MENDENHALL.INC'
IF(NCYCLE.GT.91) GOTO 73 !ncycle is number of steps in a cycle.
NCY=NCY+1
CTAVG=CTAVG+CT      !CTAVG---sum of the force calculated before
CSAVG=CSAVG+CS      !in this cycly.
CQAVG=CQAVG+CQ
CTLAVG=CTLAVG+CTL
CQLAVG=CQLAVG+CQL
CTDAVG=CTDAVG+CTD
CQDAVG=CQDAVG+CQD
CTMAVG=CTMAVG+CTM
CQMAVG=CQMAVG+CQM
C
  IF(NCY.LT.NCYCLE) GOTO 73
CTG=CTAVG/CYCLE     !calculate average force coefficient after
CSG=CSAVG/CYCLE     !complete a cycle(ncy=ncycle).
CQG=CQAVG/CYCLE
ETAG=CTG/CQG*ADVJ/PI*CFFE
CTLG=CTLAVG/CYCLE
CQLG=CQLAVG/CYCLE
CTDG=CTDAVG/CYCLE
CQDG=CQDAVG/CYCLE
CTMG=CTMAVG/CYCLE
CQMG=CQMAVG/CYCLE
DIFT=CTG-CTLG-CTDG-CTMG
DIFQ=CQG-CQLG-CQDG-CQMG
C
CRG=SQRT(CTG**2+CSG**2)  !average resultant force coefficient
   73   CONTINUE
RETURN
```

END

Appendix B

Note About the FORTRAN Programs

B.1 Program Organization

The original Mendenhall and Spangler's program(Mendenhall and Spangler 1973) was sectioned and changed into a group of subroutines with each one performing a specific function. To modify Mendenhall and Spangler's model it was necessary to modify some of those subroutines or to add some new ones.

In the main programs, there are several choices to make before starting the calculation which decide what models to use. After making these choices, there are several call statements which access the required subroutines to perform the calculations.

There are two programs given in Appendix A.

The first program in Appendix A performs the calculation for Mendenhall and Spangler's model, the modified M&S's model without wake and other blade effects, and the modified M&S's model with wake and other blade effects accounted for by the angle of attack method.

The second program in Appendix A performs the calculation for the three modified M&S's models with the dynamic stall effect included. The first one uses the Kutta condition to calculate the wake and effects of other blade. The second one does not account for the wake and effects of other blade. The third one calculates the wake and effects of other blade using the angle of attack method. The above three models use NACA-0012 sectional characteristics and Gormont's method to account for the dynamic stall effect.

Appendix C

Use of A/D Converter and SOFT500

C.1 Programs Used in Data Aquisition

Programs used in the data aquisition were written in BASIC. SOFT500 subroutines were used in those programs. It was necessary to write these programs to activate the micro computer based data acquisition system at the cavitation tunnel. The SOFT 500 subroutines were provided with the Keithley 570 A/D system.

C.1.1 Program I

This program was used in each test to record torque, side force and thrust data.

```
10 cls
11   CALL INIT
12       open "data1.dat" for output as #1
22    cls
30  VA1=0:va2=0:va3=0:stat%=0
40  call IONAME'("thru",6,0,12,1)
50  call ioname'("side",6,1,12,1)
60  call ioname'("torq",6,2,12,1)
70 'enter parameters
120 sn!=1024
122 cls
130  locate 10,1:print"press any key to start data aquisition"
131  R$=INKEY$:IF R$="" THEN 130
135   cls
140 call ANIN'("array%",sn!    ,"thru side torq",1,"done")
160 rem
170 call INTON'(20,"MIL")
180     call status'("done",stat%)
210 call grlabel'("thrust",1,3,"top","left")
212 call grlabel'("sforce",2,3,"top","left")
```

```
214 call grlabel'("torque",3,3,"top","left")
215   screen 2
220 call hgraphrt'("done","1 2 3","fast","0.000","4095.",
"-1",-1.,3,"grid")
240     if stat%<>0 then 180
280 call intoff
290   call arsave'("array%","arr.dat")
378   mean!=0:mean1!=0:mean2!=0:stdev!=0:stdev1!=0:stdev2!=0
379  call meandev'("array%",1,mean!,stdev!,1.,sn!,-1)
380  call meandev'("array%",2,mean1!,stdev1!,1.,sn!,-1)
381  call meandev'("array%",3,mean2!,stdev2!,1.,sn!,-1)
382  REM  OPEN "DATA.DAT" FOR OUTPUT AS #1
390  for t=1 to SN!
391  call argetval'("array%",t,1,va1,-1)
392  call argetval'("array%",t,2,va2,-1)
393  call argetval'("array%",t,3,va3,-1)
430  print #1,va1,va2,va3
460  next
470  call ardel'("array%")
480  locate 20,5:print"mean thrust = ";mean!
490  locate 10,5:print"mean sideforce=";mean1!
500  locate  3,5:print"mean torque = "; mean2!
510  locate 22,5:print"std =";   stdev!
520  locate 12,5:print"std = ";  stdev1!
530  locate  5,5:print"std = ";  stdev2!
550  rem
560  R$=INKEY$:if R$="" then 550
570  cls
593  CLOSE #1
600  screen 0
610  end
```

C.1.2 Program II

This program was used to monitor the propeller loads on the screen in order to check if the model transducers and the aquisition system was working properly.

```
10 cls
11   rem
15   name1$="thrust": name2$="side": name3$="torque"
20  ave=0:va1=0:va2=0:va3=0:STAT%=0:speed=0:wspeed=0:total=0:
count=0:n=0:std=0:hleft=0:hright=0:propn=0:d=0:advj=0
30      call INIT
40  call IONAME'("thru",6,0,12,1)
50  call ioname'("side",6,1,12,1)
60  call ioname'("torq",6,2,12,1)
120 sn!=1024
122 cls
140 call ANIN'("array%",sn!   ,"thru side torq",1,"done")
160 rem
170 call INTON'(20,"MIL")
180     call status'("done",stat%)
210 call grlabel'("thrust",1,3,"top","left")
```

```
212 call grlabel'("sforce",2,3,"top","left")
214 call grlabel'("torque",3,3,"top","left")
215   screen 2
220 call hgraphrt'("done","1 2 3","fast","0.000","4095.",
"-1",-1.,3,"grid")
240     if stat%<>0 then 180
280 call intoff
290   call arsave'("array%","arr.dat")
378   mean!=0:mean1!=0:mean2!=0:stdev!=0:stdev1!=0:stdev2!=0
379  call meandev'("array%",1,mean!,stdev!,1.,sn!,-1)
380  call meandev'("array%",2,mean1!,stdev1!,1.,sn!,-1)
381  call meandev'("array%",3,mean2!,stdev2!,1.,sn!,-1)
382  rem
470  call ardel'("array%")
480  locate 20,5:print"mean thrust = ";mean!
490  locate 10,5:print"mean sideforce=";mean1!
500  locate  3,5:print"mean torque = "; mean2!
510  locate 22,5:print"std =";   stdev!
520  locate 12,5:print"std = ";  stdev1!
530  locate  5,5:print"std = ";  stdev2!
540  close #1
630  end
```

C.2 Improvement of Signal Resolution

To improve the signal resolution, it was necessary to change the Keithly 570 mother board gain so that the amplifier gain could be adjusted to let the output signal magnitude for maximum forces during a test match the digital range of the A/D converter. When changing the Kethley 570 mother board gain, first turn the board off, then change the hardware settings to the required gain. Turn on the board again. Run CONFIG on the PC to change the configuration table to match the hardware gain setting.

Appendix D

Test Results

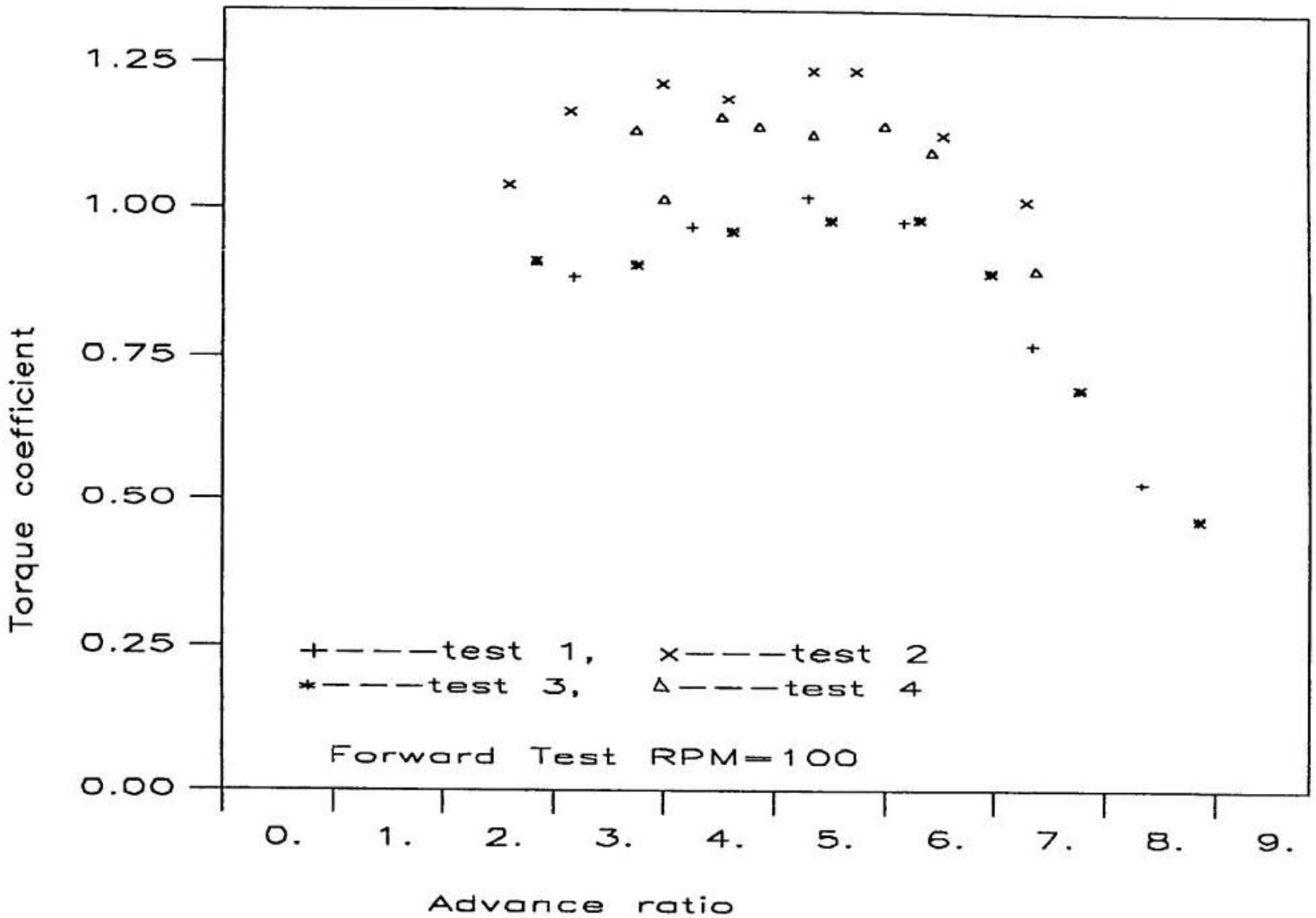


Figure D-1: Forward tests of 100 RPM — torque coefficient

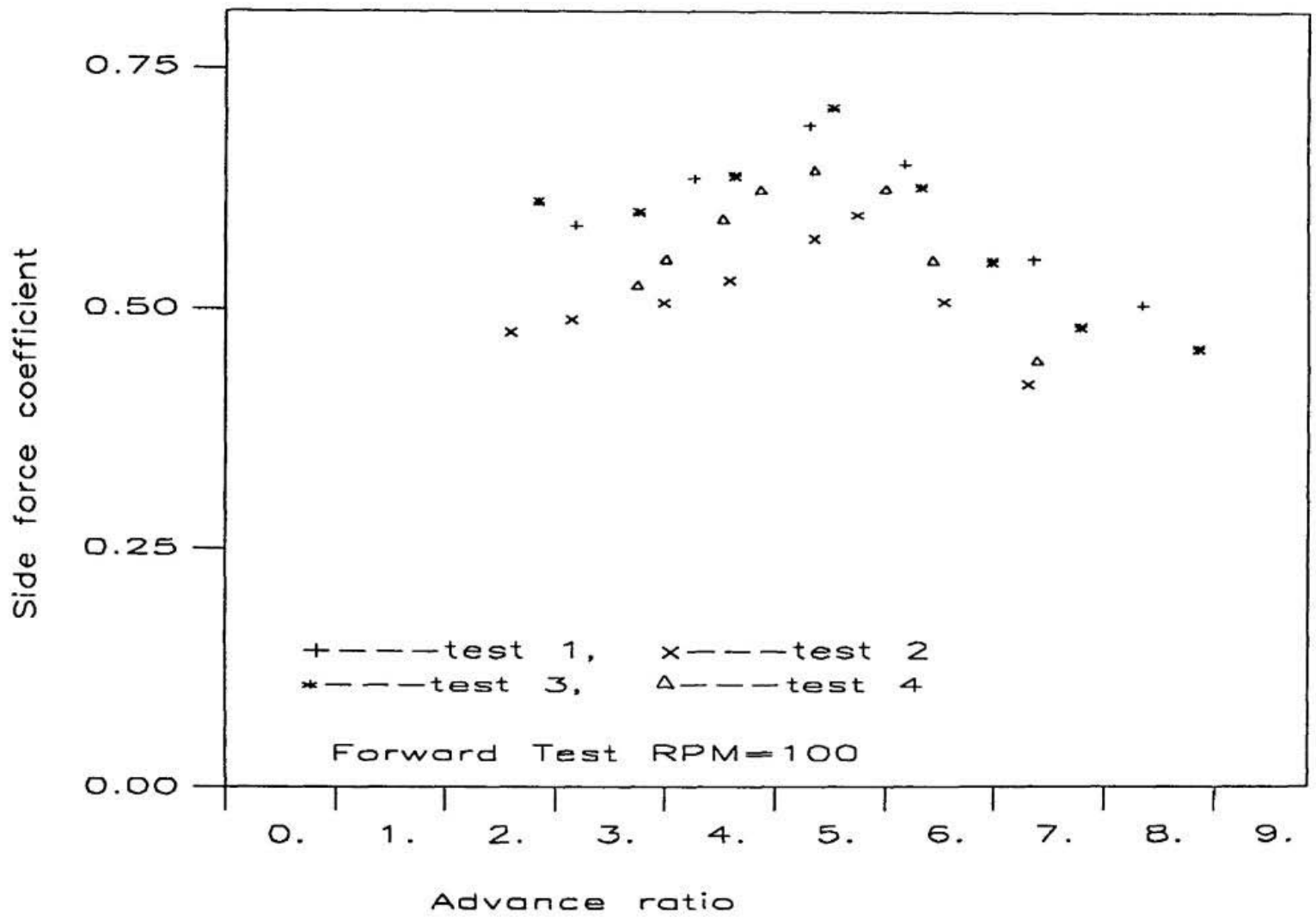


Figure D-2: Forward tests of 100 RPM — side force coefficient

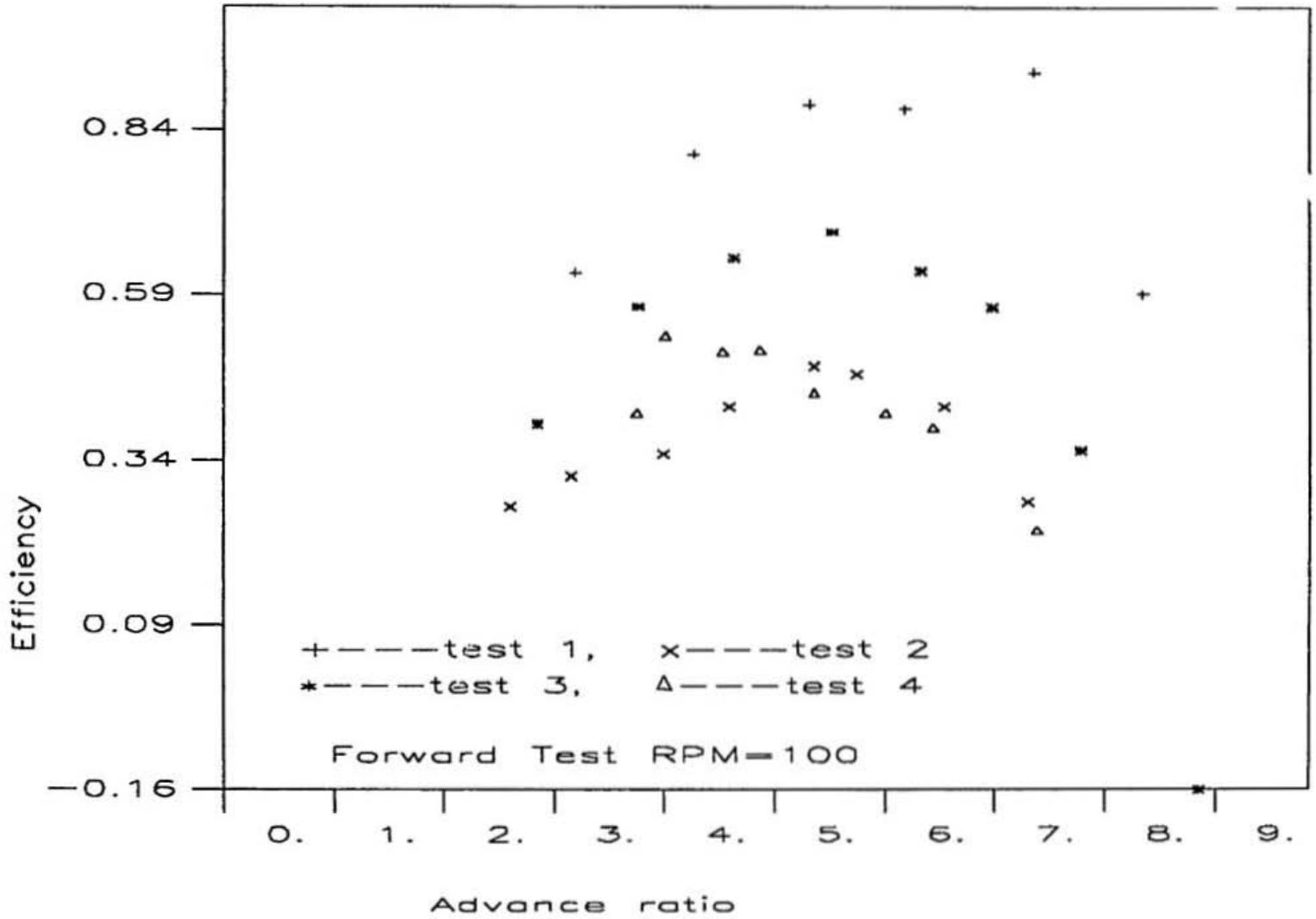


Figure D-4: Forward tests of 100 RPM — efficiency

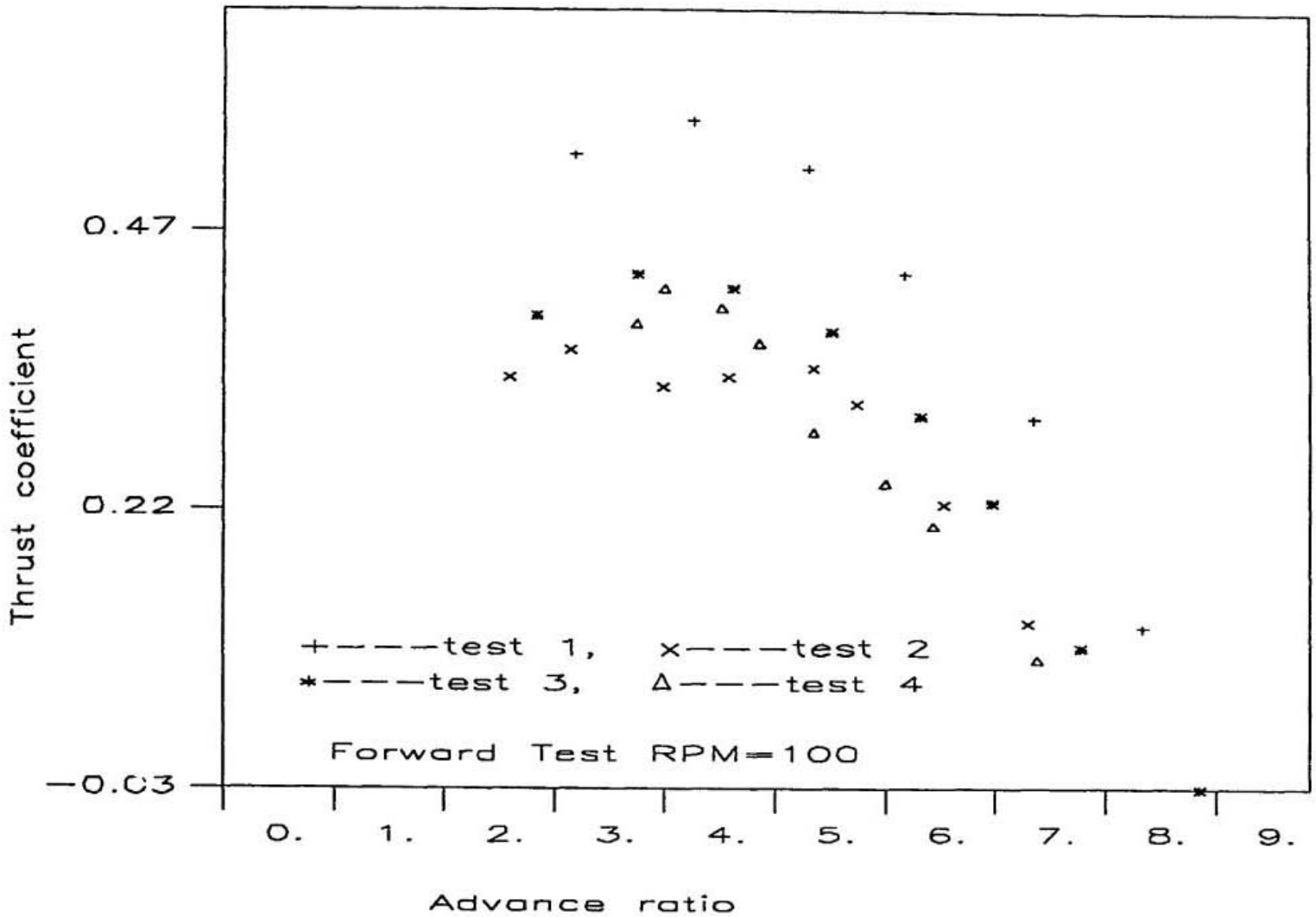


Figure D-3: Forward tests of 100 RPM — thrust coefficient

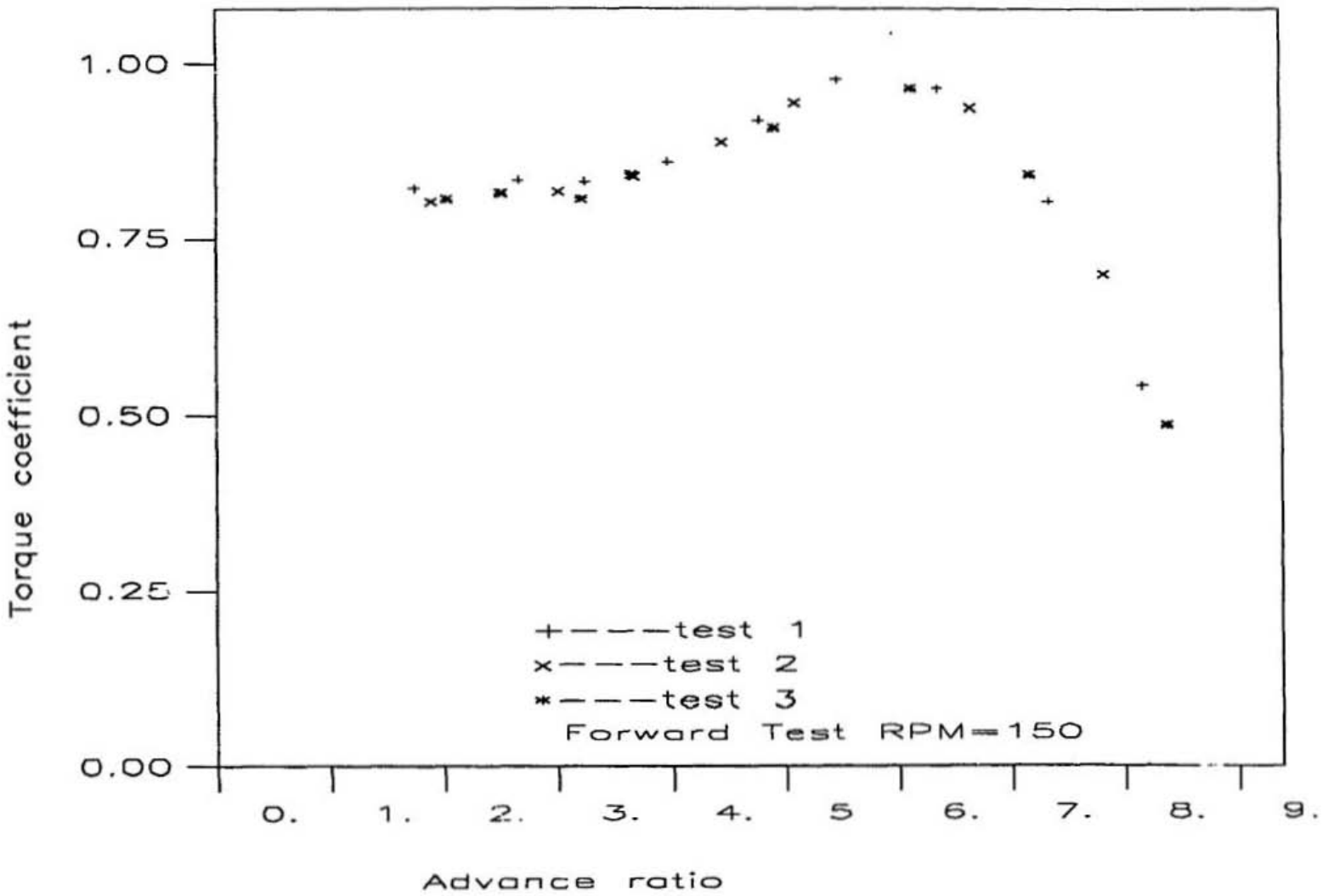


Figure D-5: Forward tests of 150 RPM — torque coefficient

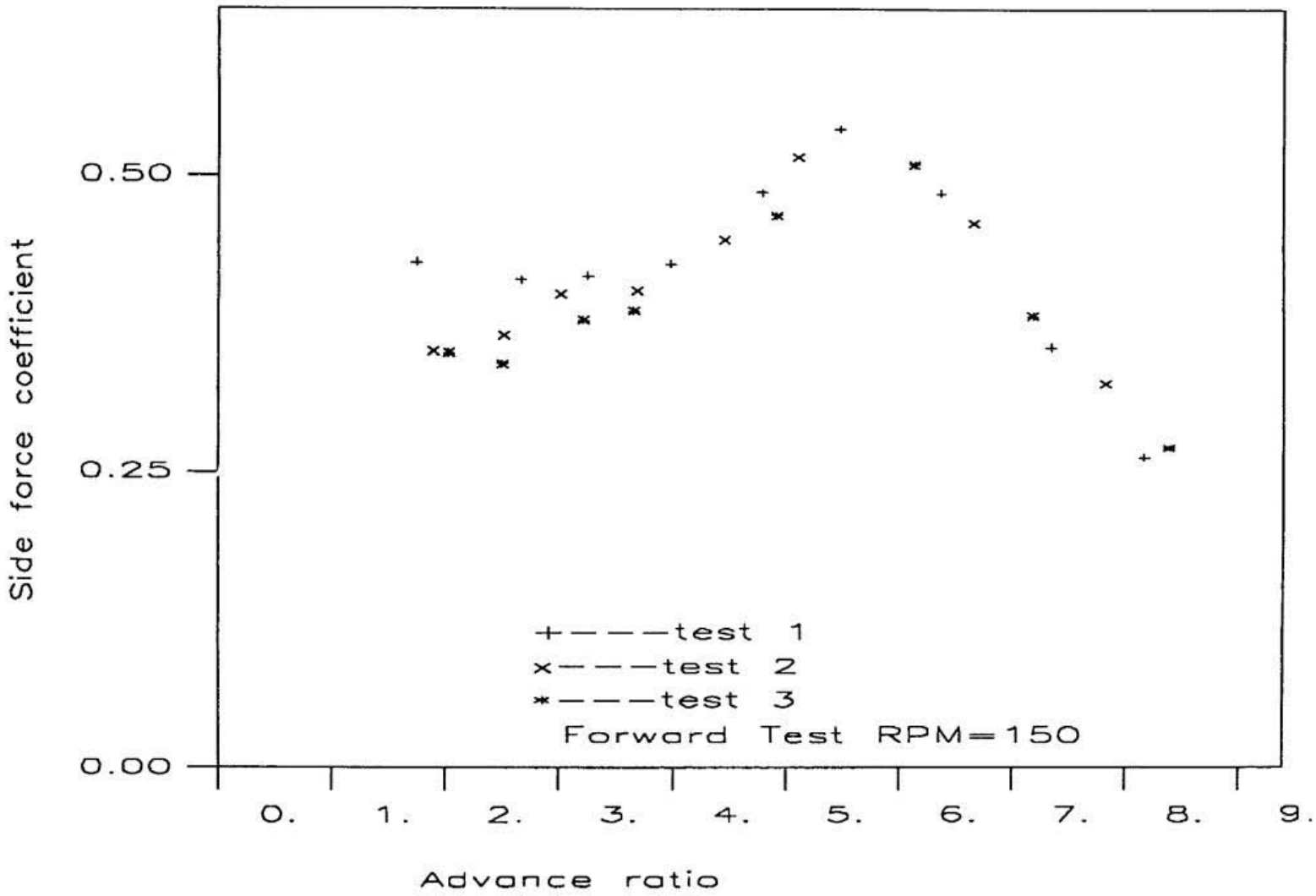


Figure D-6: Forward tests of 150 RPM — side force coefficient

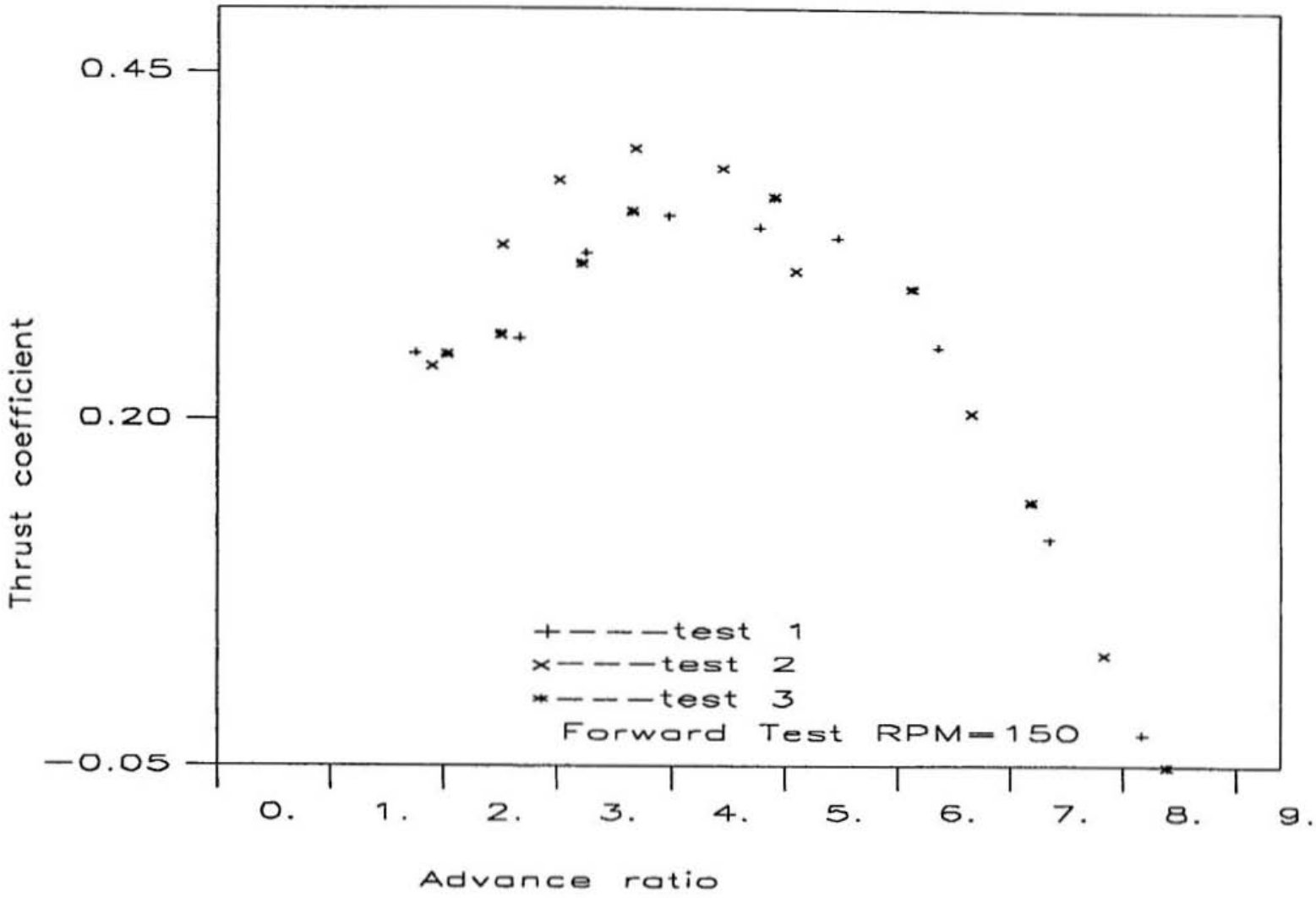


Figure D-7: Forward tests of 150 RPM — thrust coefficient

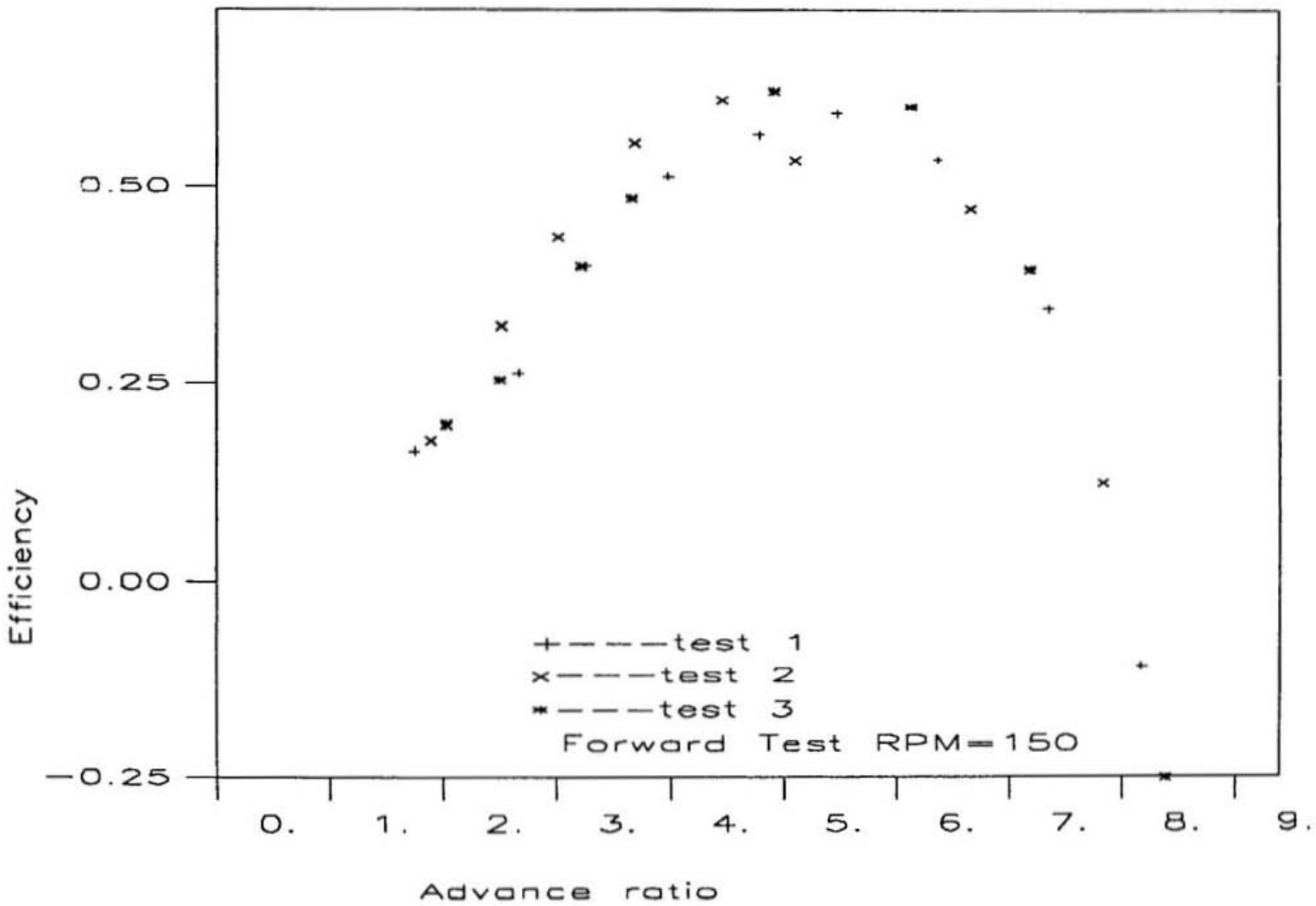


Figure D-8: Forward tests of 100 RPM -- efficiency

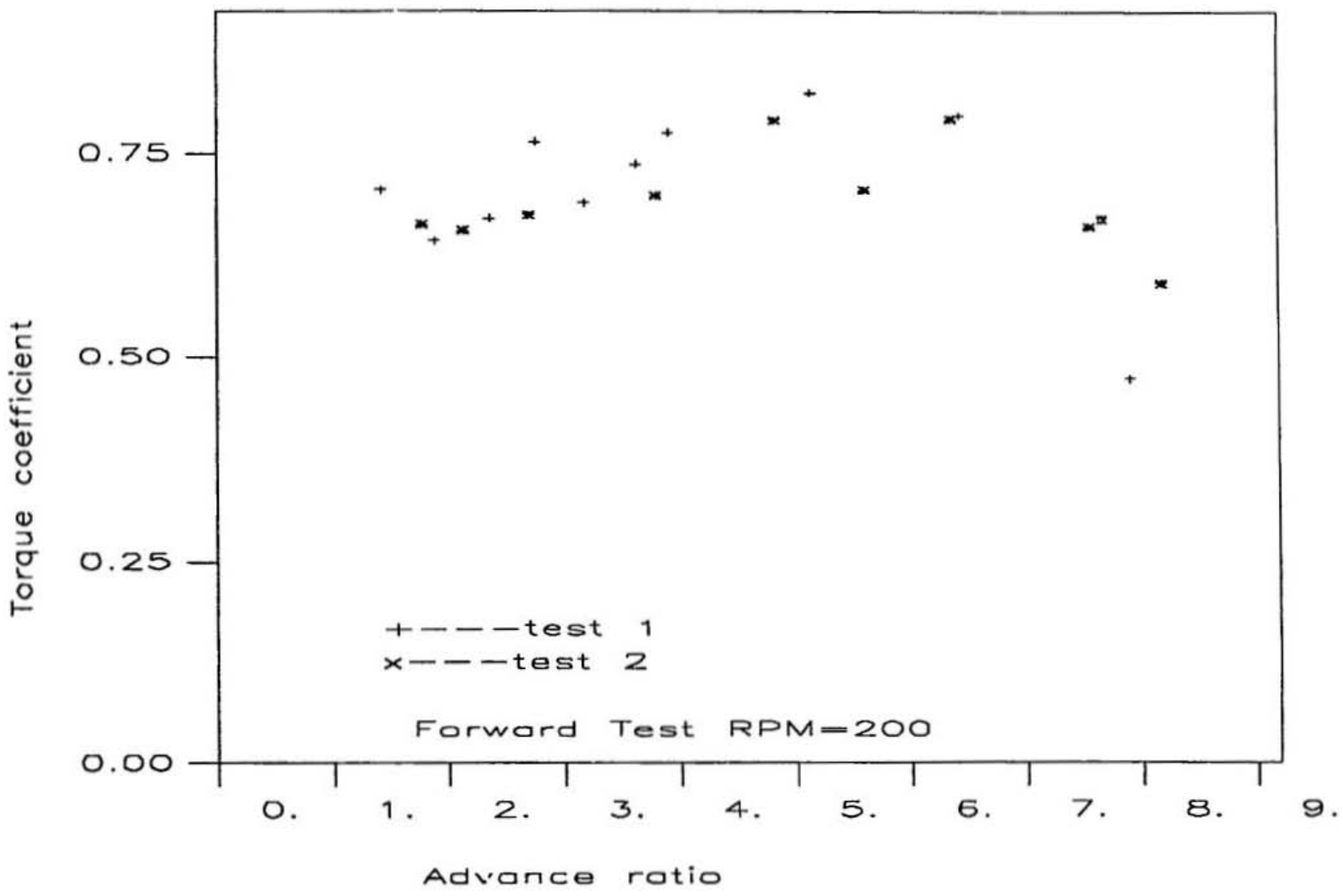


Figure D-9: Forward tests of 200 RPM — torque coefficient

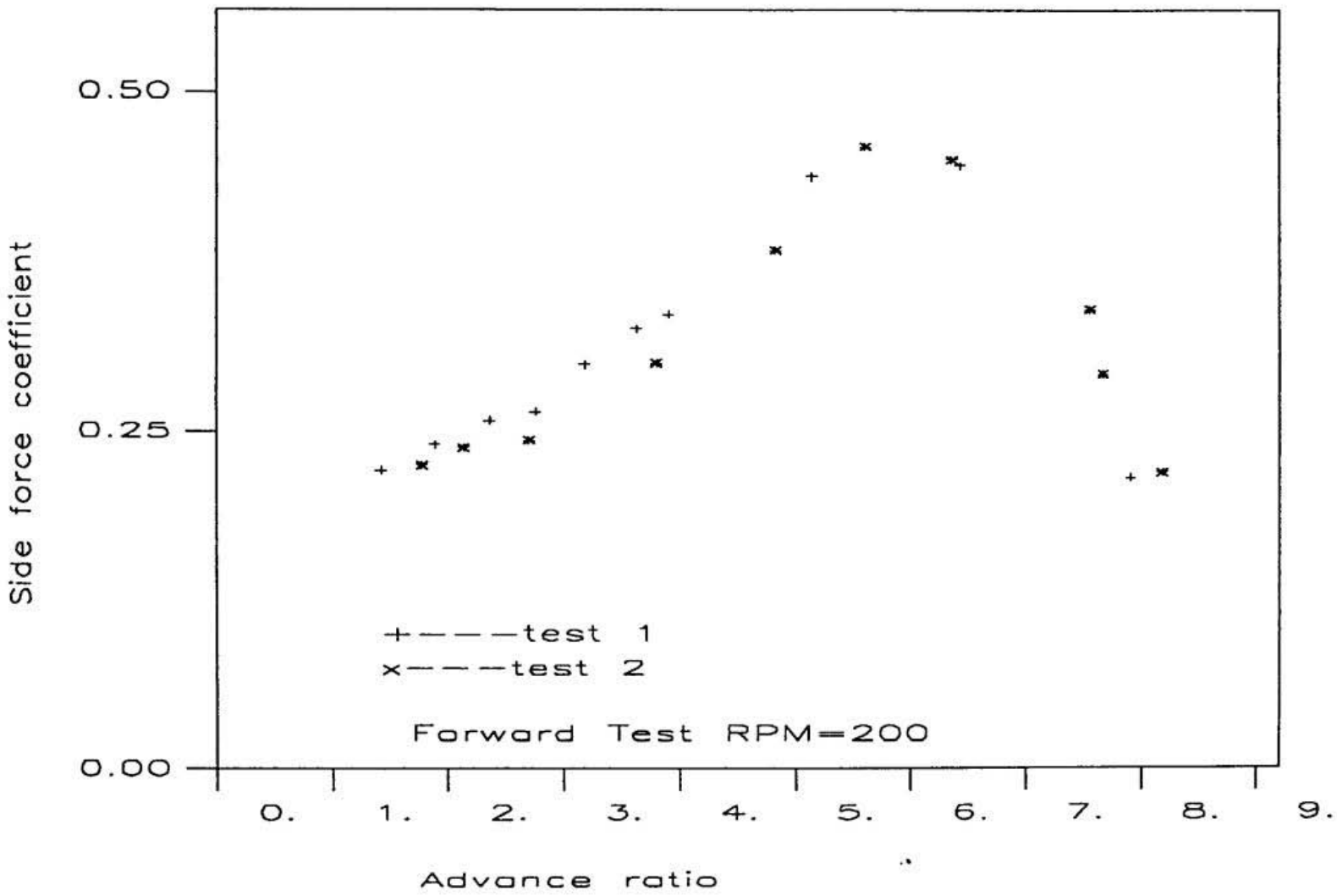


Figure D-10: Forward tests of 200 RPM — side force coefficient

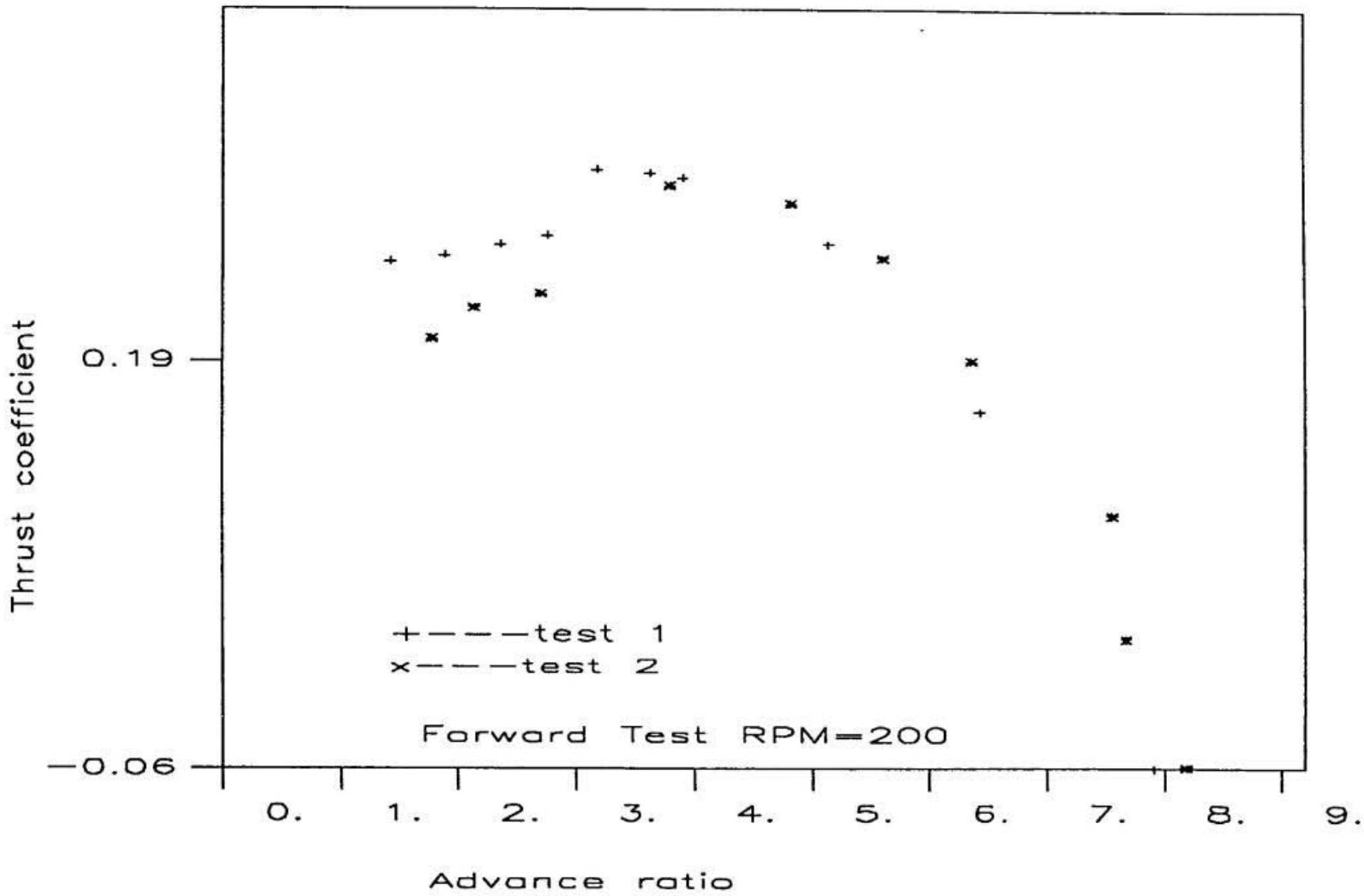


Figure D-11: Forward tests of 200 RPM — thrust coefficient

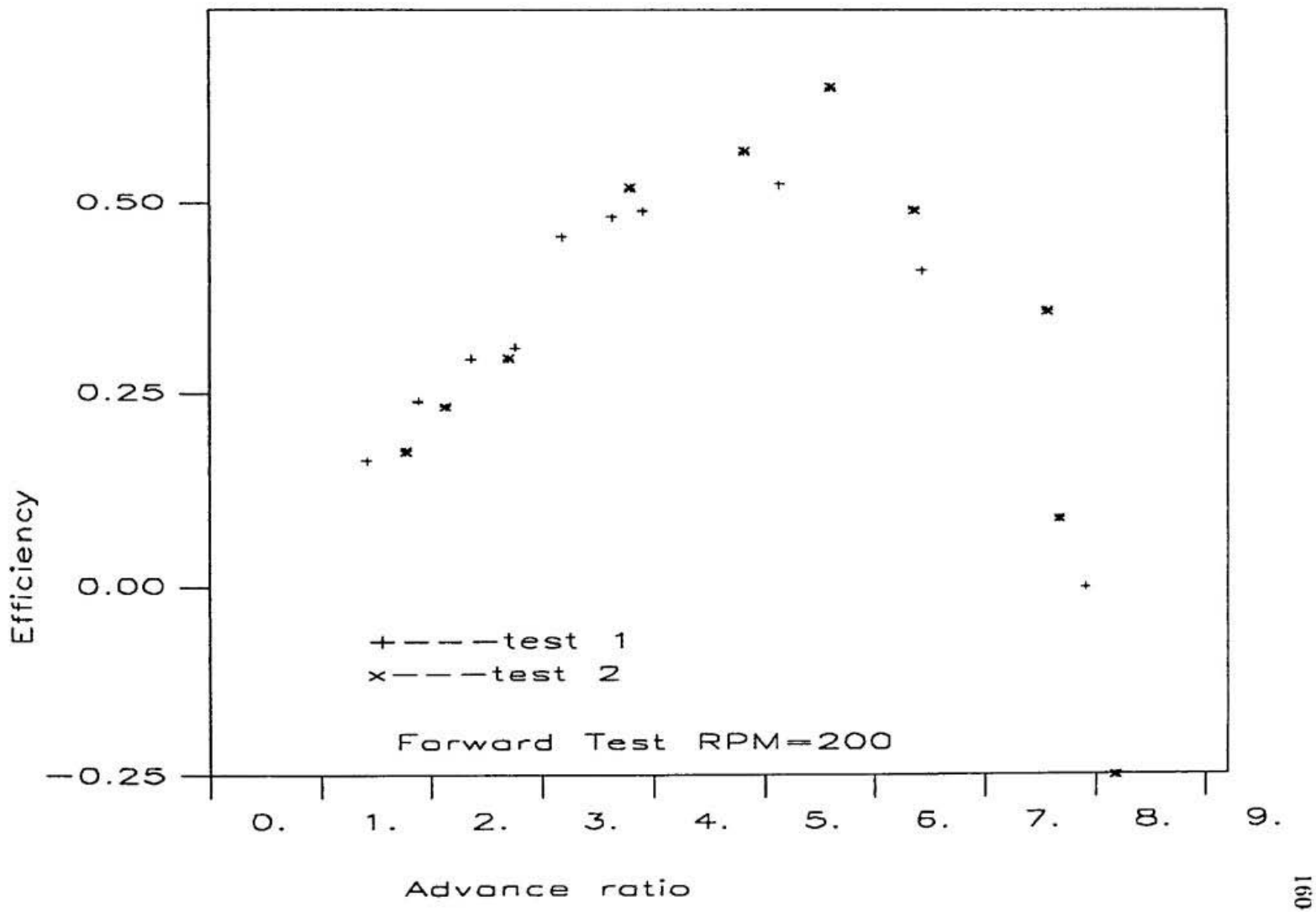


Figure D-12: Forward tests of 200 RPM — efficiency

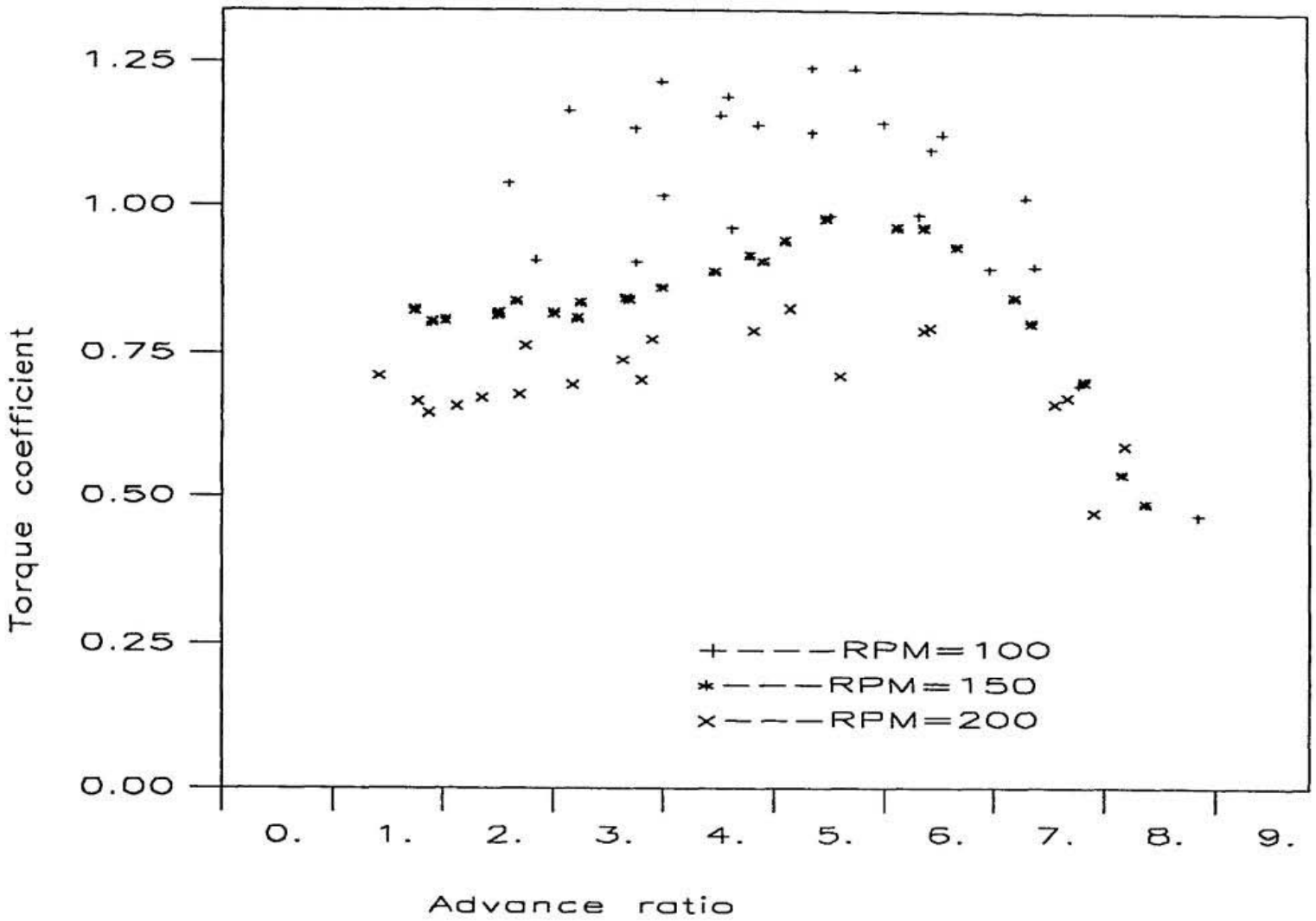


Figure D-13: Comparison of test results -- torque coefficient

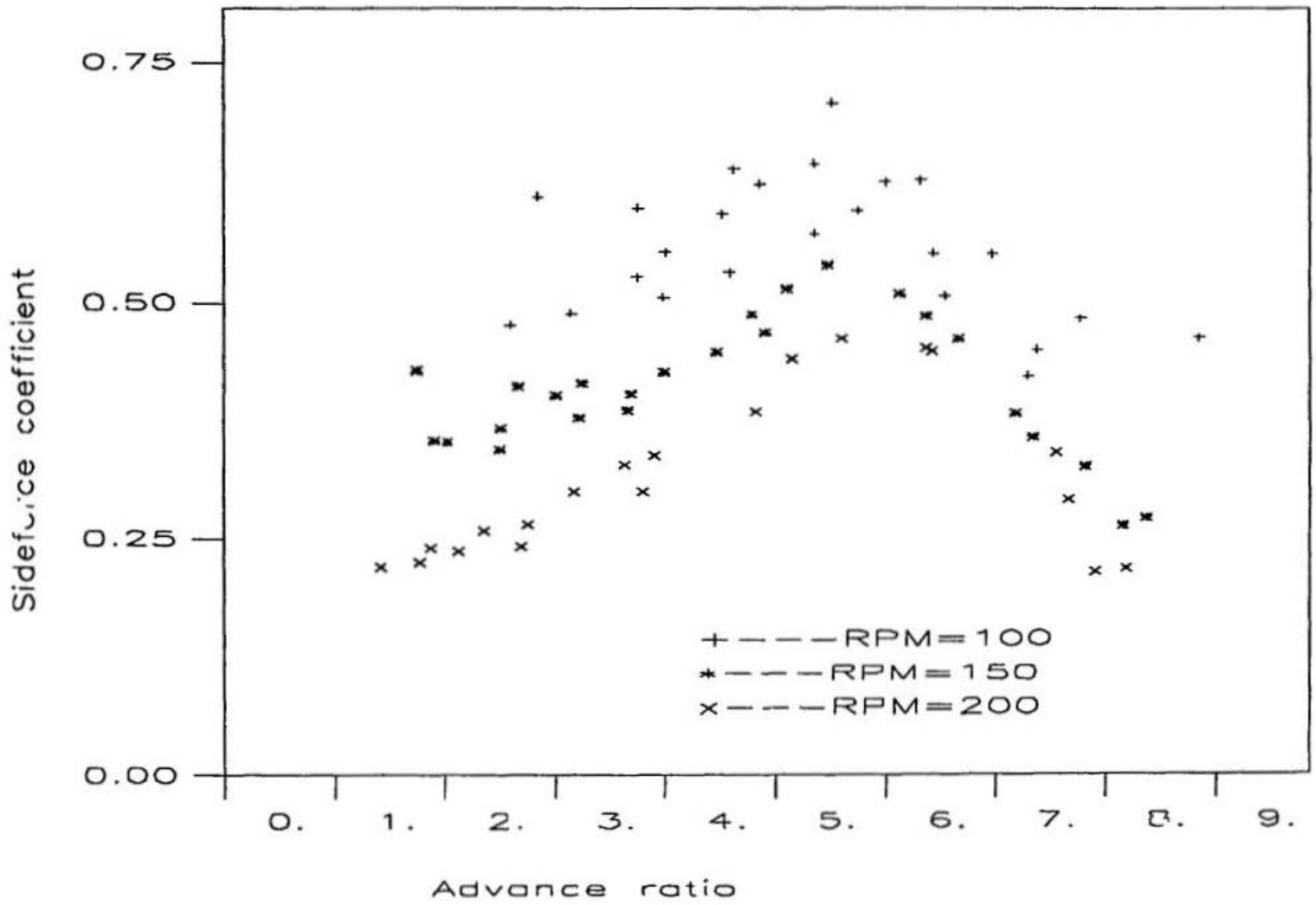


Figure D-14: Comparison of test results — side force coefficient

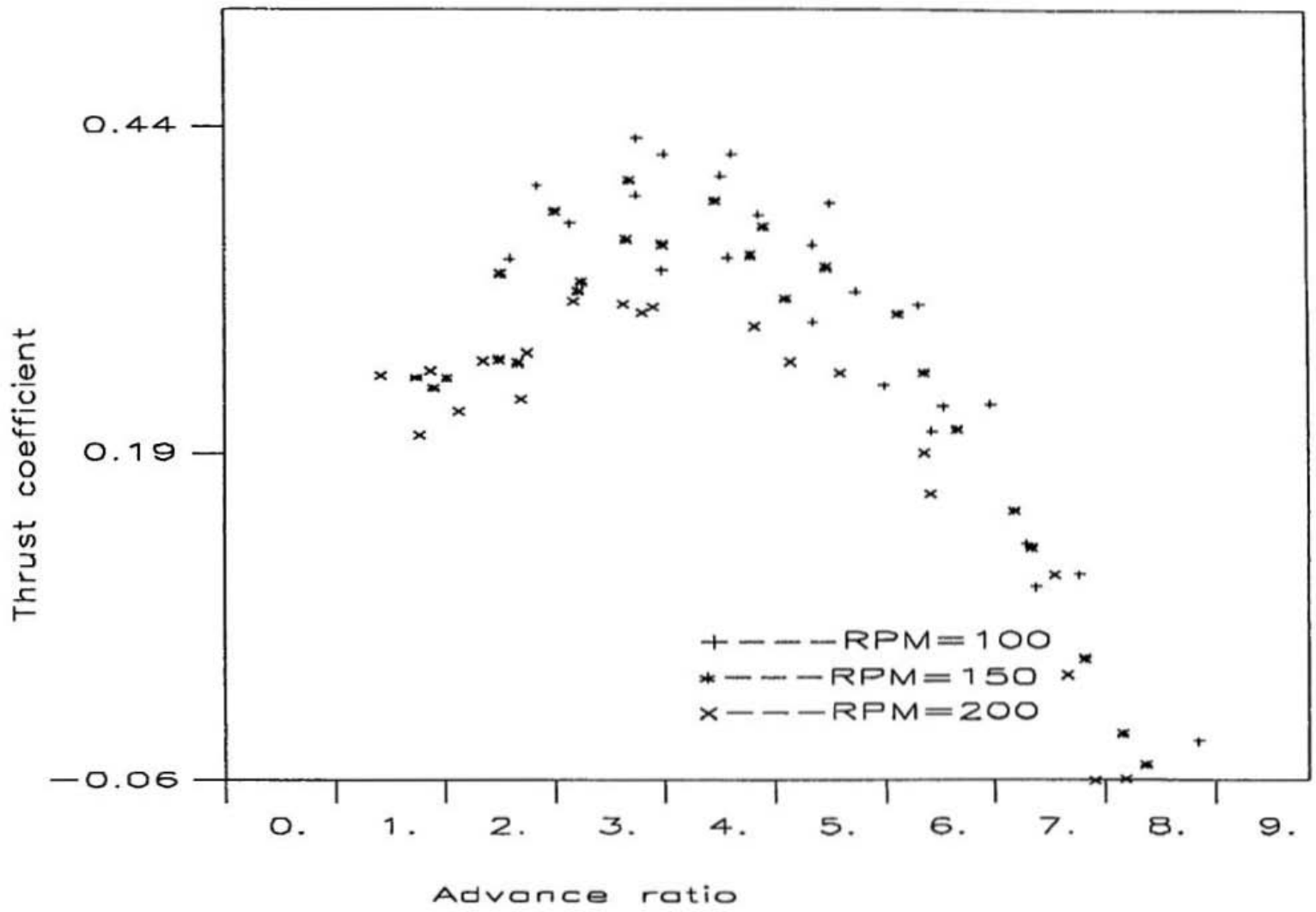


Figure D-15: Comparison of test results — thrust coefficient

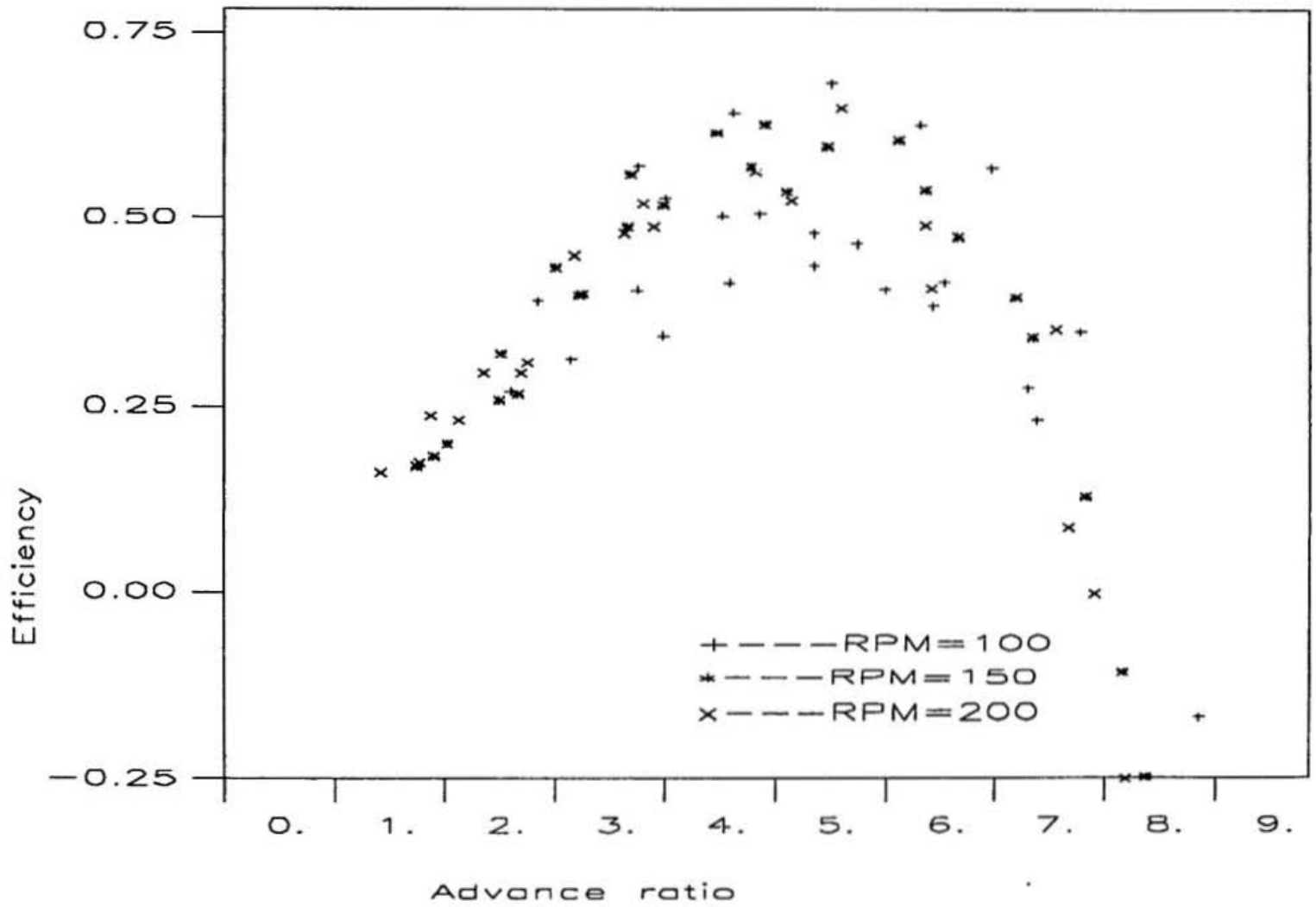


Figure D-16: Comparison of test results — efficiency

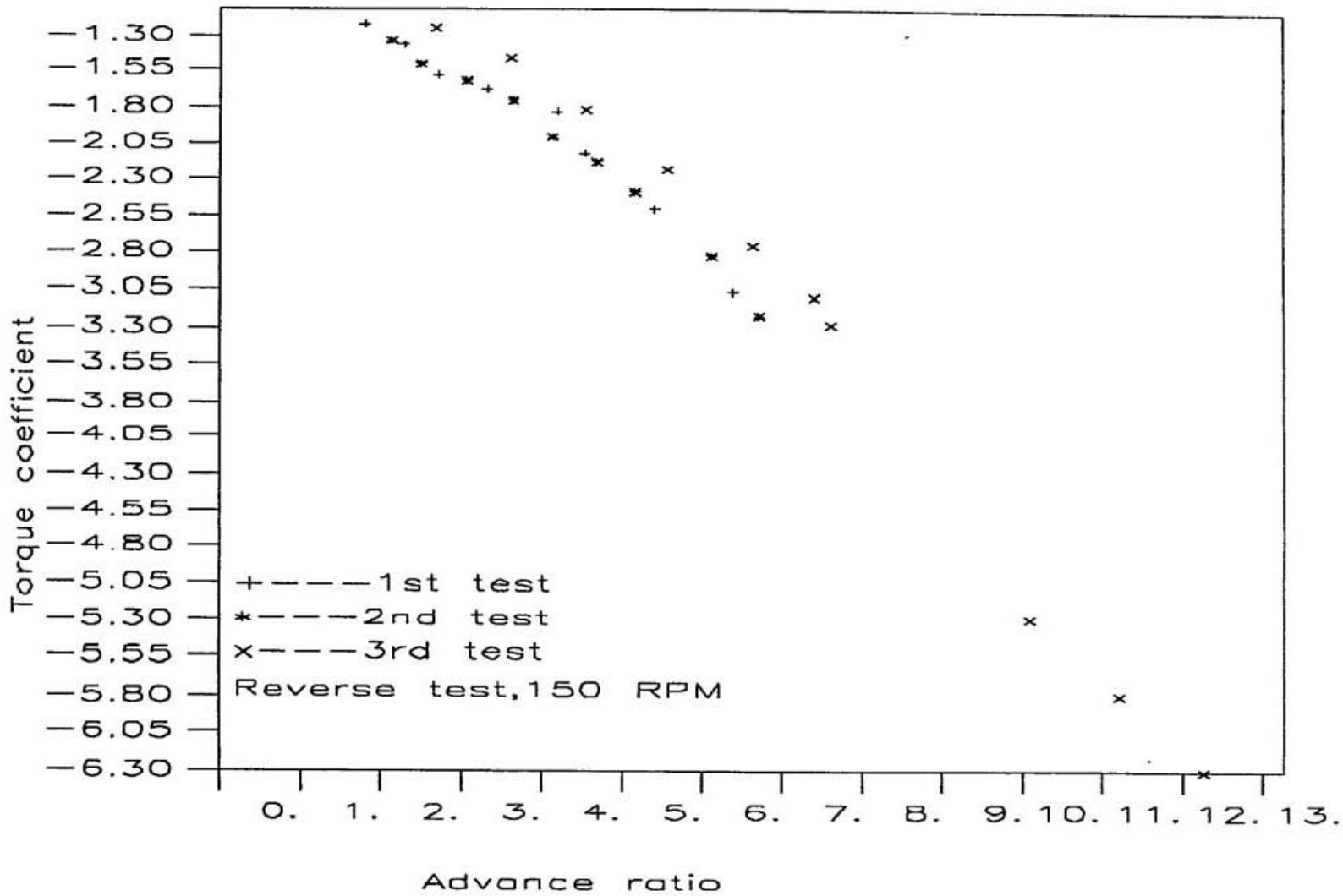


Figure D-17: Reverse tests of 150 RPM — torque coefficient

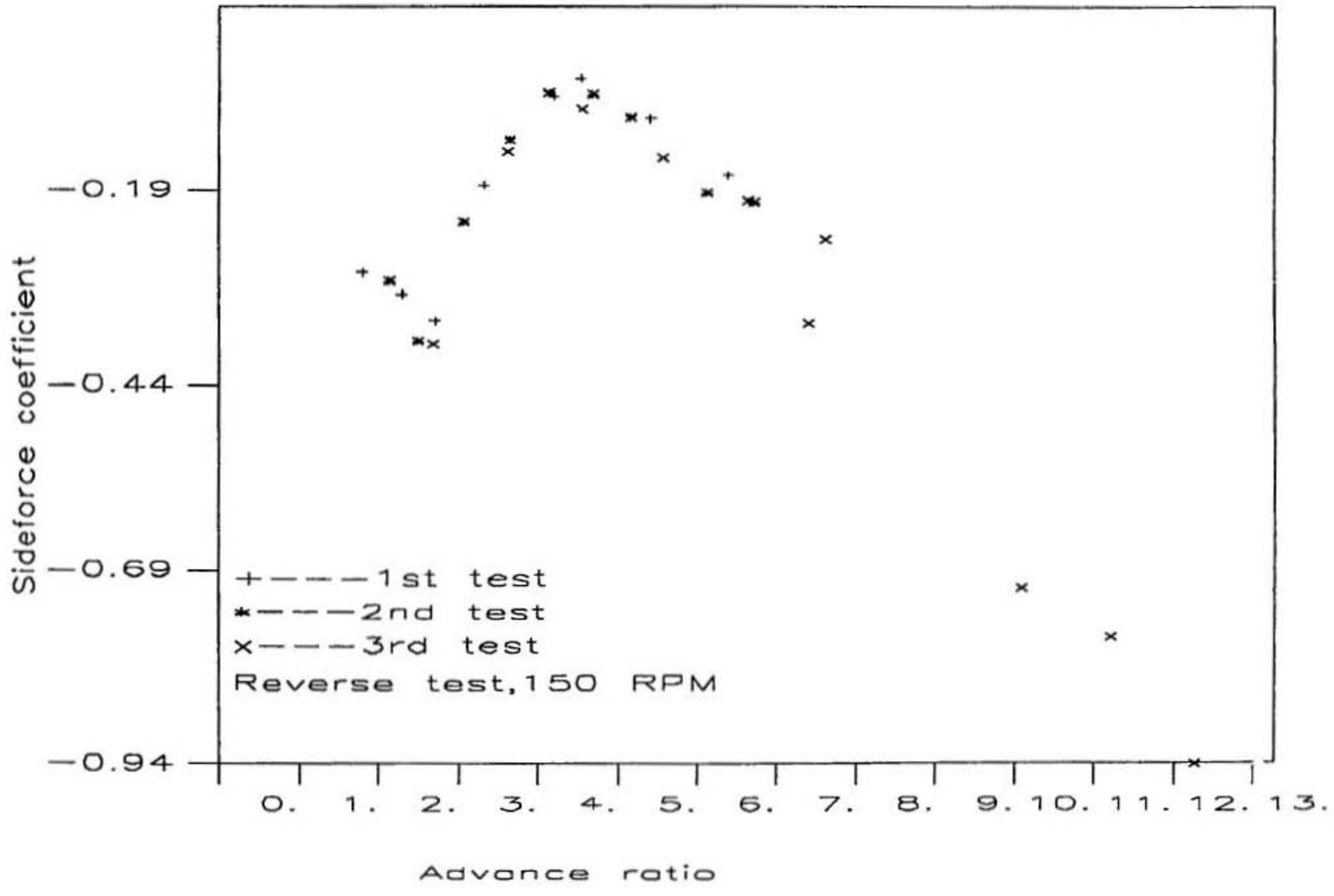


Figure D-18: Reverse tests of 150 RPM — side force coefficient

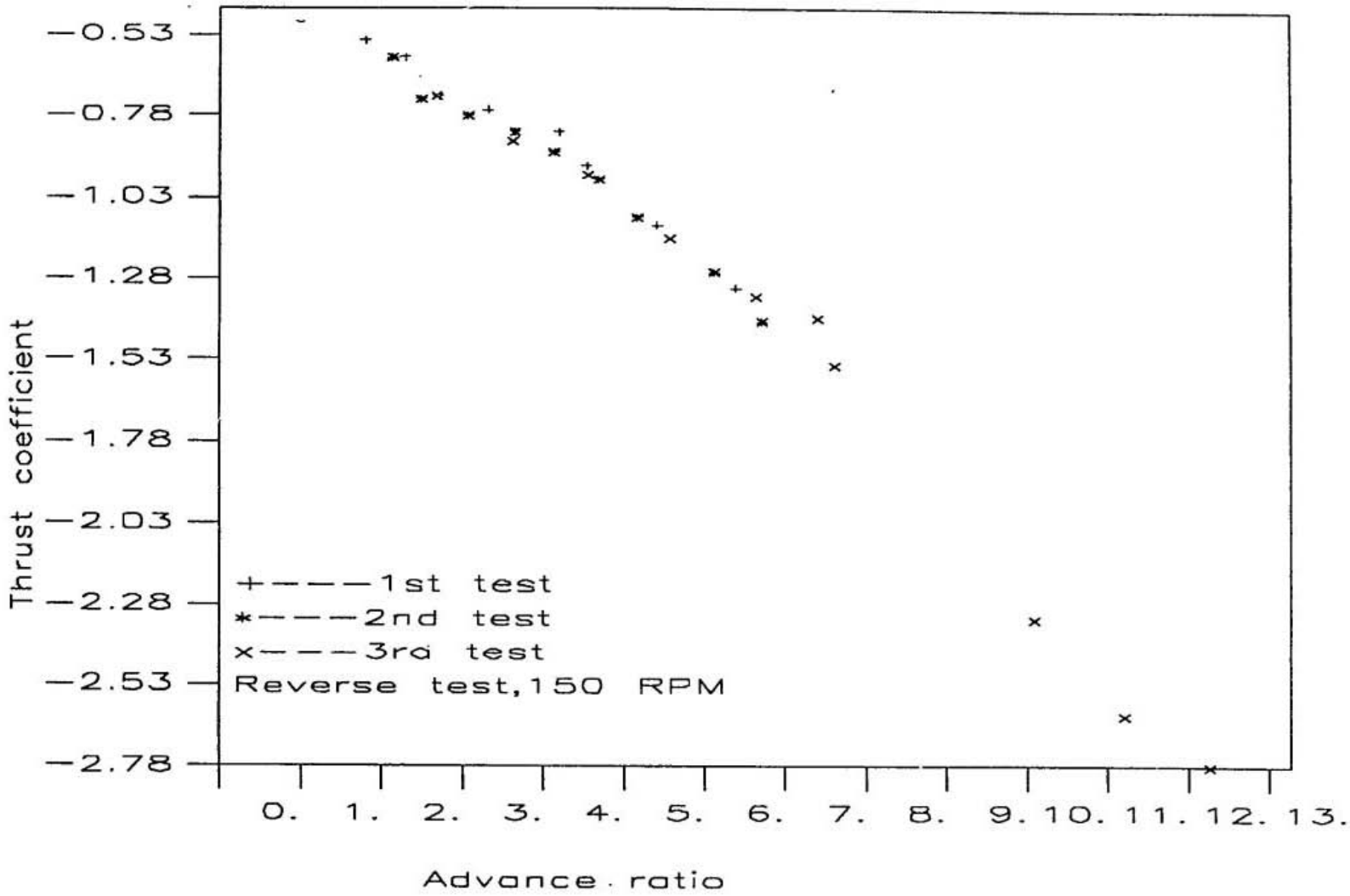


Figure D-19: Reverse tests of 150 RPM — thrust coefficient

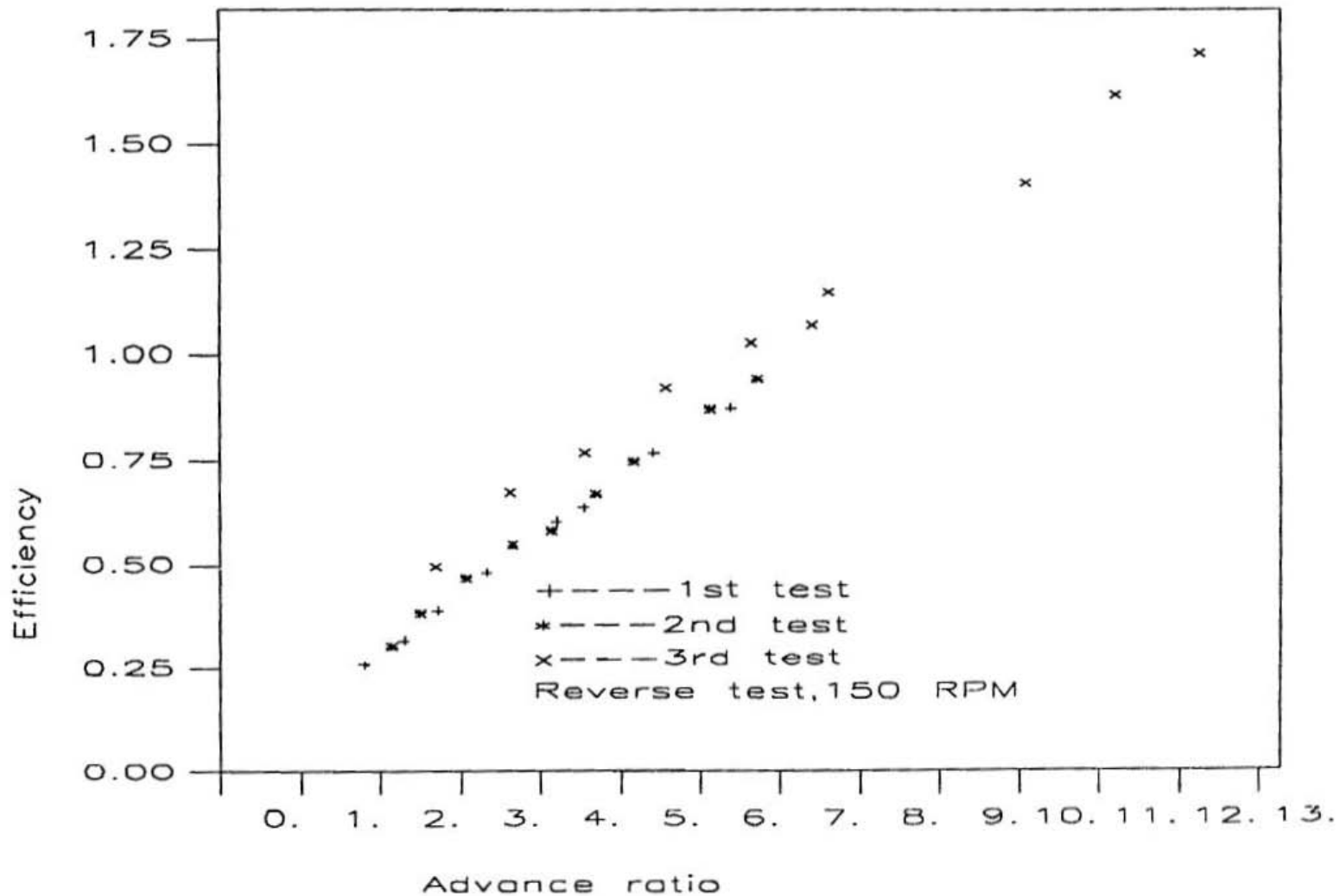


Figure D-20: Reverse tests of 150 RPM - efficiency

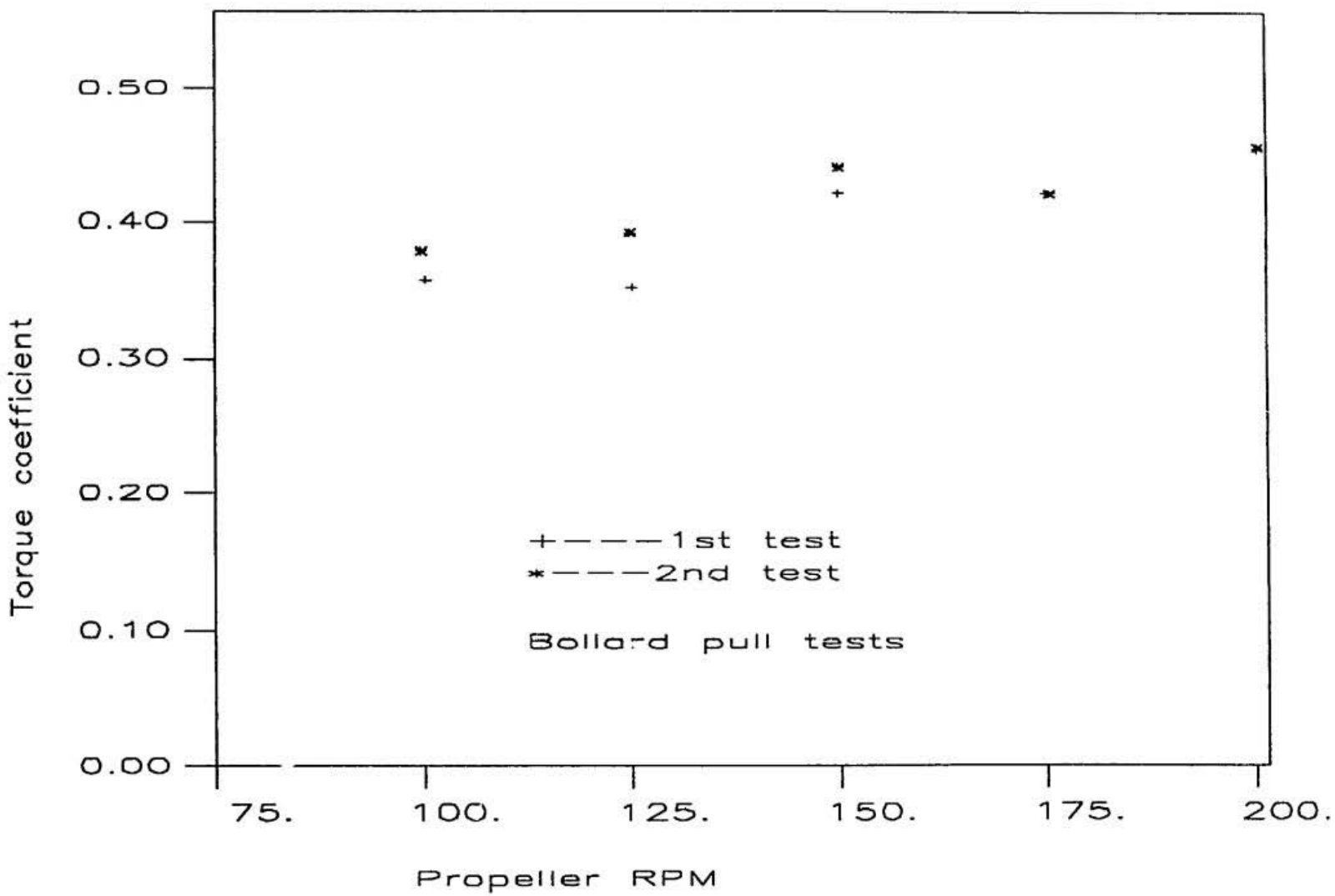


Figure D-21: Torque coefficient of propeller at zero speed

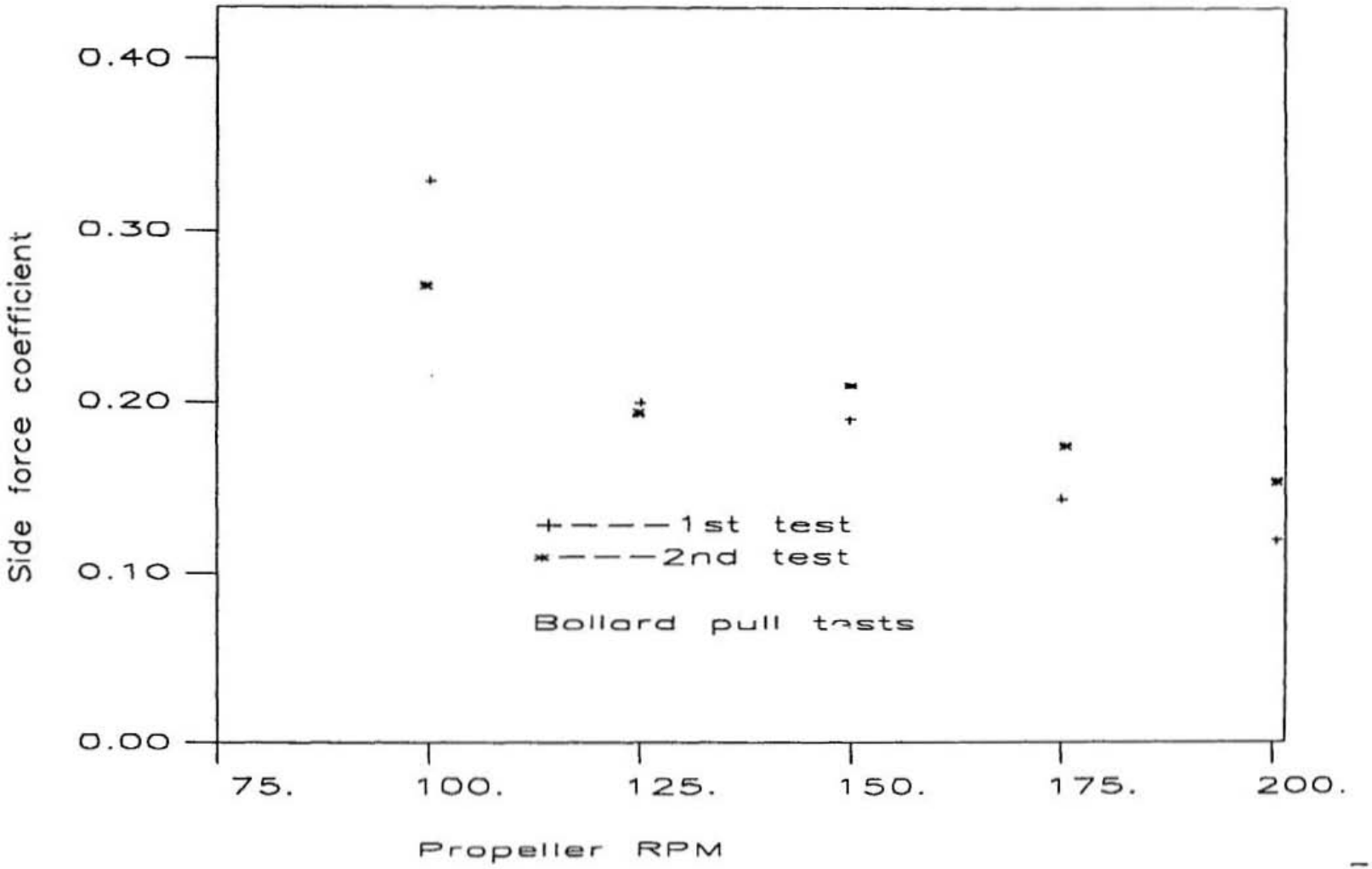


Figure D-22: Side force coefficient of propeller at zero speed

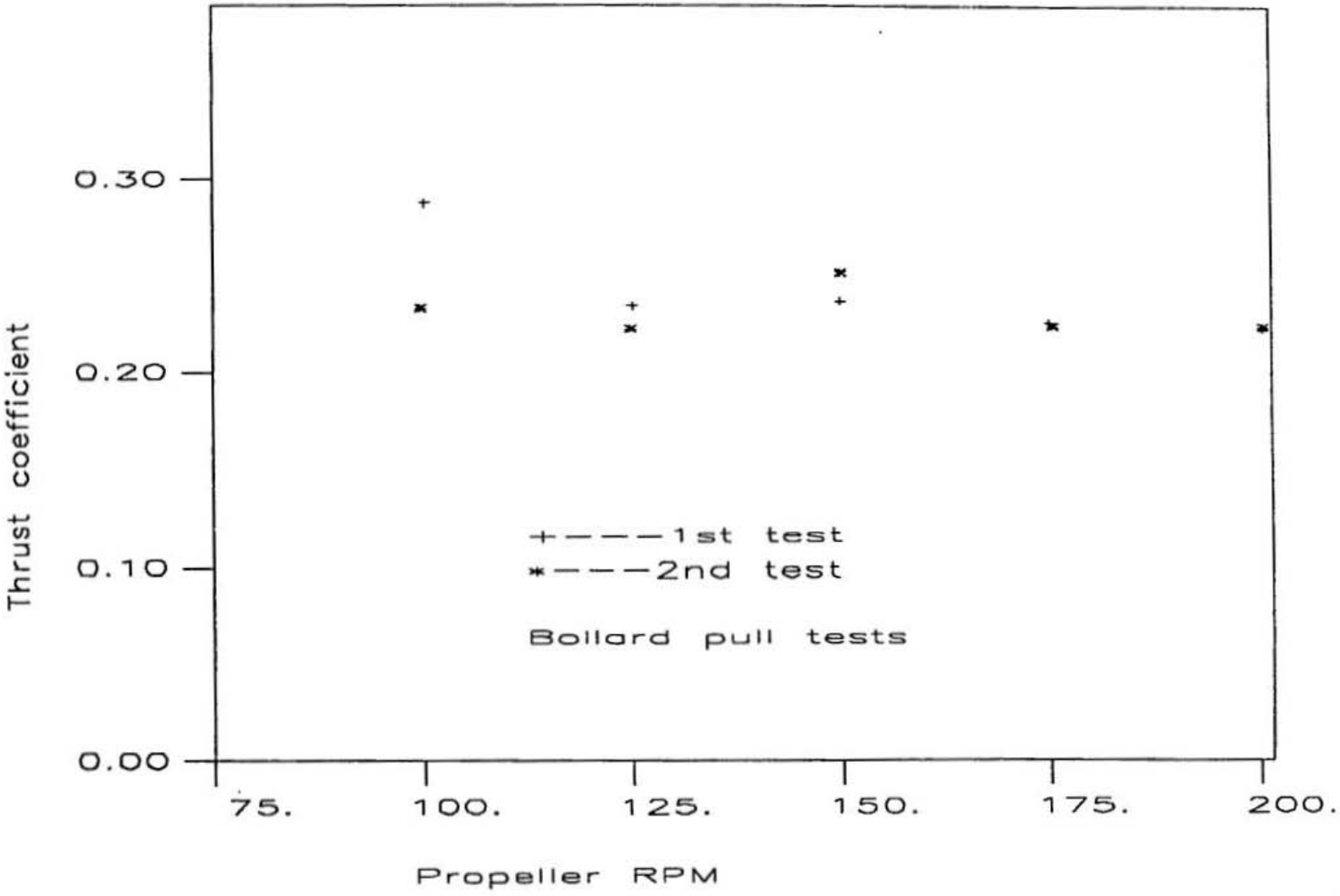


Figure D-23: Thrust coefficient of propeller at zero speed

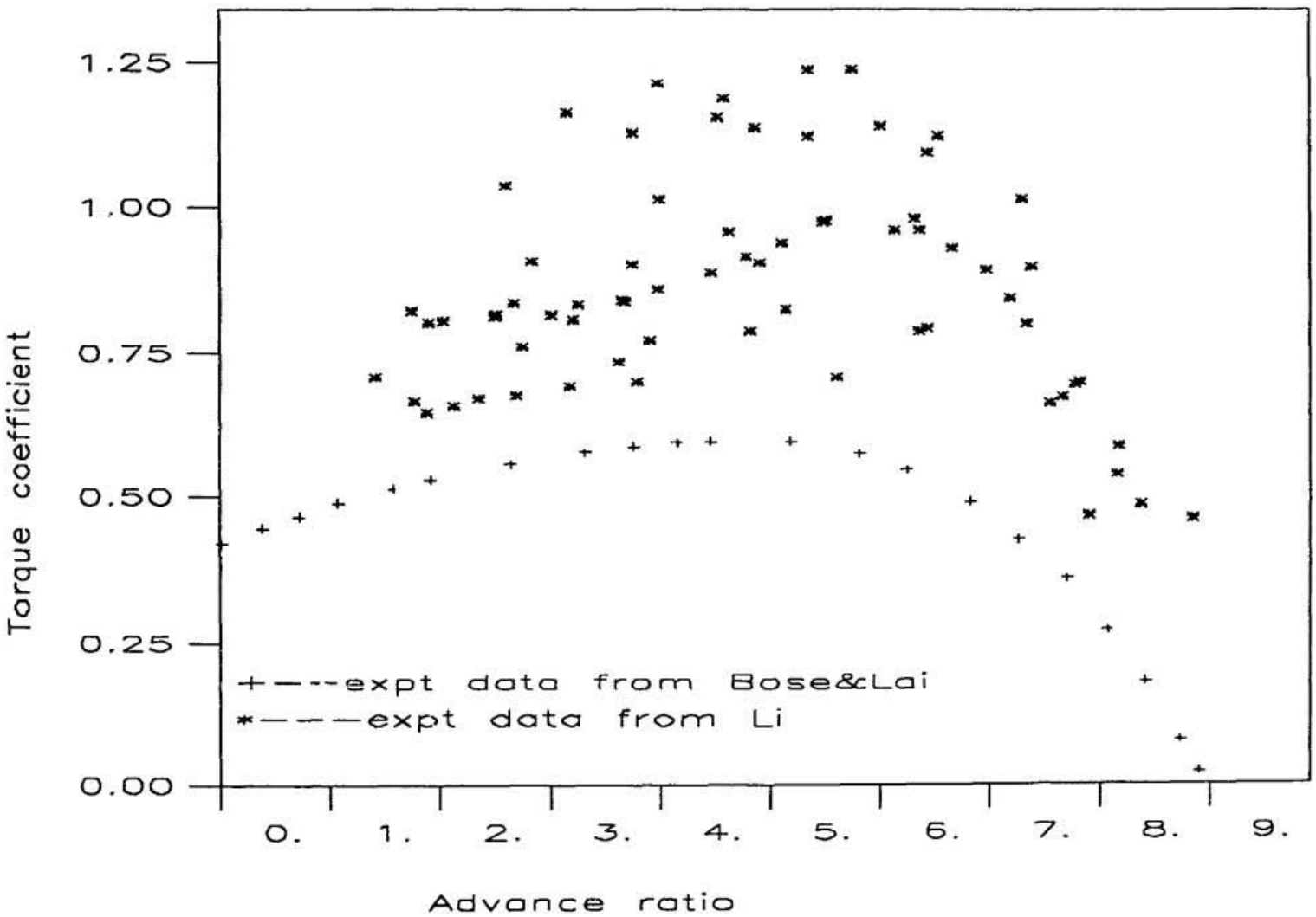


Figure D-24: Comparison of open water test with tunnel test — torque coefficient

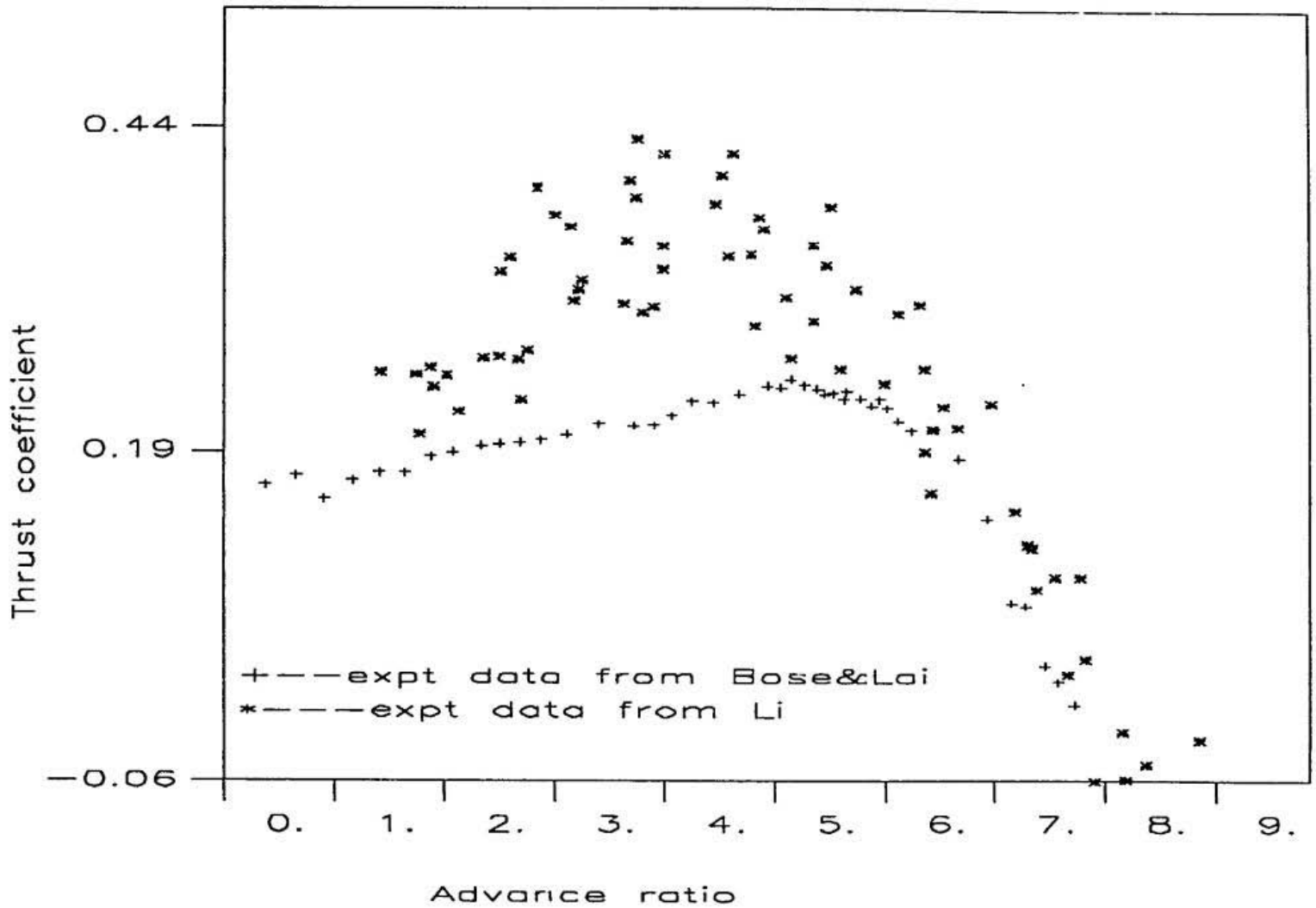


Figure D-25: Comparison of open water test with tunnel test — thrust coefficient

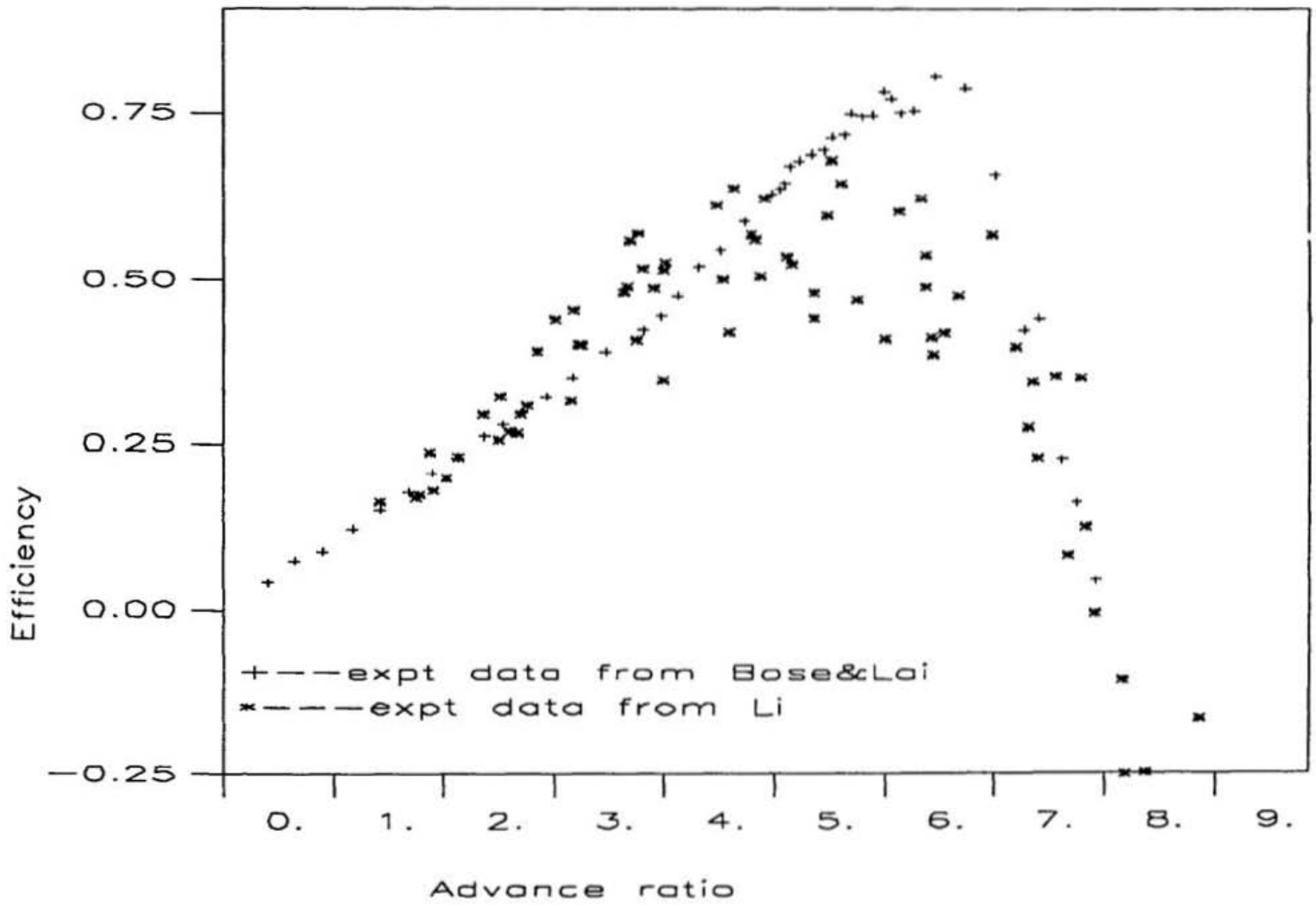


Figure D-26: Comparison of open water test with tunnel test — efficiency

Appendix E

Theoretical Results — Part I

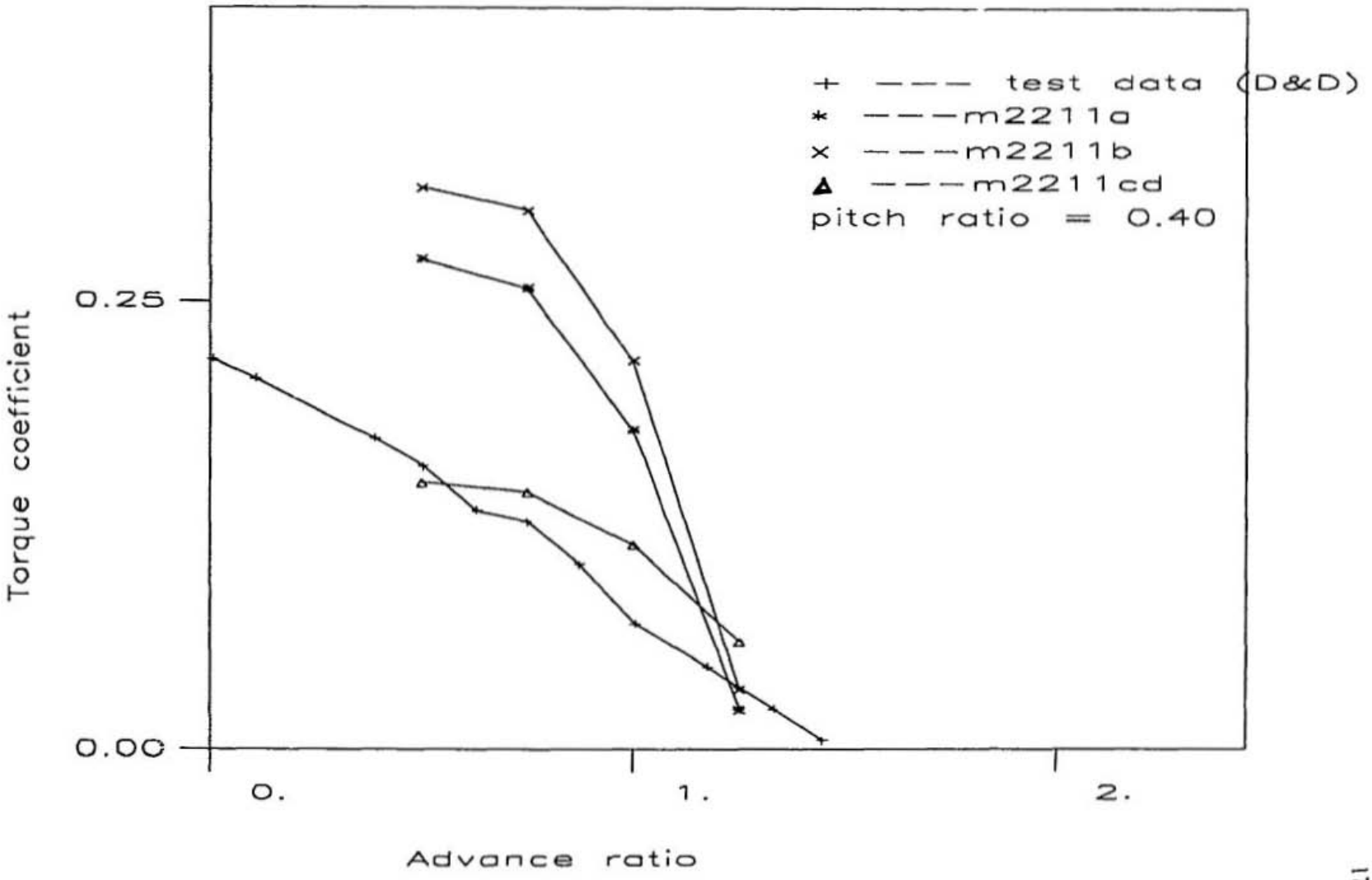


Figure E-1: Comparison of theoretical results with test results torque coefficient(pitch ratio=0.4π)

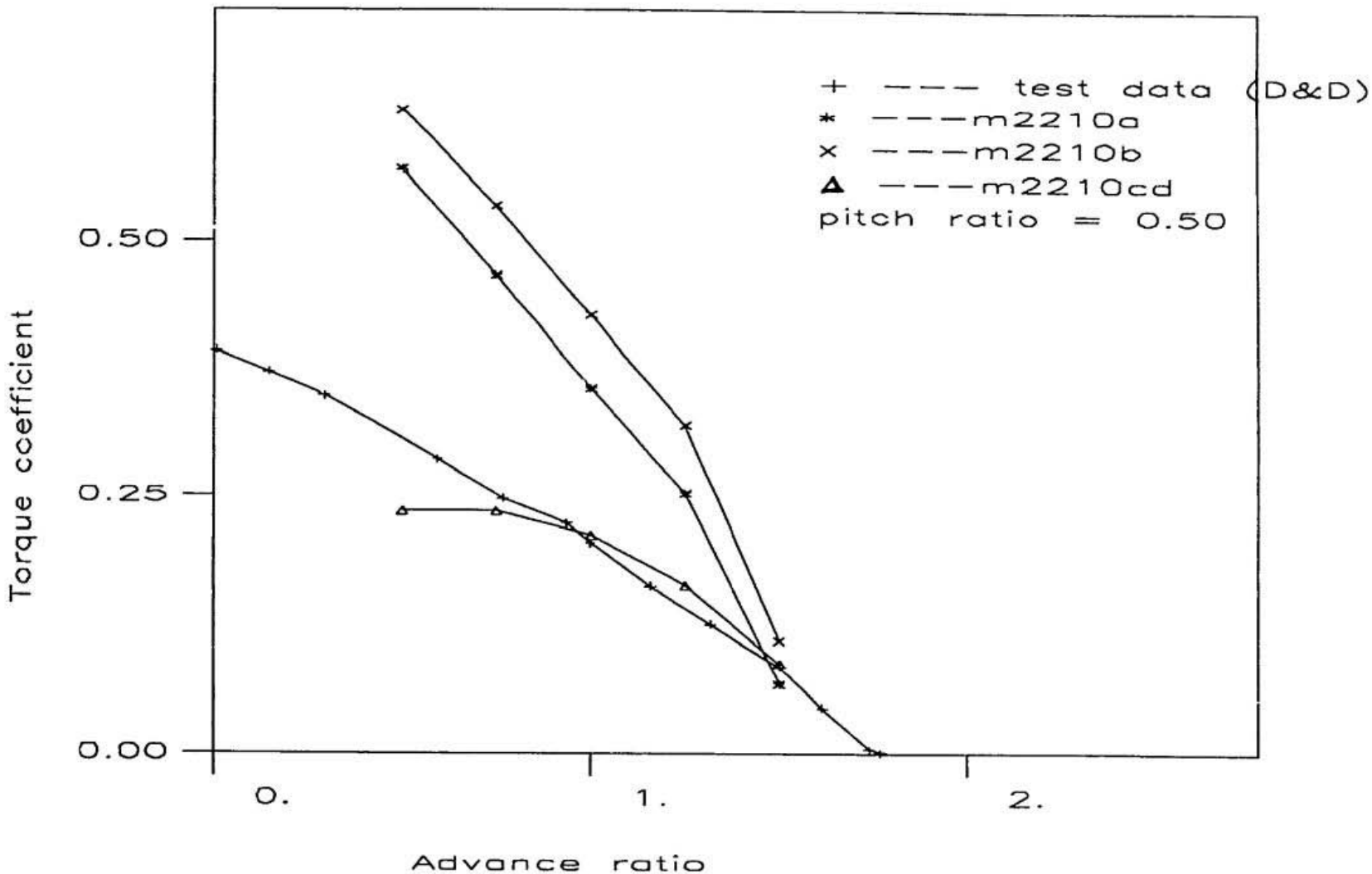


Figure E-2: Comparison of theoretical results with test results -- torque coefficient(pitch ratio=0.5π)

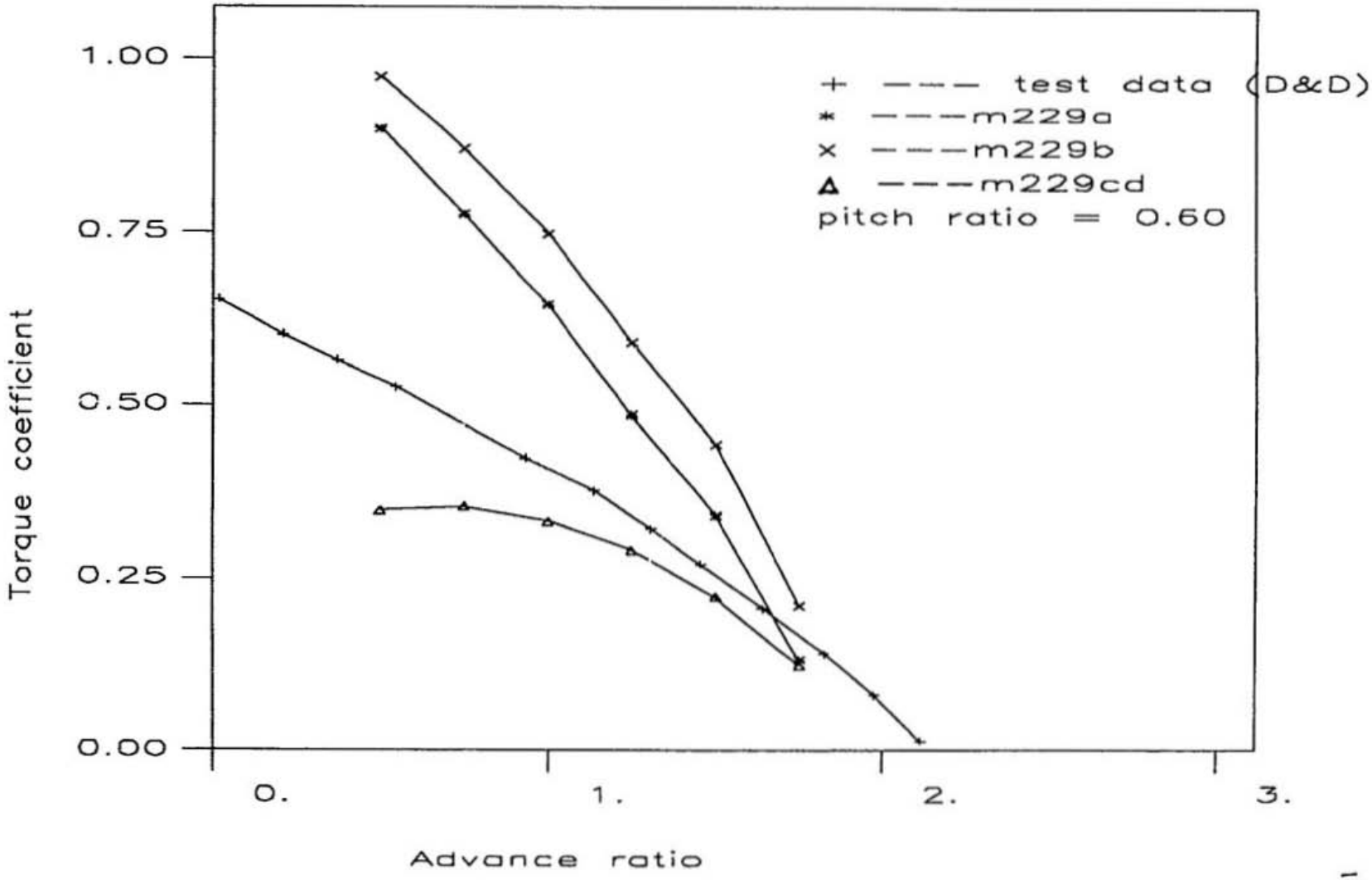


Figure E-3: Comparison of theoretical results with test results -- torque coefficient(pitch ratio=0.6π)

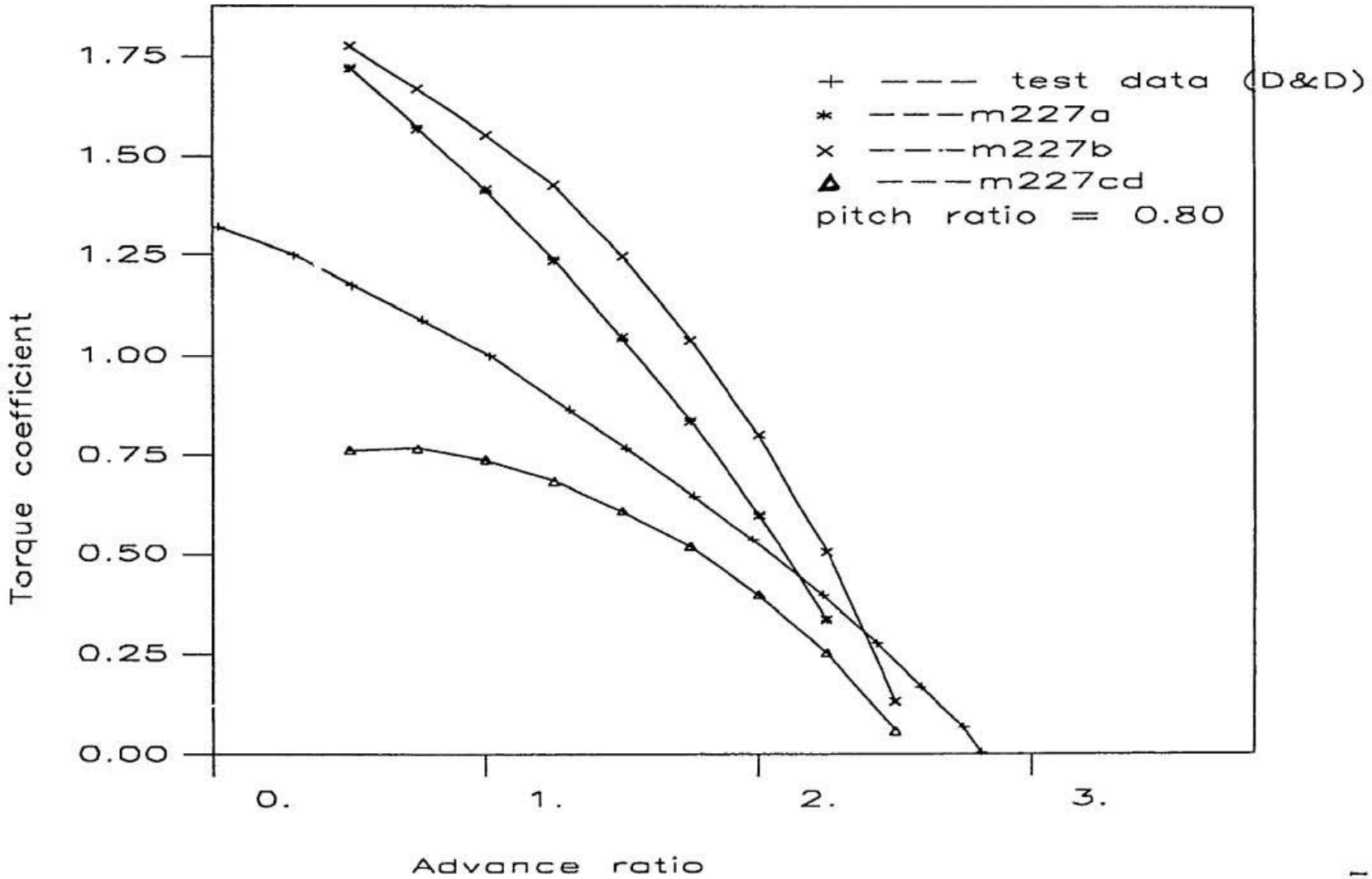


Figure E-5: Comparison of theoretical results with test results — torque coefficient(pitch ratio=0.8π)

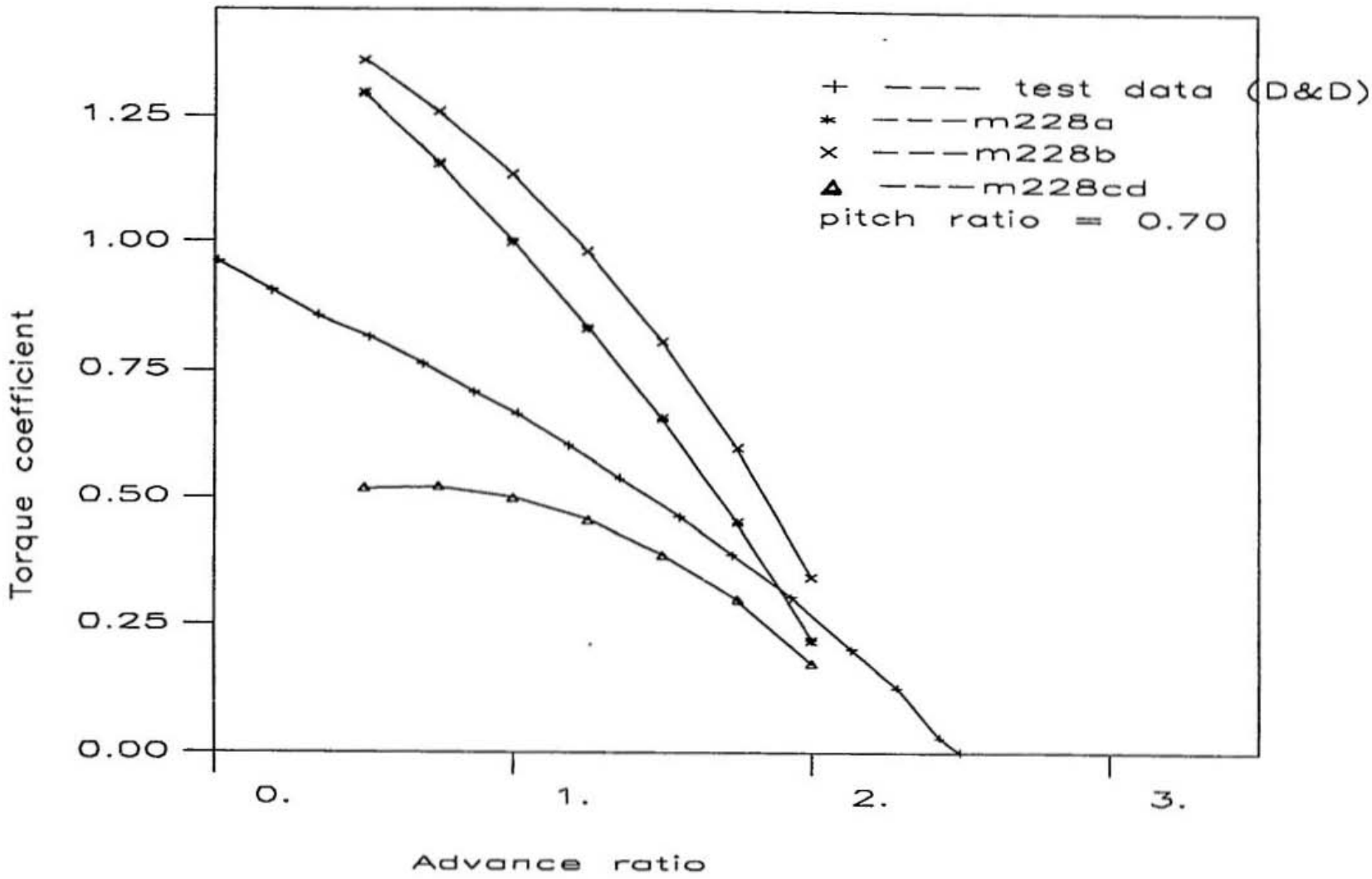


Figure E-4: Comparison of theoretical results with test results — torque coefficient(pitch ratio=0.7π)

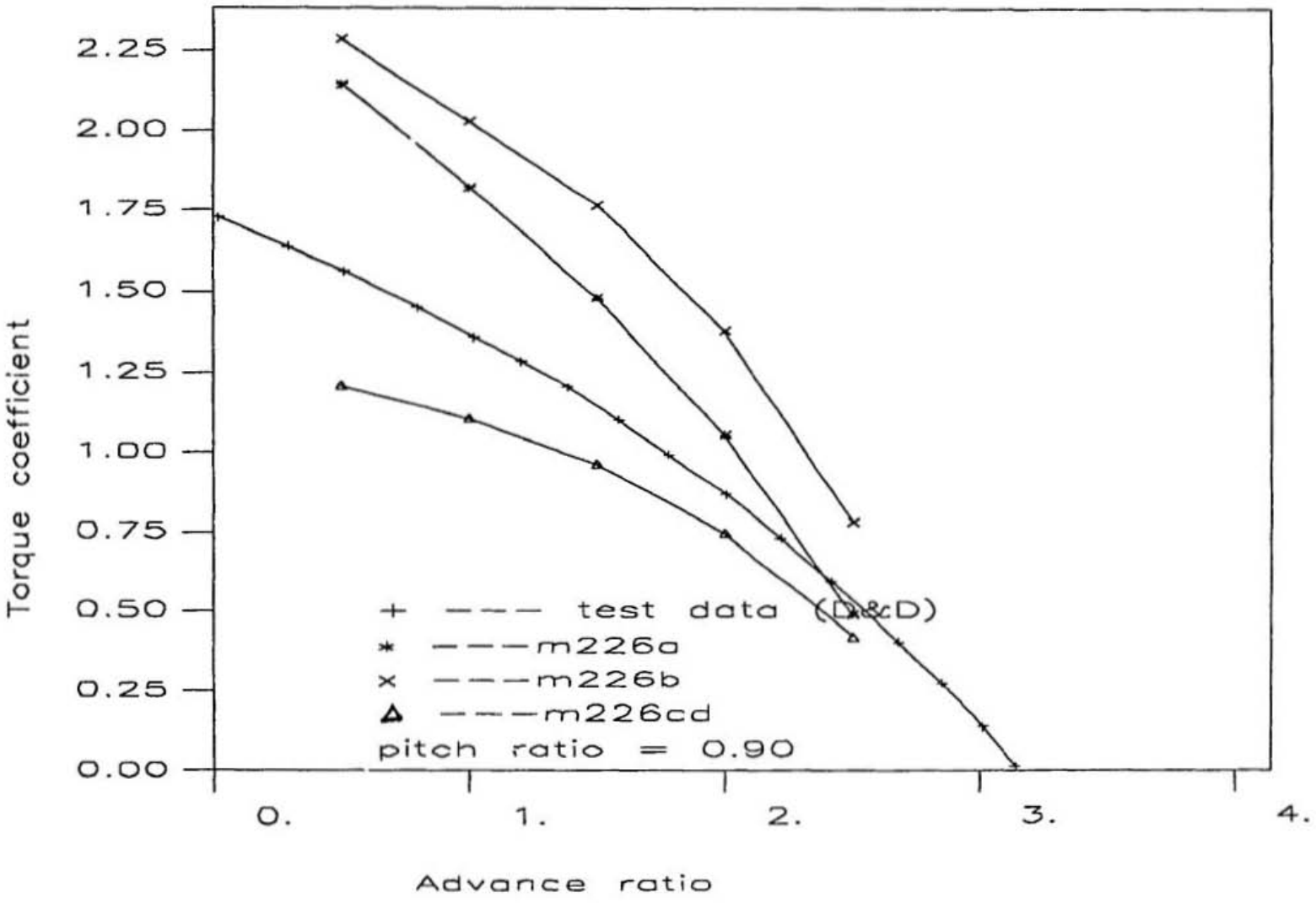


Figure E-6: Comparison of theoretical results with test results — torque coefficient(pitch ratio=0.9π)

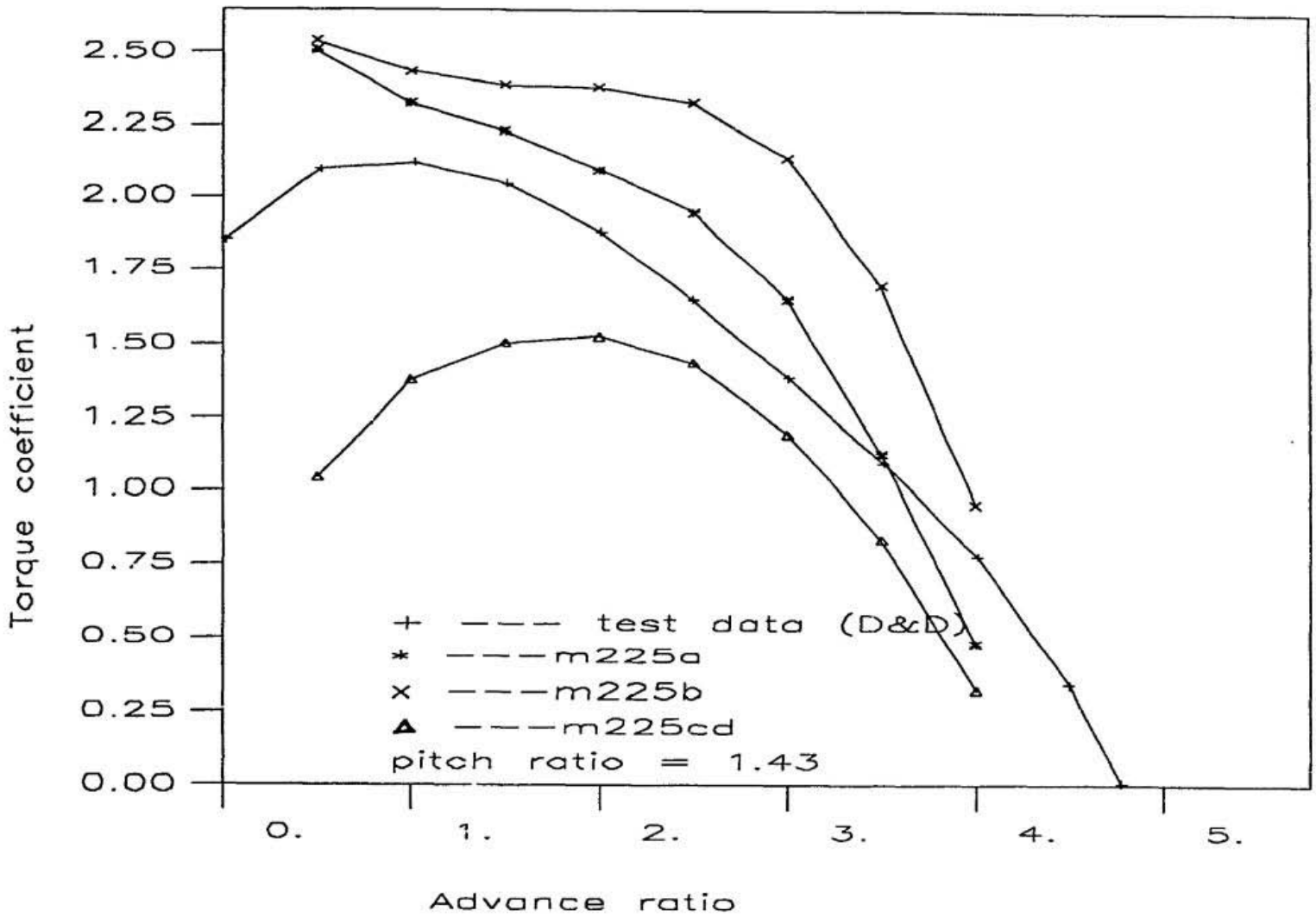


Figure E-7: Comparison of theoretical results with test results — torque coefficient(pitch ratio=1.429π)

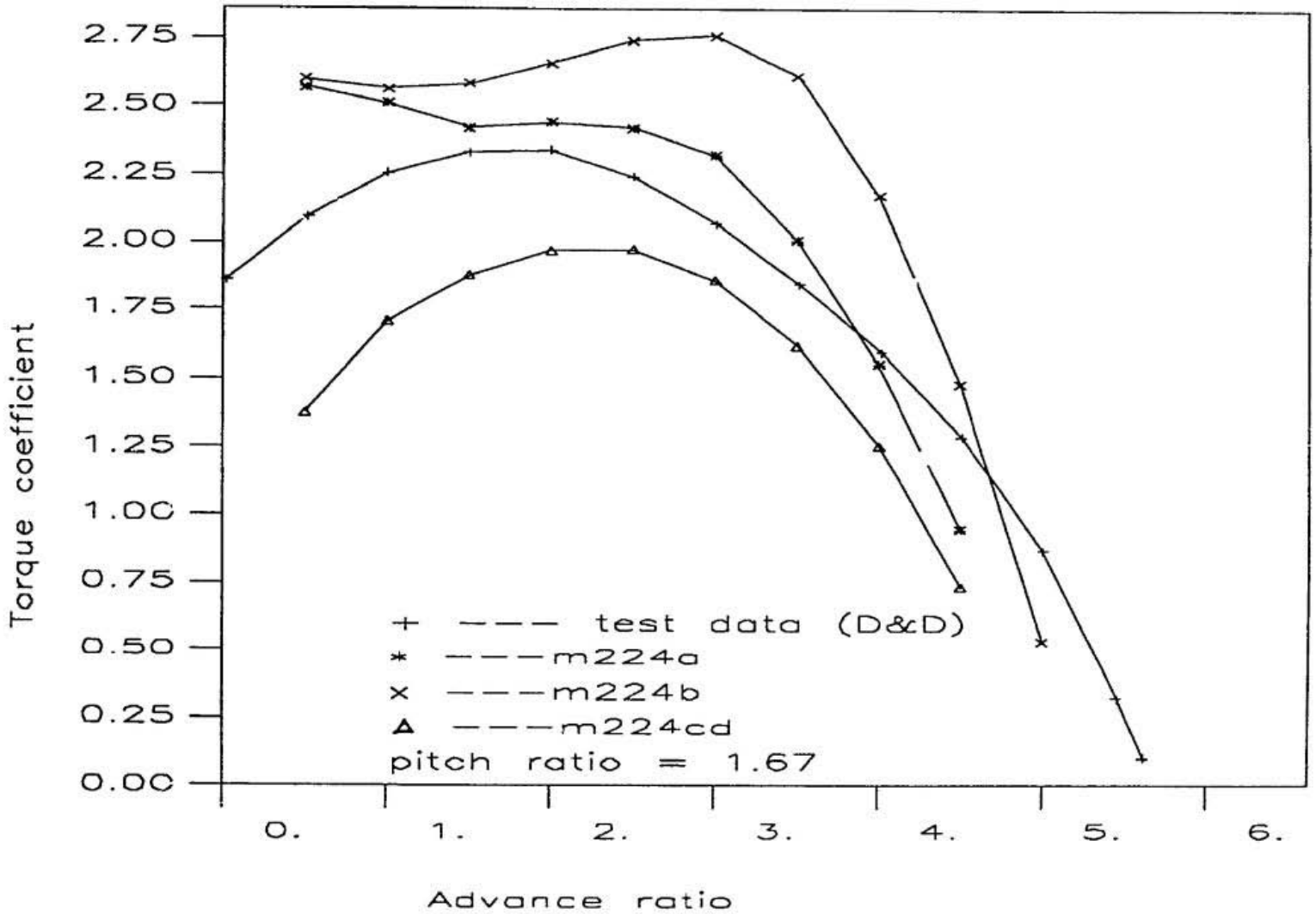


Figure E-8: Comparison of theoretical results with test results — torque coefficient(pitch ratio=1.667π)

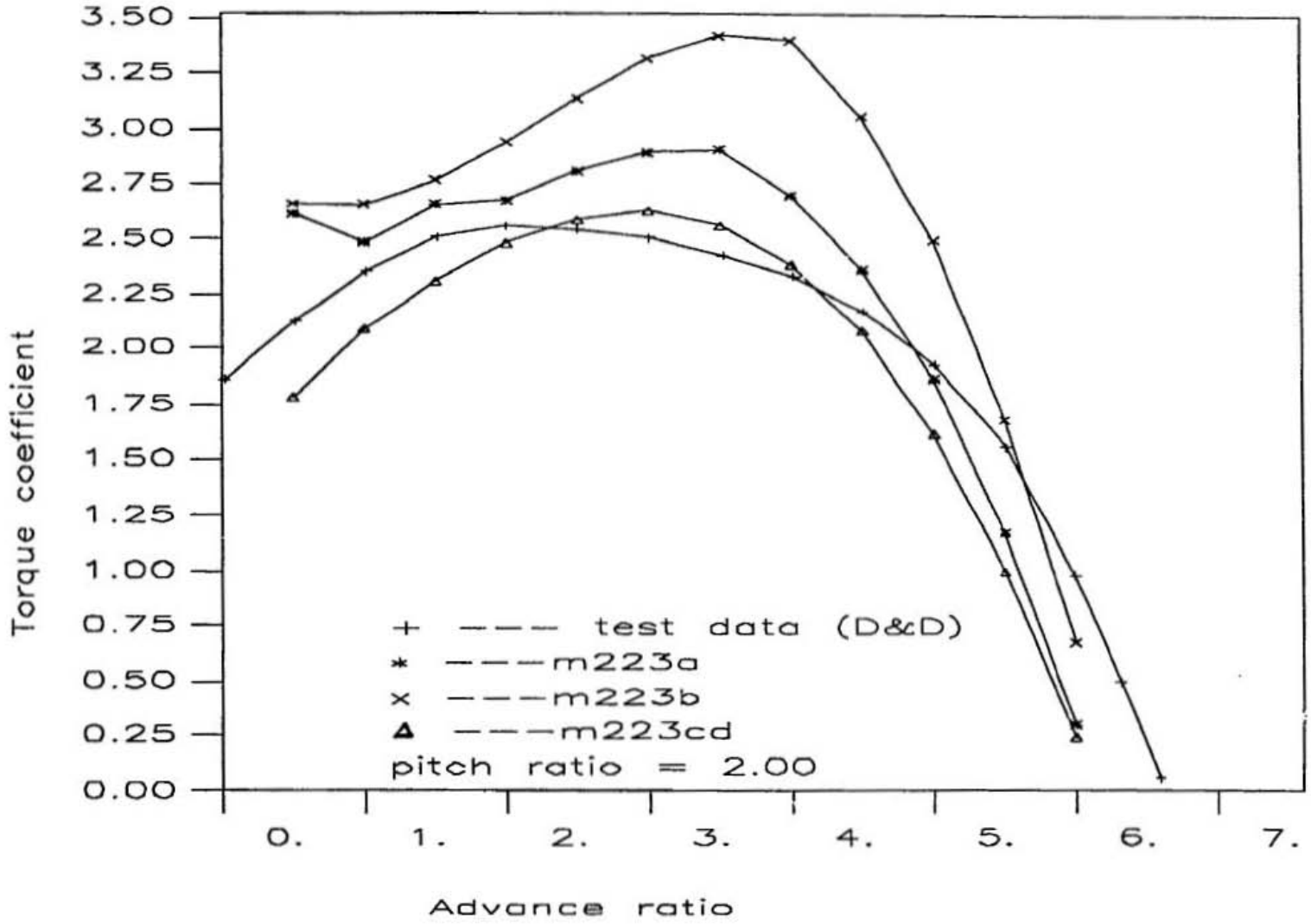


Figure E-9: Comparison of theoretical results with test results — torque coefficient(pitch ratio=2.000π)

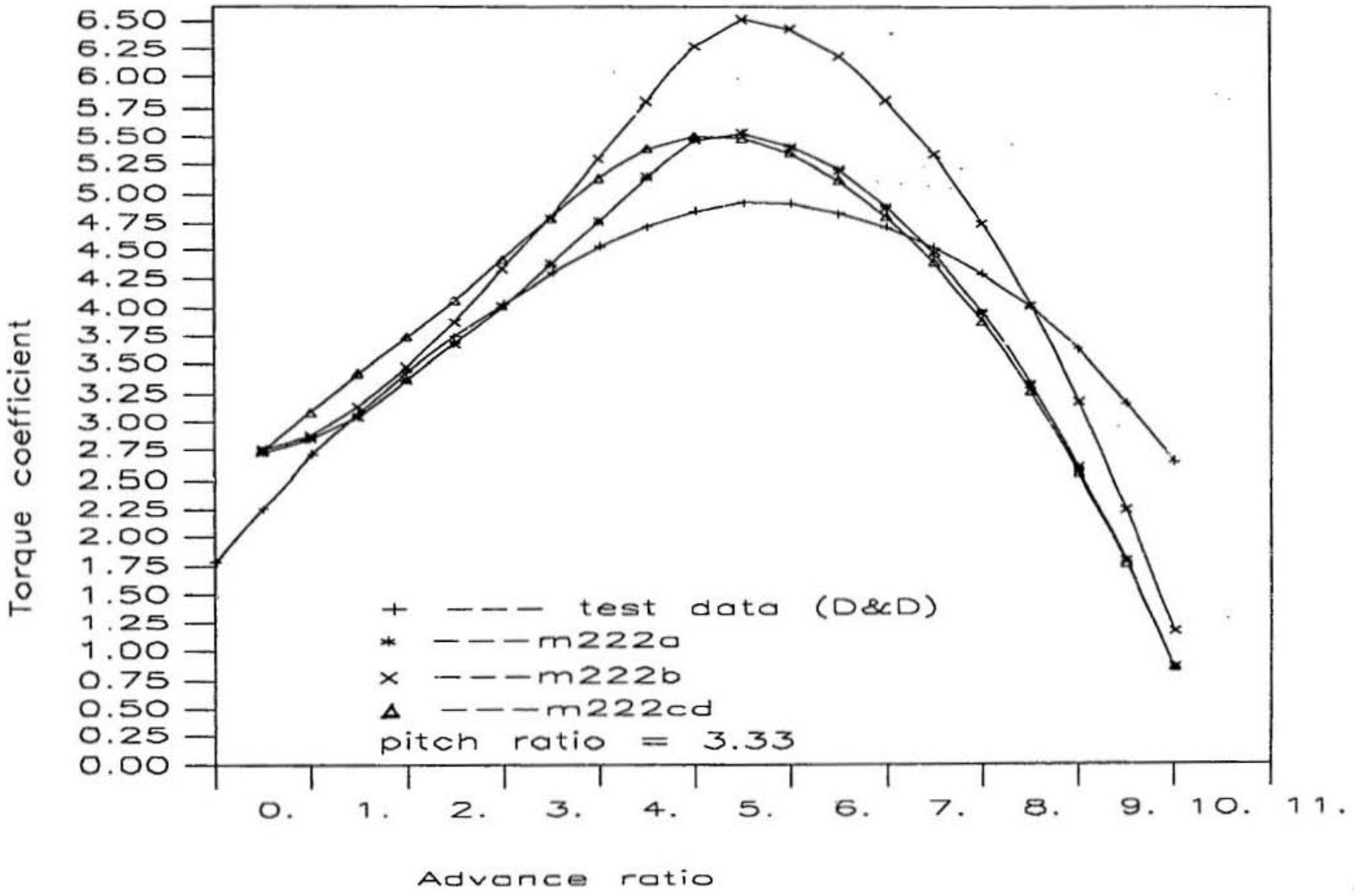


Figure E-10: Comparison of theoretical results with test results — torque coefficient(pitch ratio=3.333π)

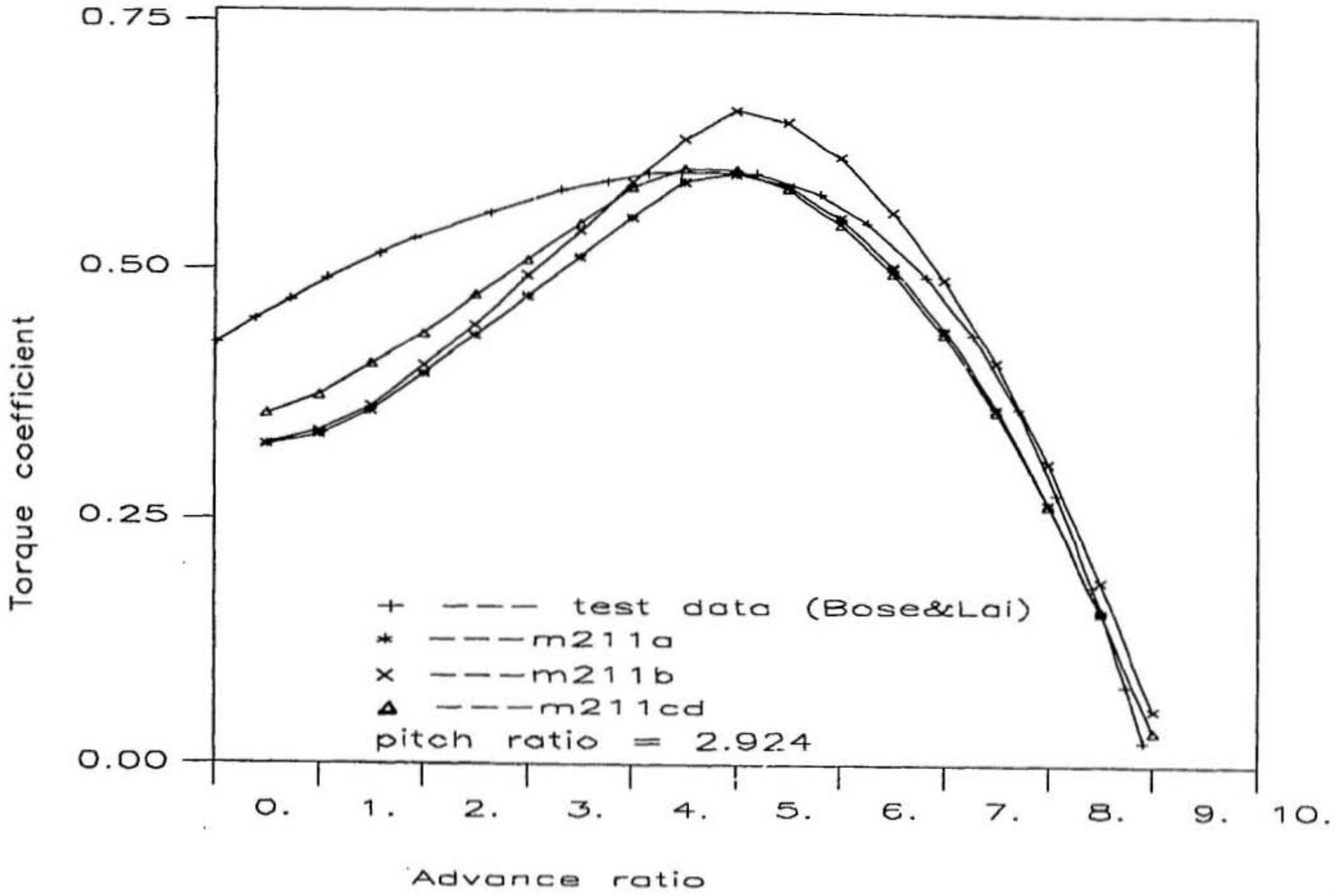


Figure E-11: Comparison of theoretical results with test results — torque coefficient(pitch ratio=2.924π)

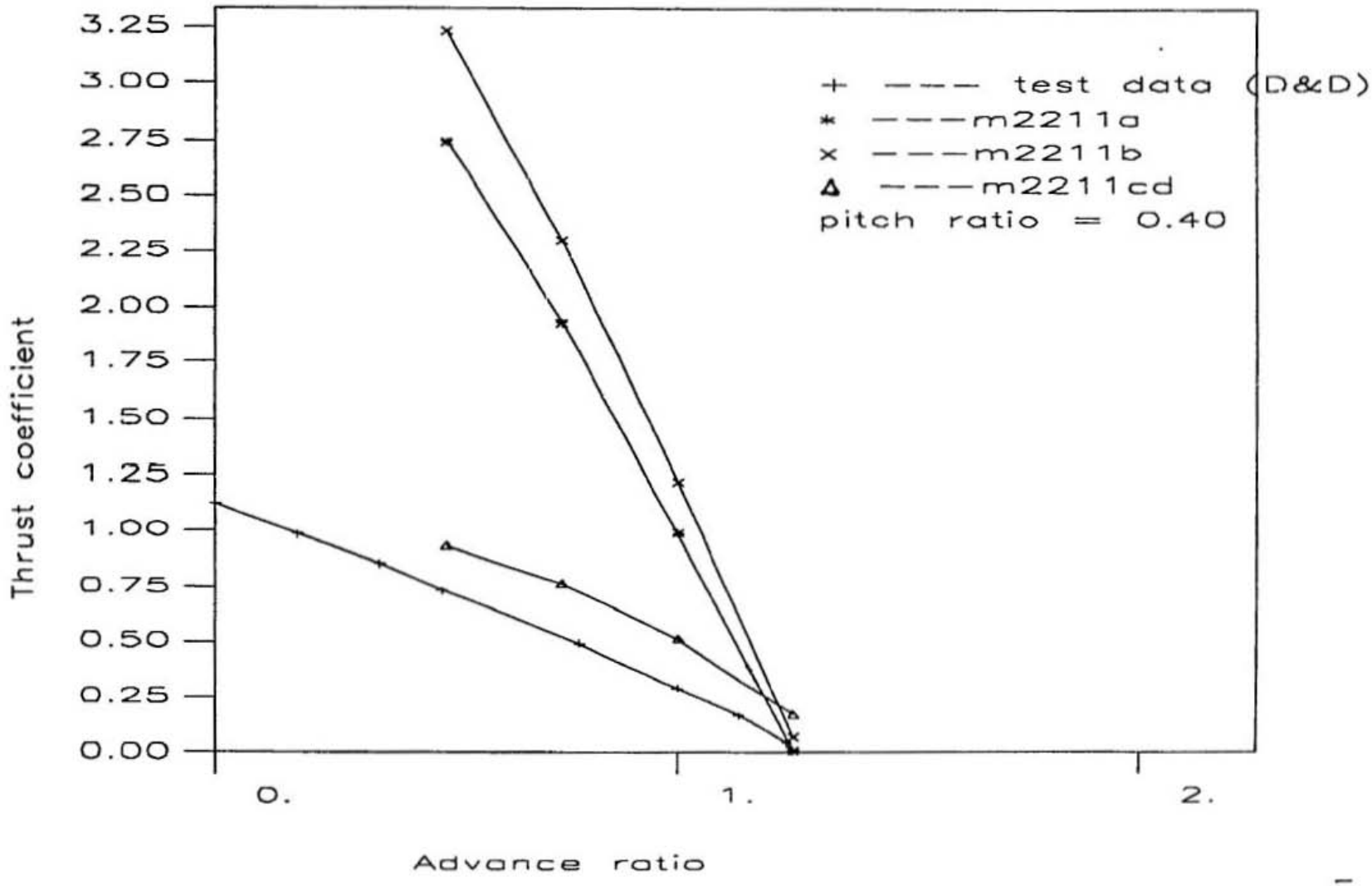


Figure E-12: Comparison of theoretical results with test results – thrust coefficient(pitch ratio=0.4π)

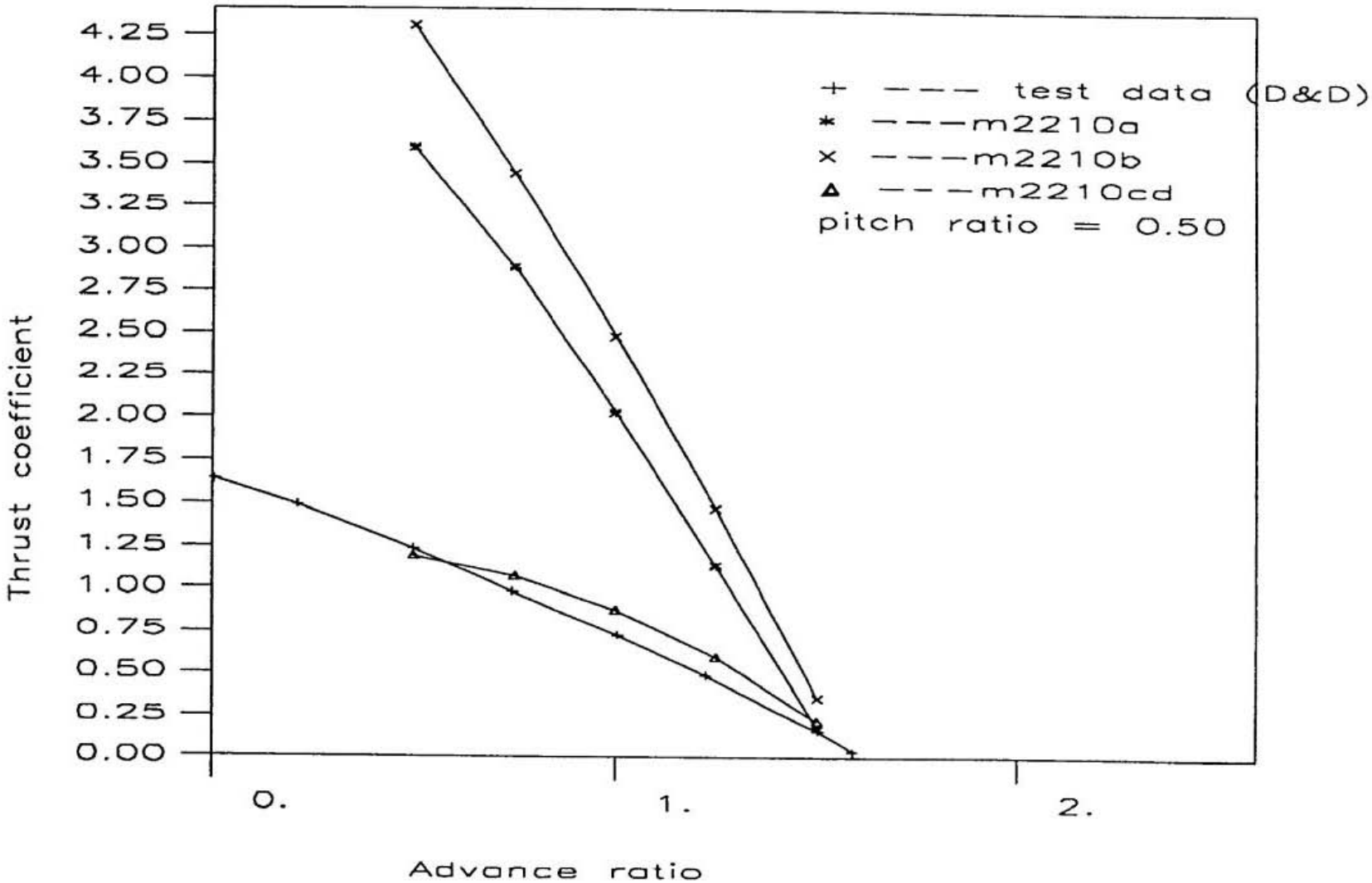


Figure E-13: Comparison of theoretical results with test results -- thrust coefficient(pitch ratio=0.5π)

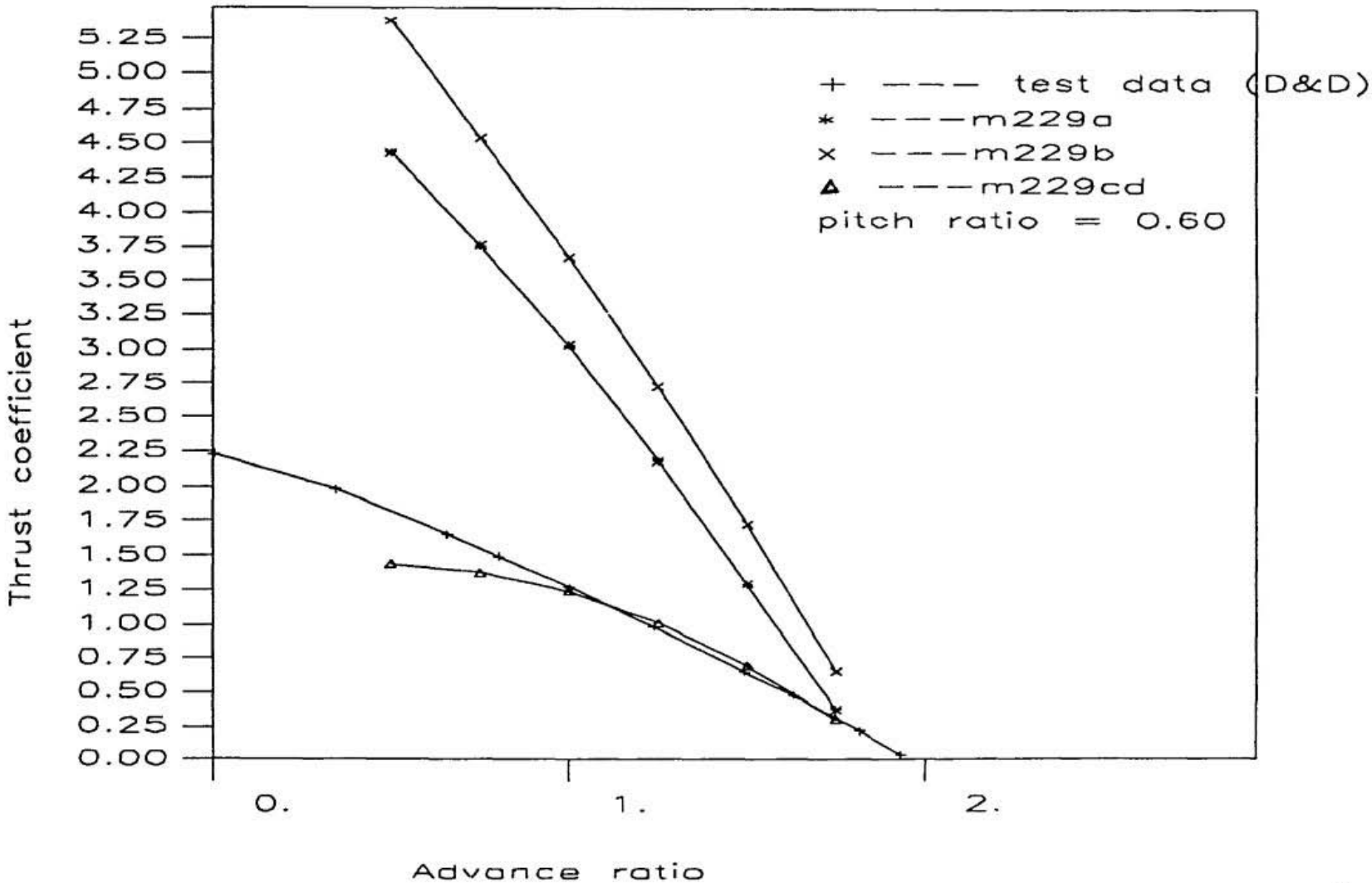
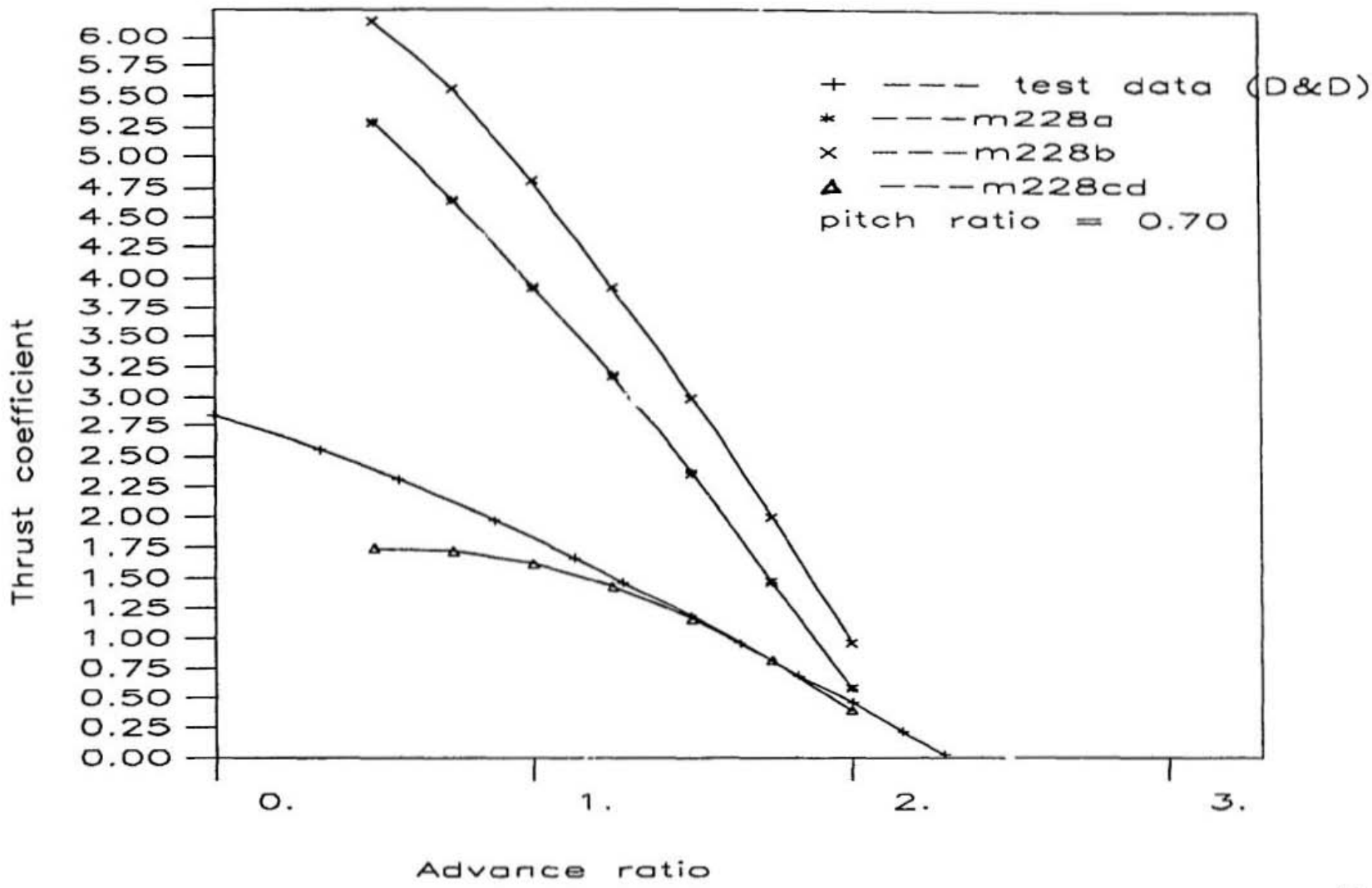


Figure E-14: Comparison of theoretical results with test results – thrust coefficient(pitch ratio=0.6π)



061

Figure E-15: Comparison of theoretical results with test results — thrust coefficient(pitch ratio=0.7π)

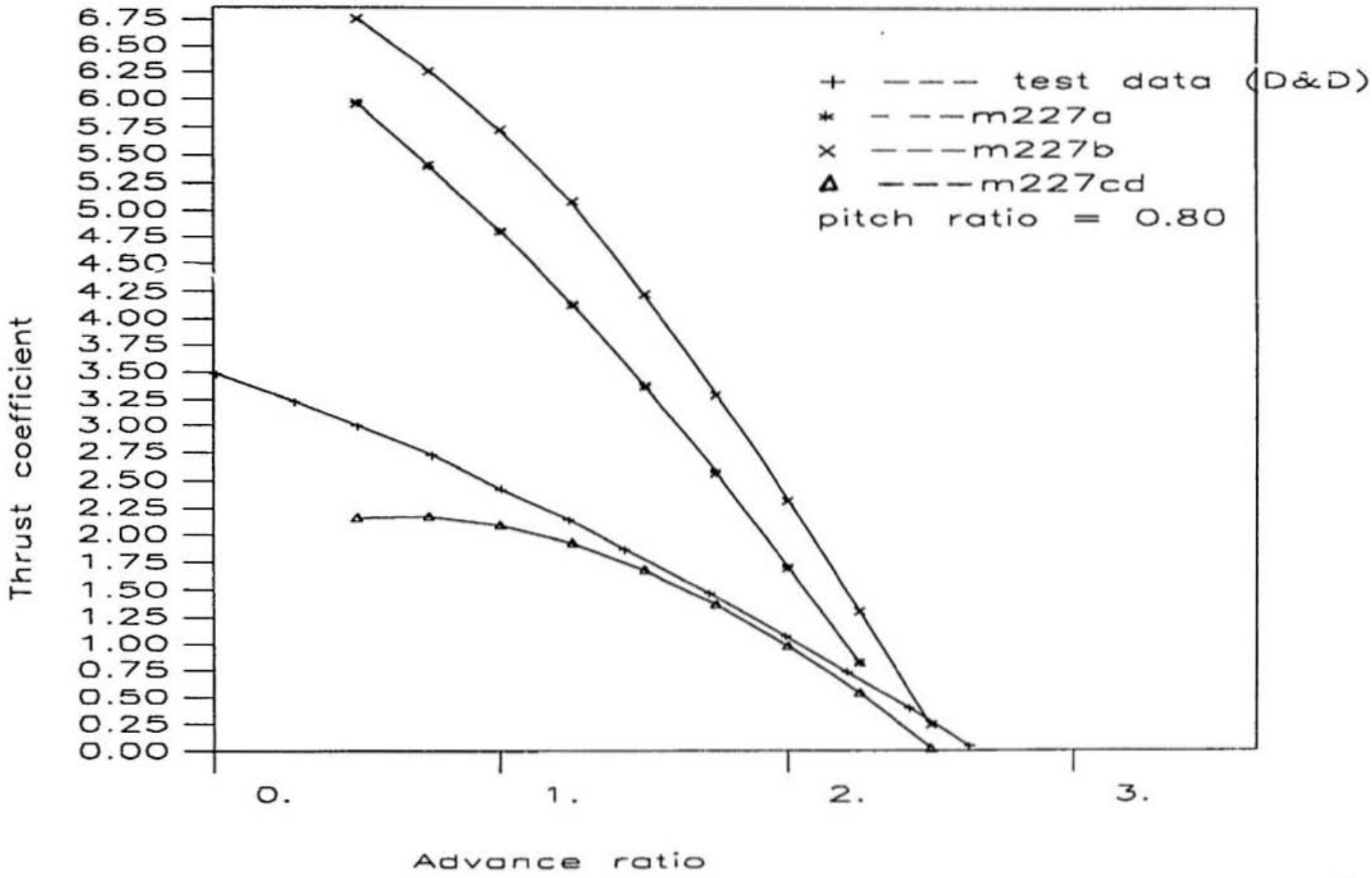


Figure E-16: Comparison of theoretical results with test results — thrust coefficient(pitch ratio=0.8π)

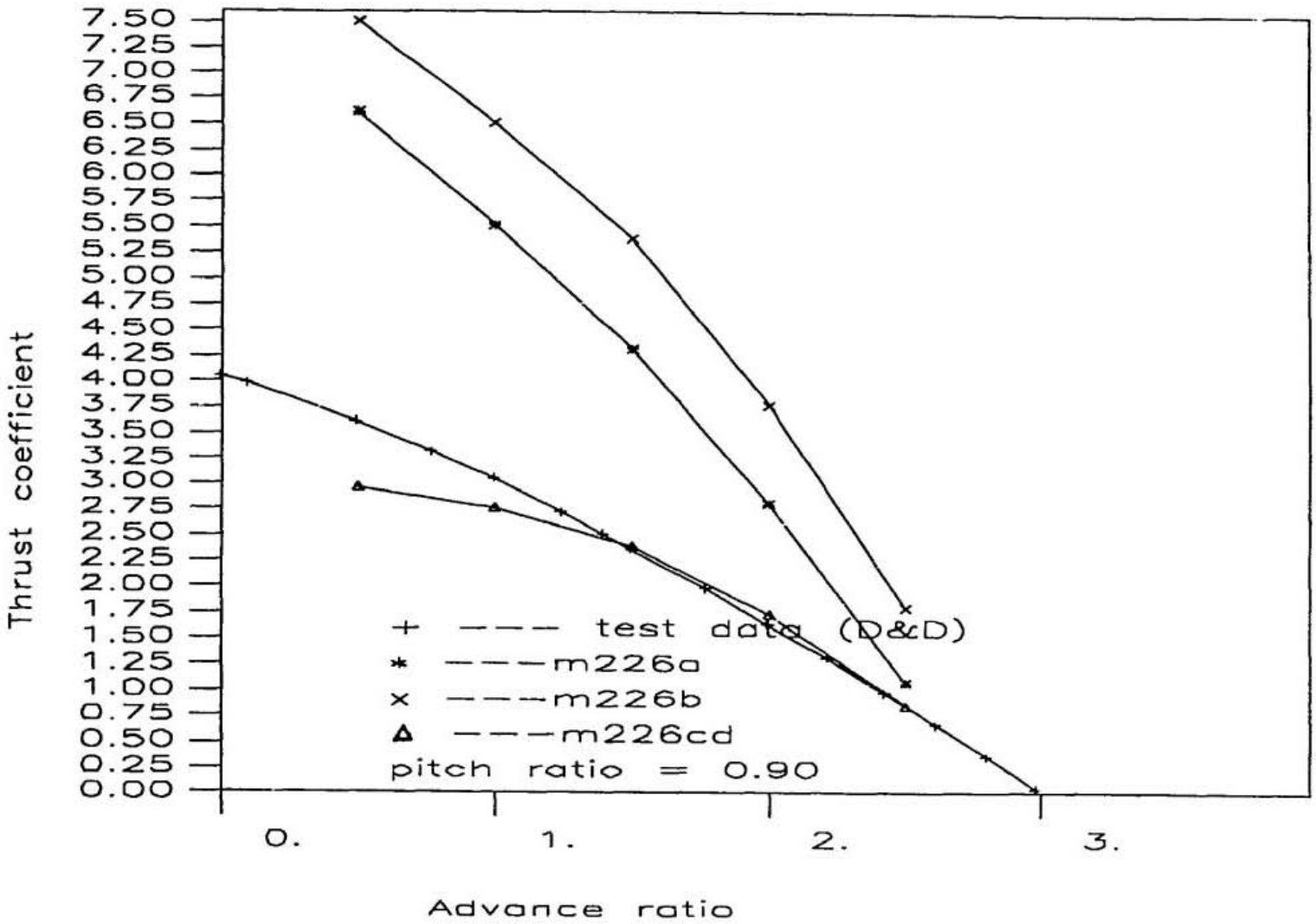


Figure E-17: Comparison of theoretical results with test results — thrust coefficient(pitch ratio=0.9π)

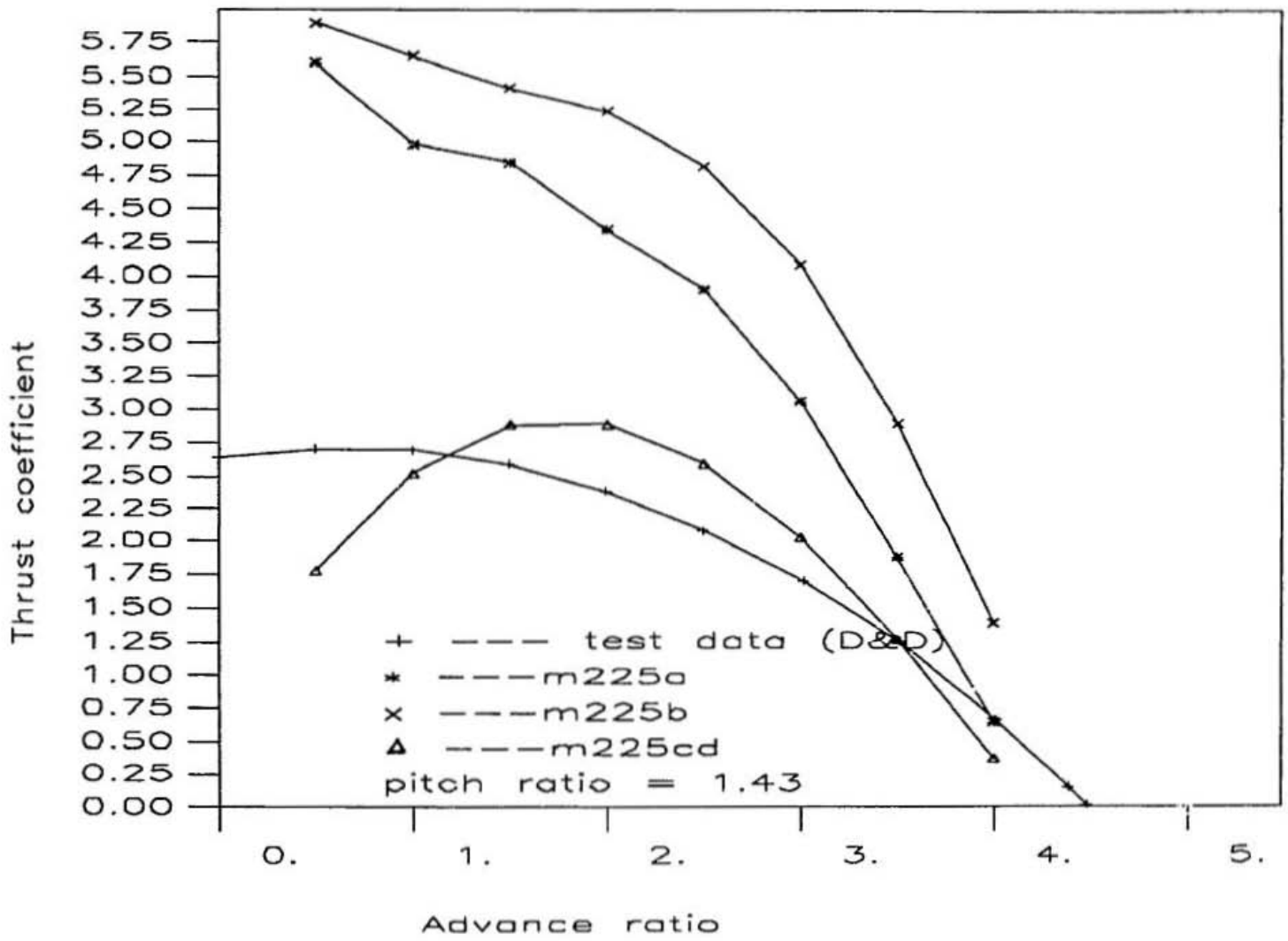


Figure E-18: Comparison of theoretical results with test results — thrust coefficient(pitch ratio=1.429π)

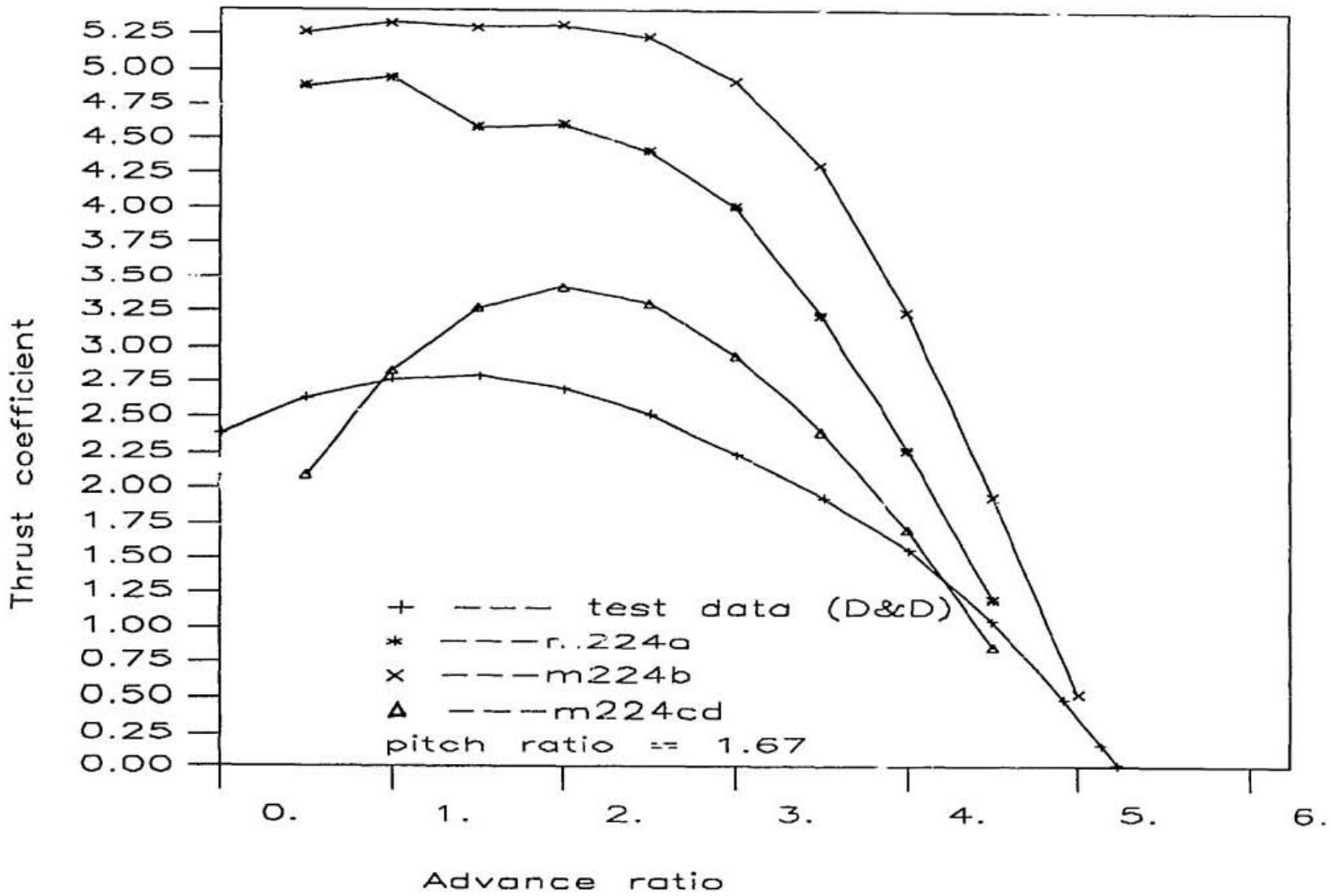


Figure E-19: Comparison of theoretical results with test results — thrust coefficient(pitch ratio=1.667π)

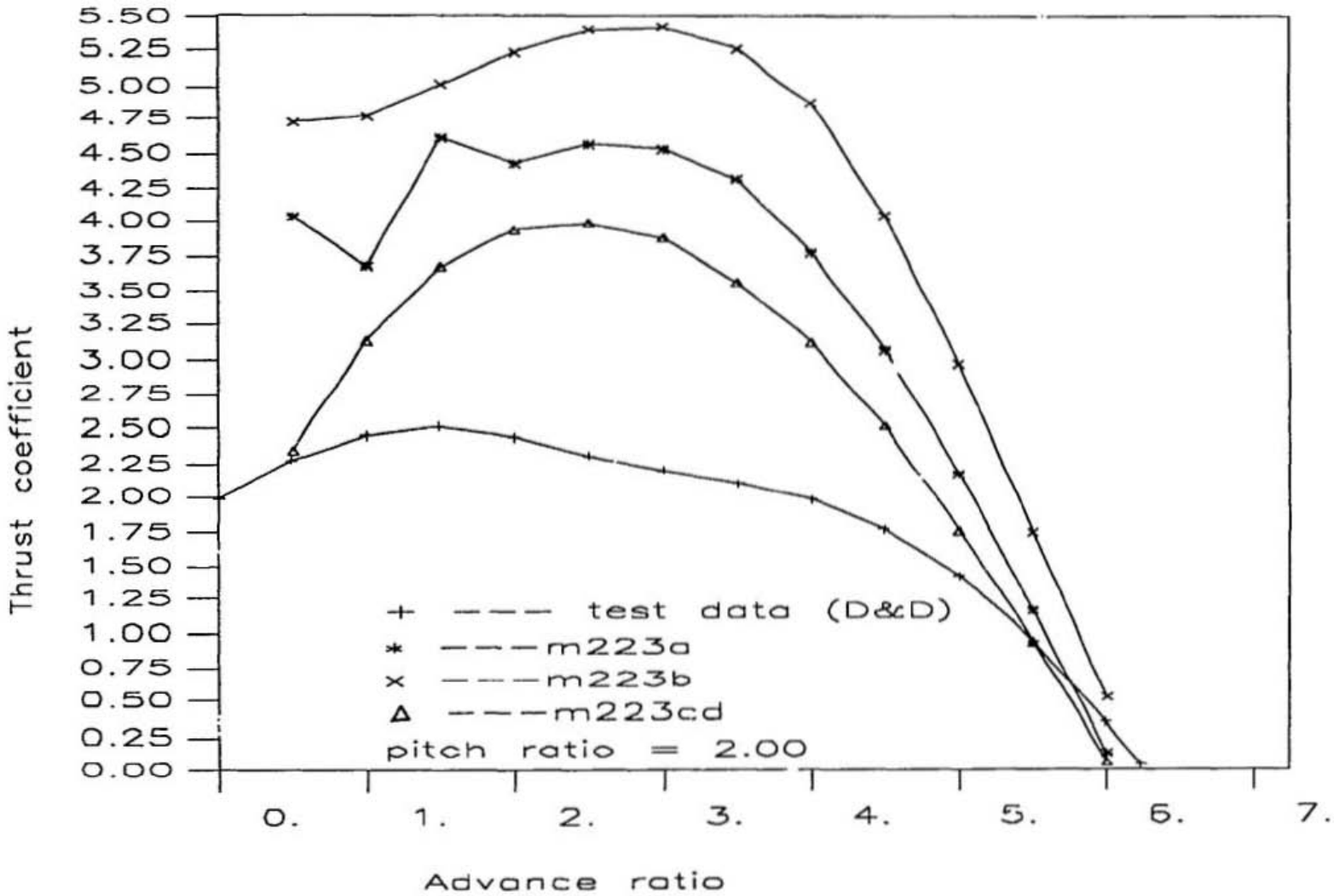


Figure E-20: Comparison of theoretical results with test results — thrust coefficient(pitch ratio=2.000π)

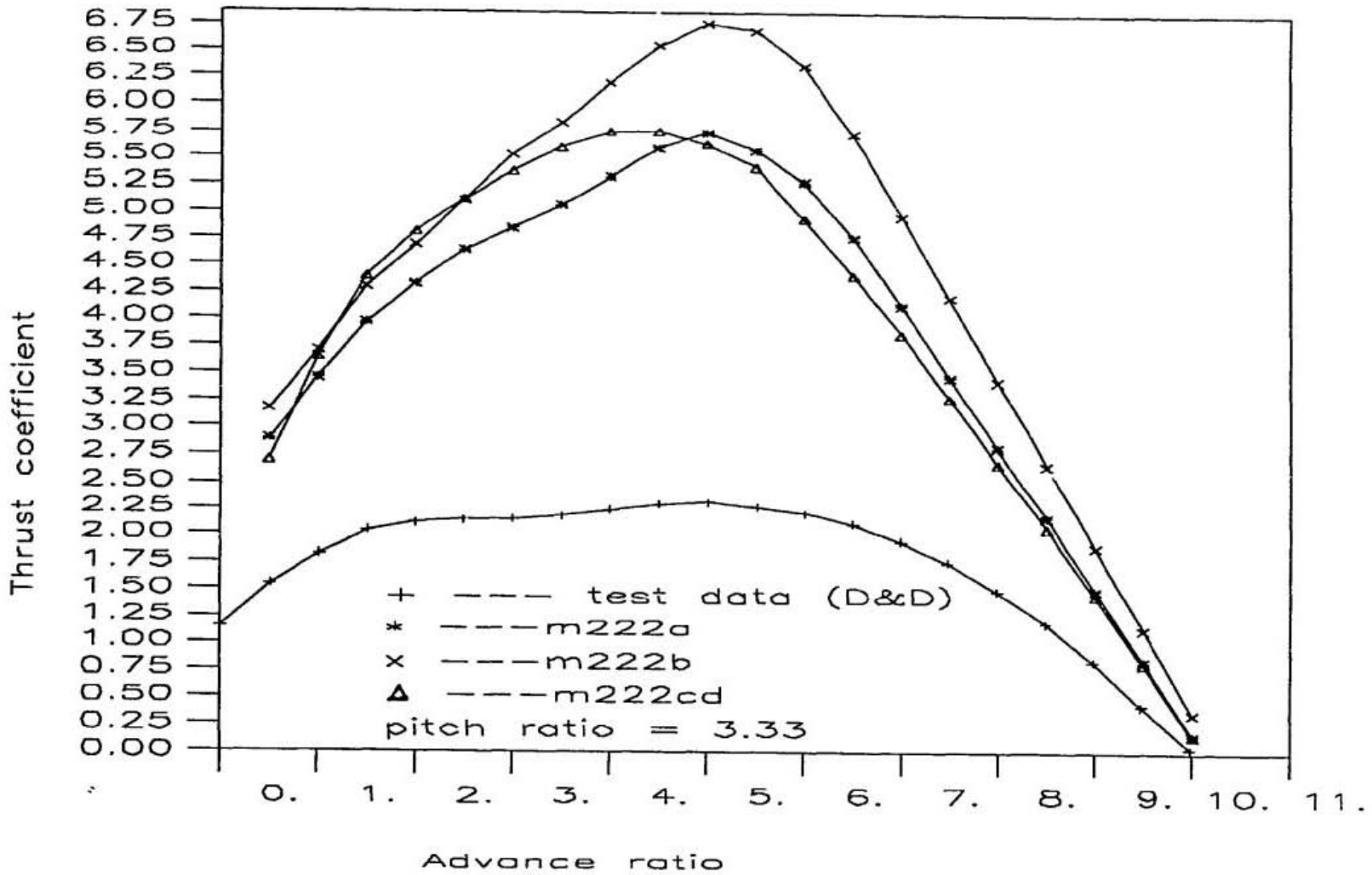


Figure E-21: Comparison of theoretical results with test results — thrust coefficient(pitch ratio=3.333π)

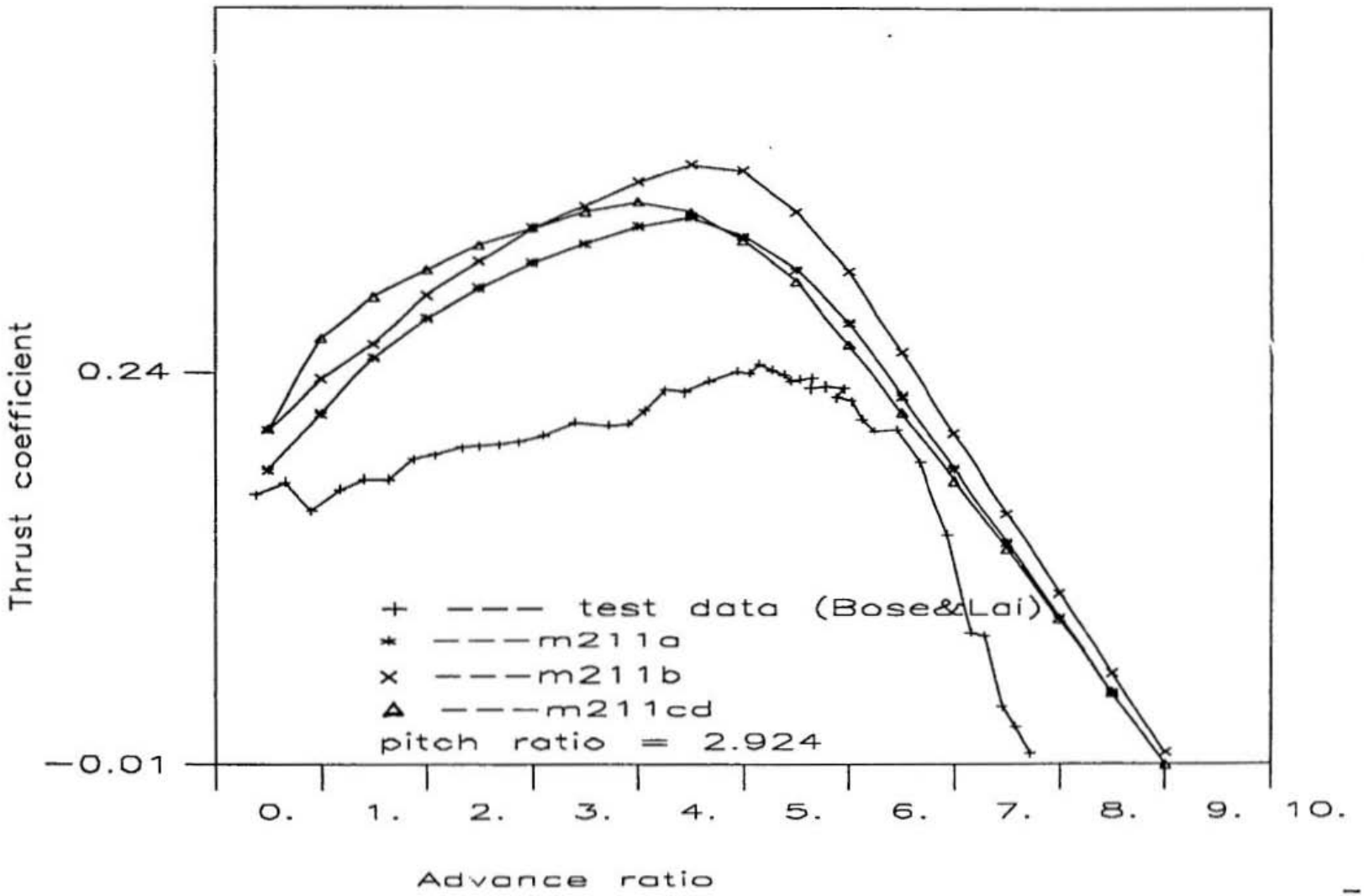


Figure E-22: Comparison of theoretical results with test results — thrust coefficient(pitch ratio=2.924π)

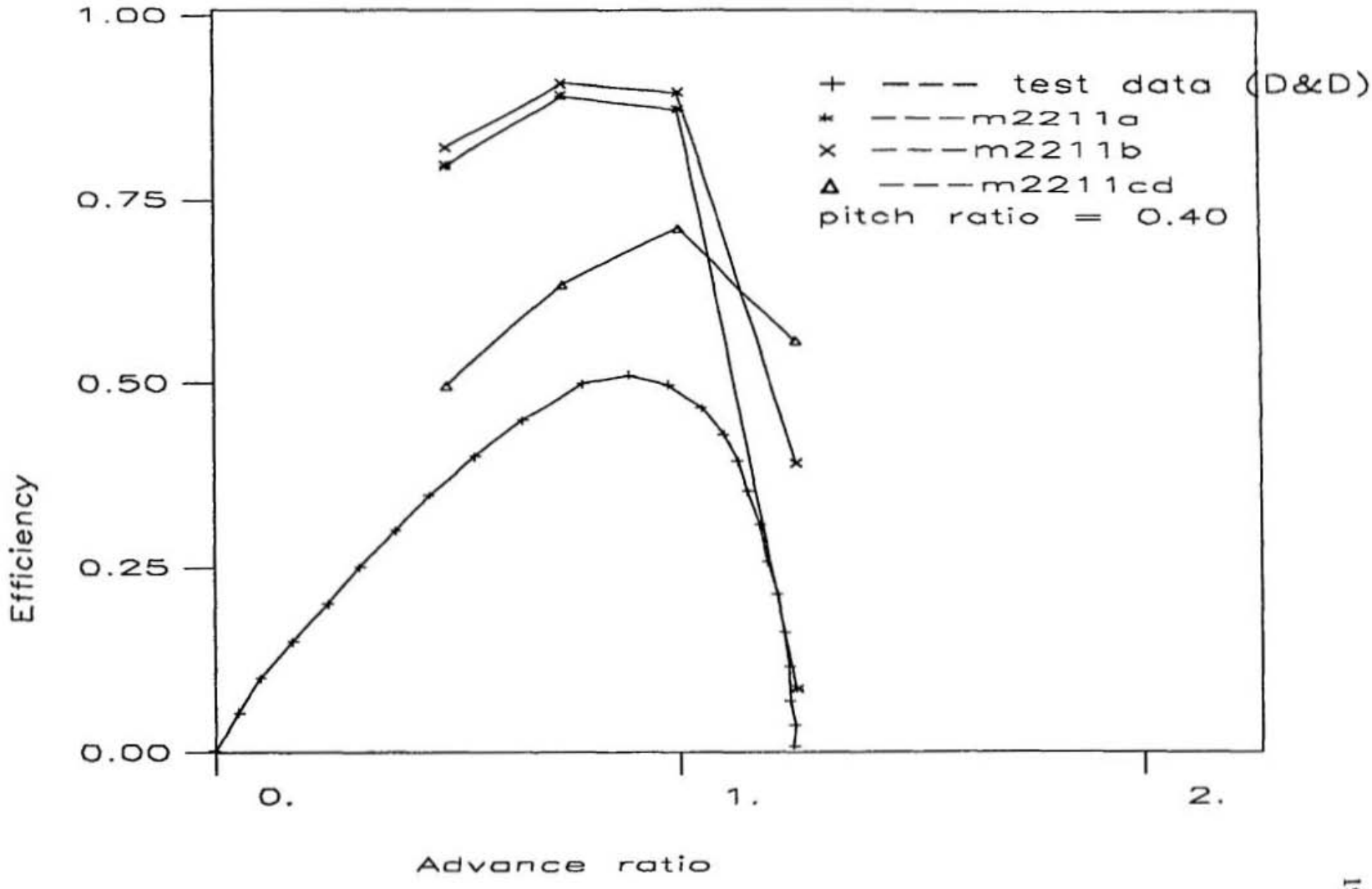


Figure E-23: Comparison of theoretical results with test results — efficiency(pitch ratio=0.4π)

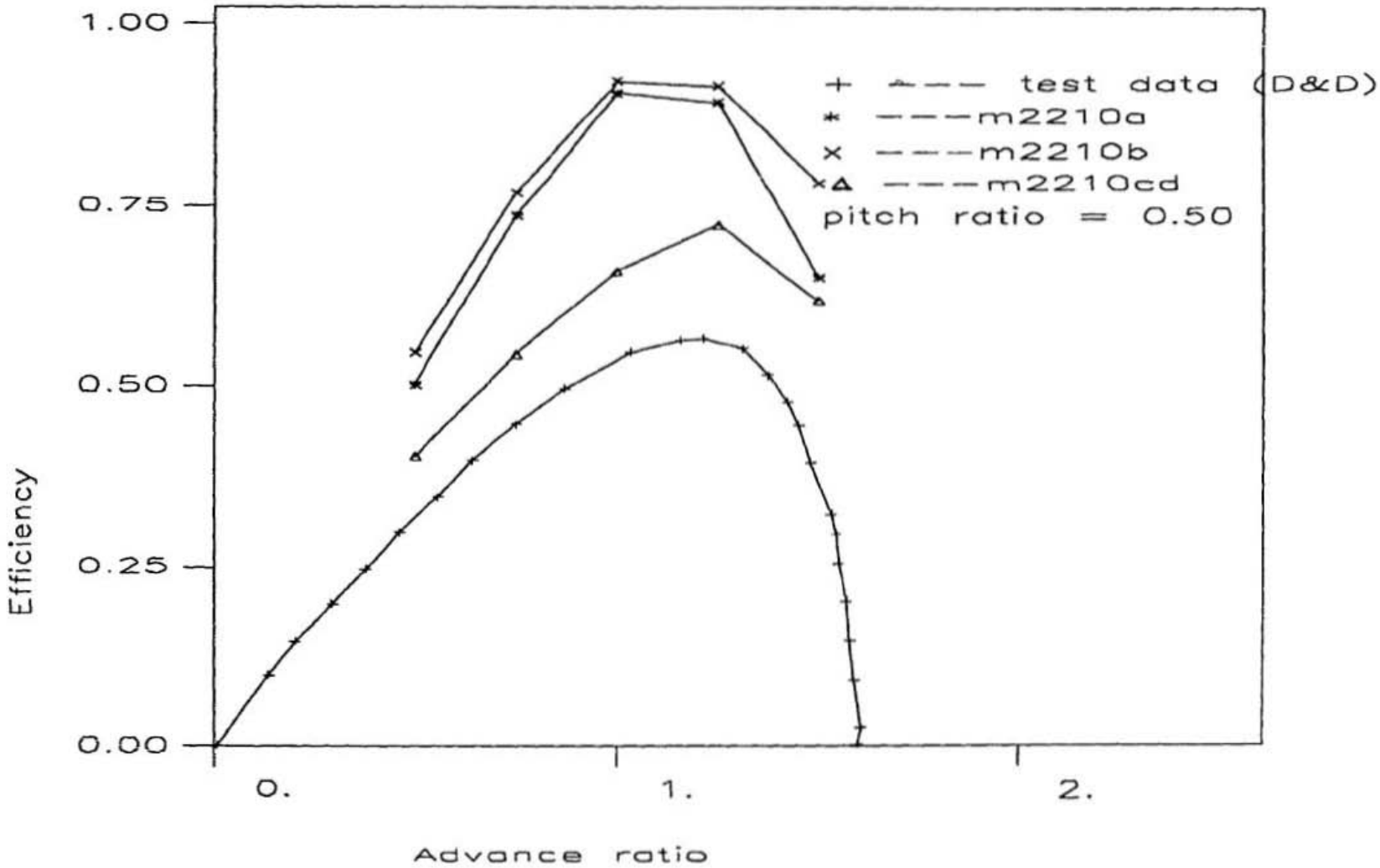


Figure E-24: Comparison of theoretical results with test results — efficiency(pitch ratio=0.5π)

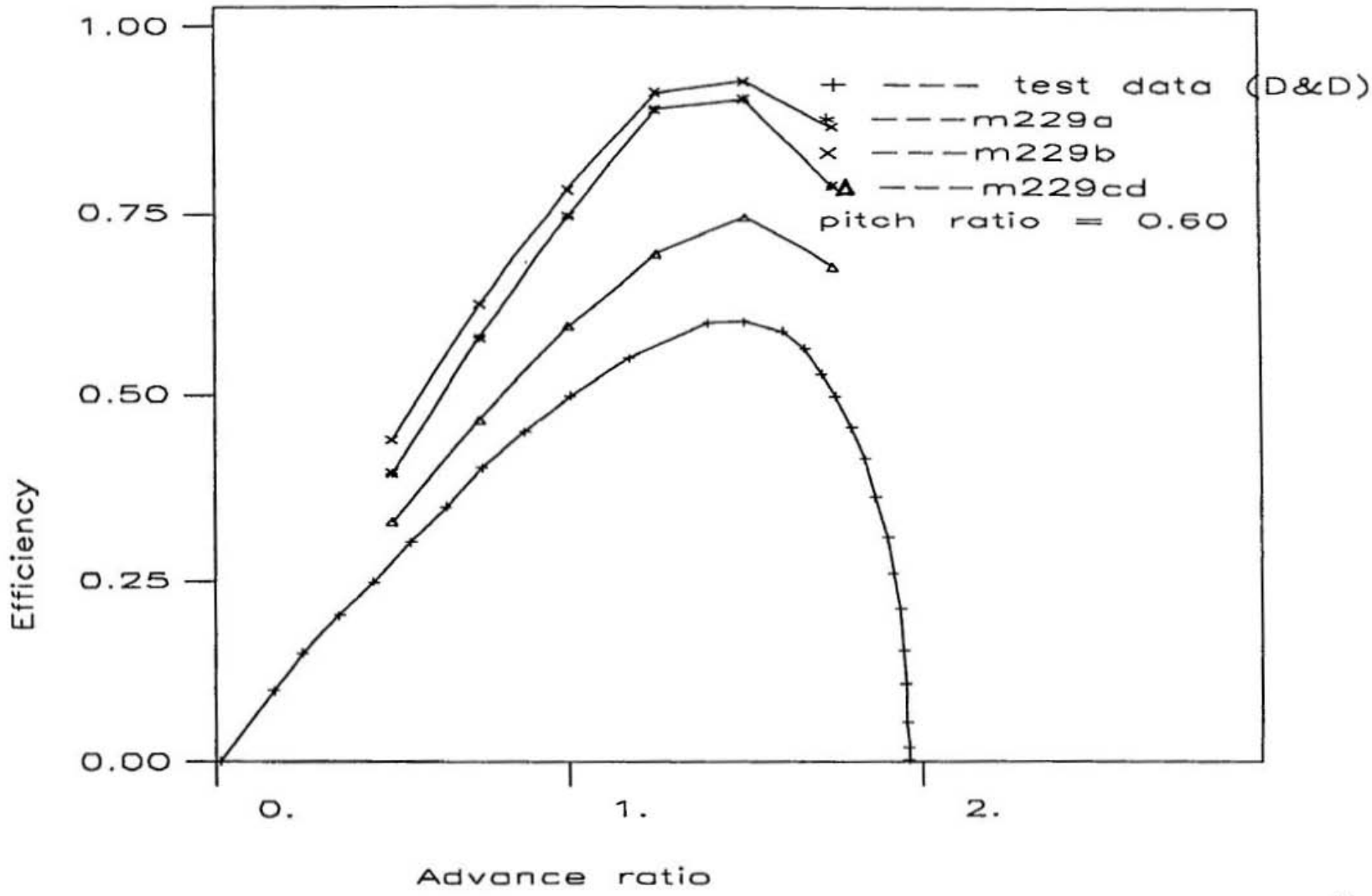


Figure E-25: Comparison of theoretical results with test results — efficiency(pitch ratio=0.6π)

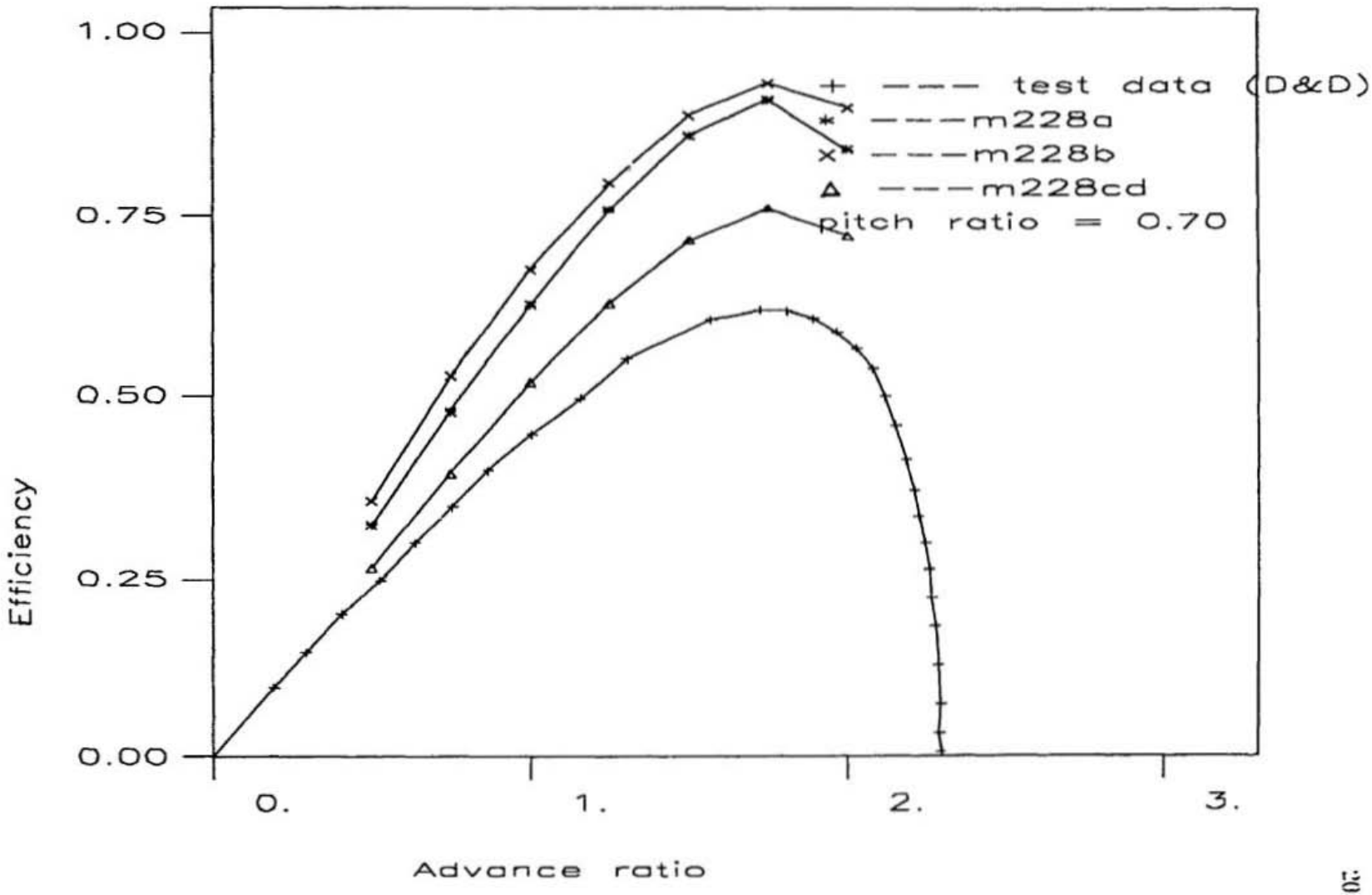


Figure E-26: Comparison of theoretical results with test results — efficiency(pitch ratio=0.7π)

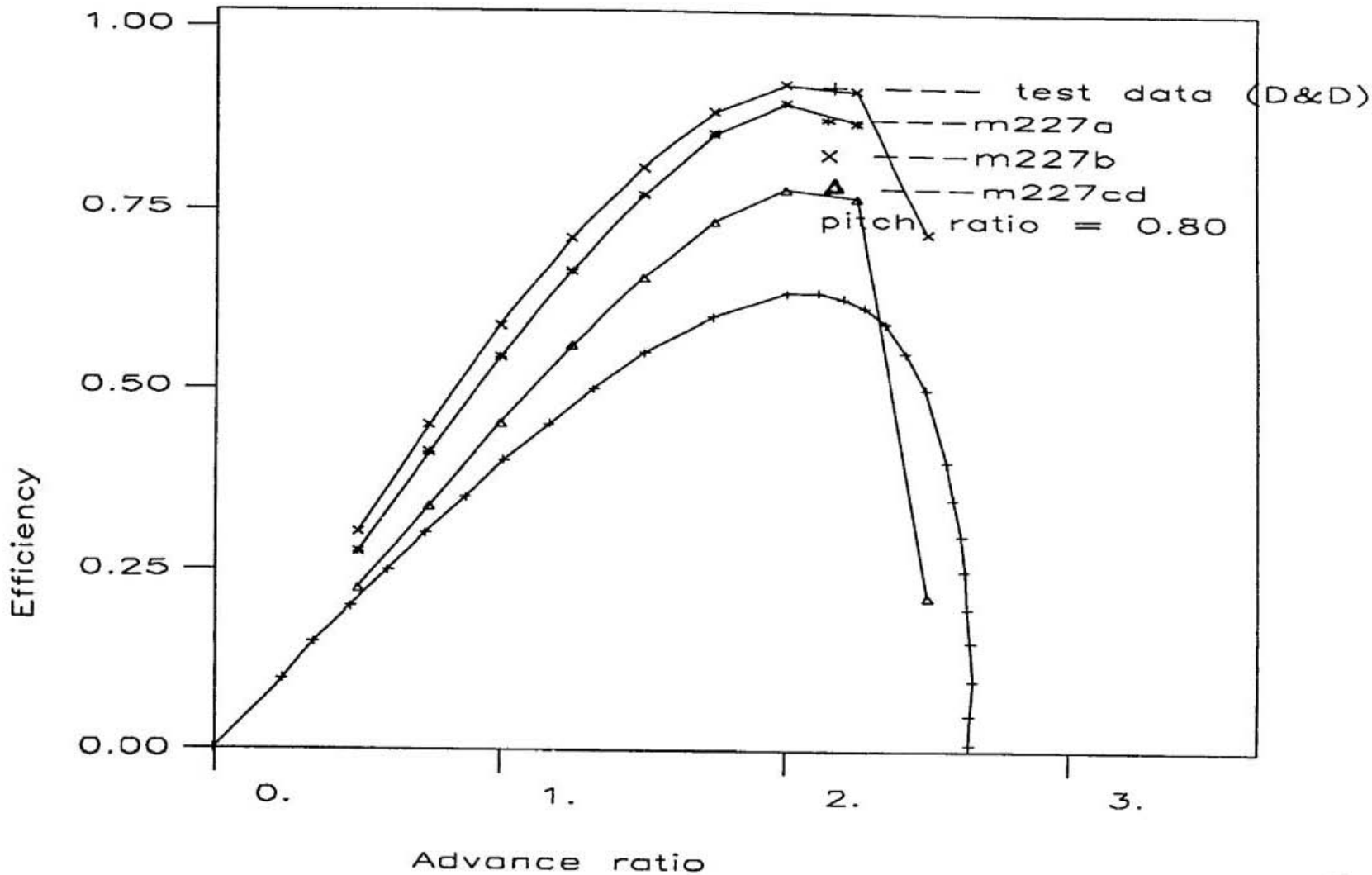


Figure E-27: Comparison of theoretical results with test results — efficiency(pitch ratio=0.8π)

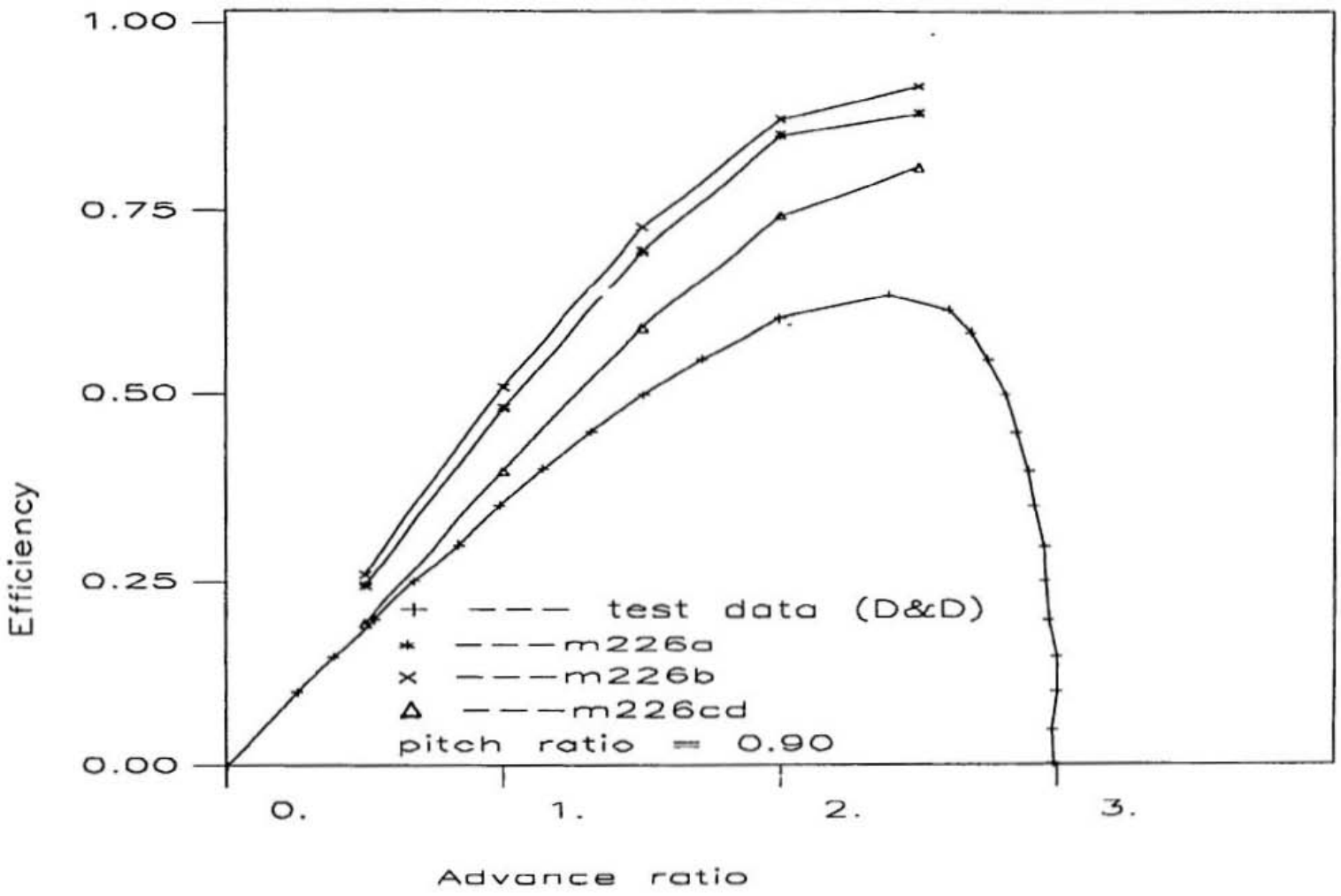


Figure E-28: Comparison of theoretical results with test results — efficiency(pitch ratio=0.9π)

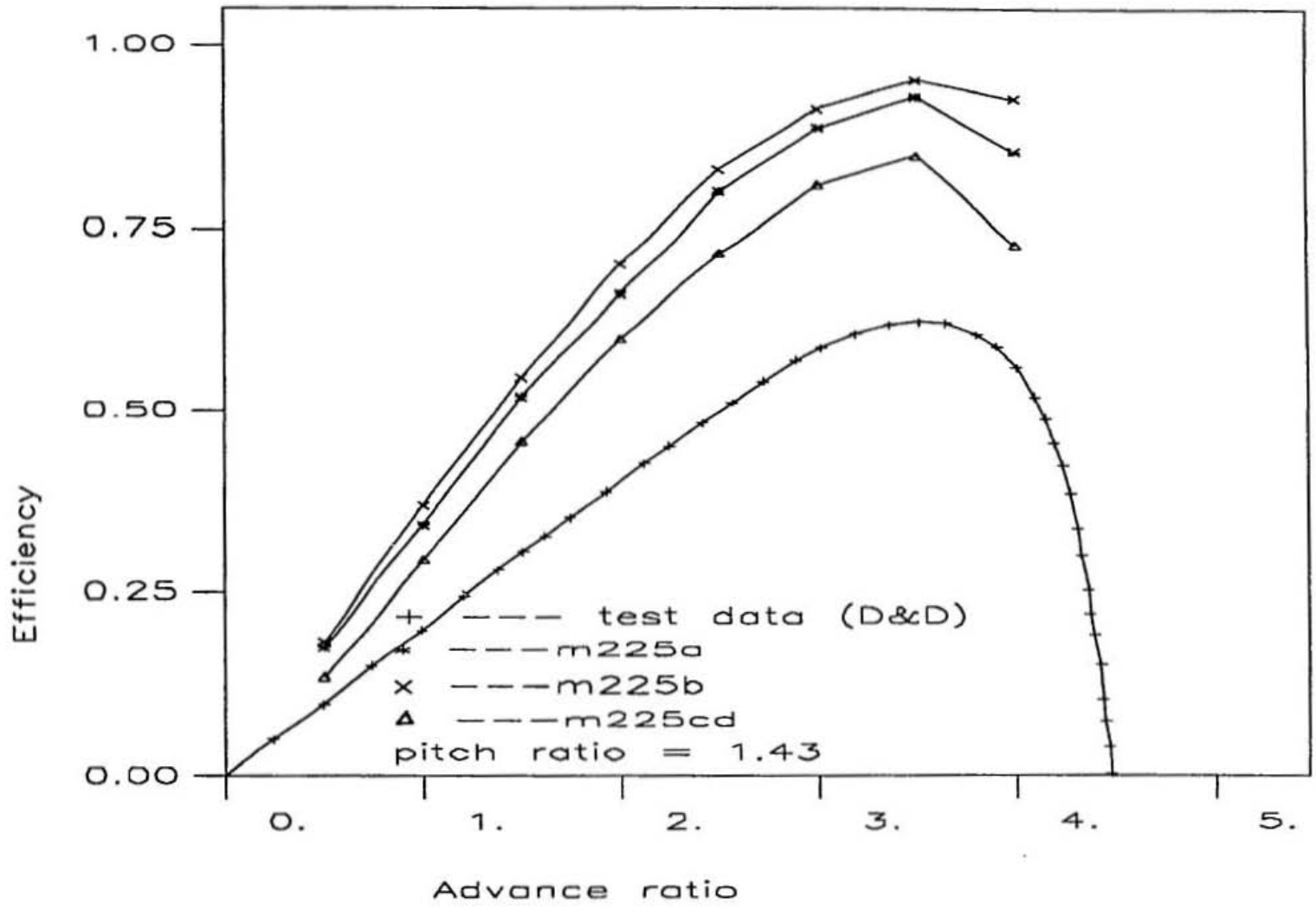


Figure E-29: Comparison of theoretical results with test results — efficiency(pitch ratio=1.429π)

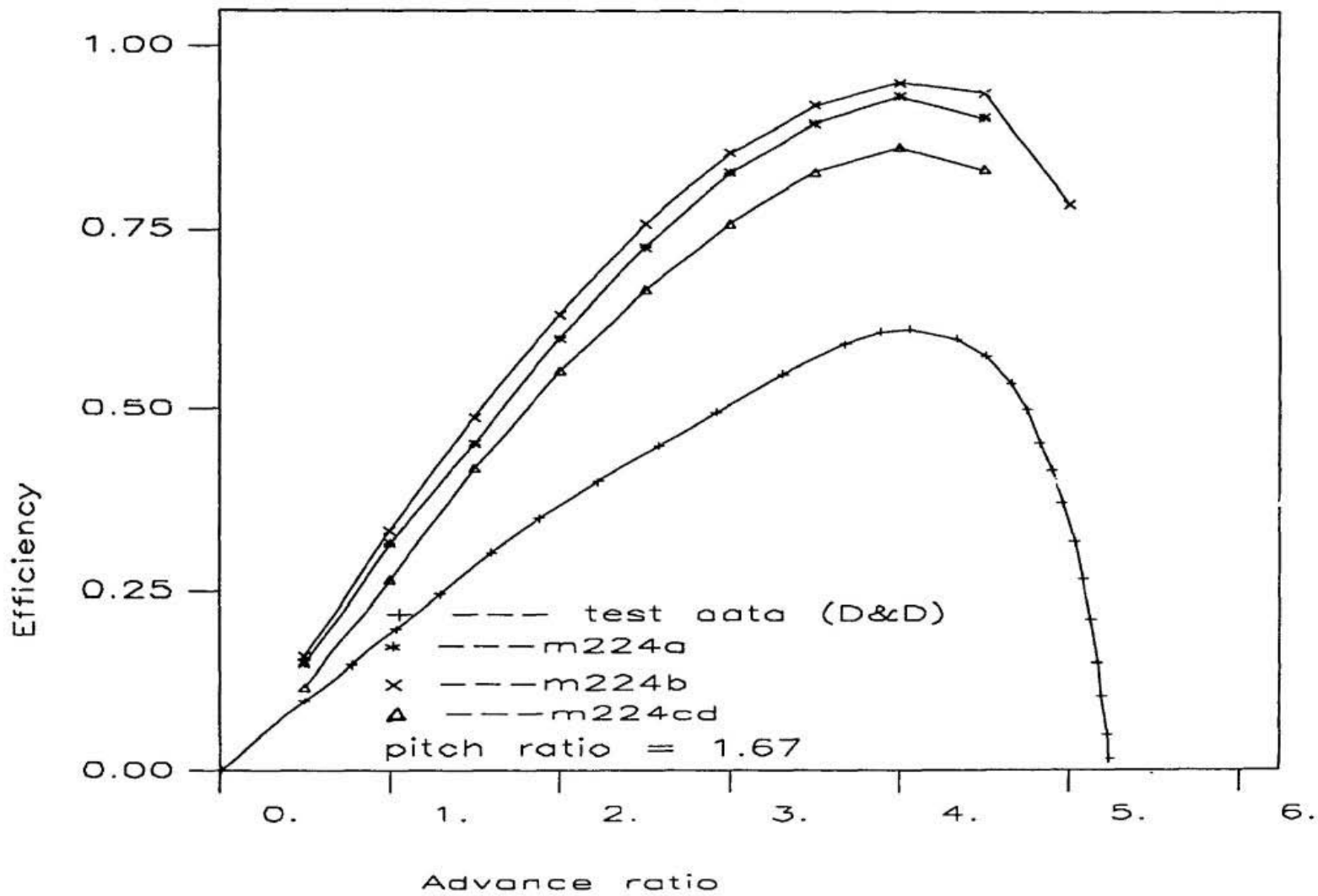


Figure E-30: Comparison of theoretical results with test results — efficiency(pitch ratio=1.667π)

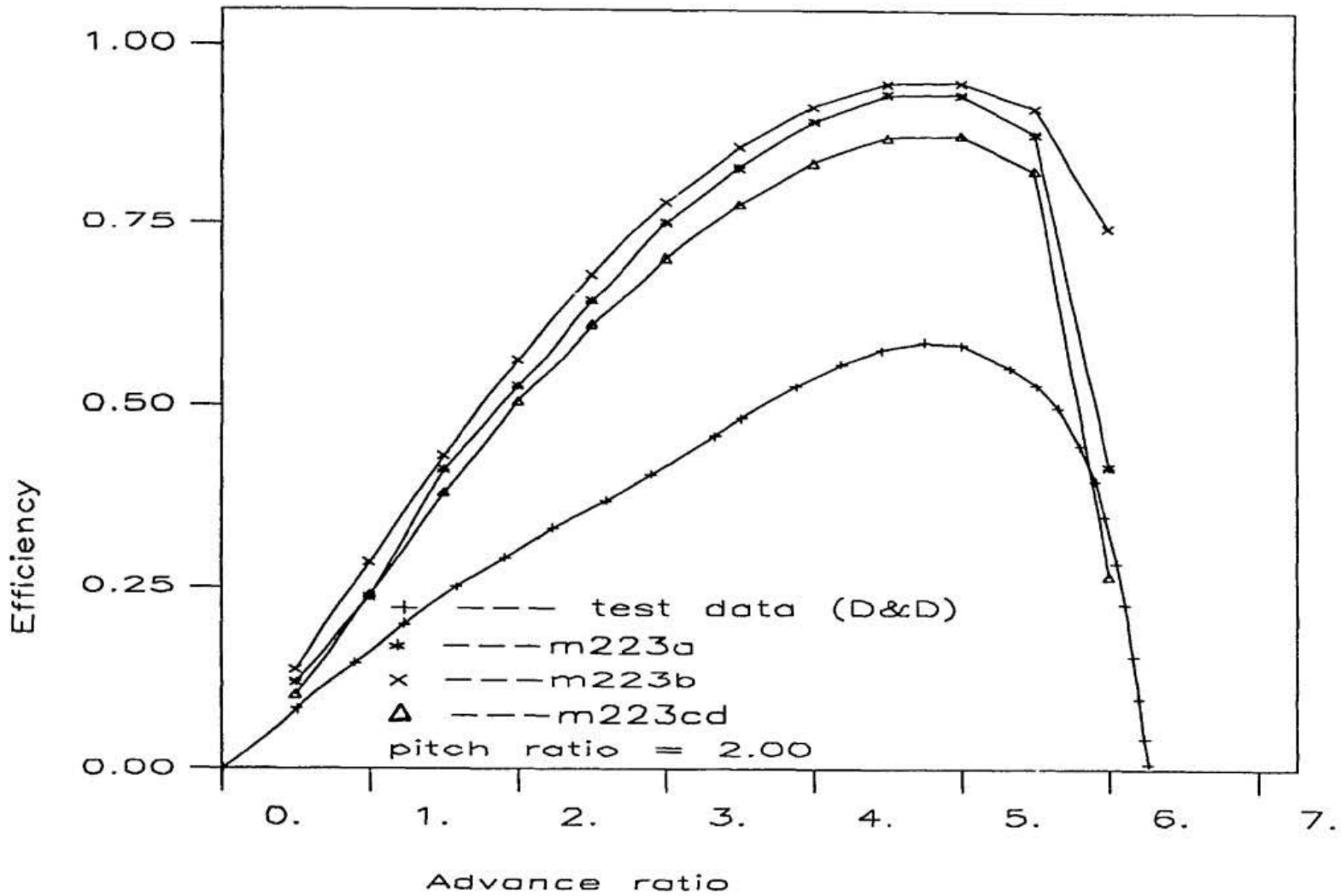


Figure E-31: Comparison of theoretical results with test results — efficiency(pitch ratio=2.000π)

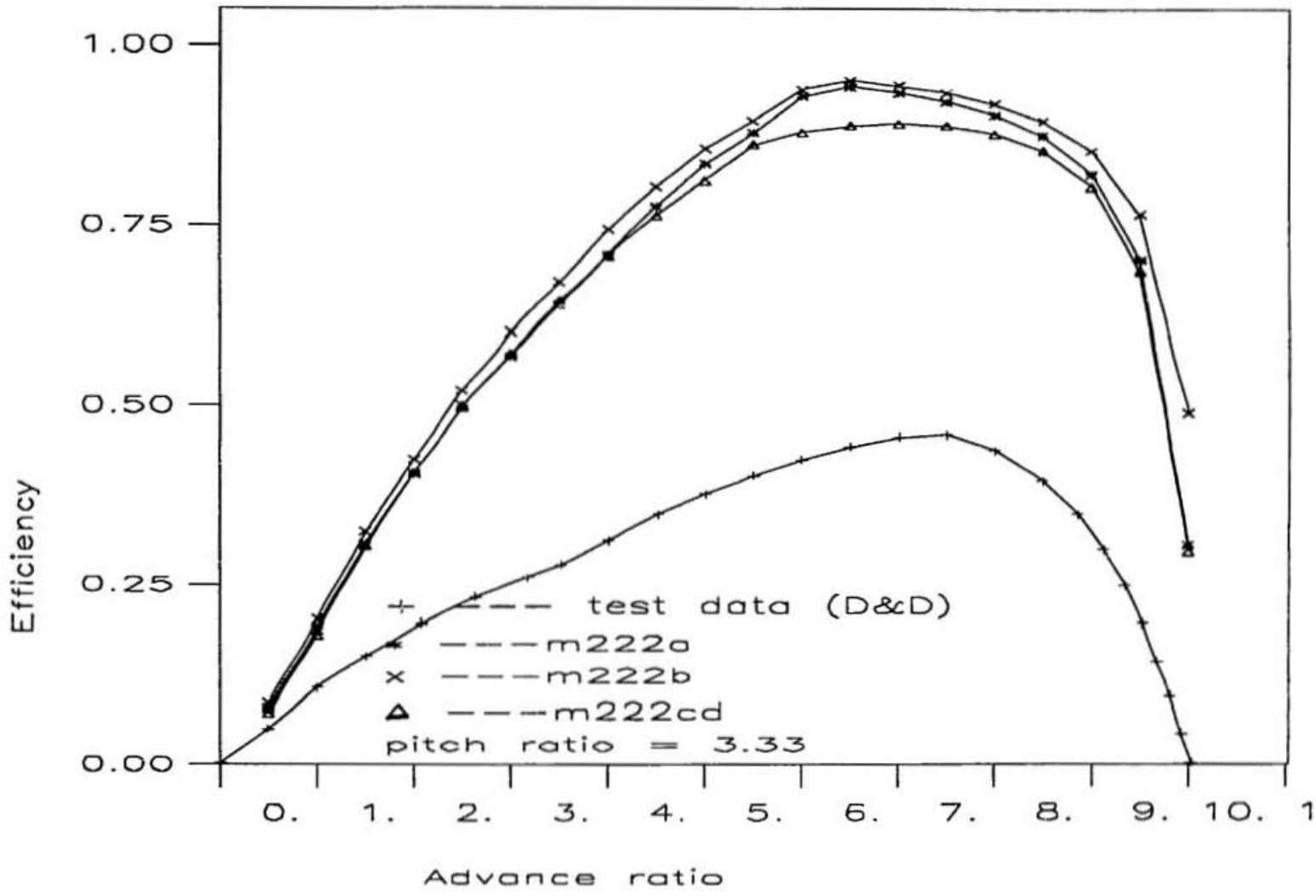


Figure E-32: Comparison of theoretical results with test results — efficiency(pitch ratio=3.333π)

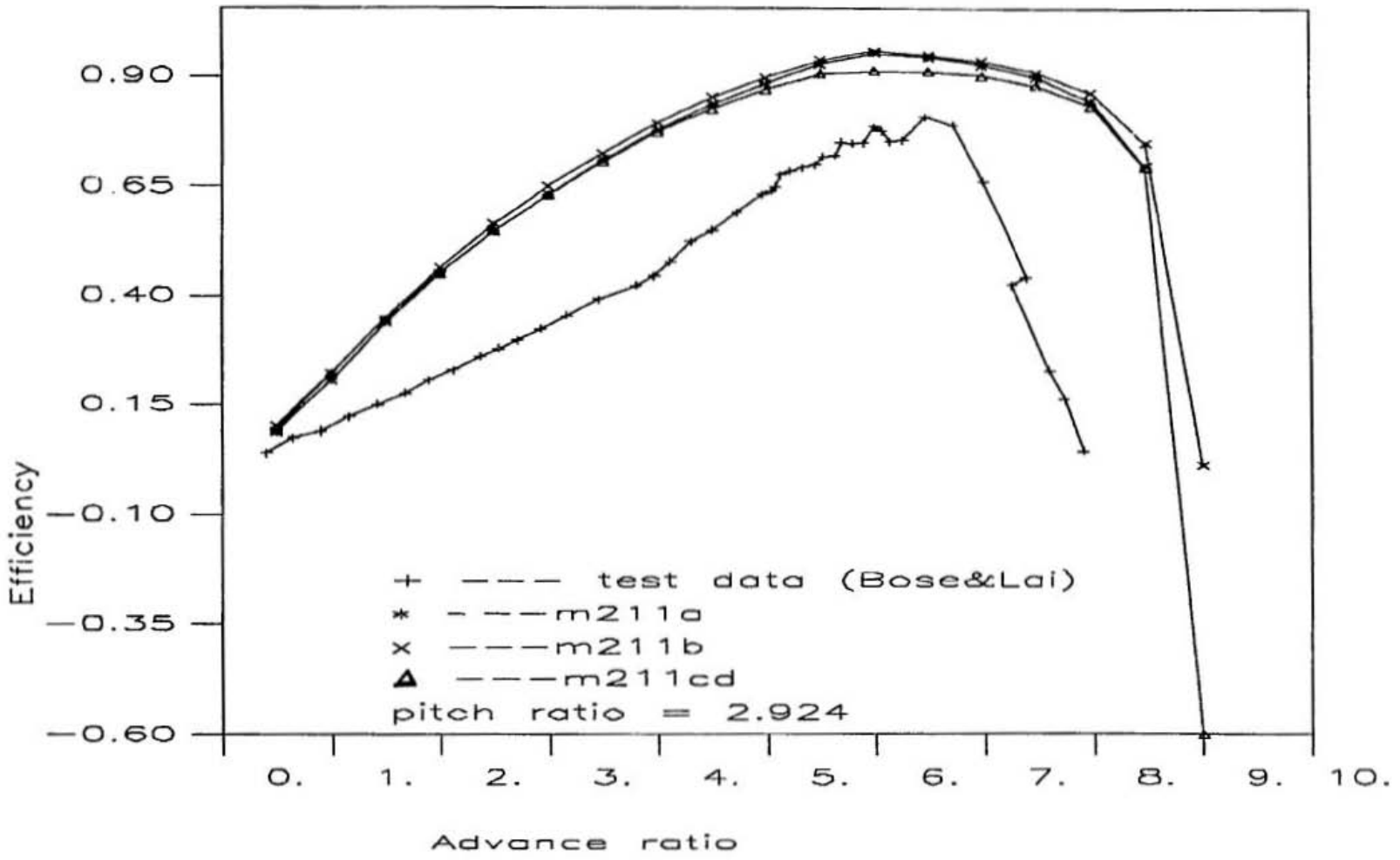


Figure E-33: Comparison of theoretical results with test results — efficiency(pitch ratio=2.924π)

Appendix F

Theoretical Results — Part II

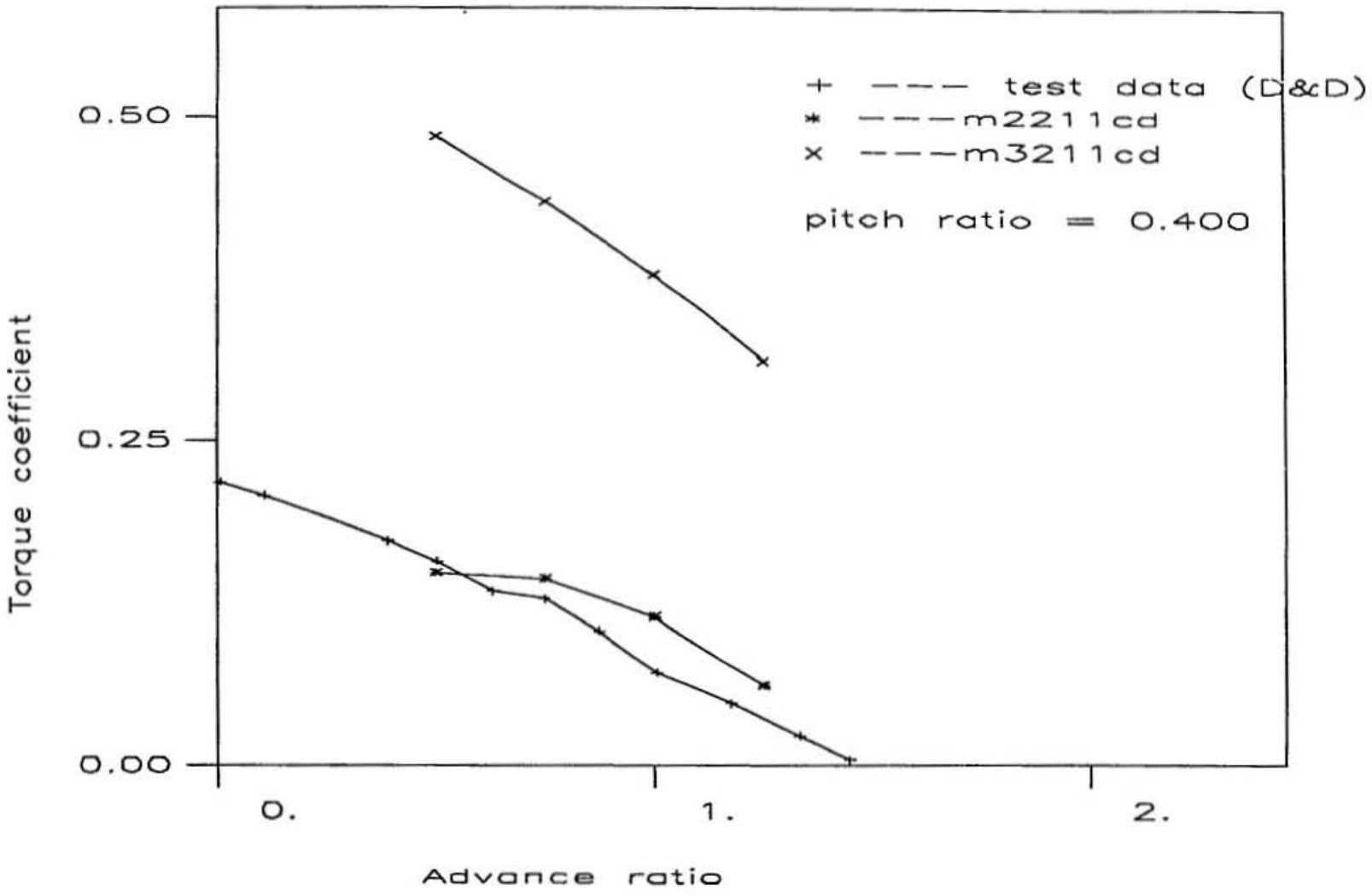


Figure F-1: Comparison of theoretical results with test results — torque coefficient(pitch ratio=0.4π)

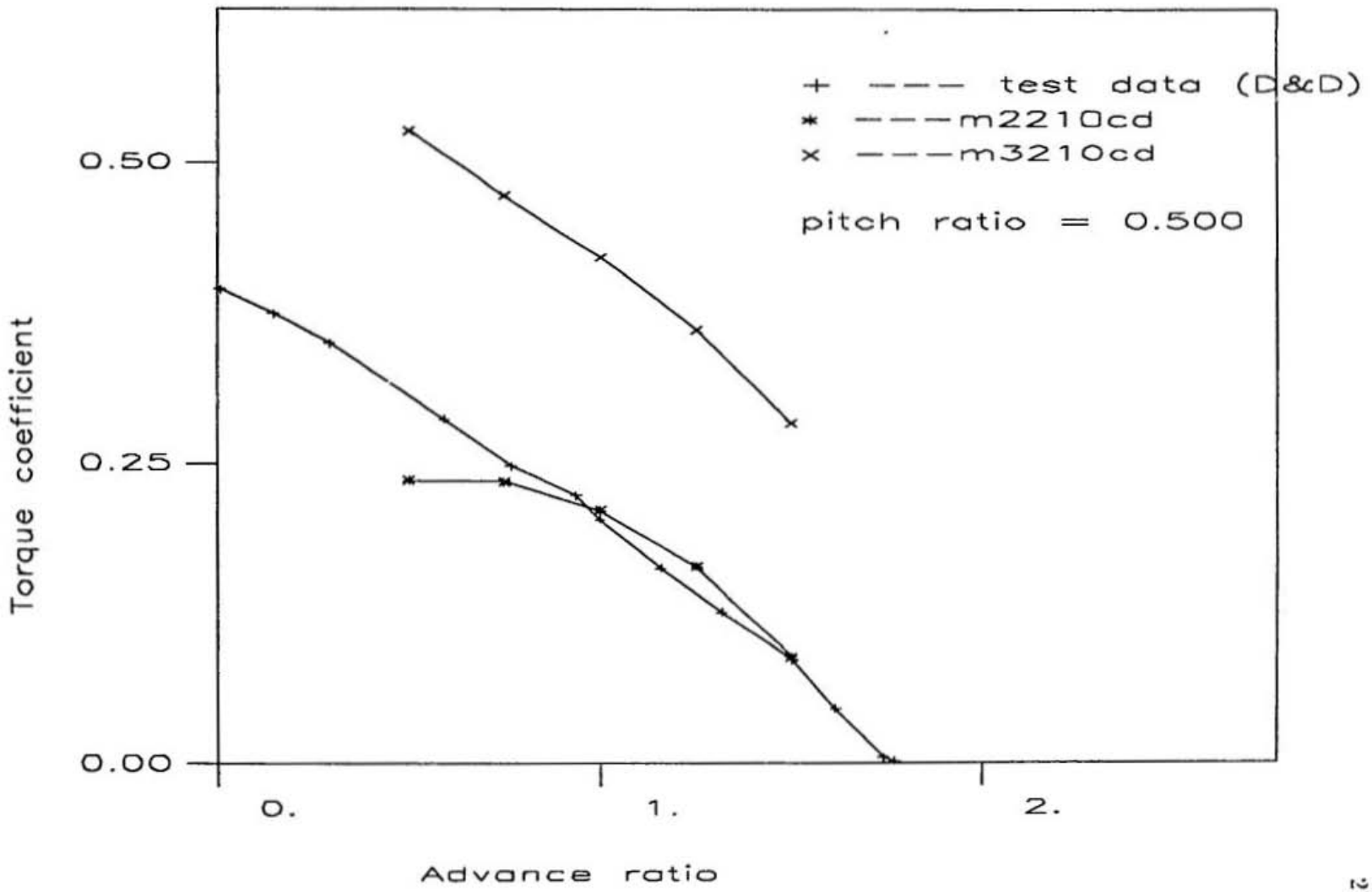


Figure F-2: Comparison of theoretical results with test results — torque coefficient(pitch ratio=0.5π)

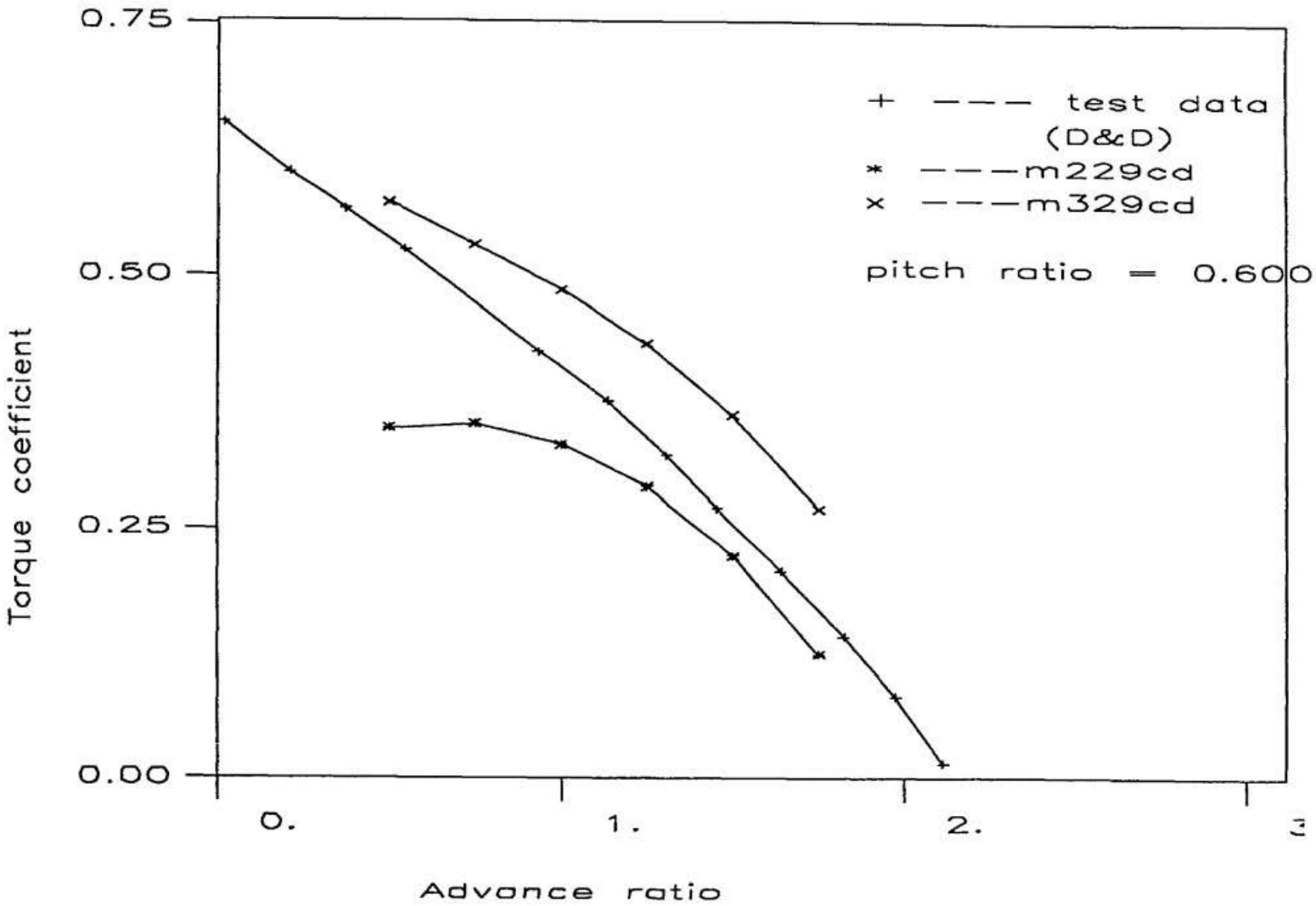


Figure F-3: Comparison of theoretical results with test results — torque coefficient(pitch ratio=0.6π)

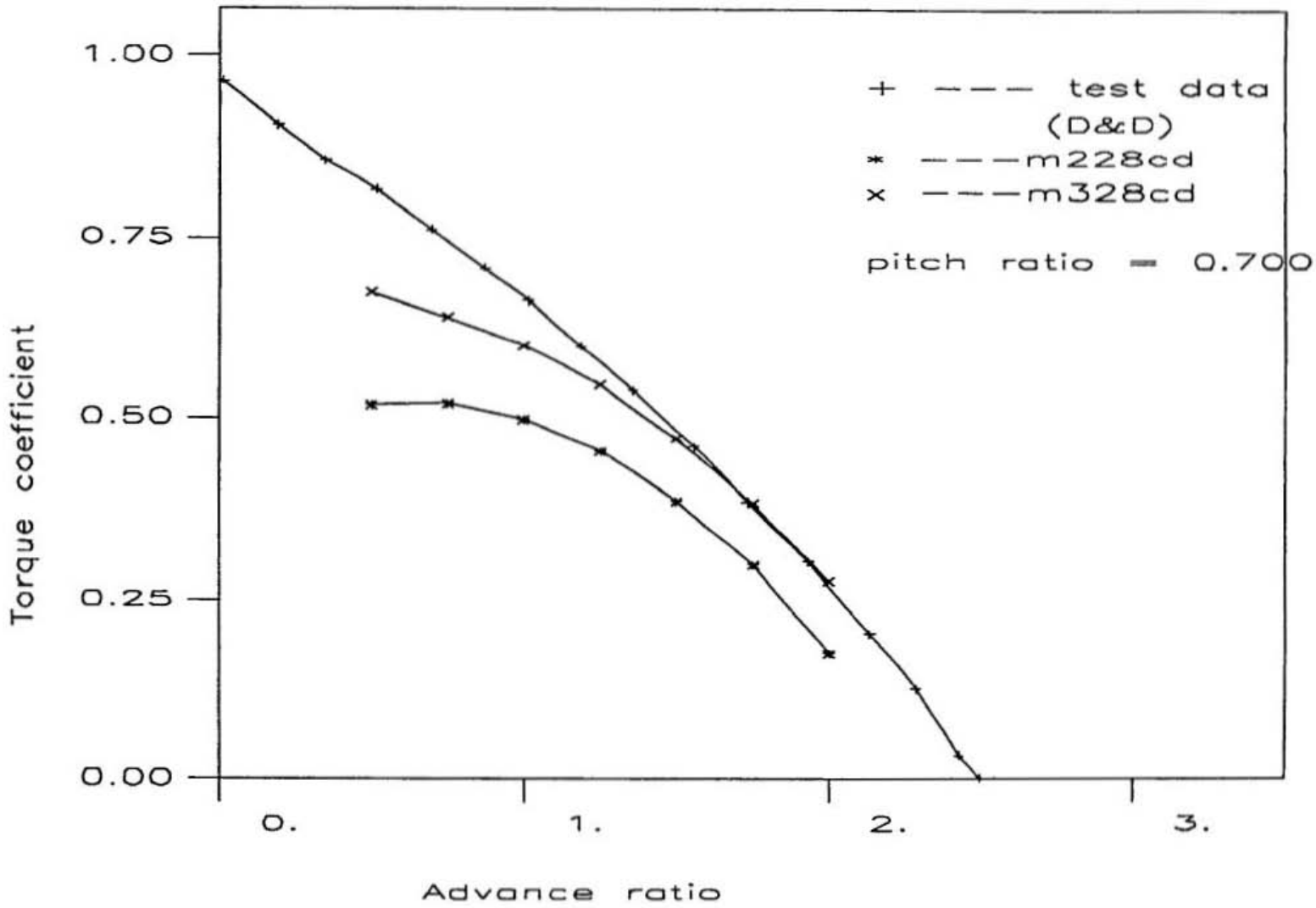


Figure F-4: Comparison of theoretical results with test results — torque coefficient(pitch ratio=0.7π)

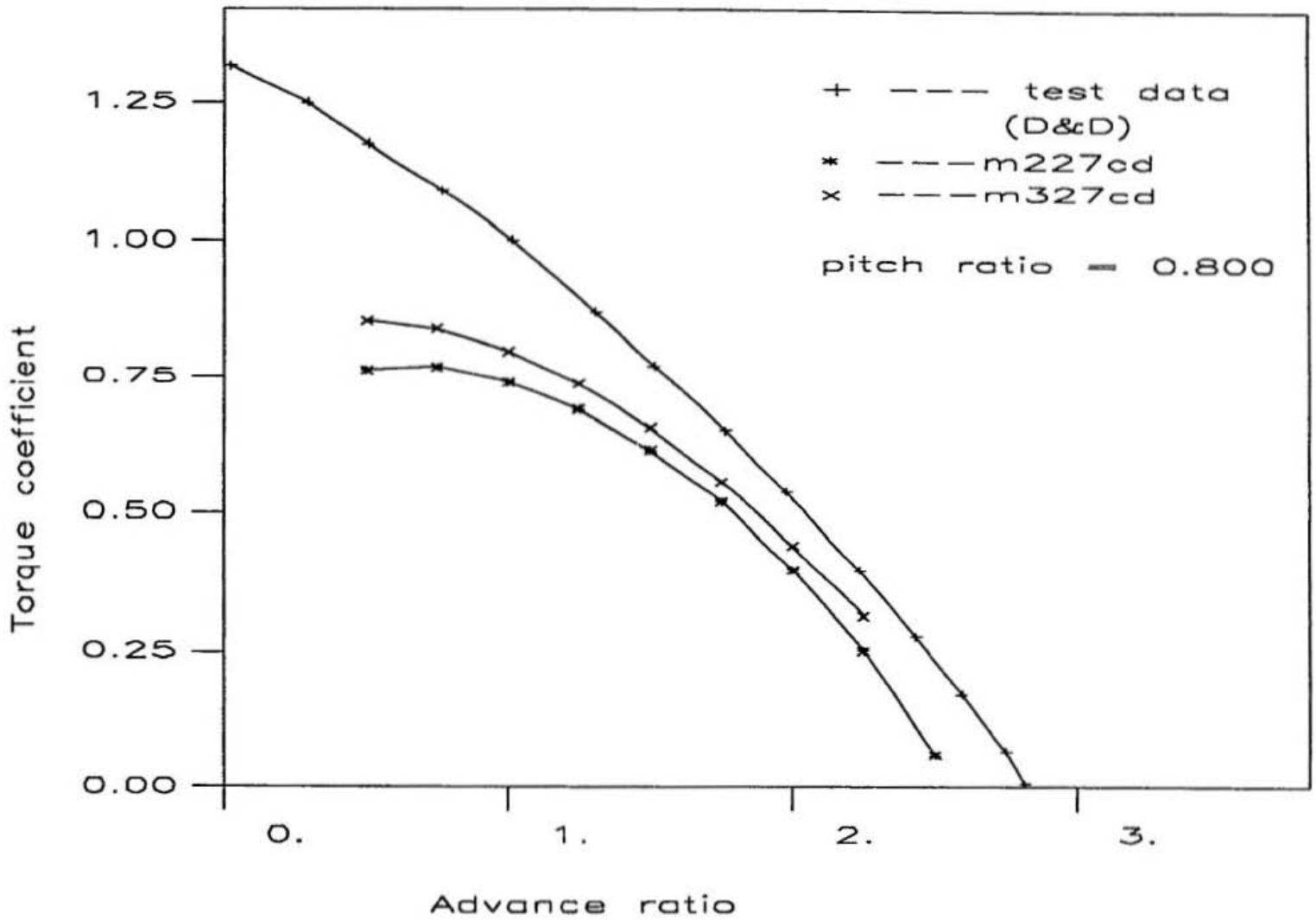


Figure F-5: Comparison of theoretical results with test results — torque coefficient(pitch ratio=0.8π)

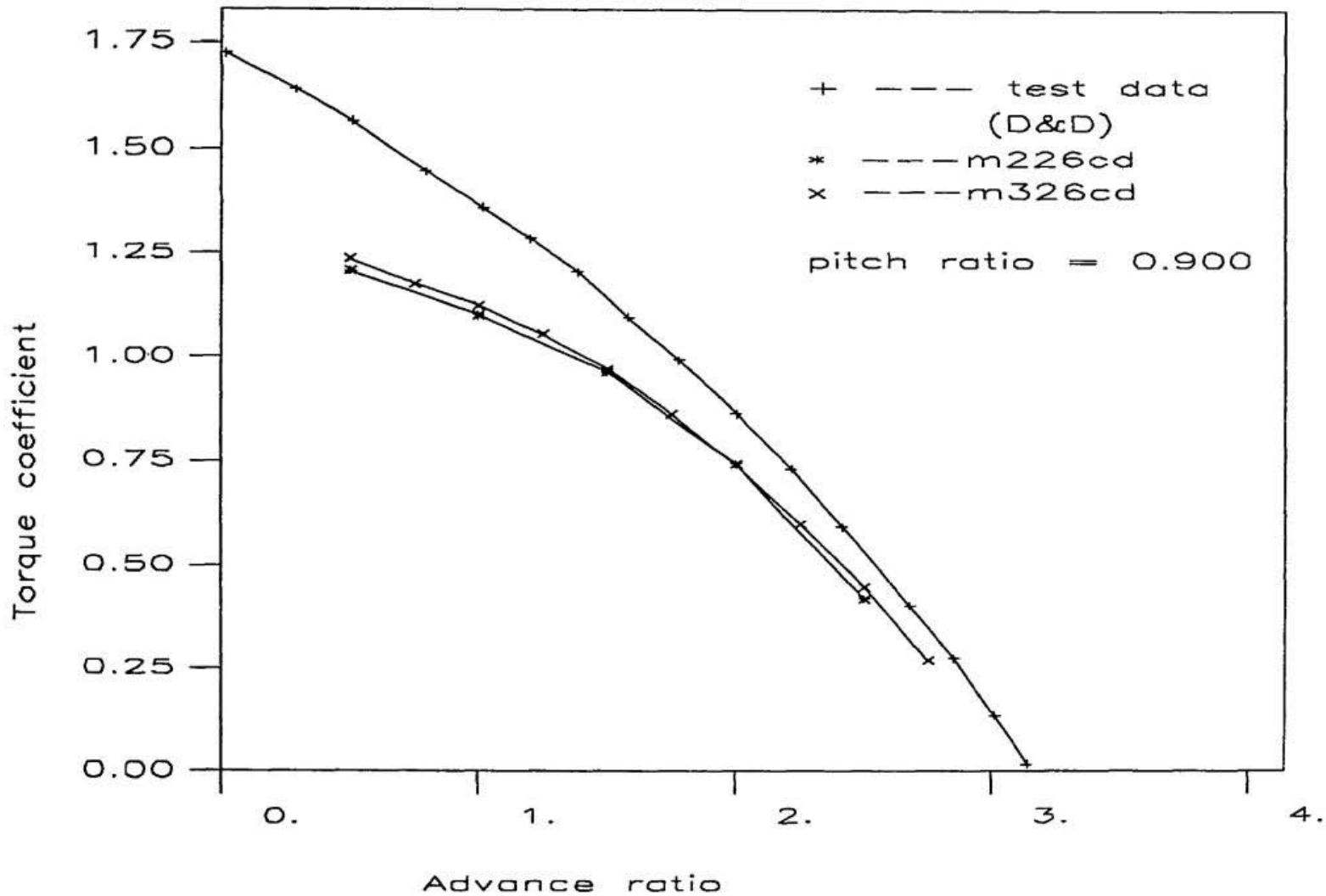


Figure F-6: Comparison of theoretical results with test results — torque coefficient(pitch ratio=0.9π)

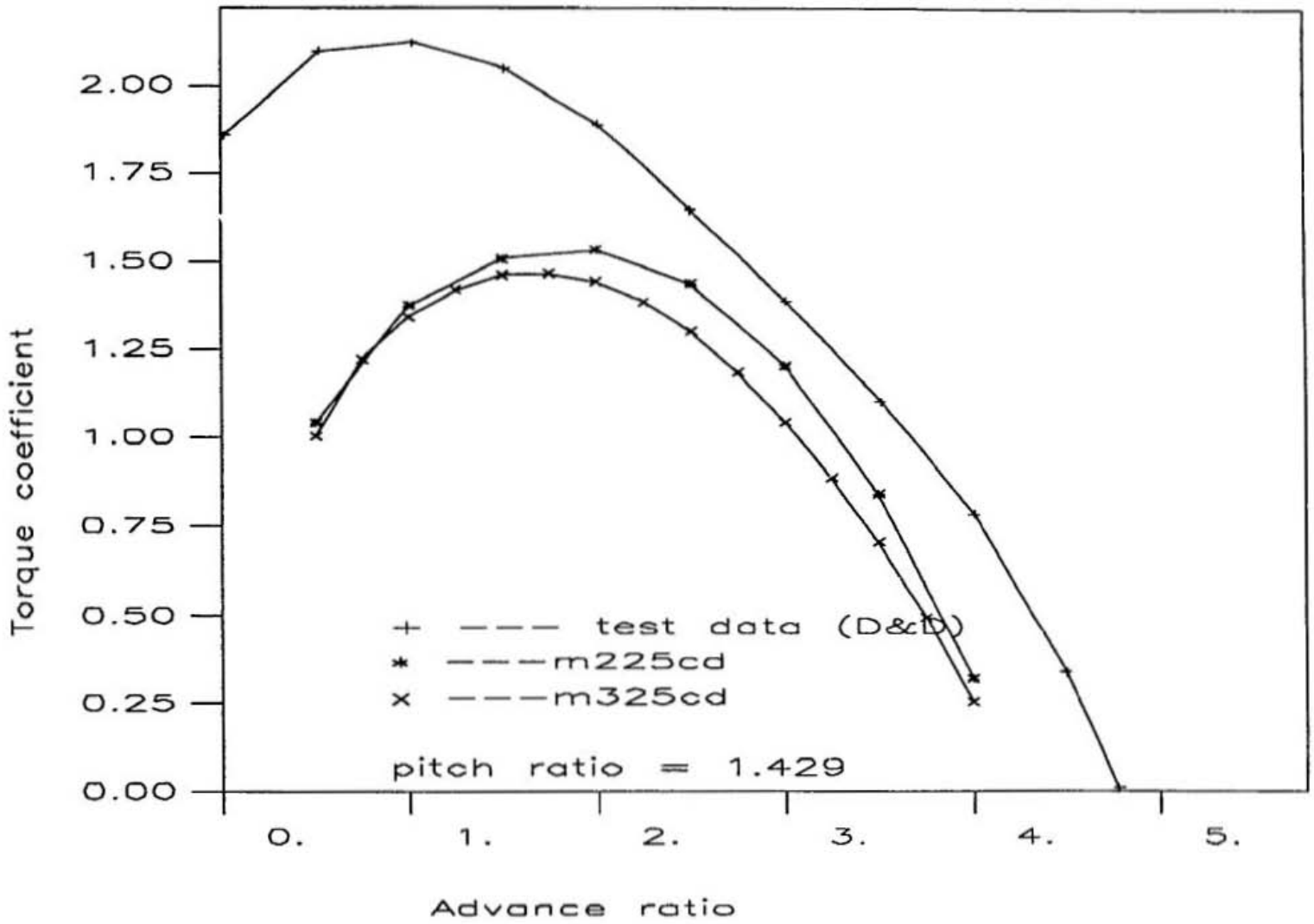


Figure F-7: Comparison of theoretical results with test results — torque coefficient(pitch ratio=1.429π)

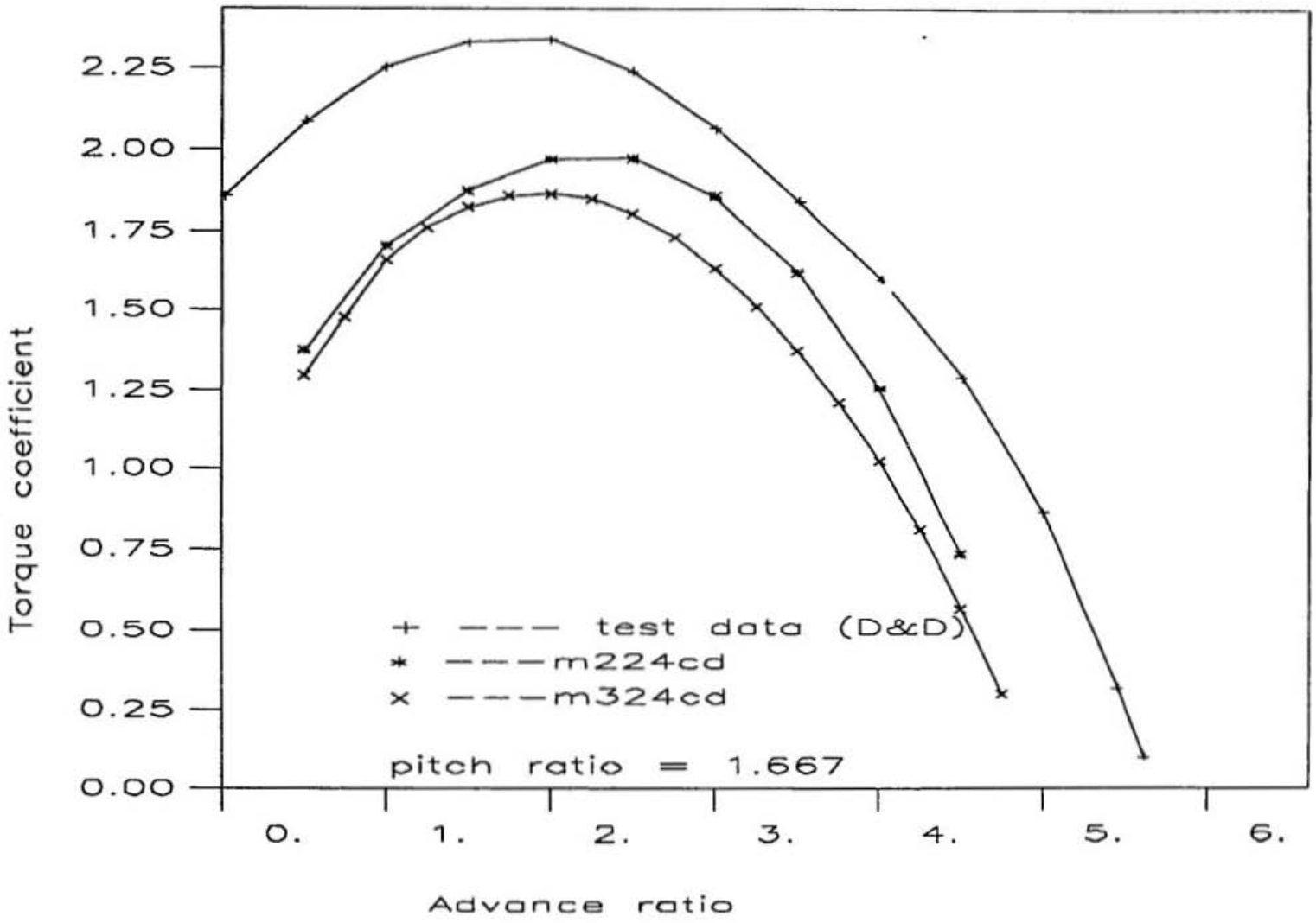


Figure F-8: Comparison of theoretical results with test results — torque coefficient(pitch ratio=1.667π)

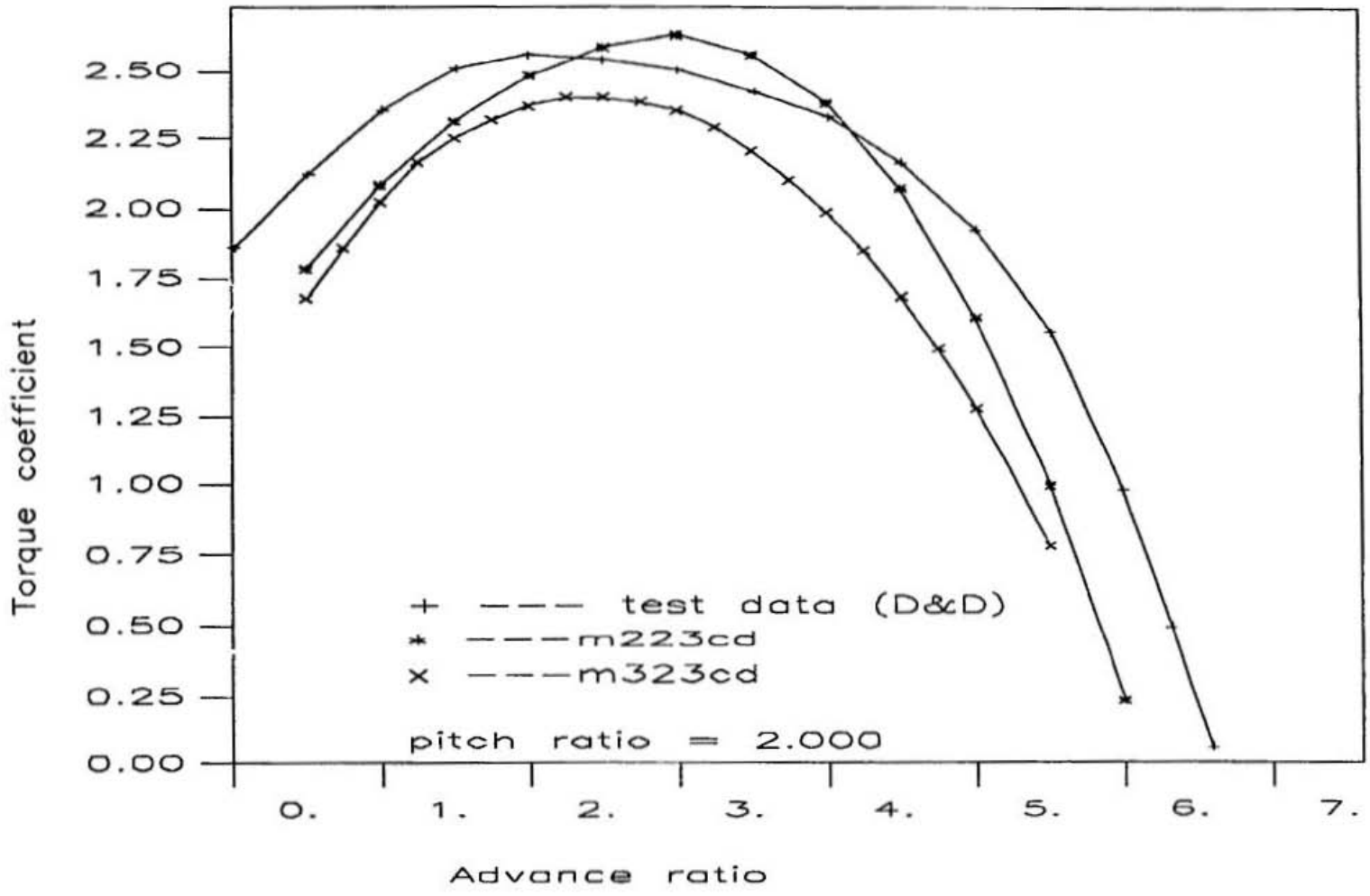


Figure F-9: Comparison of theoretical results with test results — torque coefficient(pitch ratio=2.000π)

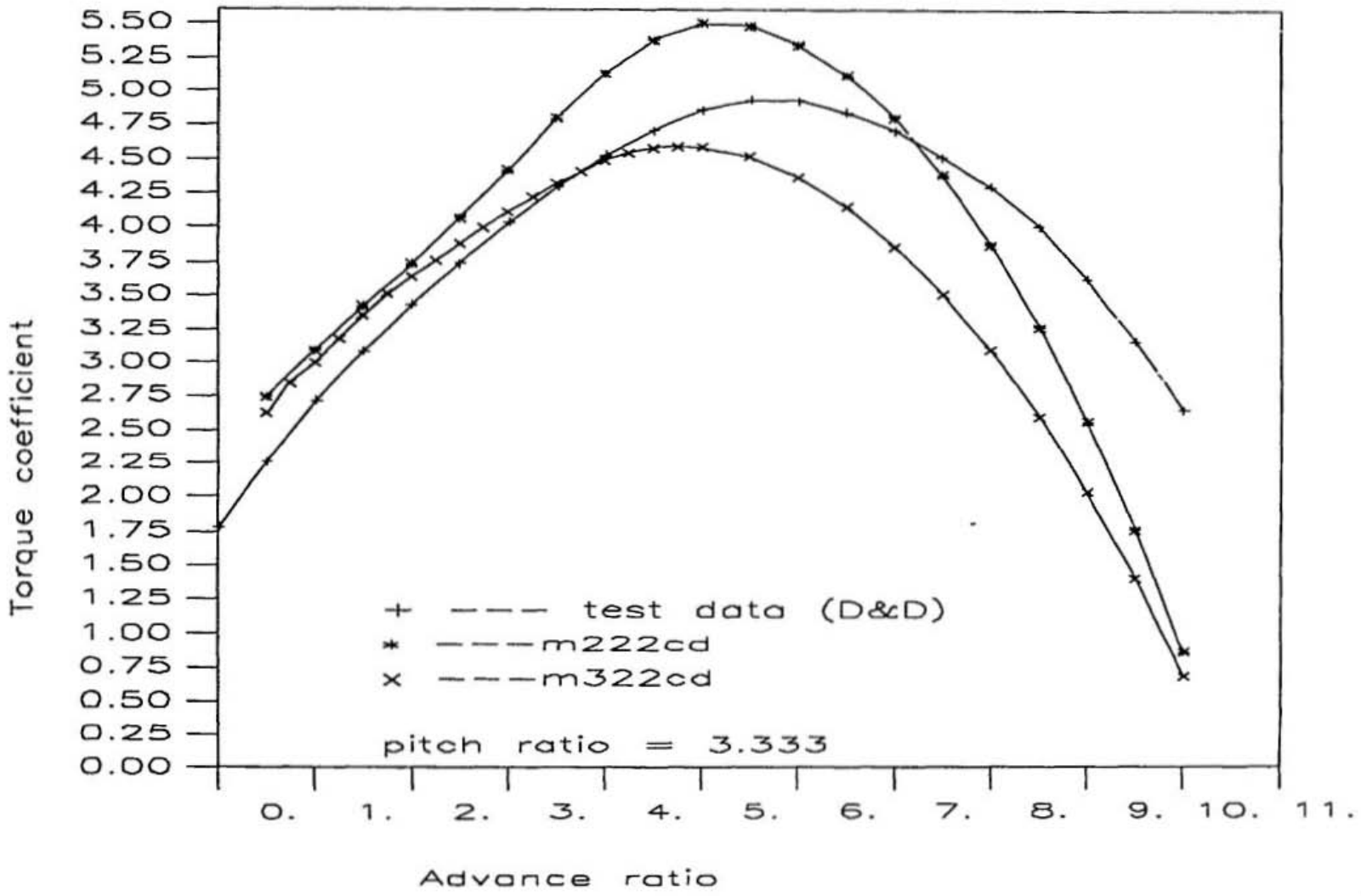


Figure F-10: Comparison of theoretical results with test results — torque coefficient(pitch ratio=3.333π)

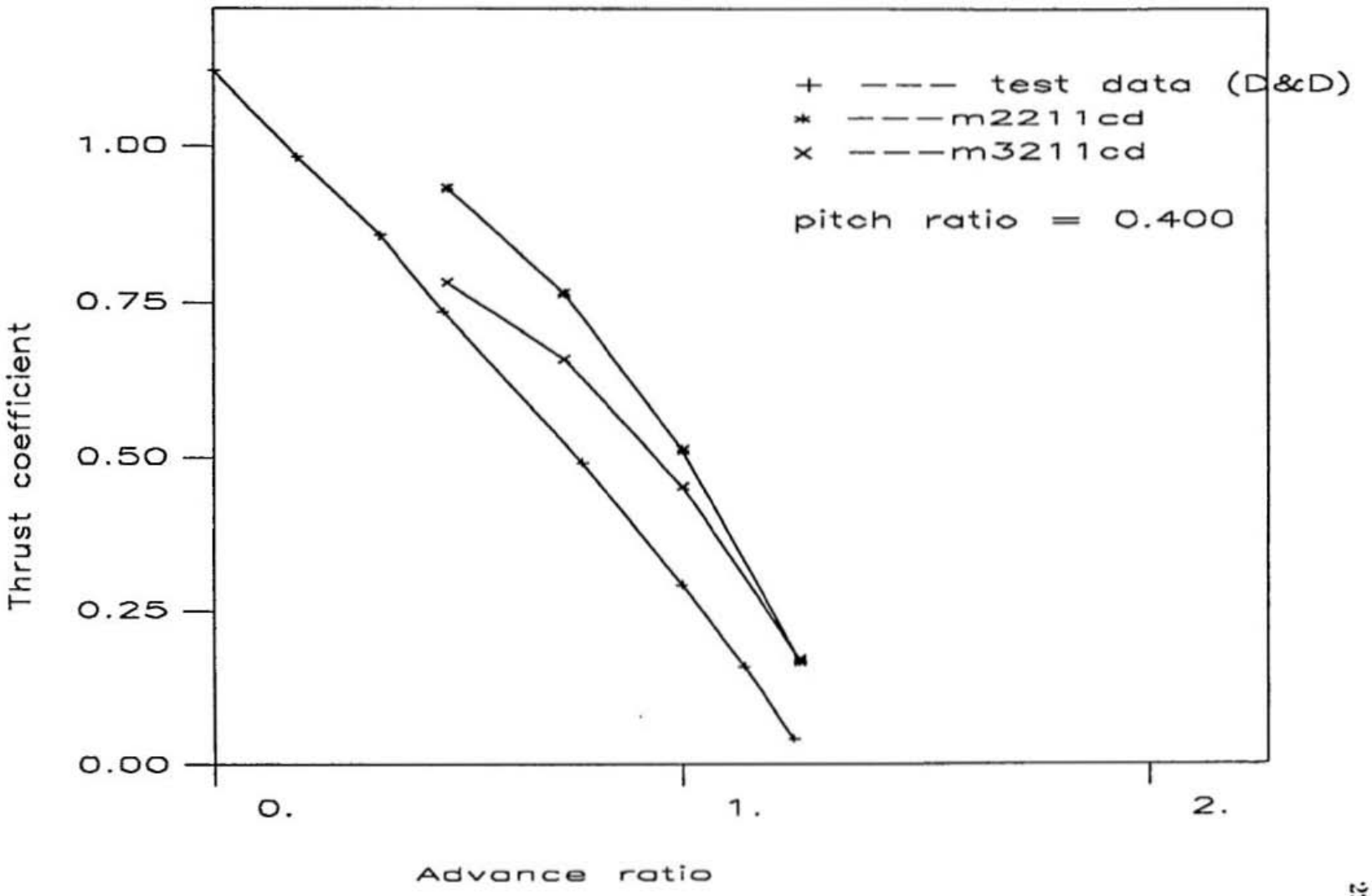


Figure F-12: Comparison of theoretical results with test results — thrust coefficient(pitch ratio=0.4π)

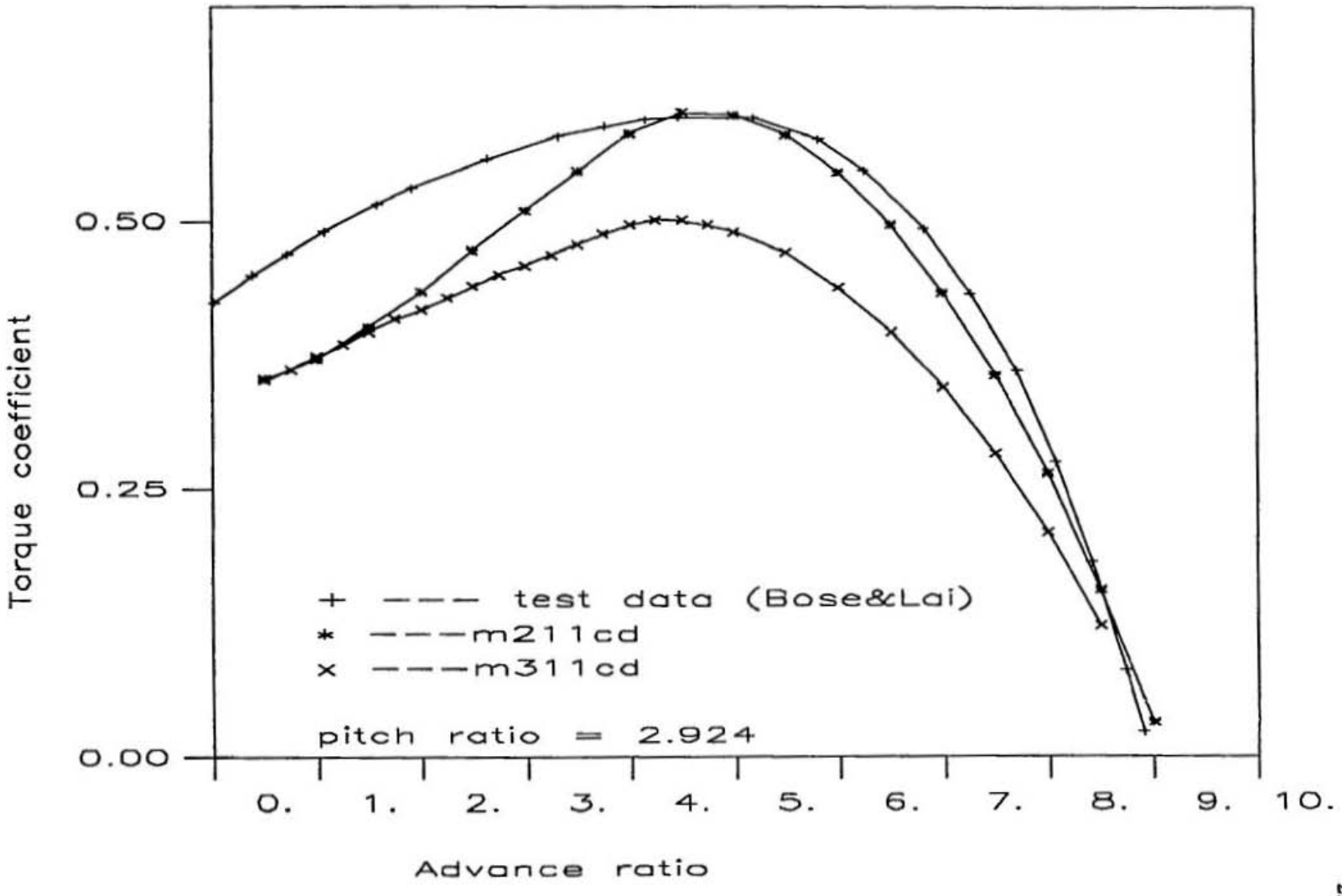


Figure F-11: Comparison of theoretical results with test results — torque coefficient(pitch ratio=2.924π)

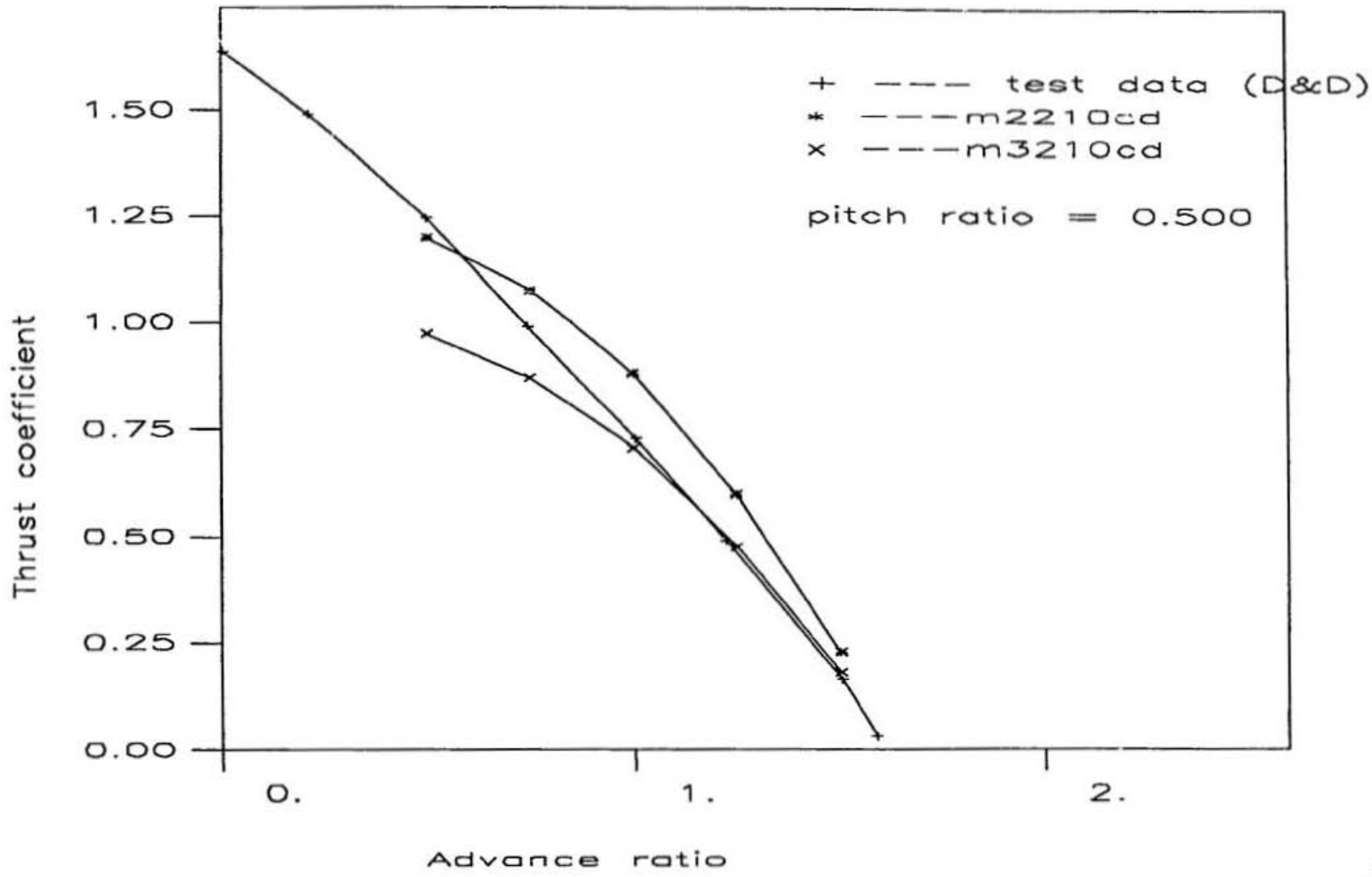


Figure F-13: Comparison of theoretical results with test results — thrust coefficient(pitch ratio=0.5π)

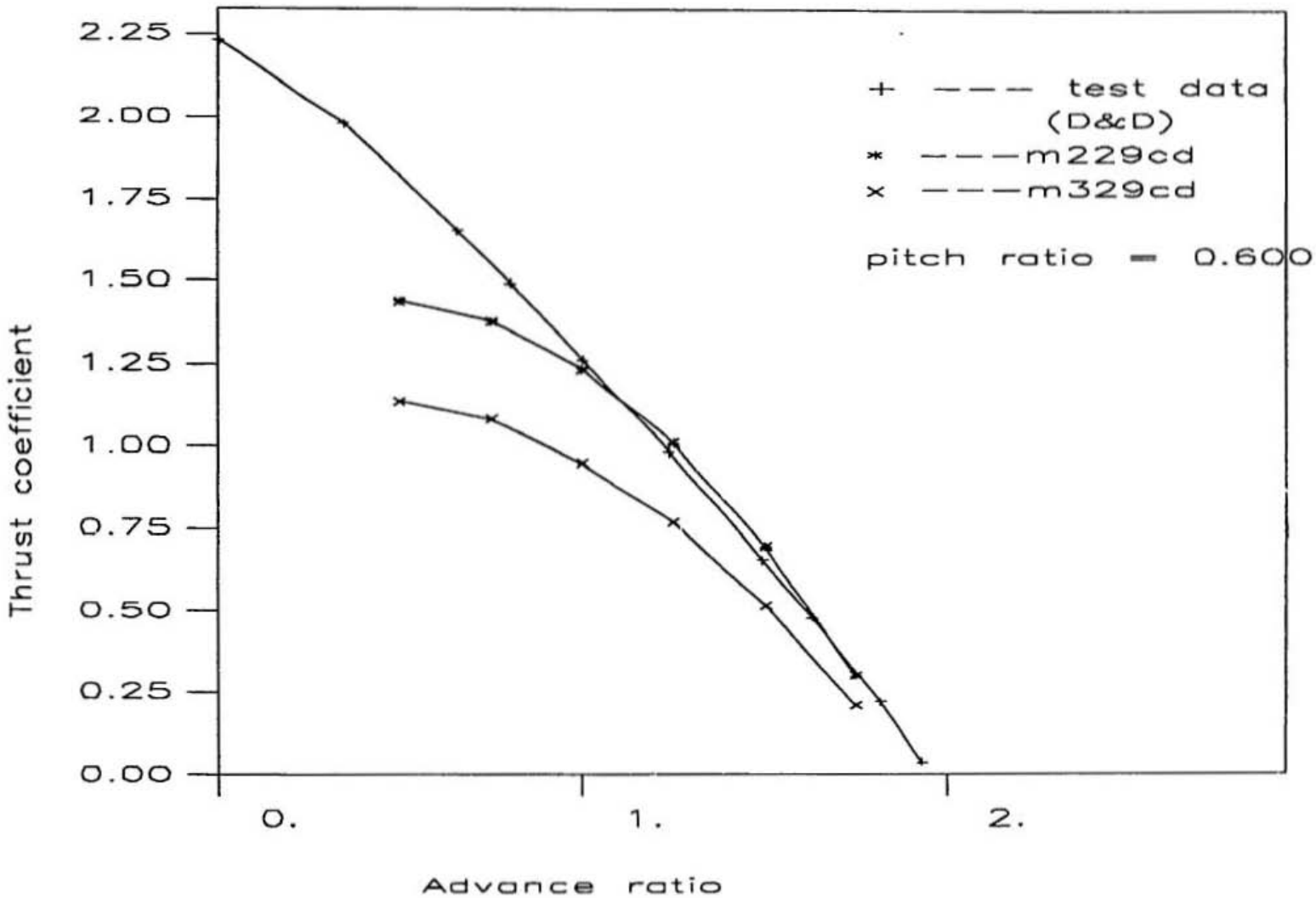


Figure F-14: Comparison of theoretical results with test results — thrust coefficient(pitch ratio=0.6π)

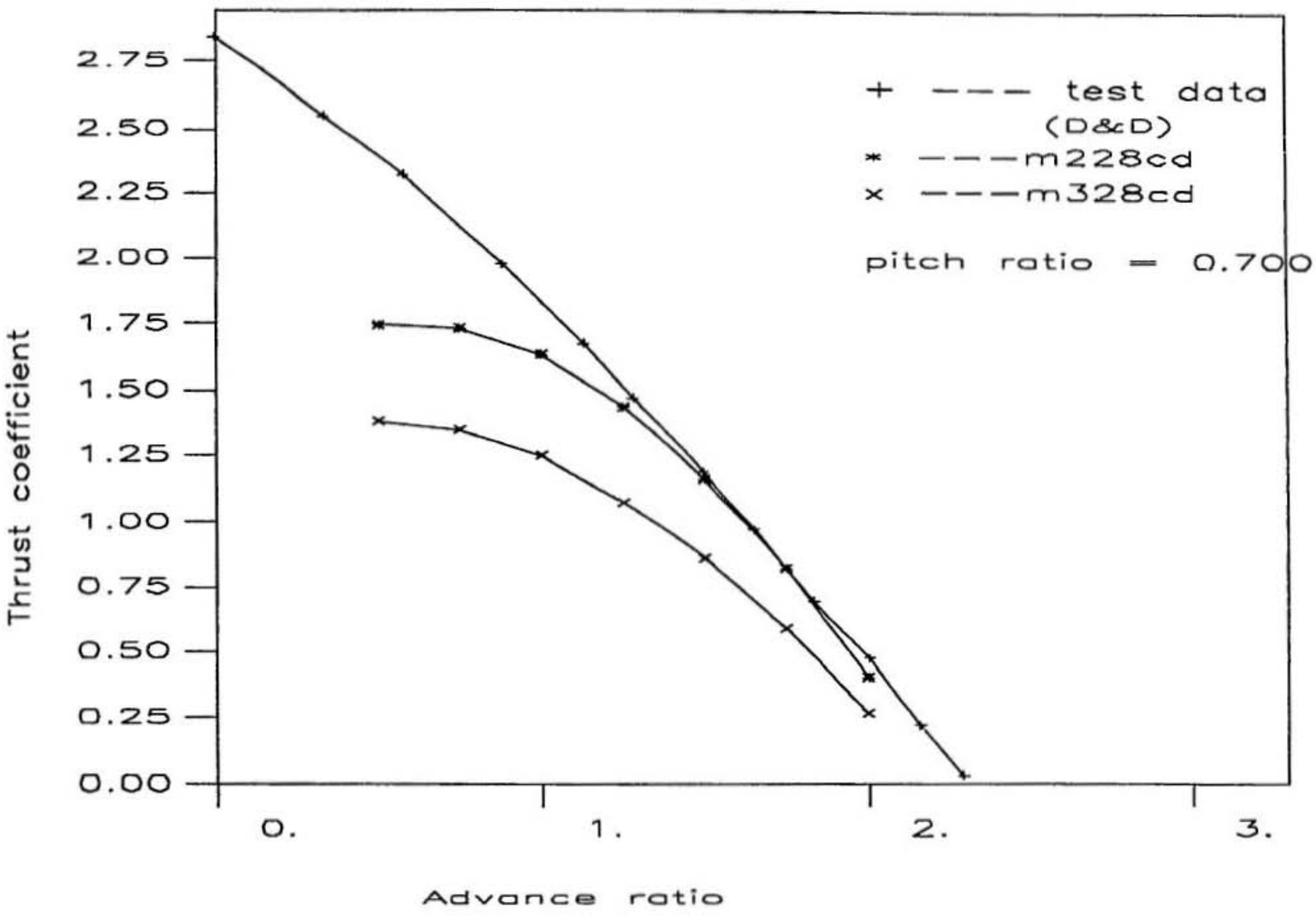


Figure F-15: Comparison of theoretical results with test results — thrust coefficient(pitch ratio=0.7π)

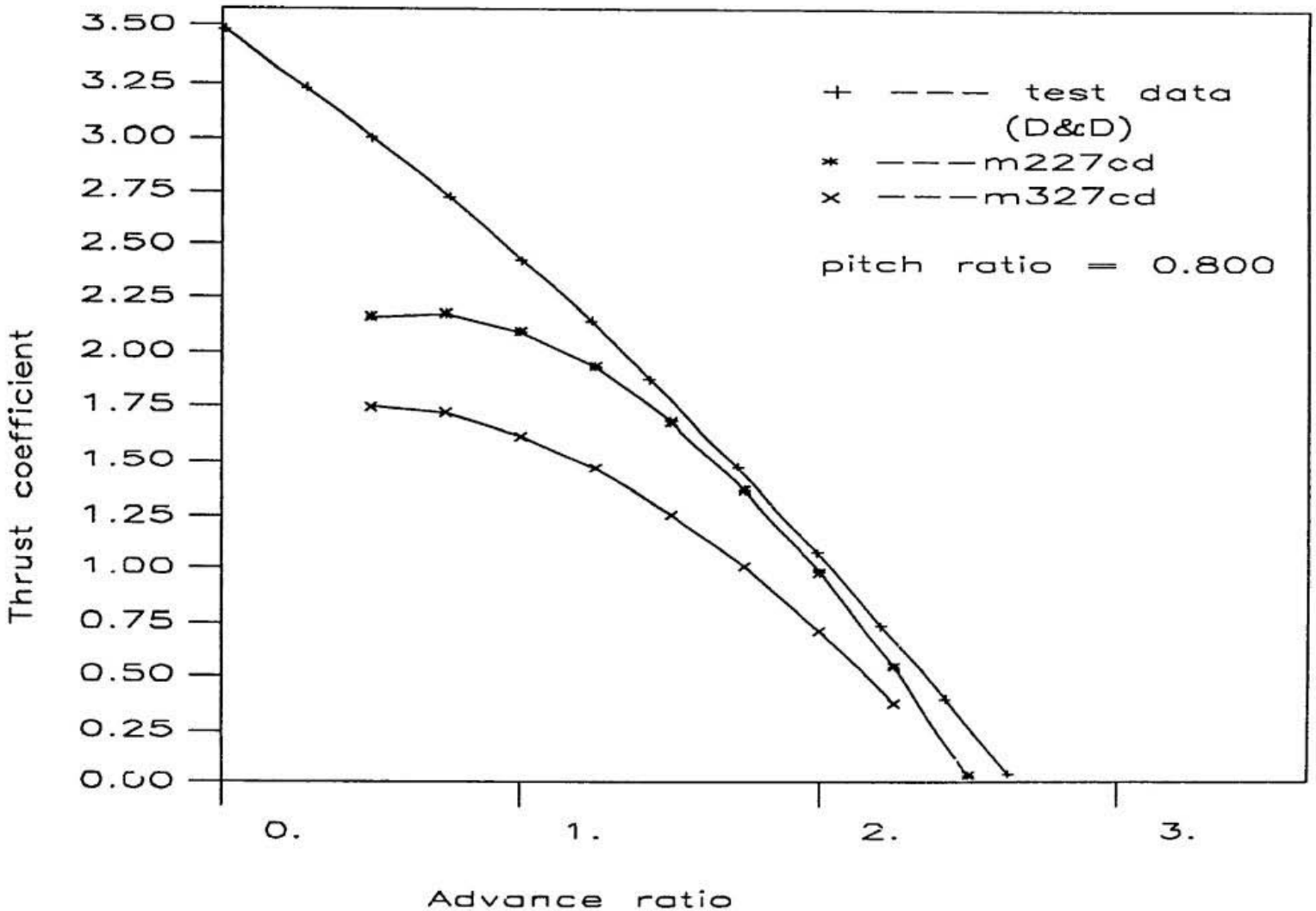


Figure F-16: Comparison of theoretical results with test results — thrust coefficient(pitch ratio=0.8π)

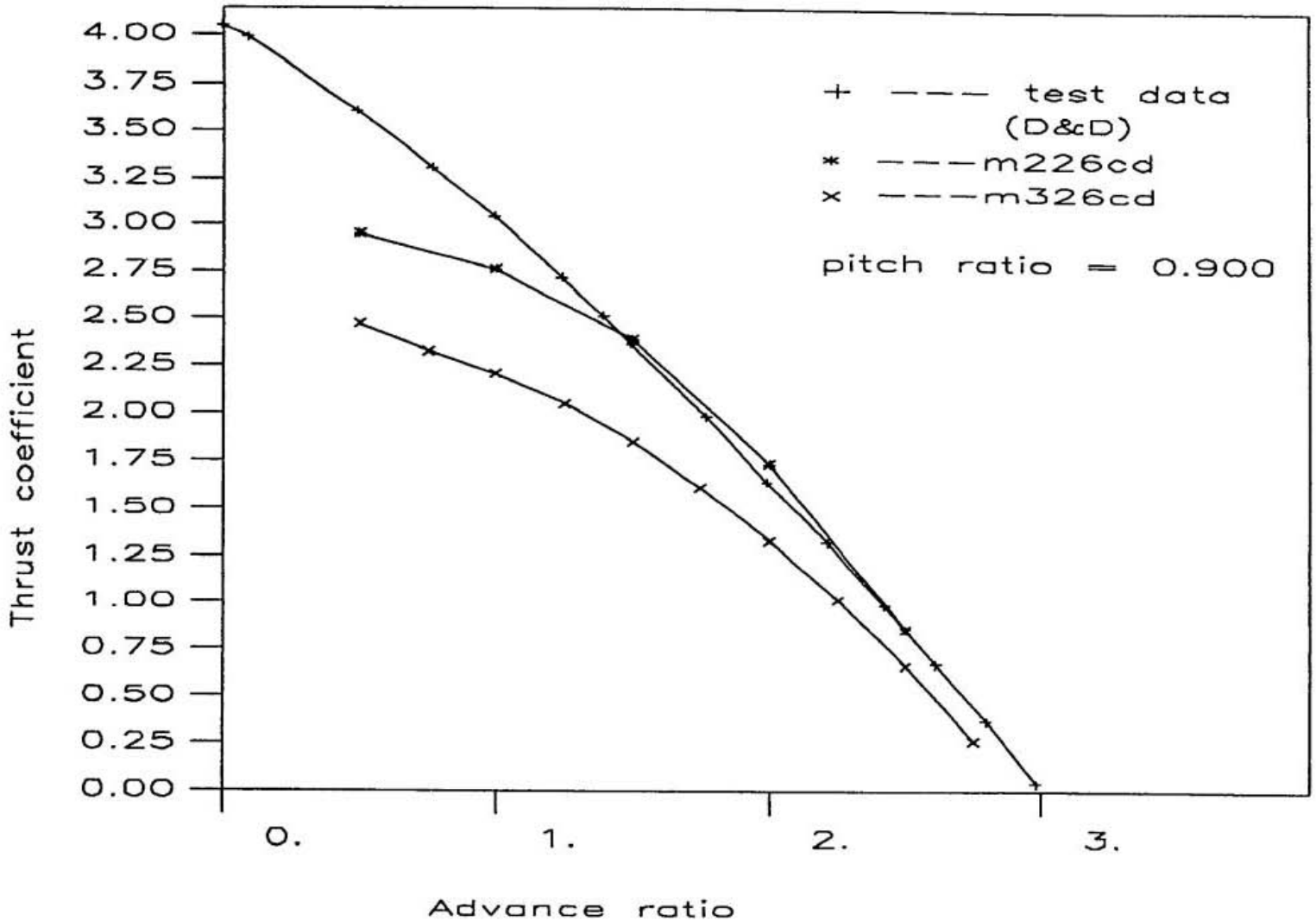


Figure F-17: Comparison of theoretical results with test results — thrust coefficient(pitch ratio=0.9π)

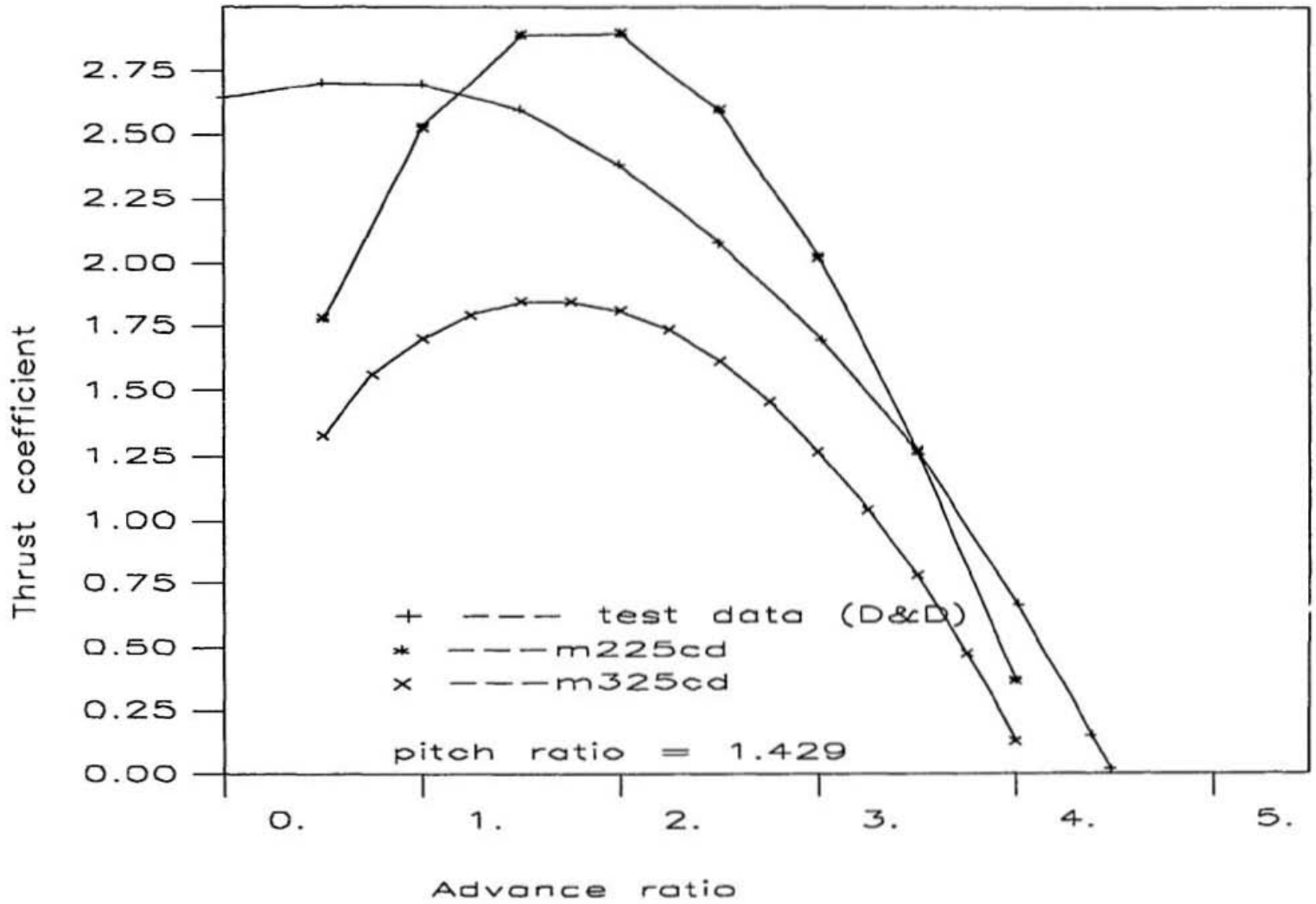


Figure F-18: Comparison of theoretical results with test results — thrust coefficient(pitch ratio=1.429π)

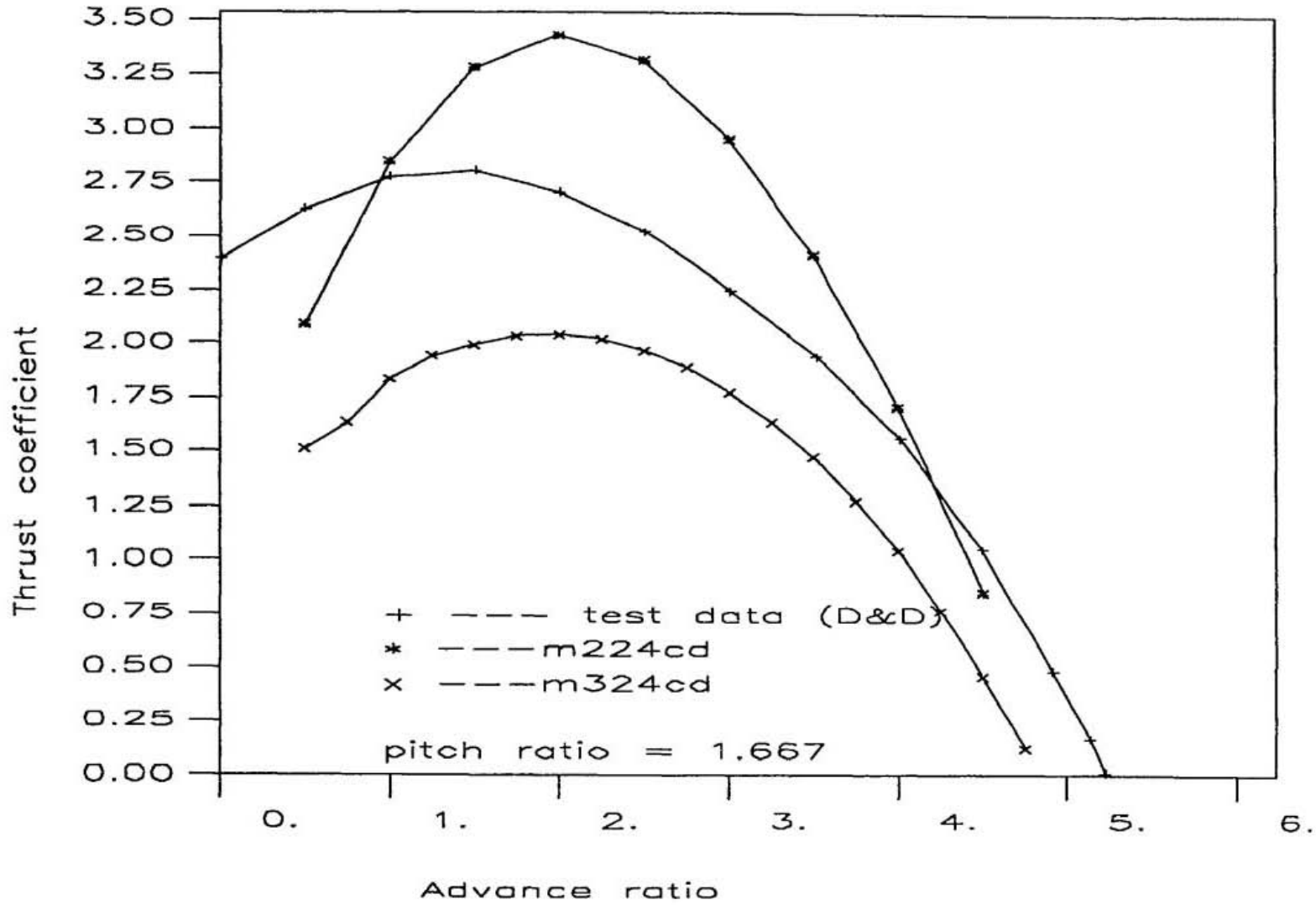


Figure F-19: Comparison of theoretical results with test results — thrust coefficient(pitch ratio=1.667π)

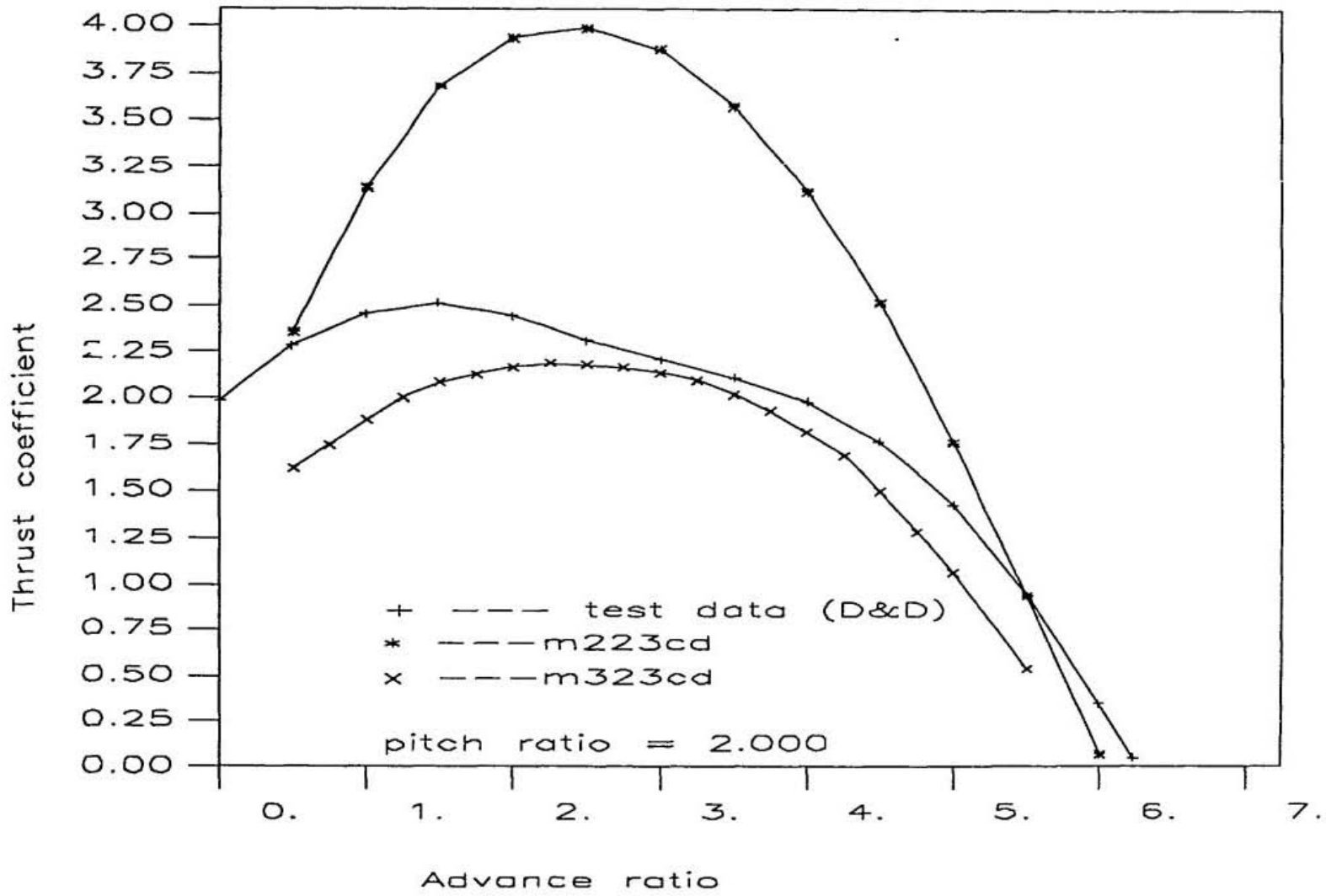


Figure F-20: Comparison of theoretical results with test results — thrust coefficient(pitch ratio=2.000π)

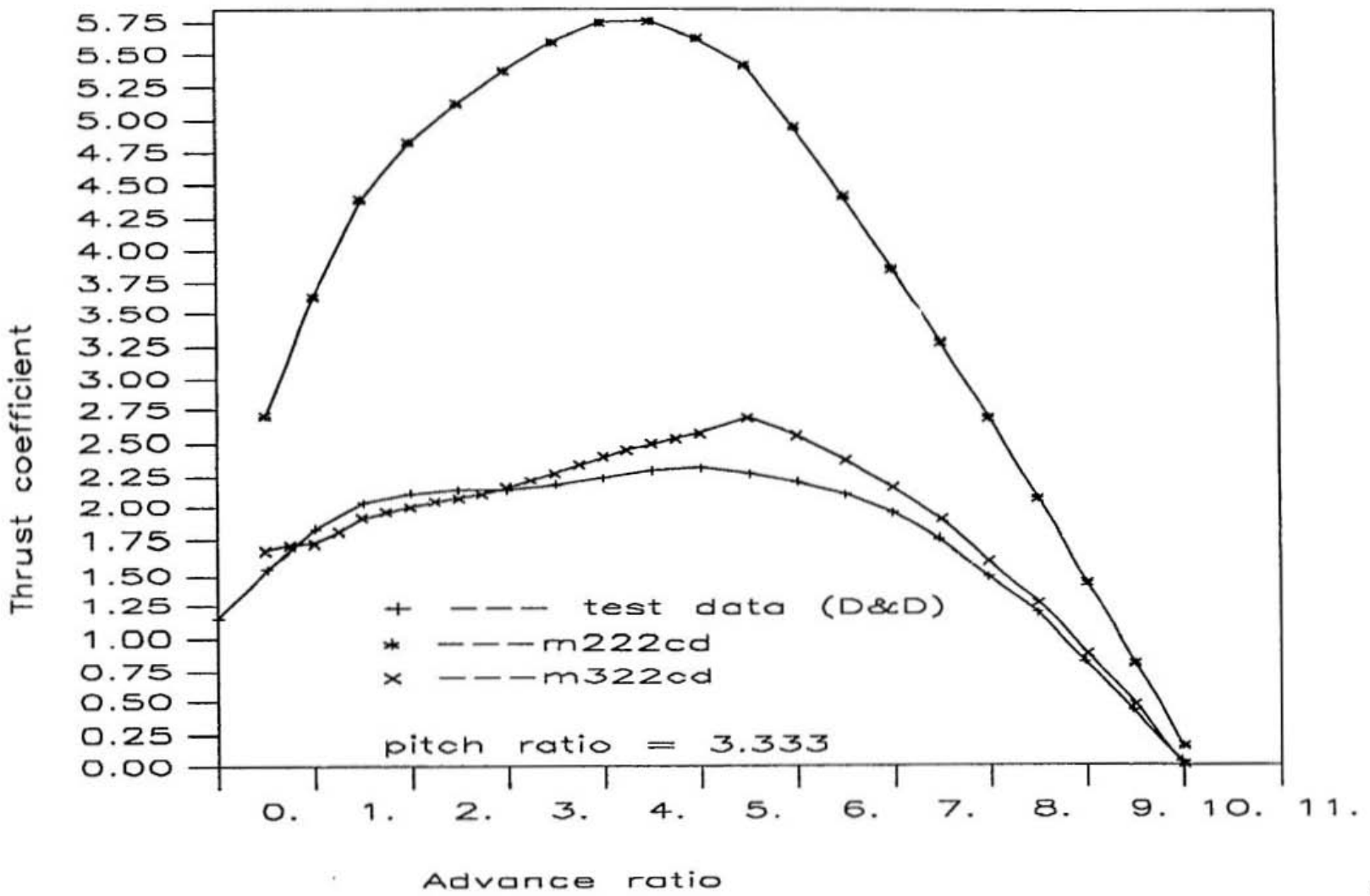


Figure F-21: Comparison of theoretical results with test results — thrust coefficient(pitch ratio=3.333π)

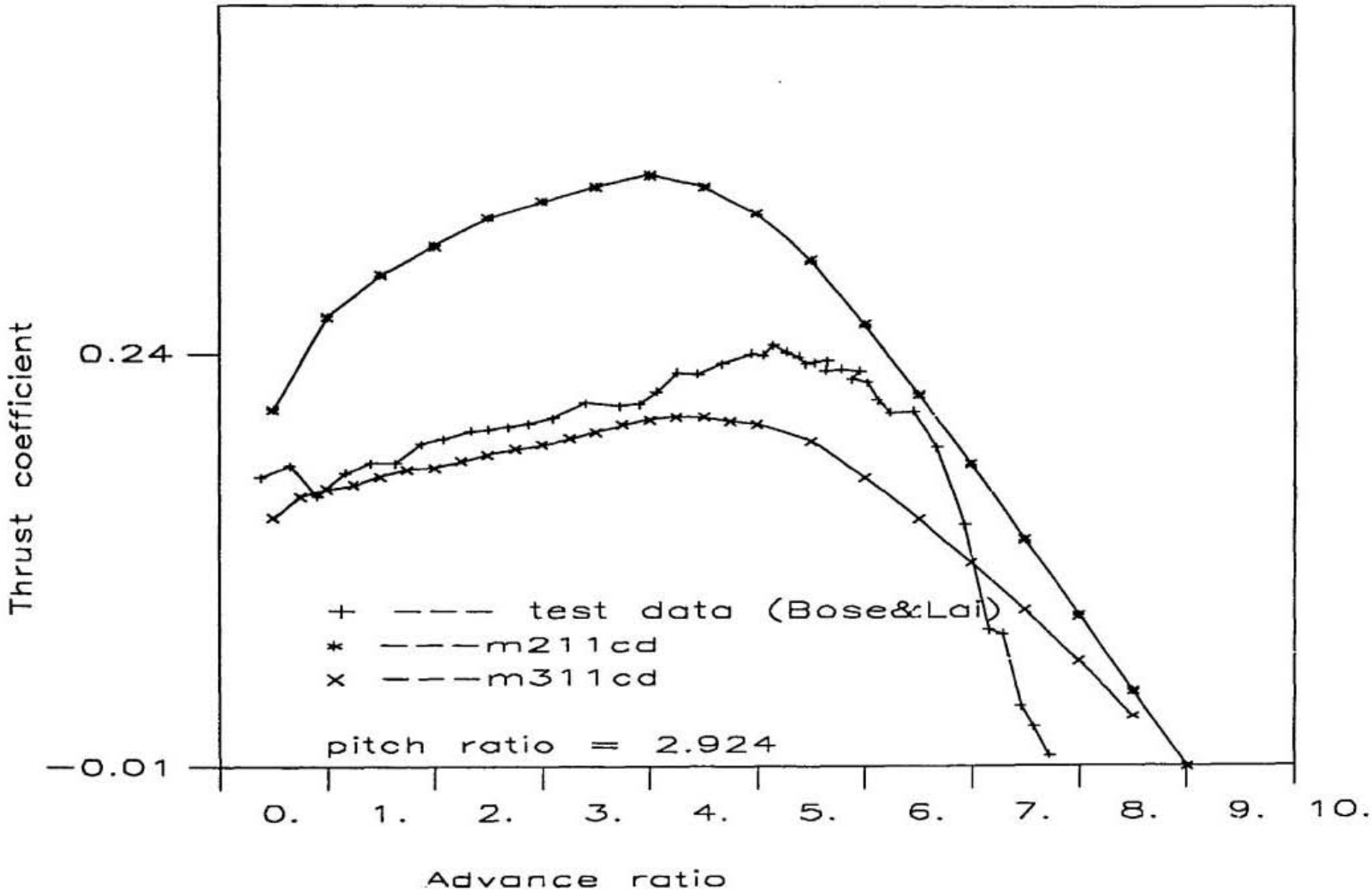


Figure F-22: Comparison of theoretical results with test results — thrust coefficient(pitch ratio=2.924π)

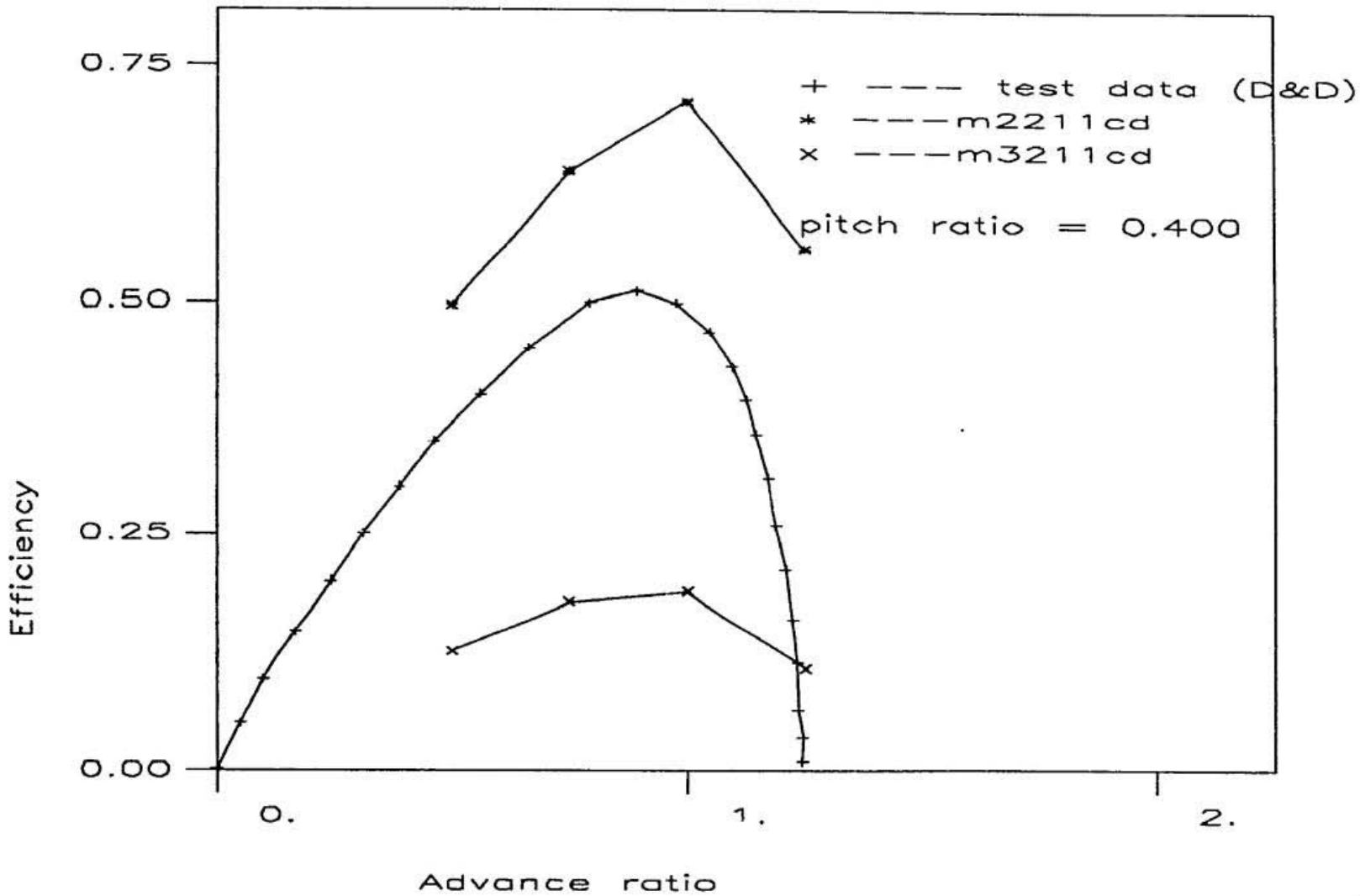


Figure F-23: Comparison of theoretical results with test results — efficiency (pitch ratio=0.4π)

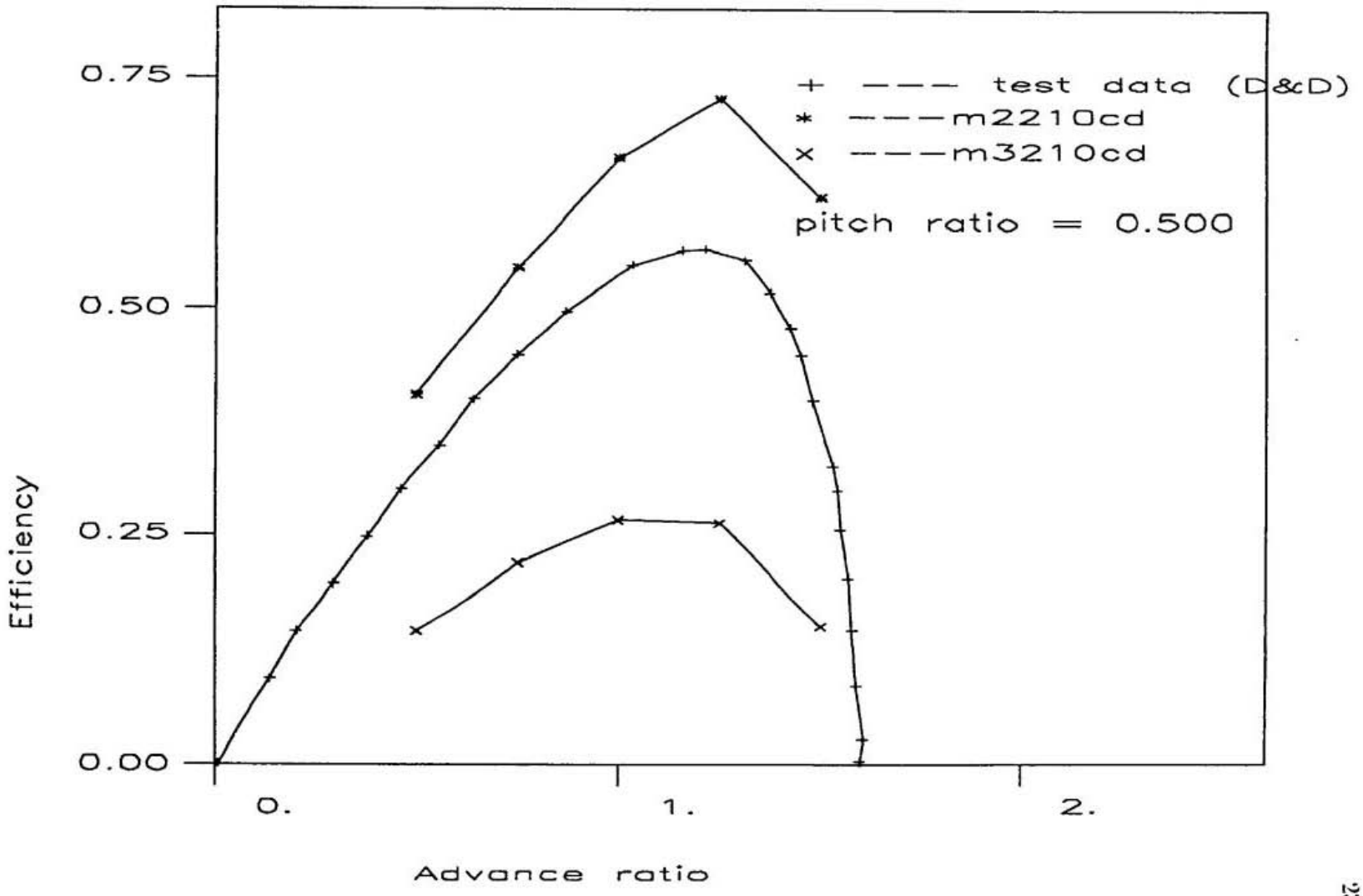


Figure F-24: Comparison of theoretical results with test results — efficiency (pitch ratio=0.5π)

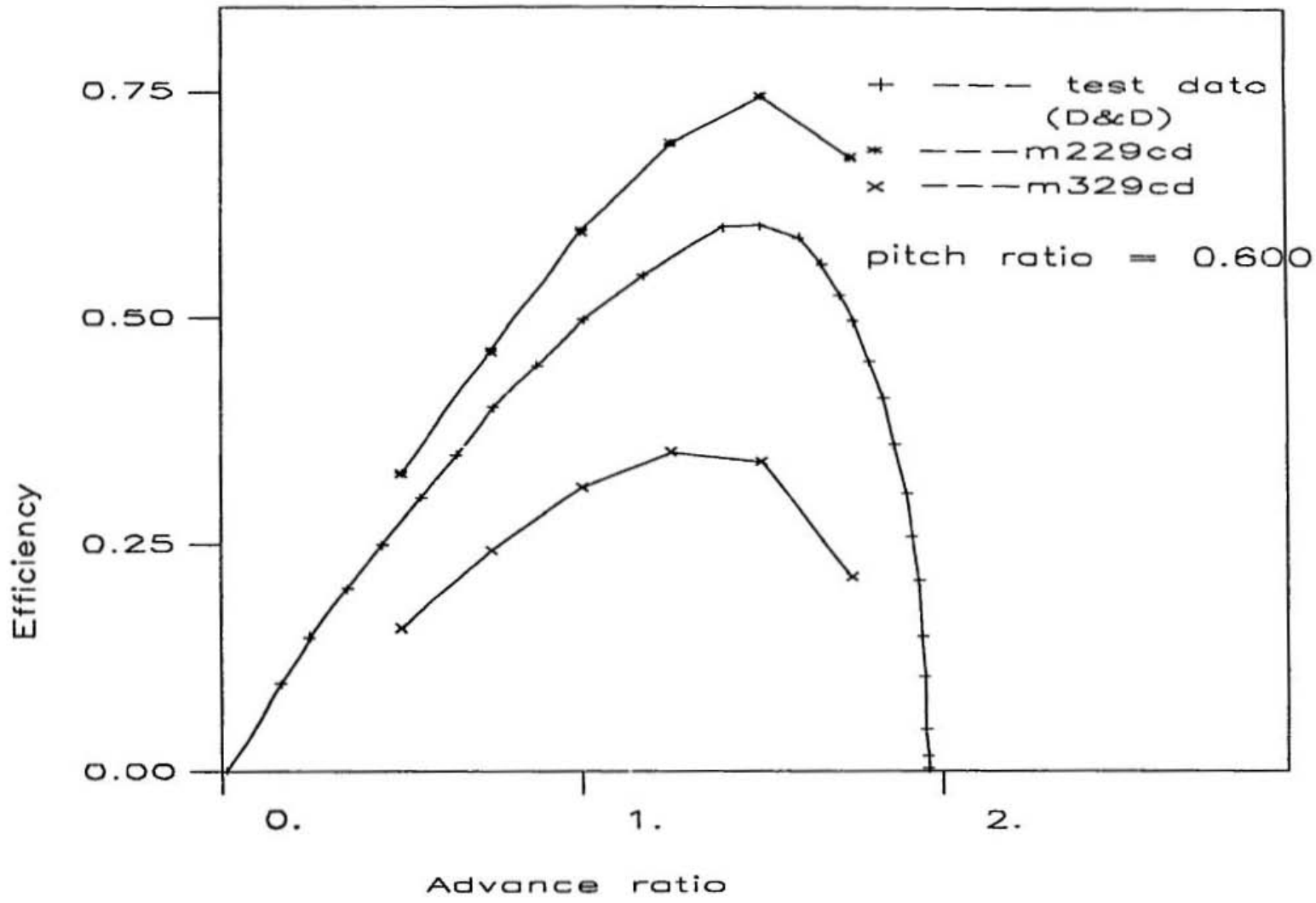


Figure F-25: Comparison of theoretical results with test results — efficiency (pitch ratio=0.6π)

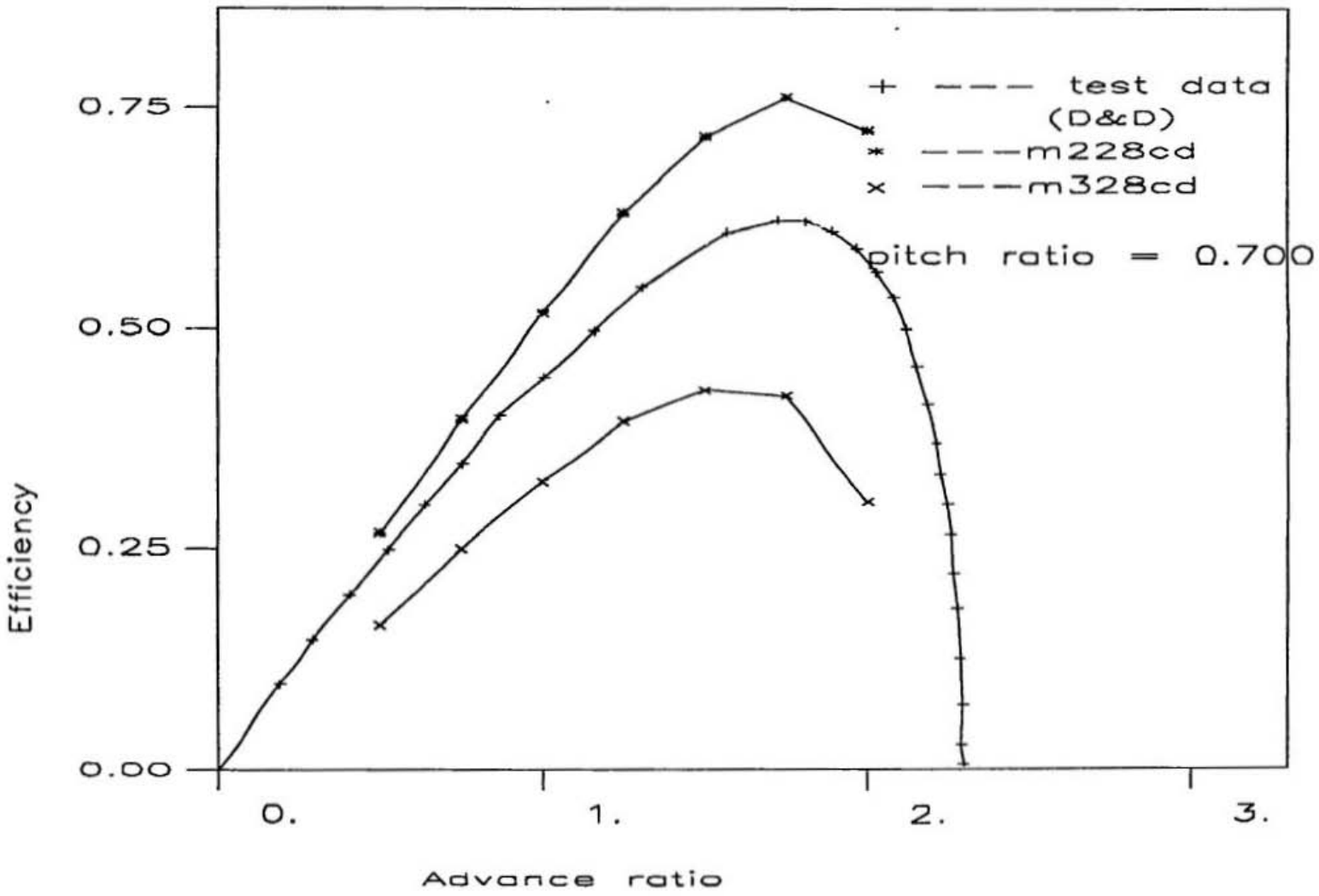


Figure F-26: Comparison of theoretical results with test results — efficiency (pitch ratio=0.7π)

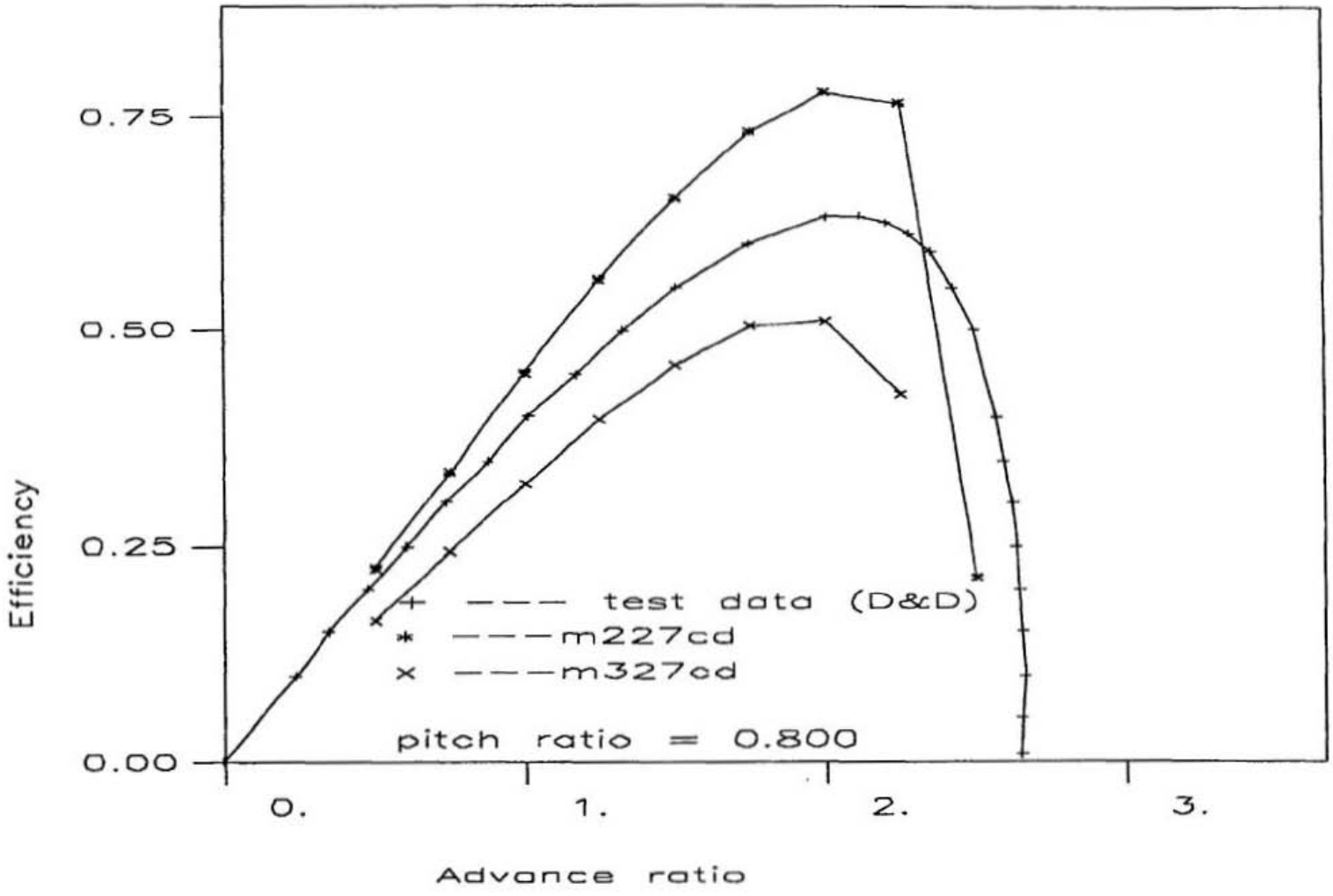


Figure F-27: Comparison of theoretical results with test results — efficiency (pitch ratio=0.8π)

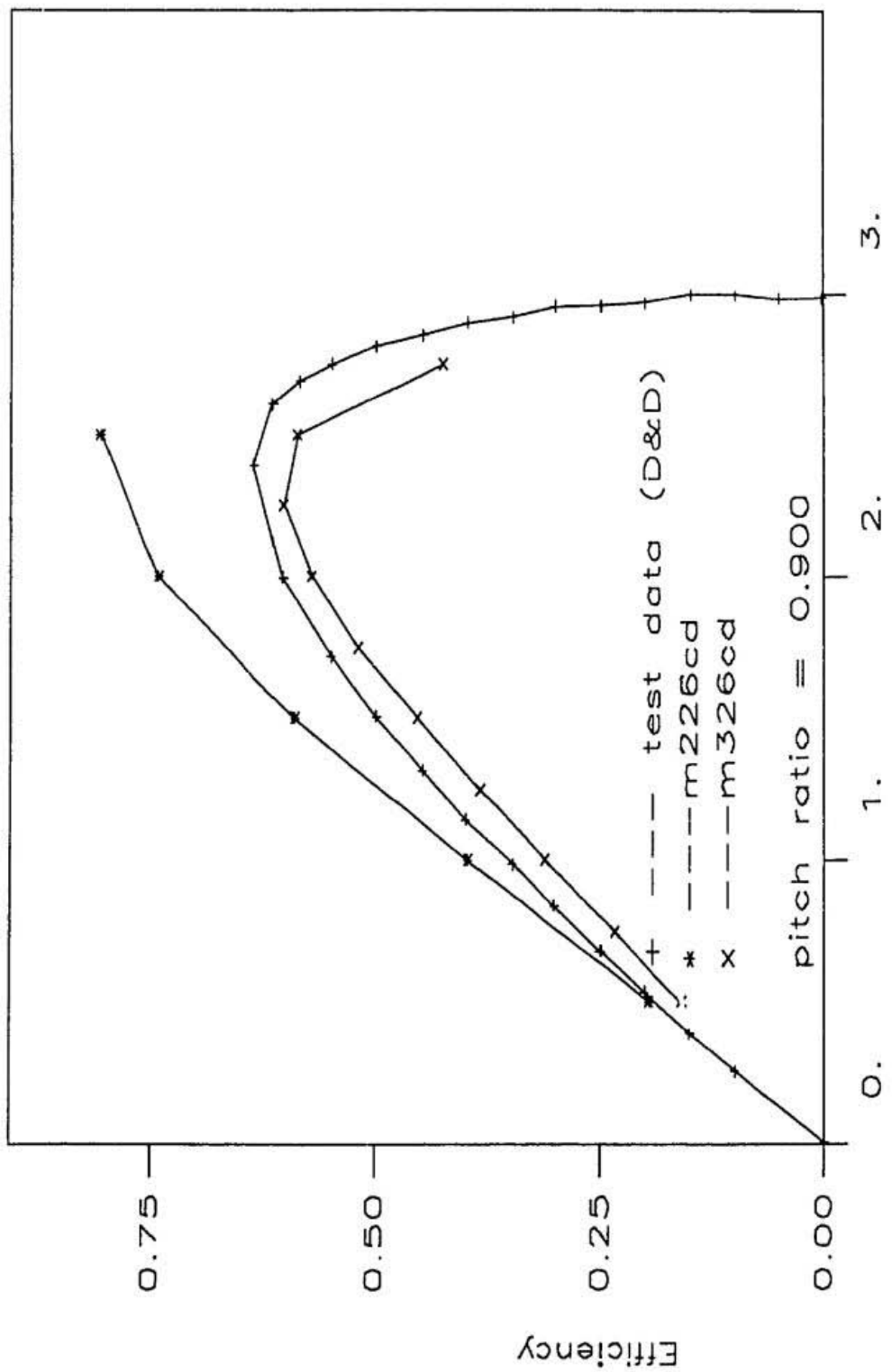


Figure F-28: Comparison of theoretical results with test results — efficiency (pitch ratio=0.9π)

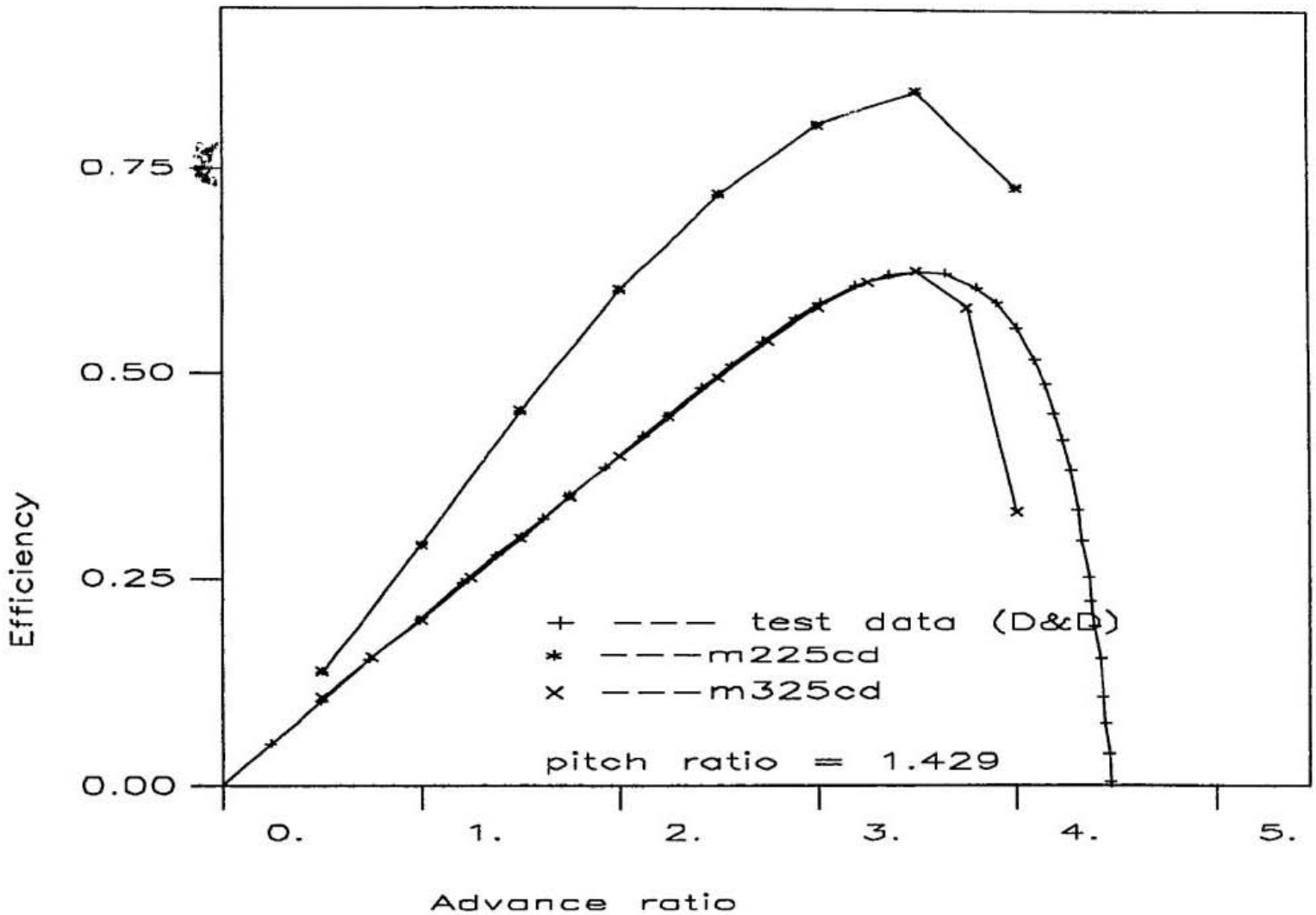


Figure F-29: Comparison of theoretical results with test results — efficiency (pitch ratio=1.429π)

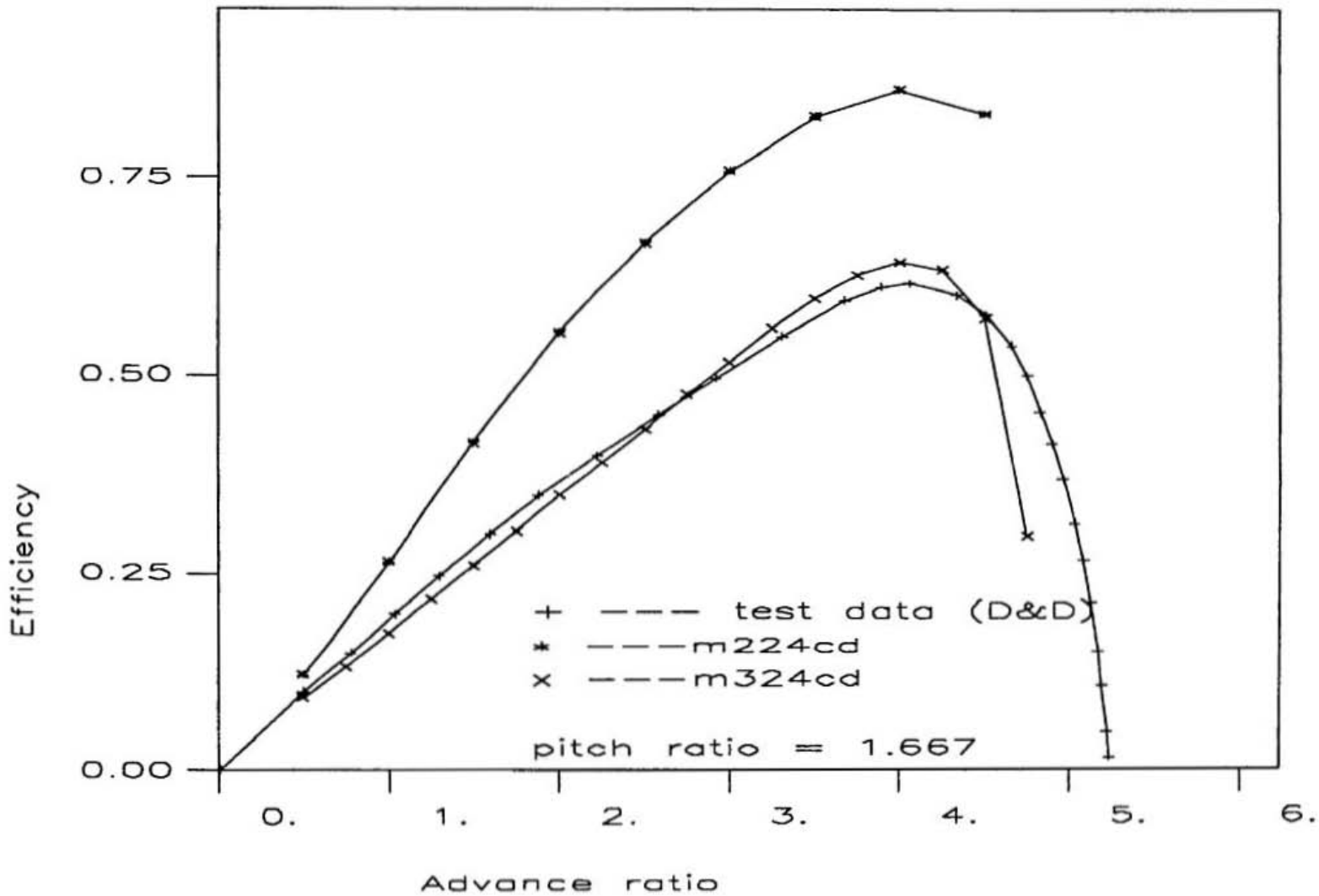


Figure F-30: Comparison of theoretical results with test results — efficiency (pitch ratio=1.667π)

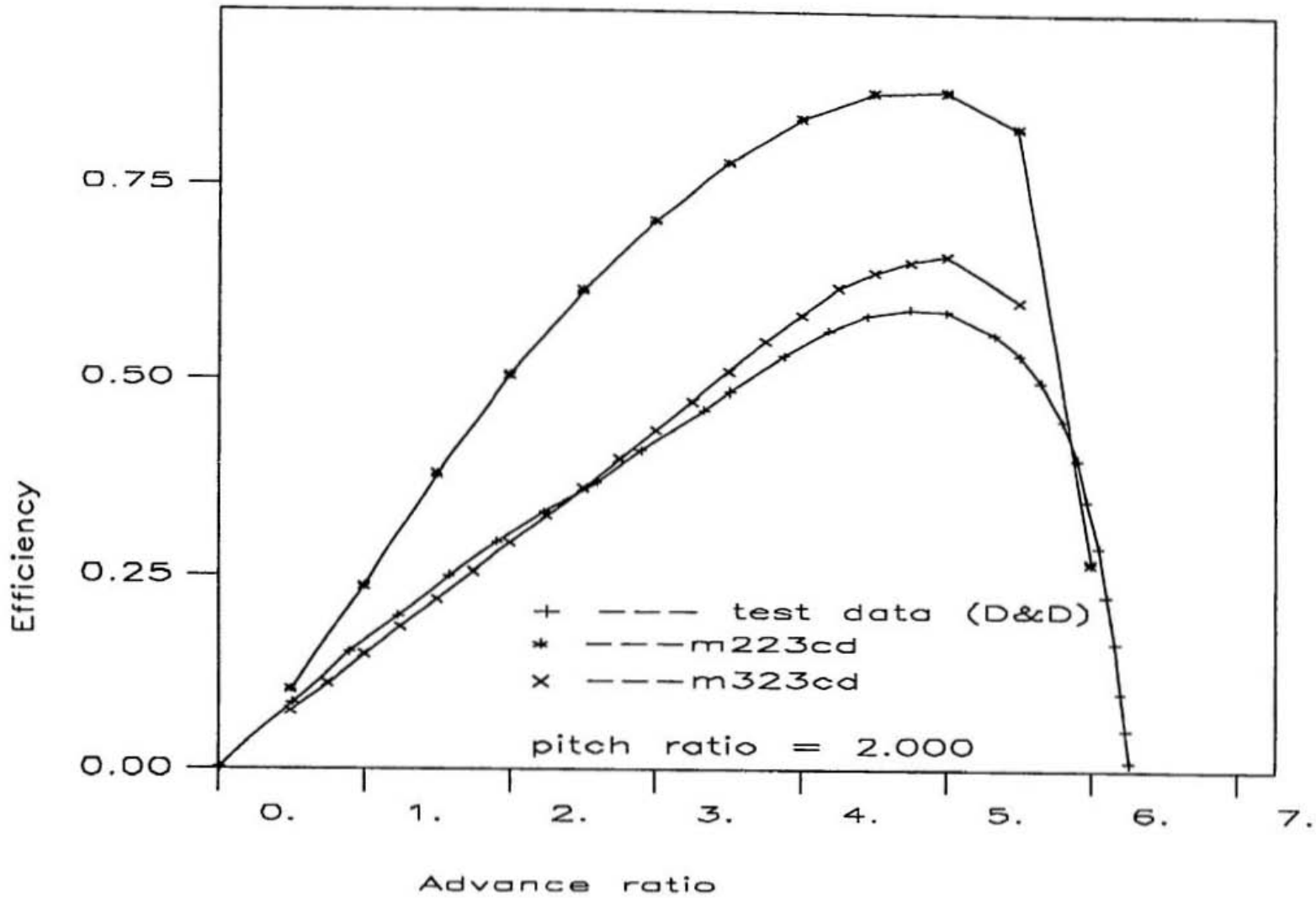


Figure F-31: Comparison of theoretical results with test results — efficiency (pitch ratio=2.000π)

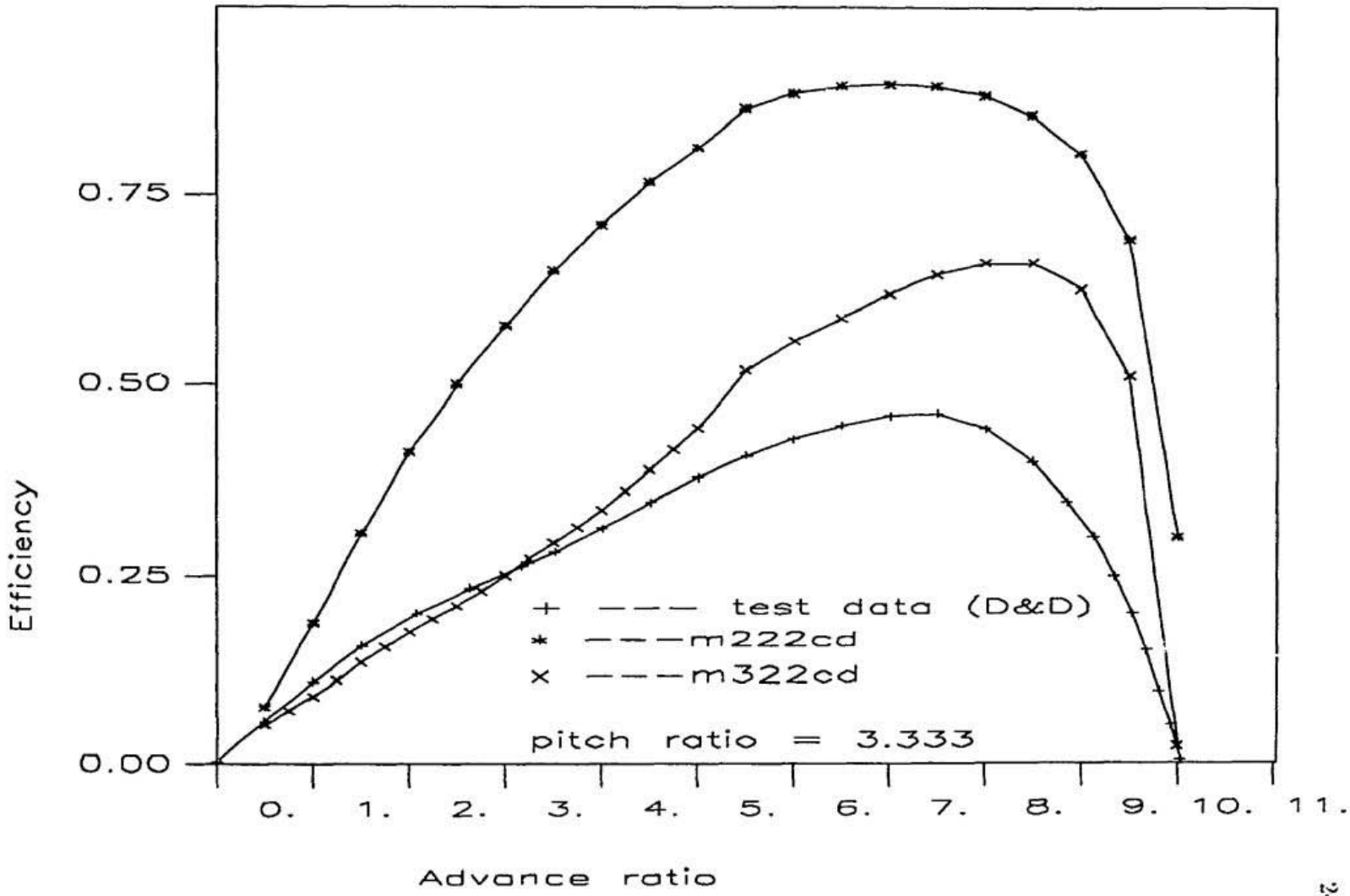


Figure F-32: Comparison of theoretical results with test results — efficiency (pitch ratio=3.333π)

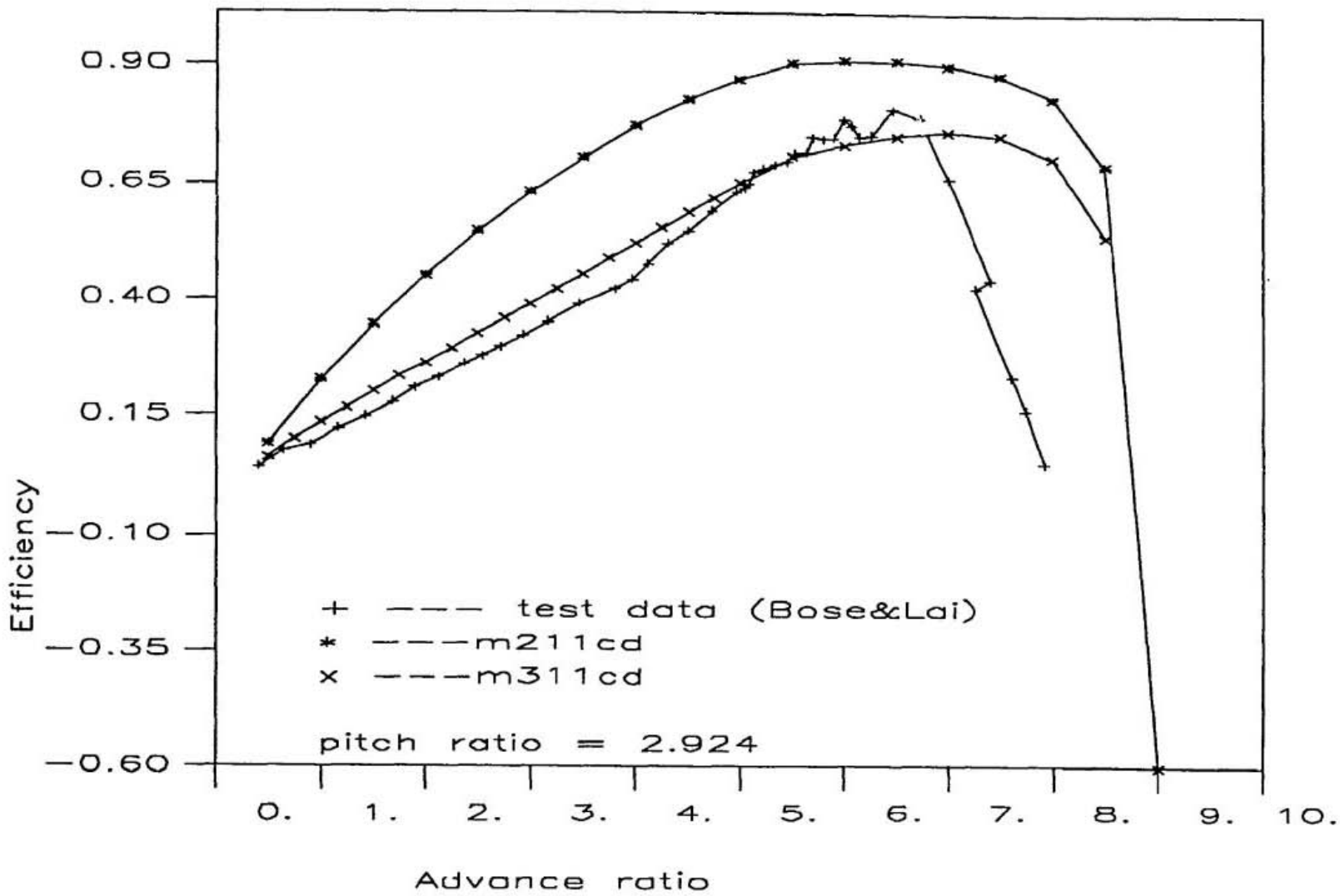


Figure F-33: Comparison of theoretical results with test results — efficiency (pitch ratio=2.924π)

Appendix G

Theoretical Results — Part III

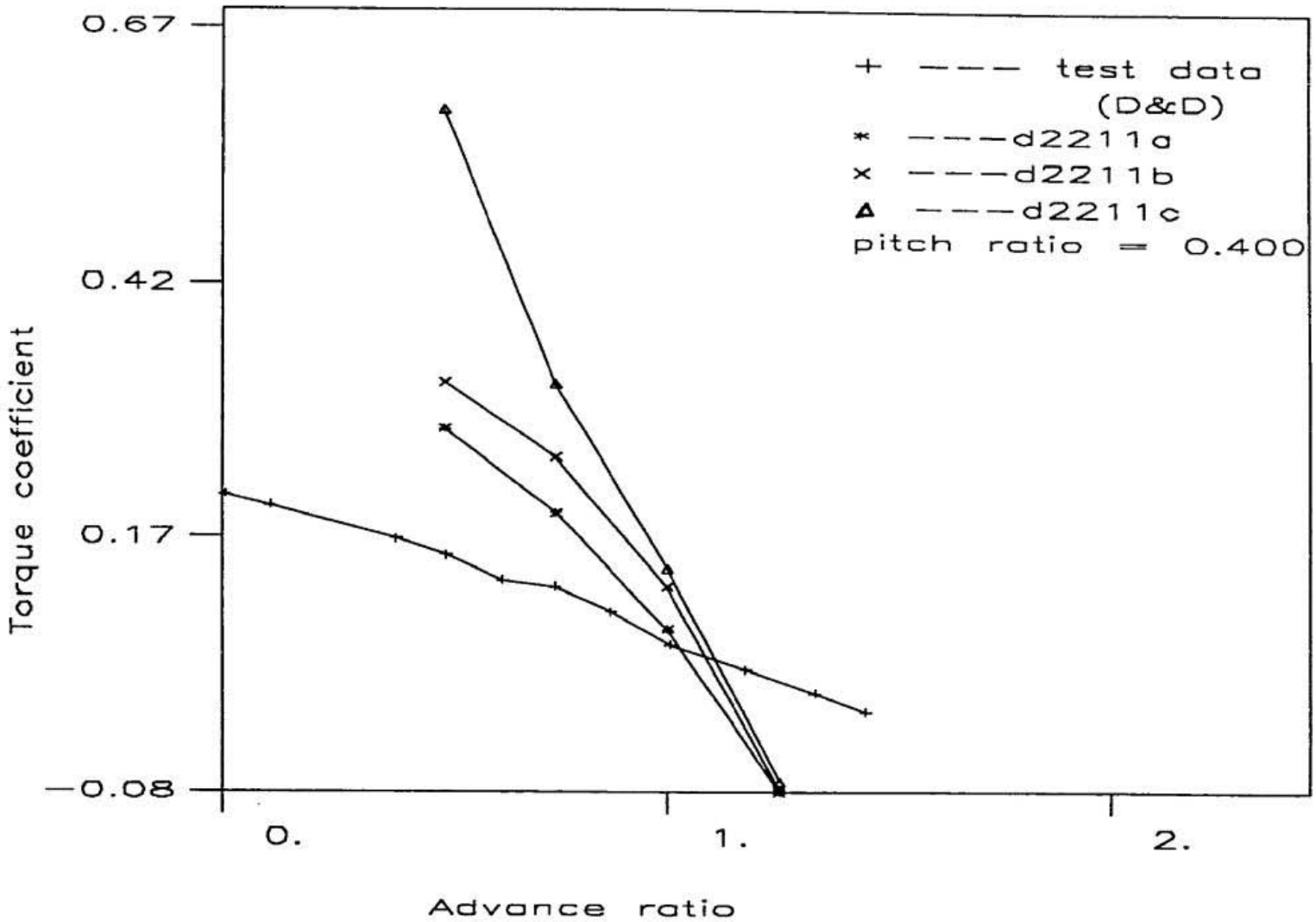


Figure G-1: Comparison of theoretical results with test results — torque coefficient(pitch ratio=0.4π)

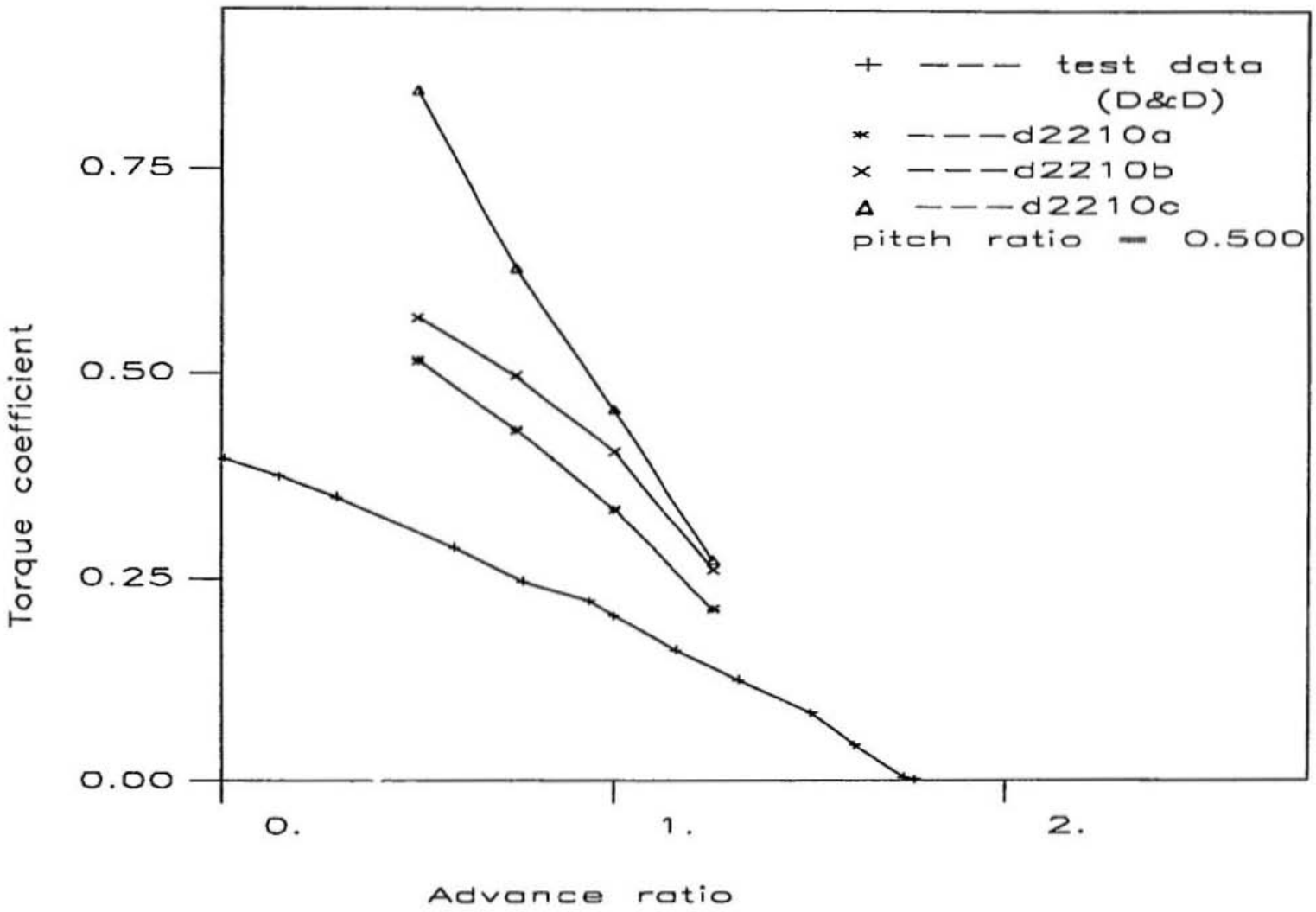


Figure G-2: Comparison of theoretical results with test results — torque coefficient(pitch ratio=0.5π)

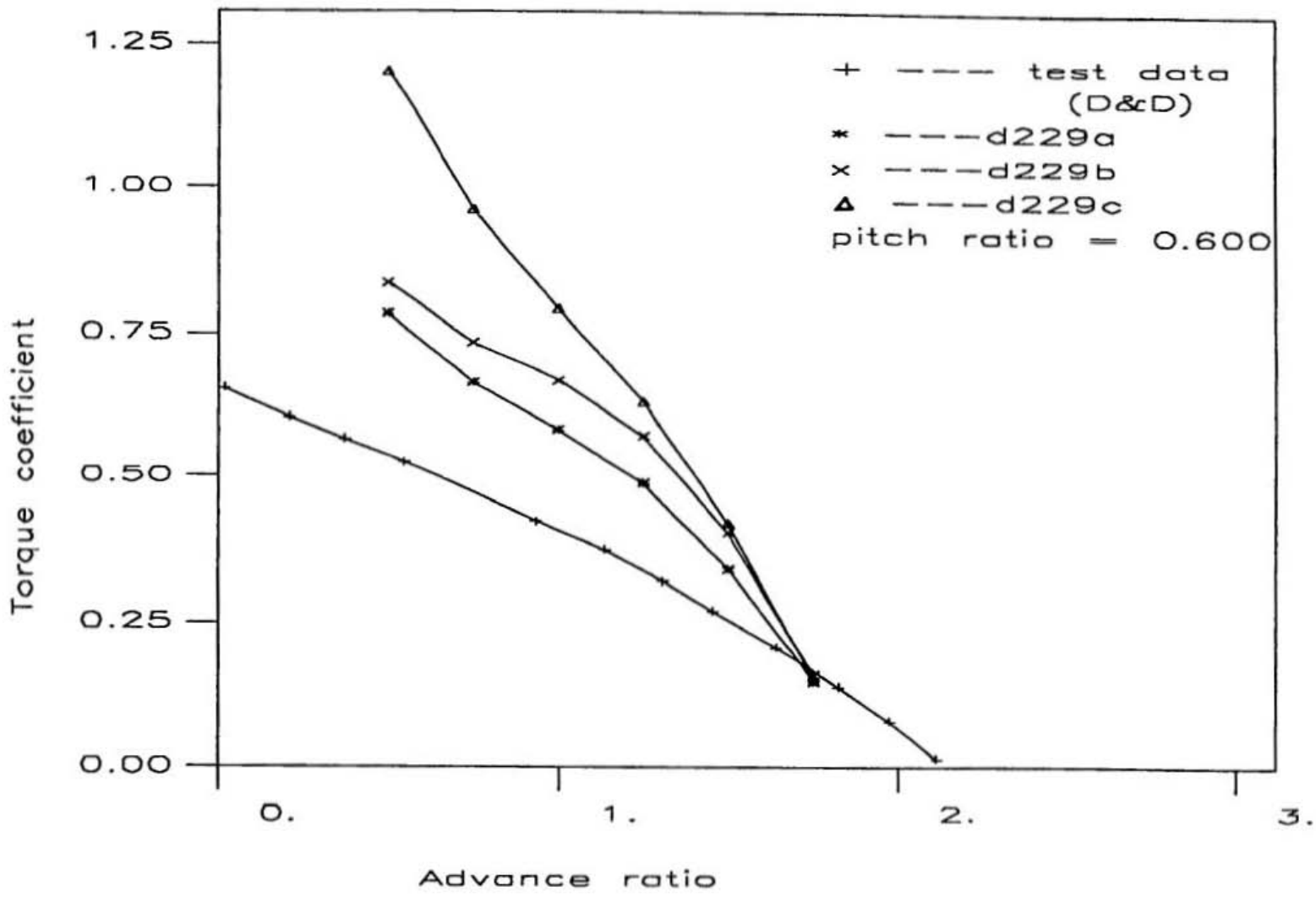


Figure G-3: Comparison of theoretical results with test results — torque coefficient(pitch ratio=0.6π)

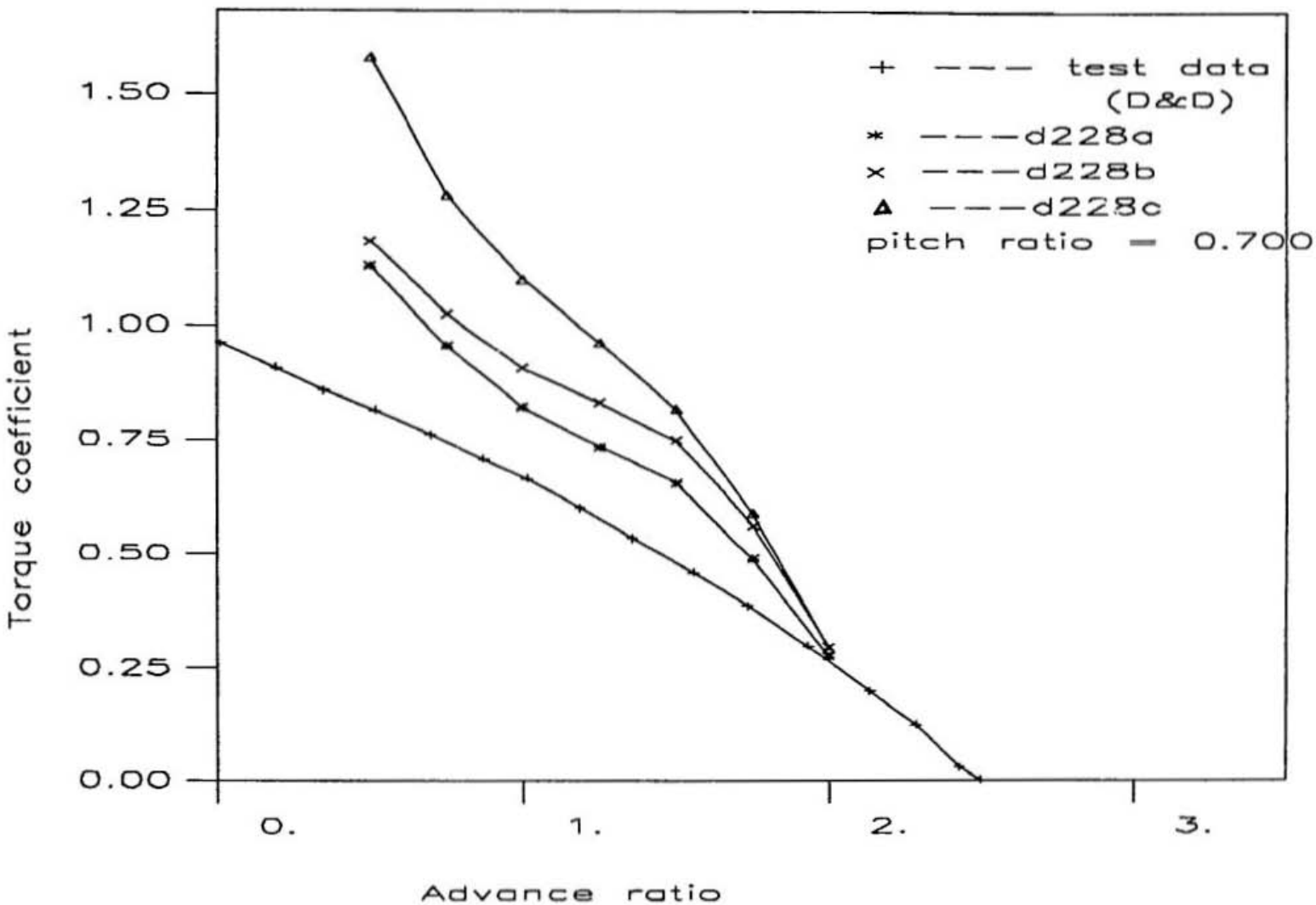


Figure G-4: Comparison of theoretical results with test results — torque coefficient(pitch ratio=0.7π)

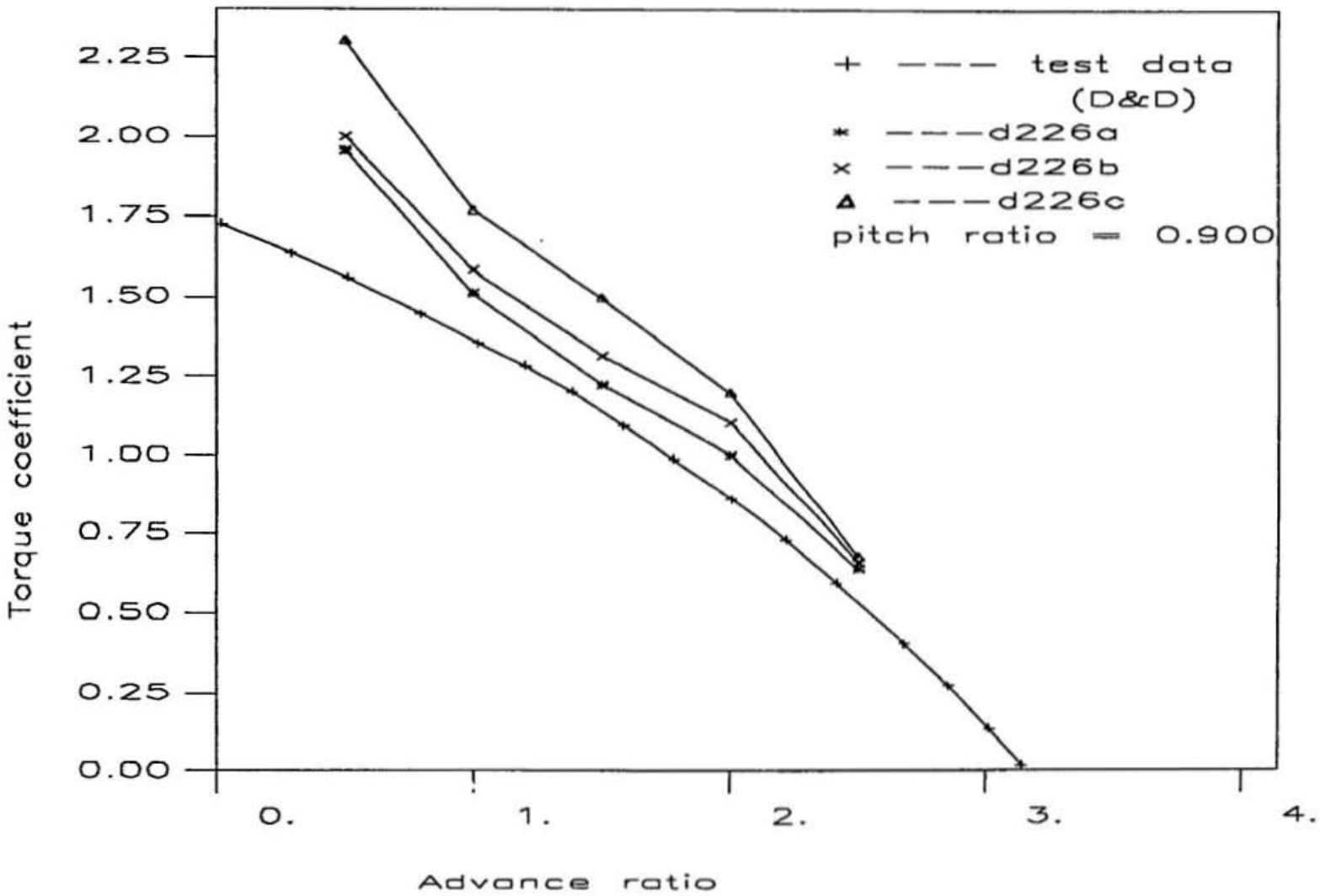


Figure G-6: Comparison of theoretical results with test results — torque coefficient(pitch ratio=0.9π)

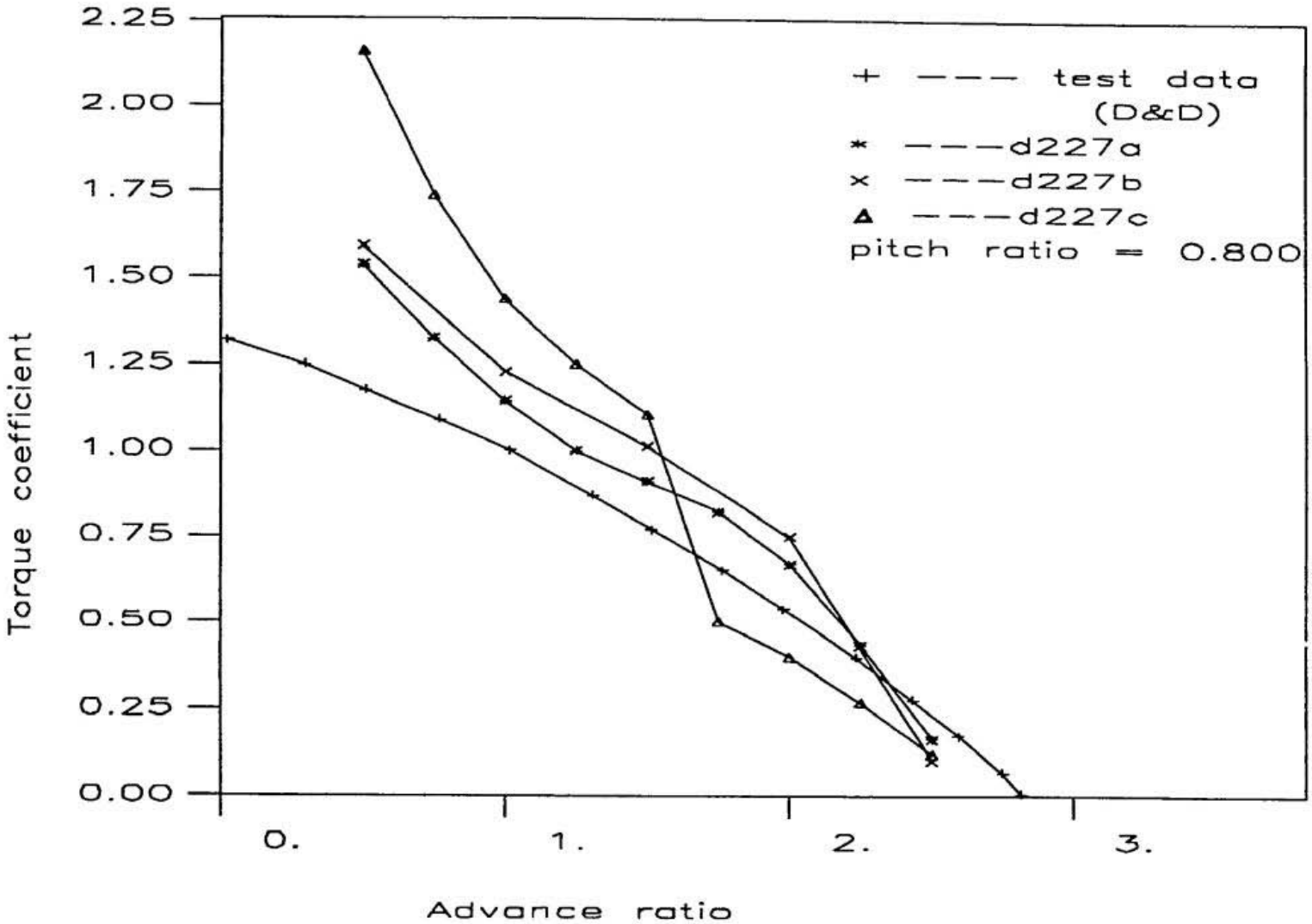


Figure G-5: Comparison of theoretical results with test results — torque coefficient(pitch ratio=0.8π)

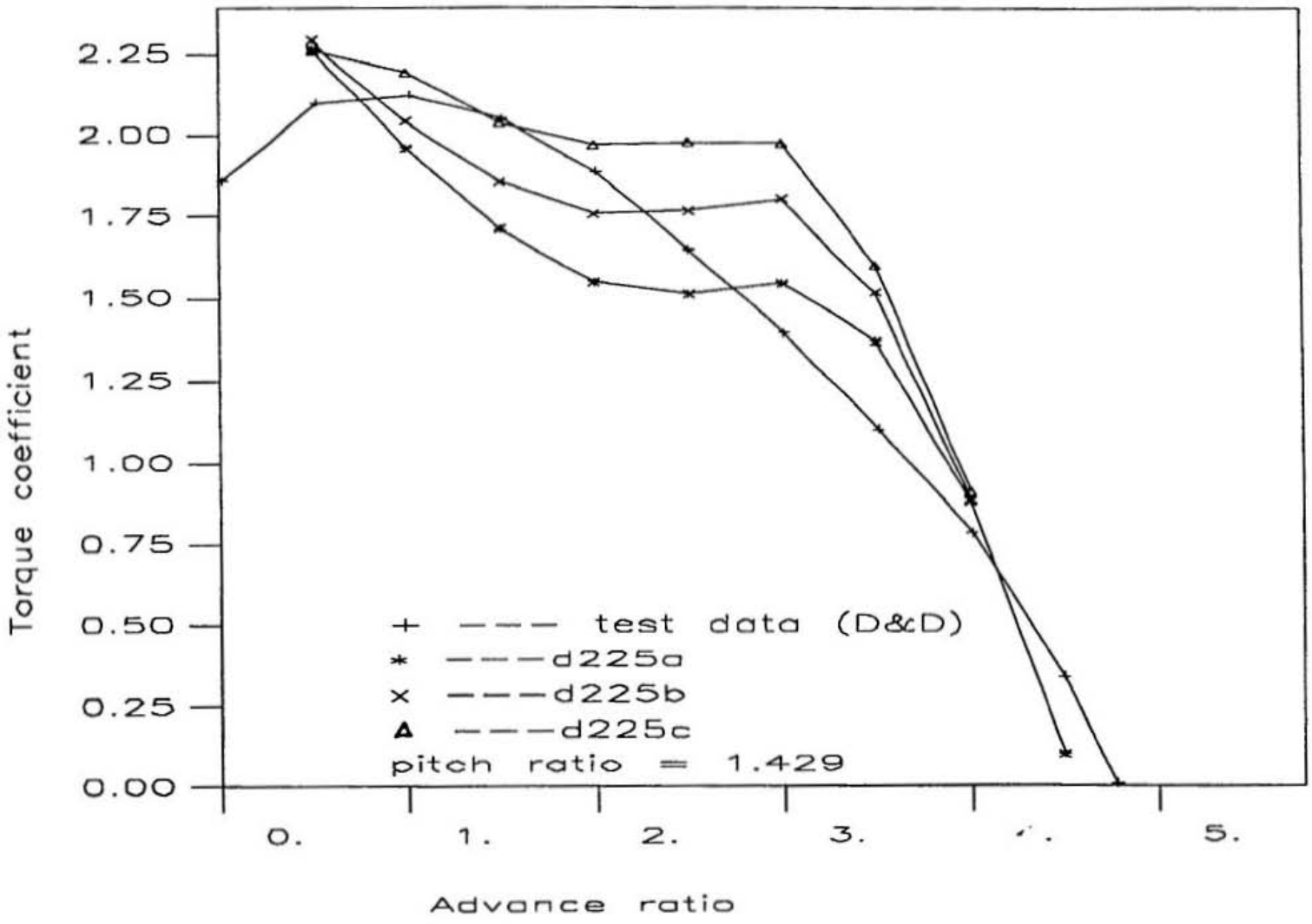


Figure G-7: Comparison of theoretical results with test results — torque coefficient(pitch ratio=1.429π)

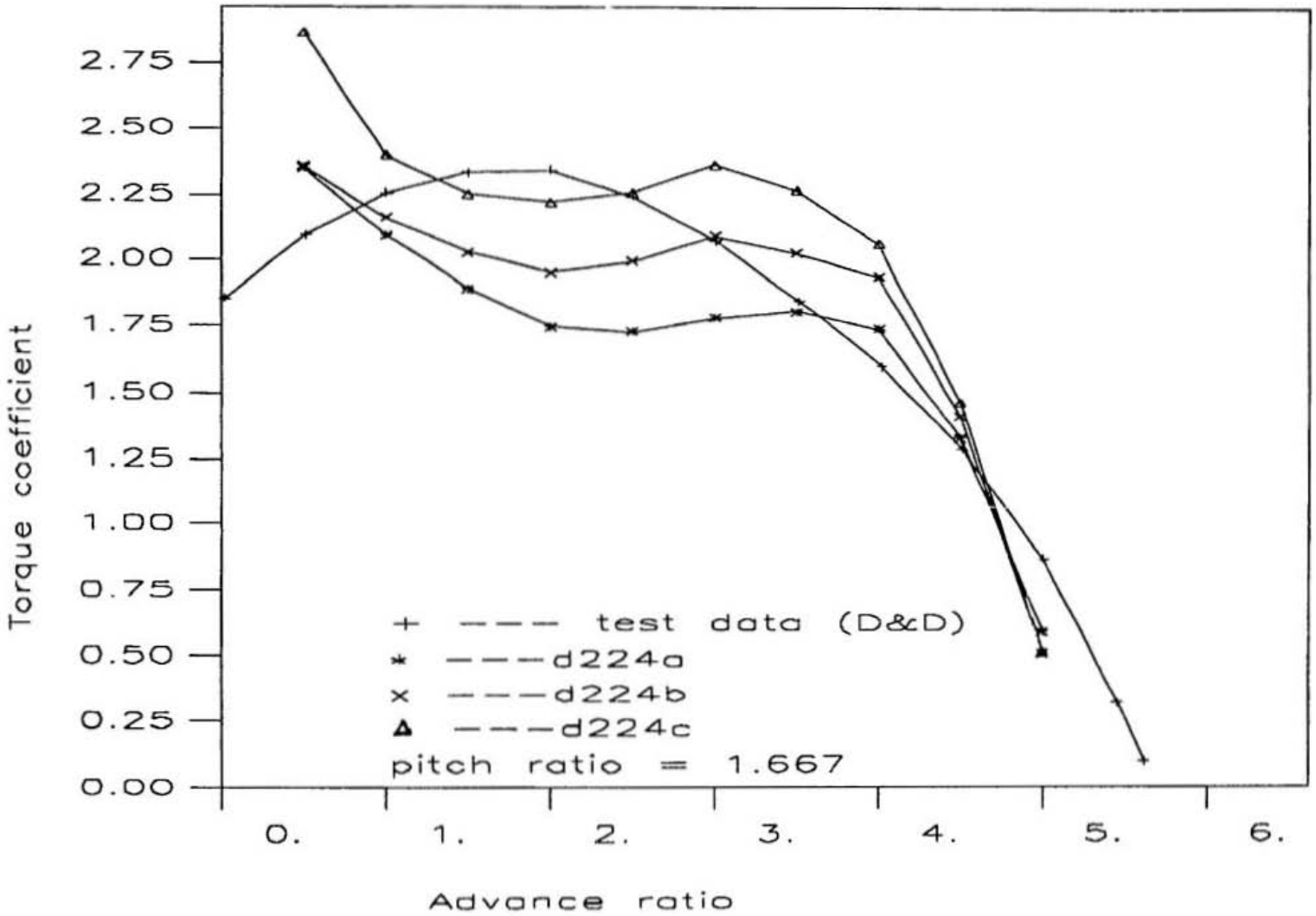


Figure G-8: Comparison of theoretical results with test results — torque coefficient (pitch ratio=1.667π)

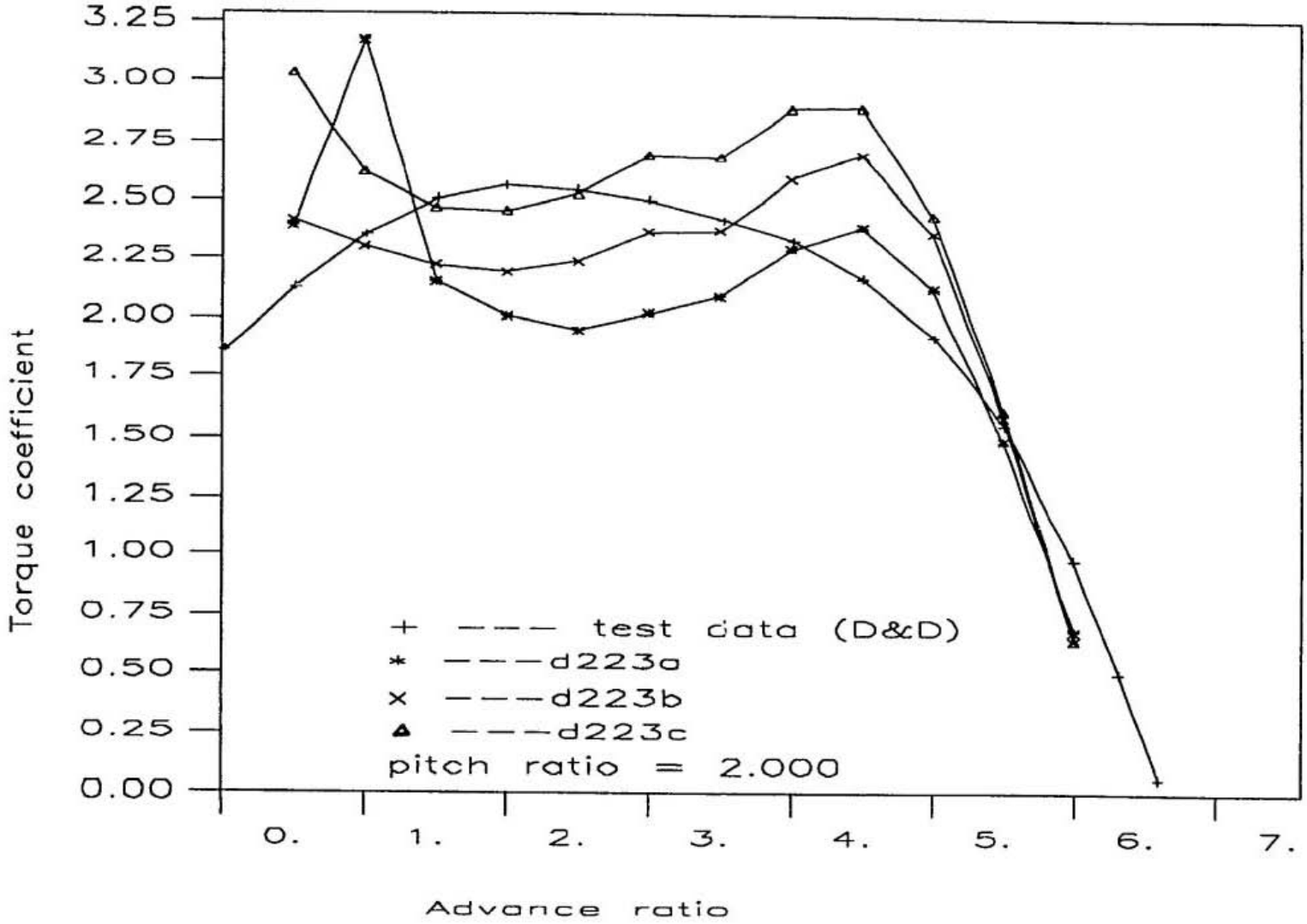


Figure G-9: Comparison of theoretical results with test results — torque coefficient(pitch ratio=2.000π)

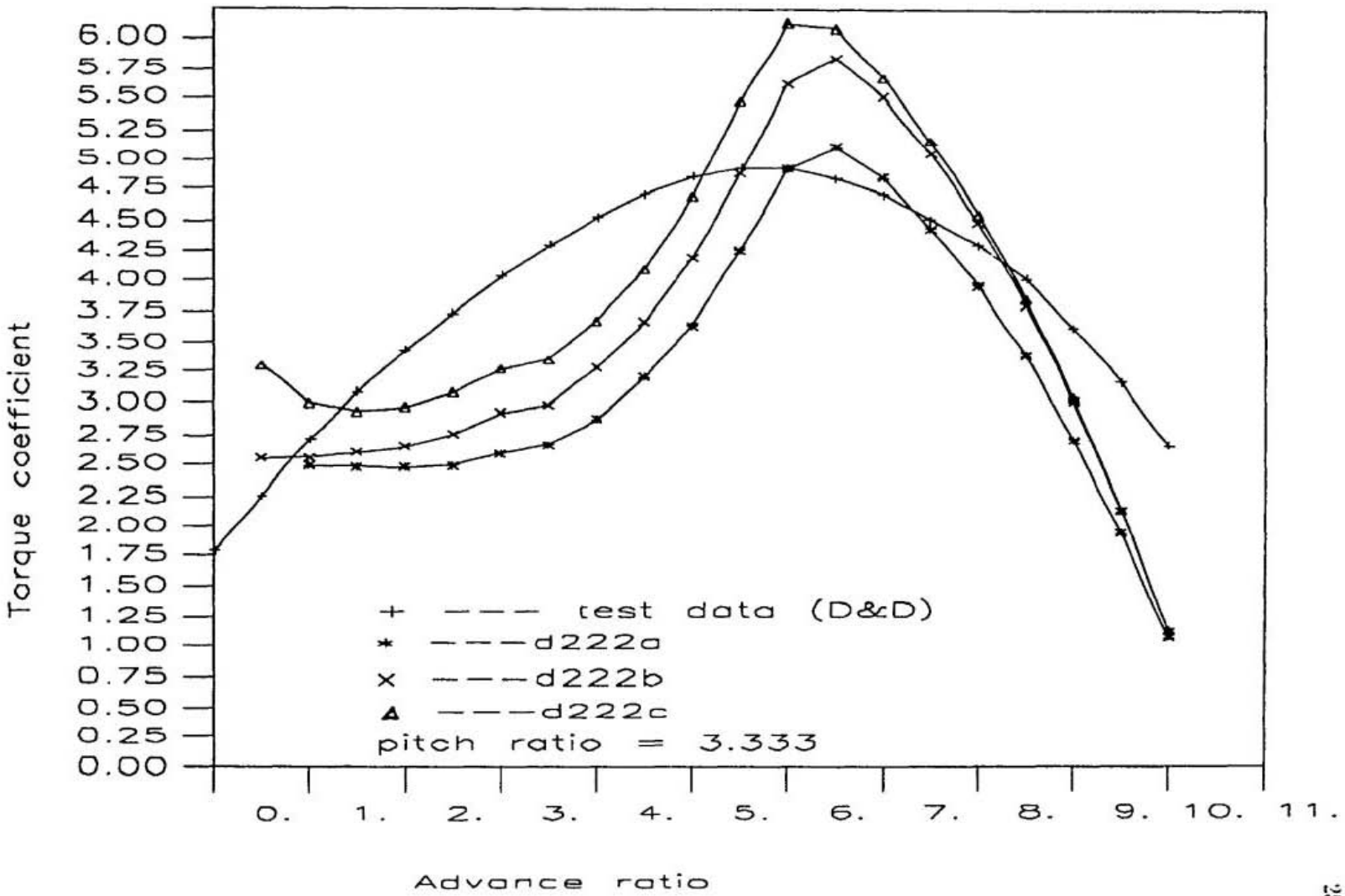


Figure G-10: Comparison of theoretical results with test results — torque coefficient(pitch ratio=3.333π)

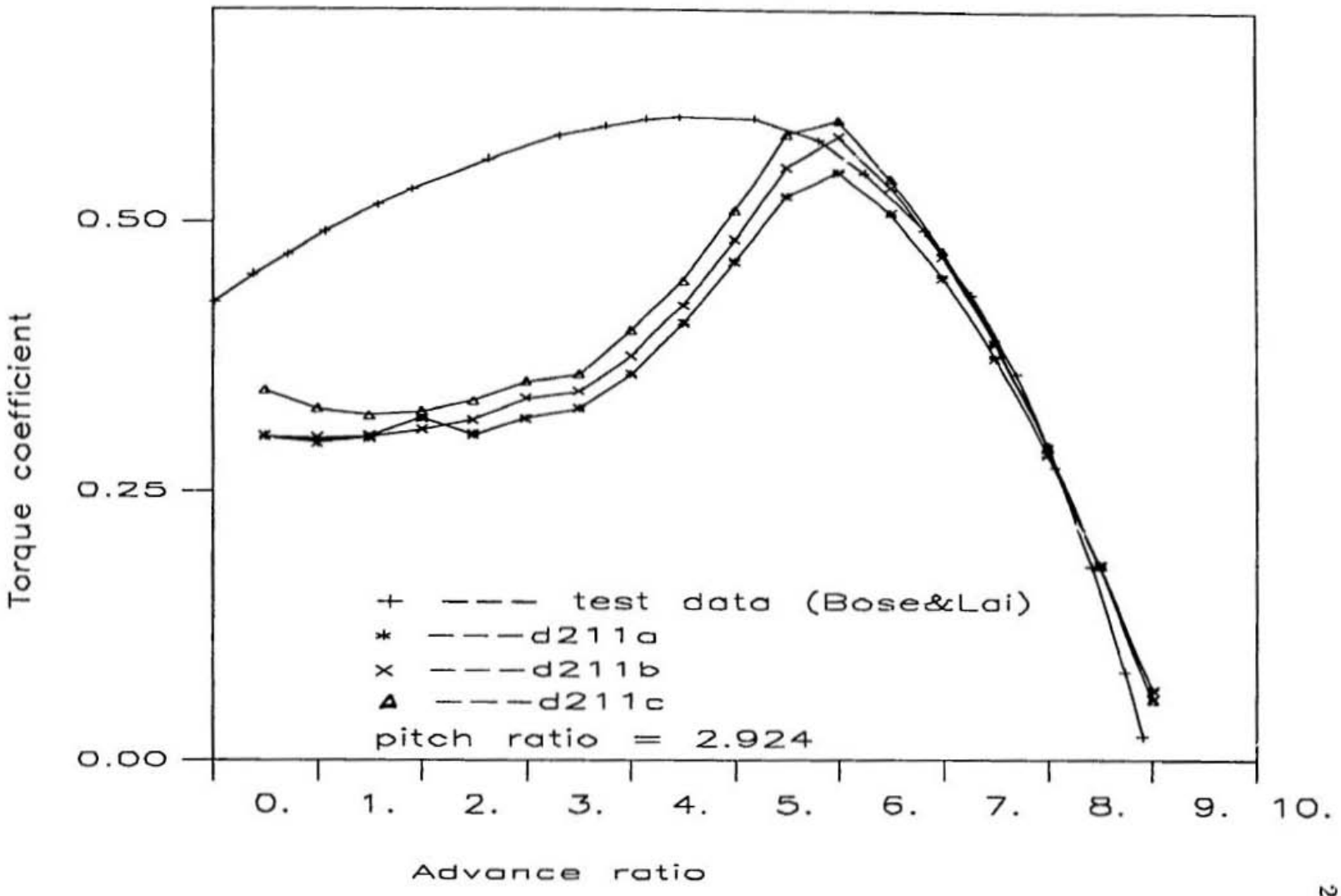


Figure G-11: Comparison of theoretical results with test results — torque coefficient(pitch ratio=2.924π)

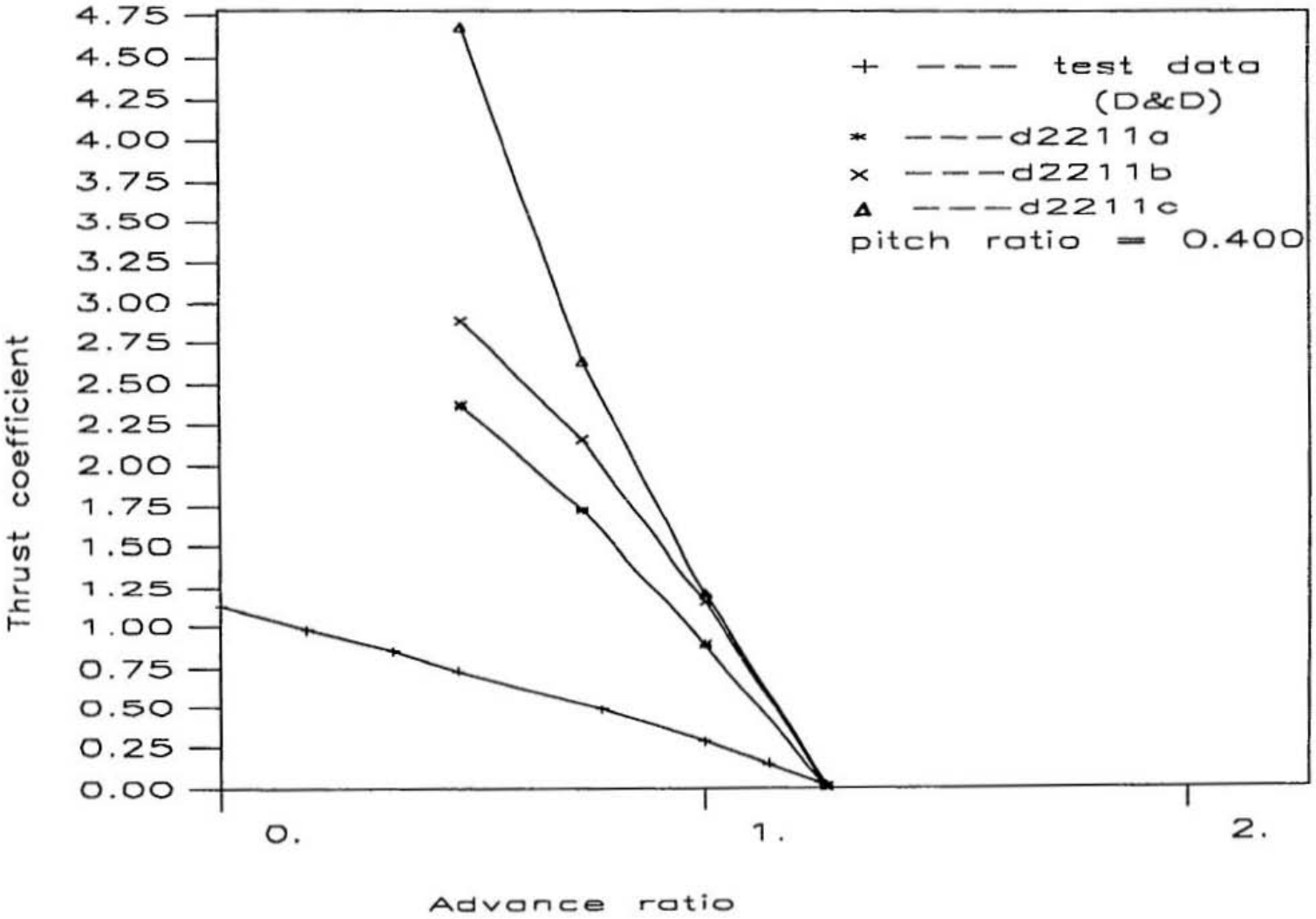


Figure G-12: Comparison of theoretical results with test results — thrust coefficient(pitch ratio=0.4π)

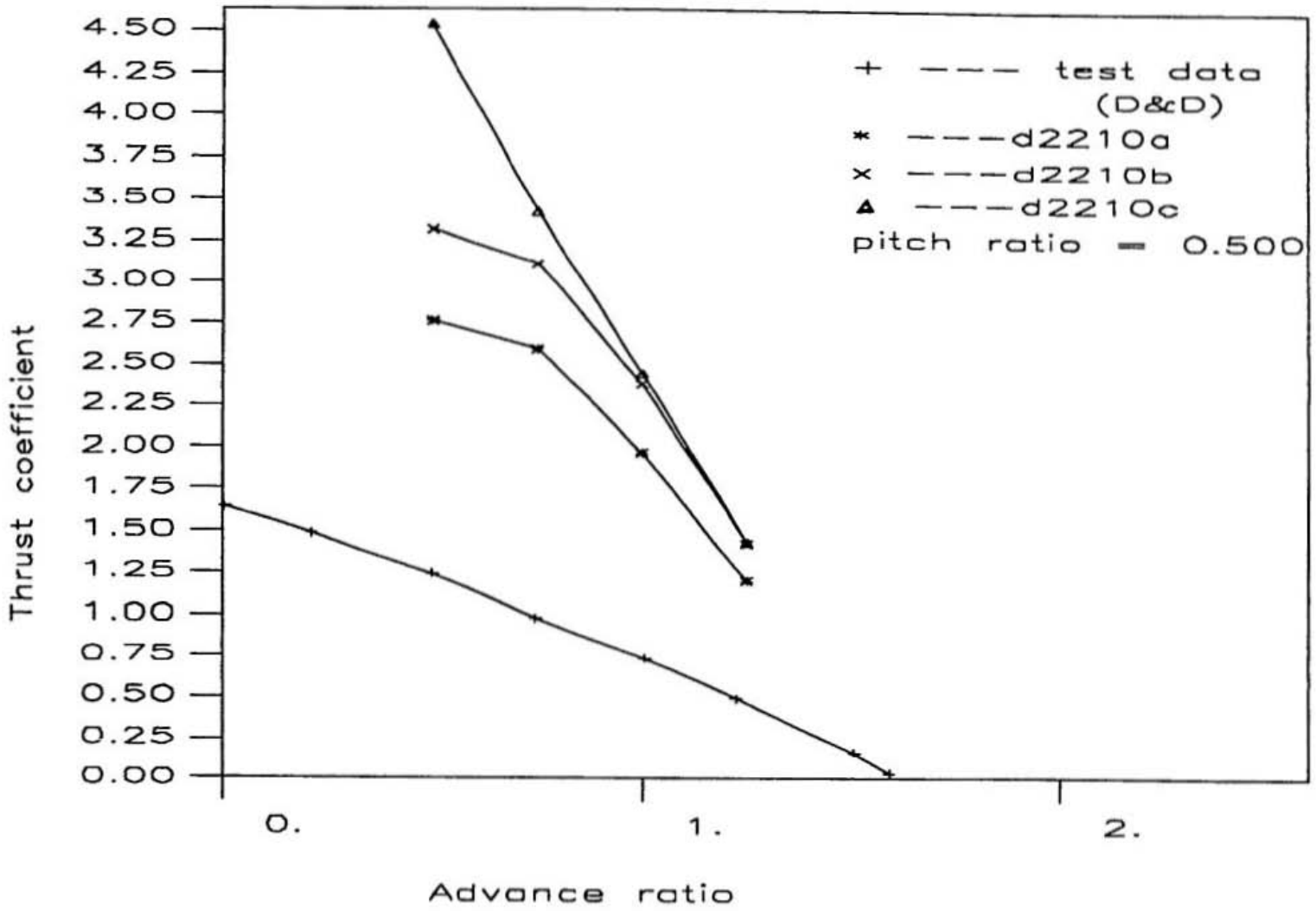


Figure G-13: Comparison of theoretical results with test results — thrust coefficient(pitch ratio=0.5π)

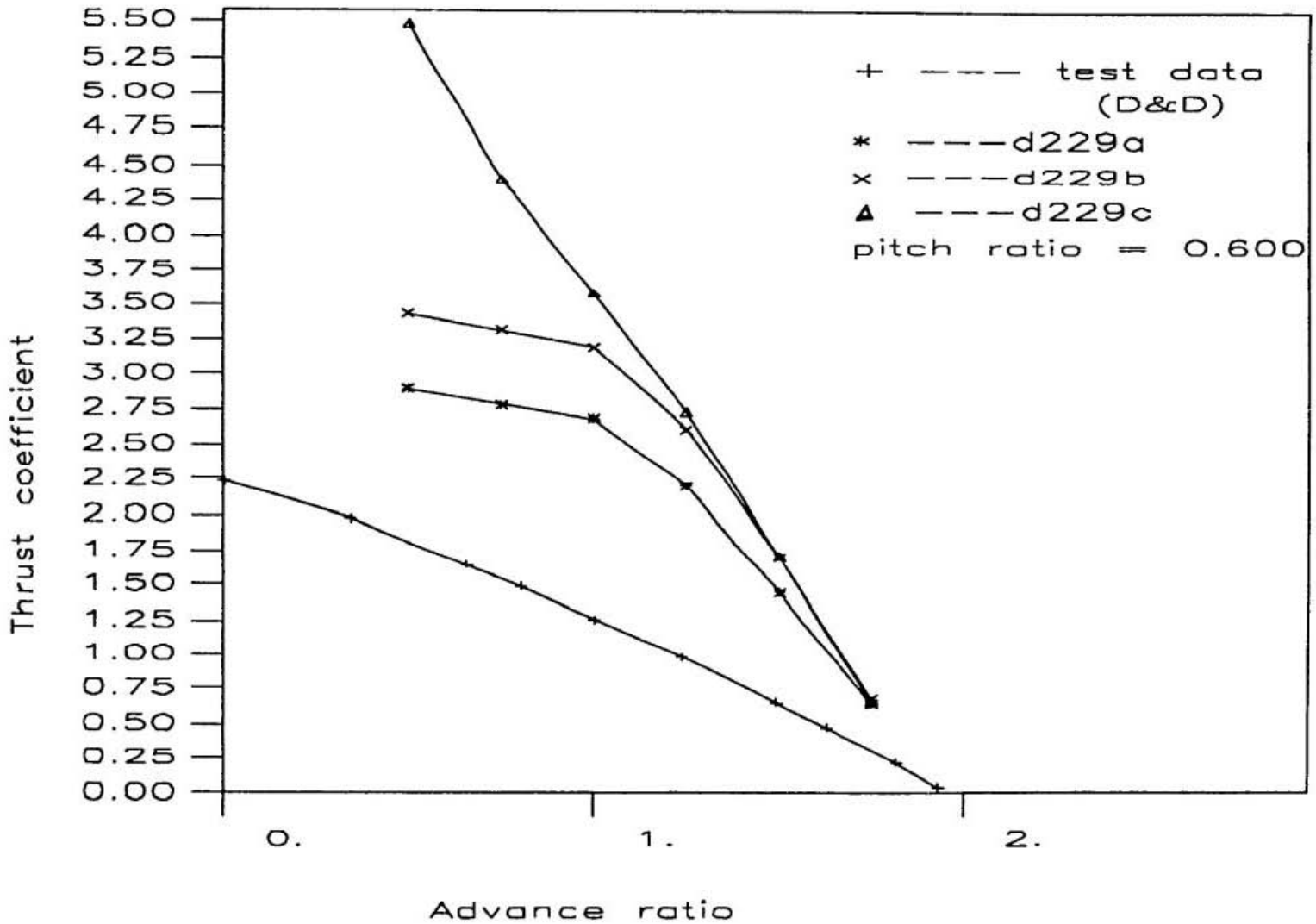


Figure G-14: Comparison of theoretical results with test results — thrust coefficient(pitch ratio=0.6π)

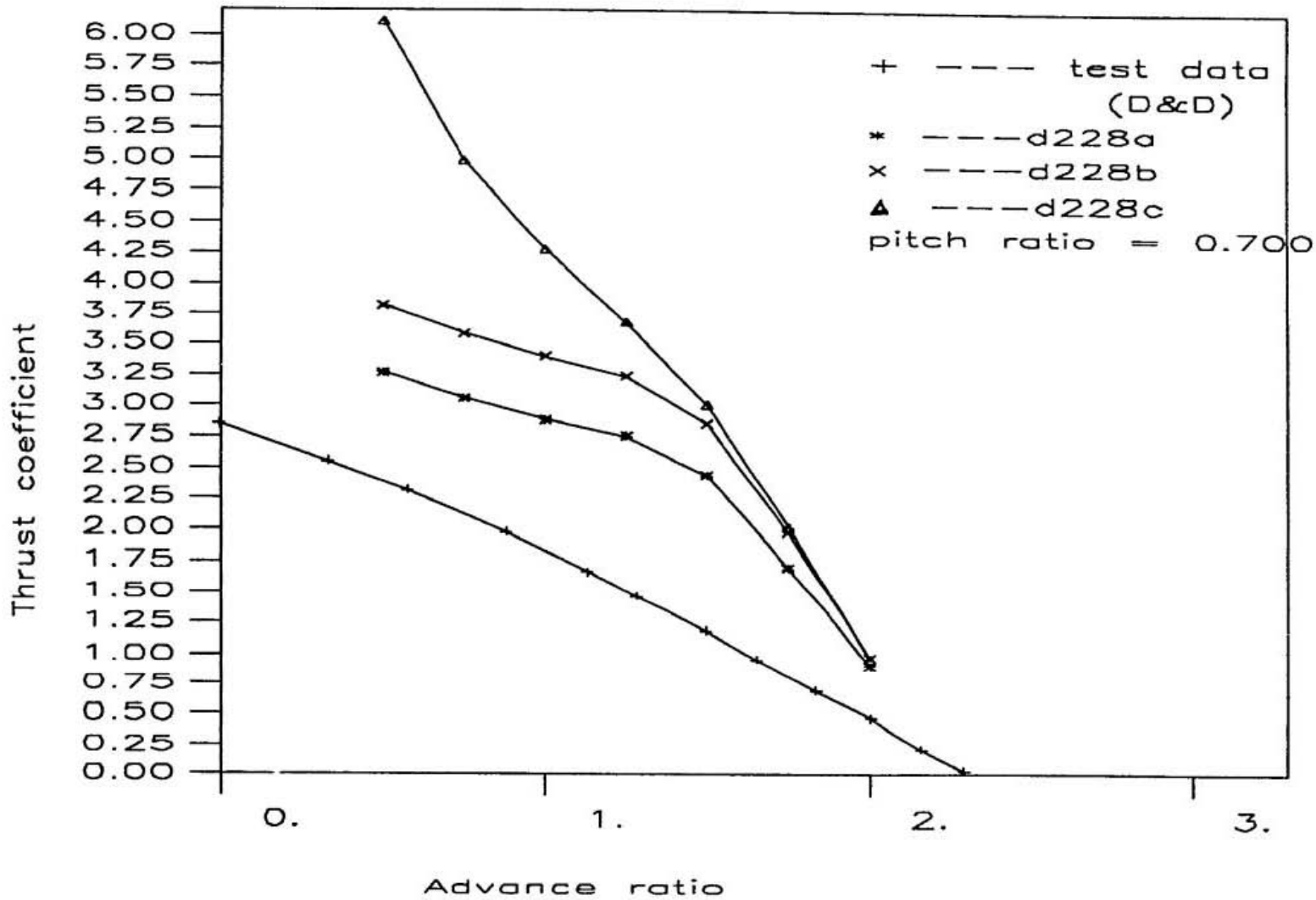


Figure G-15: Comparison of theoretical results with test results — thrust coefficient(pitch ratio=0.7π)

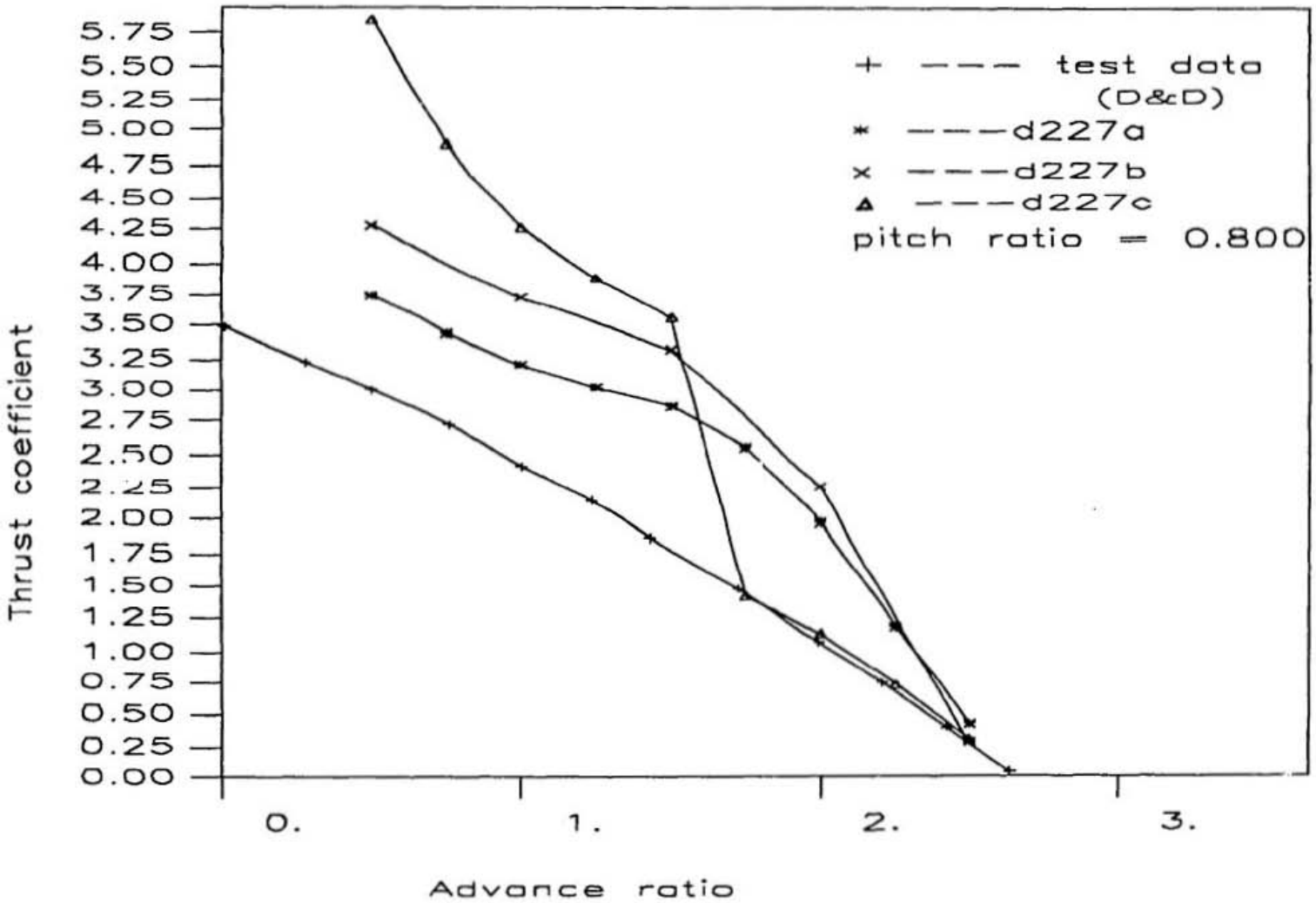


Figure G-16: Comparison of theoretical results with test results — thrust coefficient(pitch ratio=0.8π)

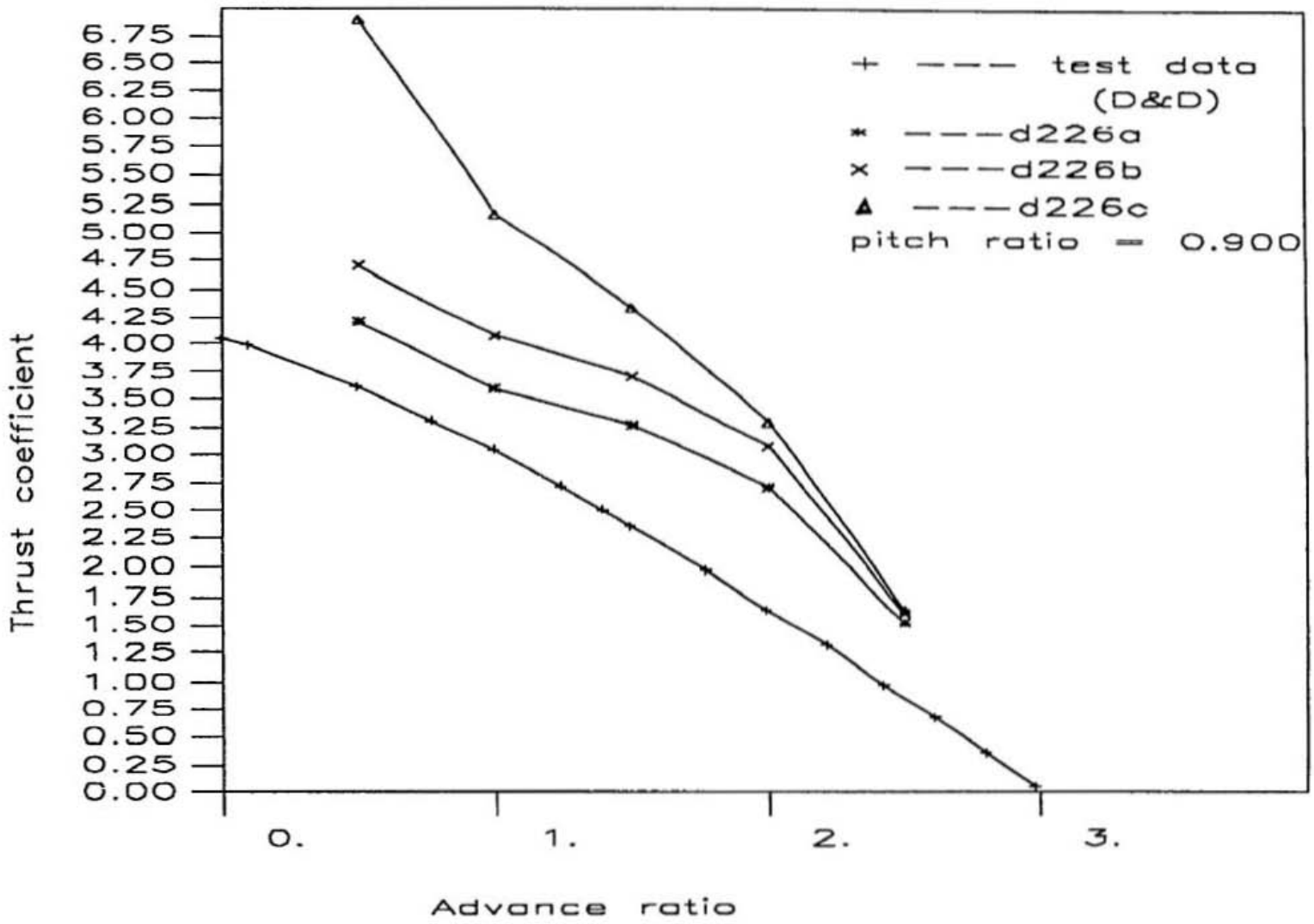


Figure G-17: Comparison of theoretical results with test results — thrust coefficient(pitch ratio=0.9π)

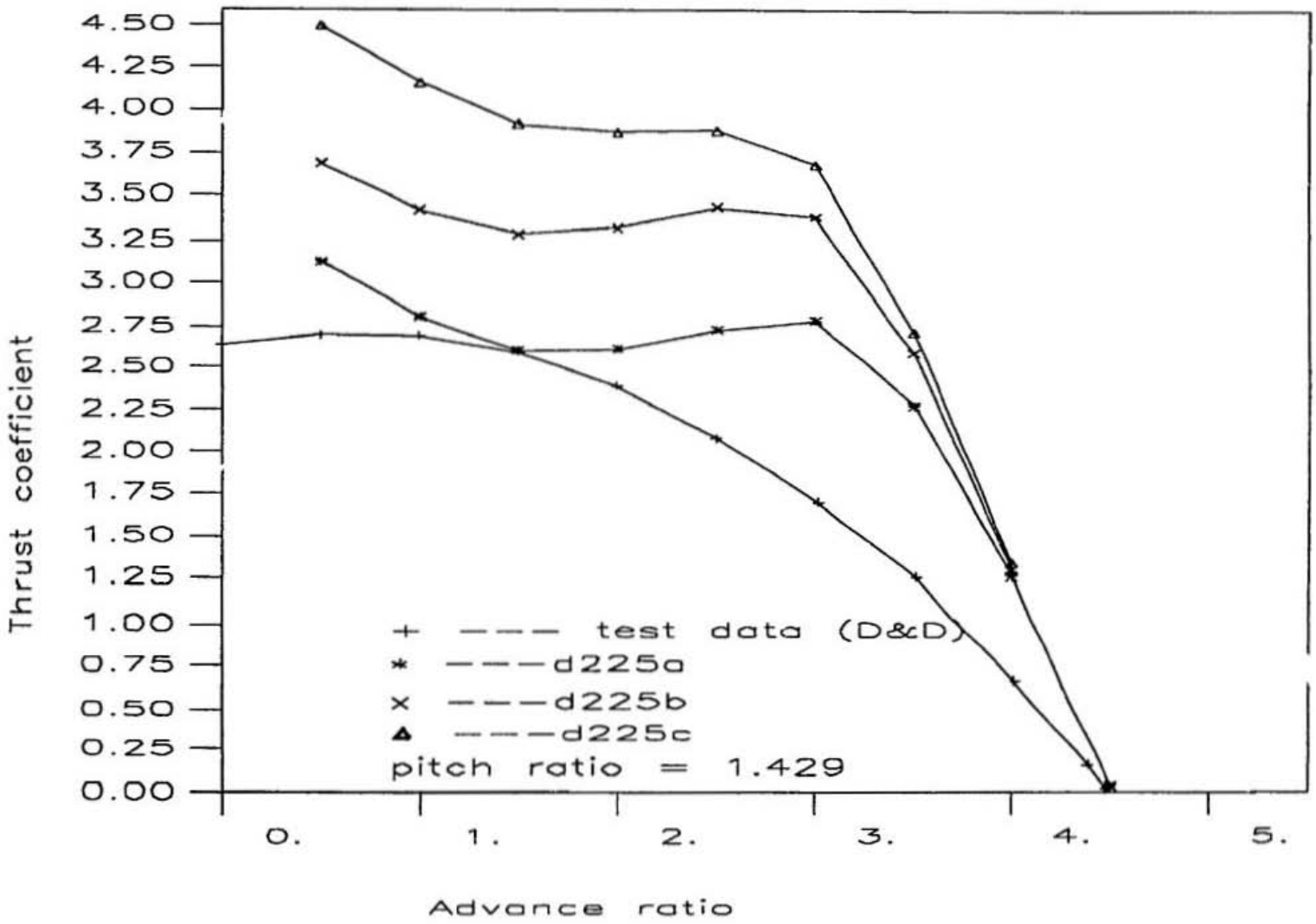


Figure G-18: Comparison of theoretical results with test results — thrust coefficient(pitch ratio=1.429π)

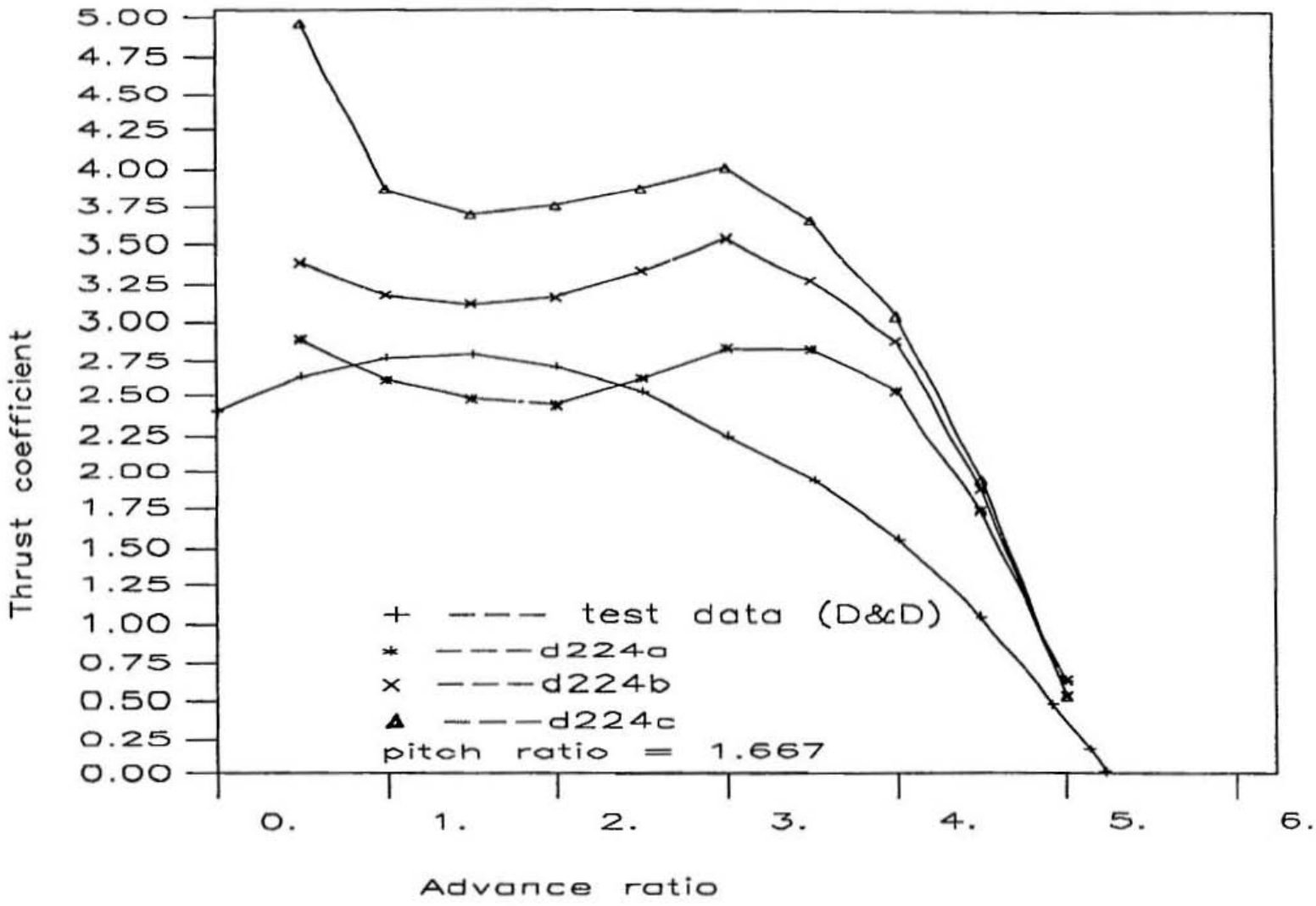


Figure G-19: Comparison of theoretical results with test results — thrust coefficient(pitch ratio=1.667π)

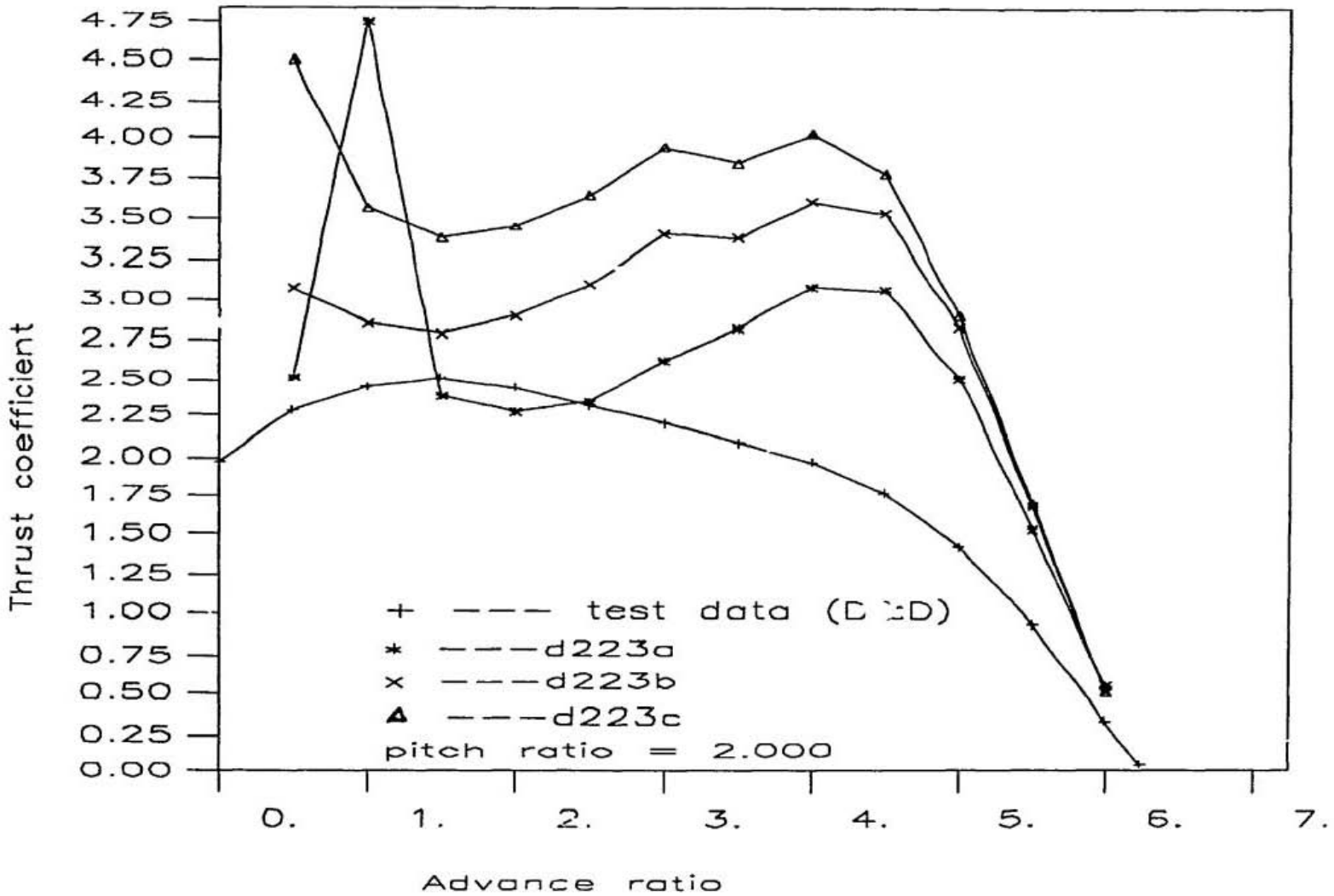


Figure G-20: Comparison of theoretical results with test results — thrust coefficient(pitch ratio=2.000π)

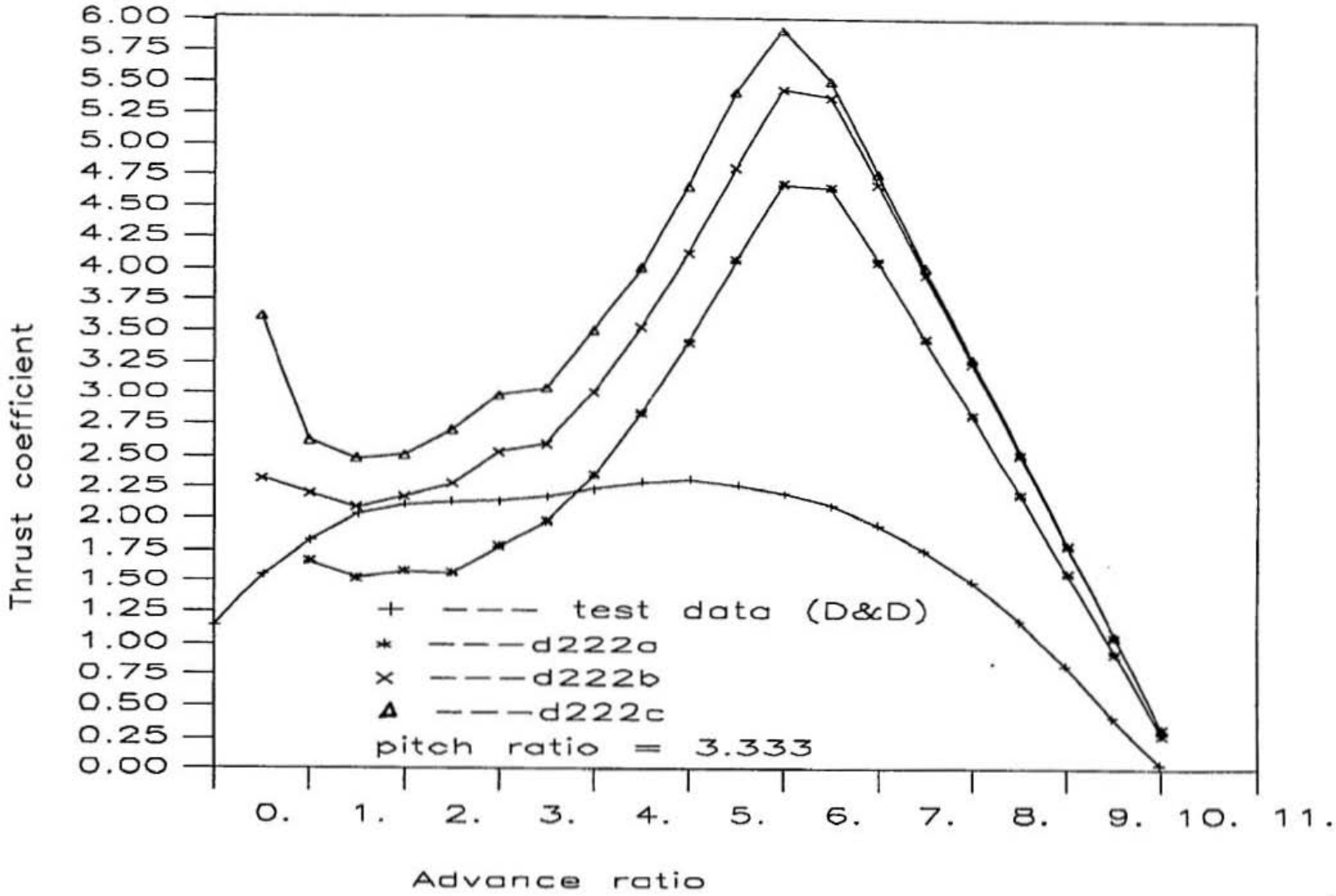


Figure G-21: Comparison of theoretical results with test results — thrust coefficient(pitch ratio=3.333π)

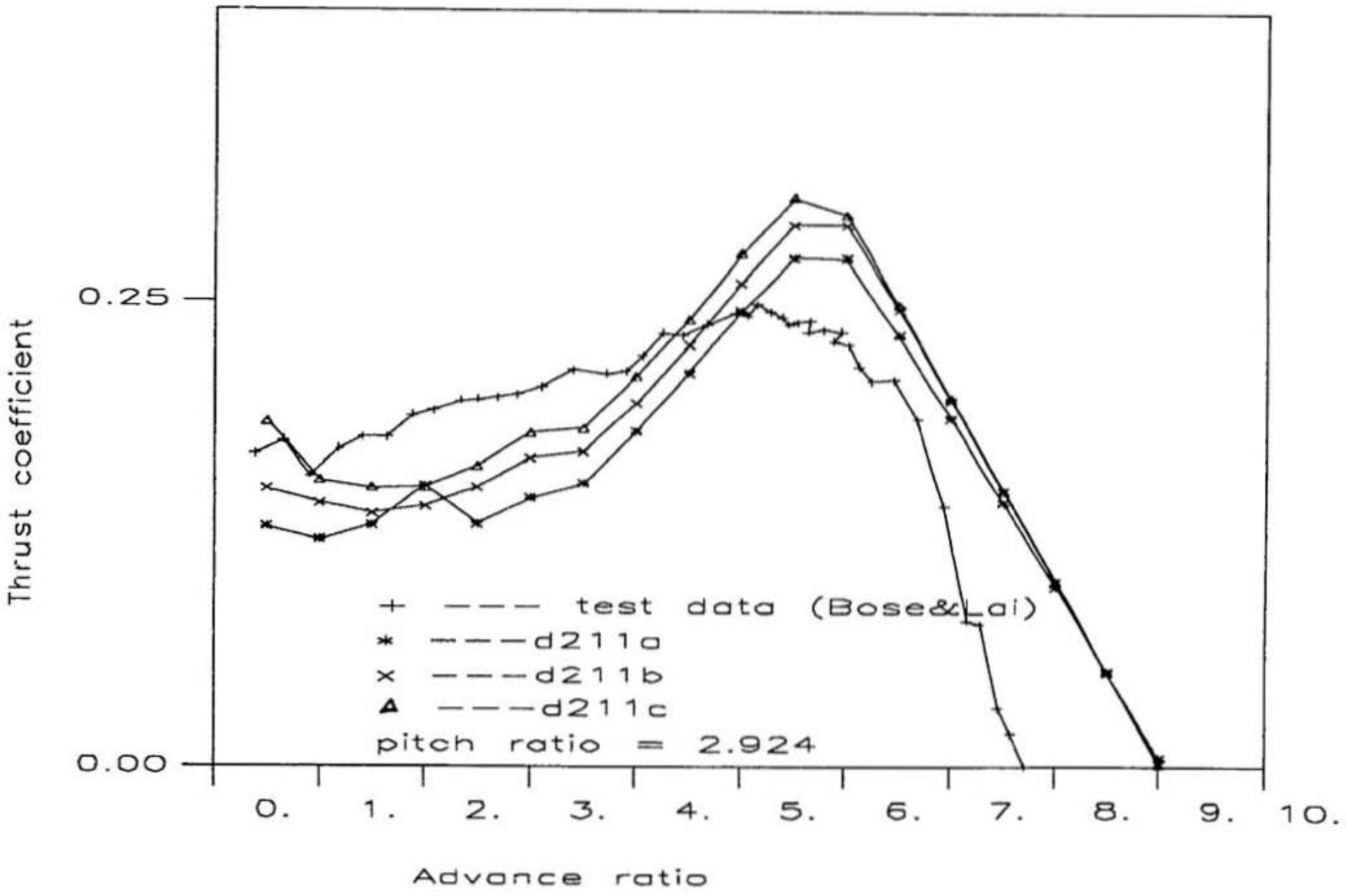


Figure G-22: Comparison of theoretical results with test results — thrust coefficient(pitch ratio=2.924π)

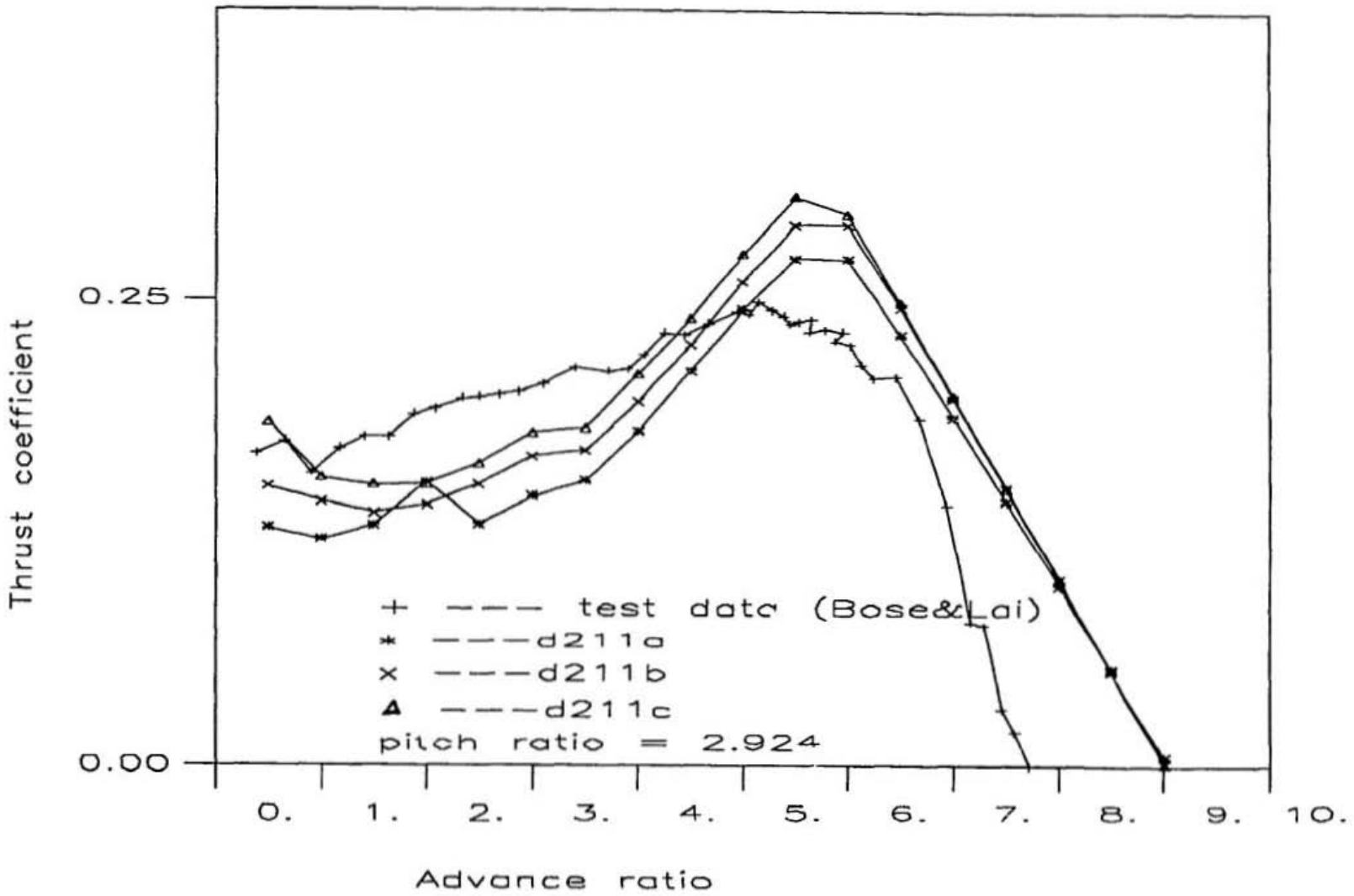


Figure G-22: Comparison of theoretical results with test results — thrust coefficient(pitch ratio=2.924π)

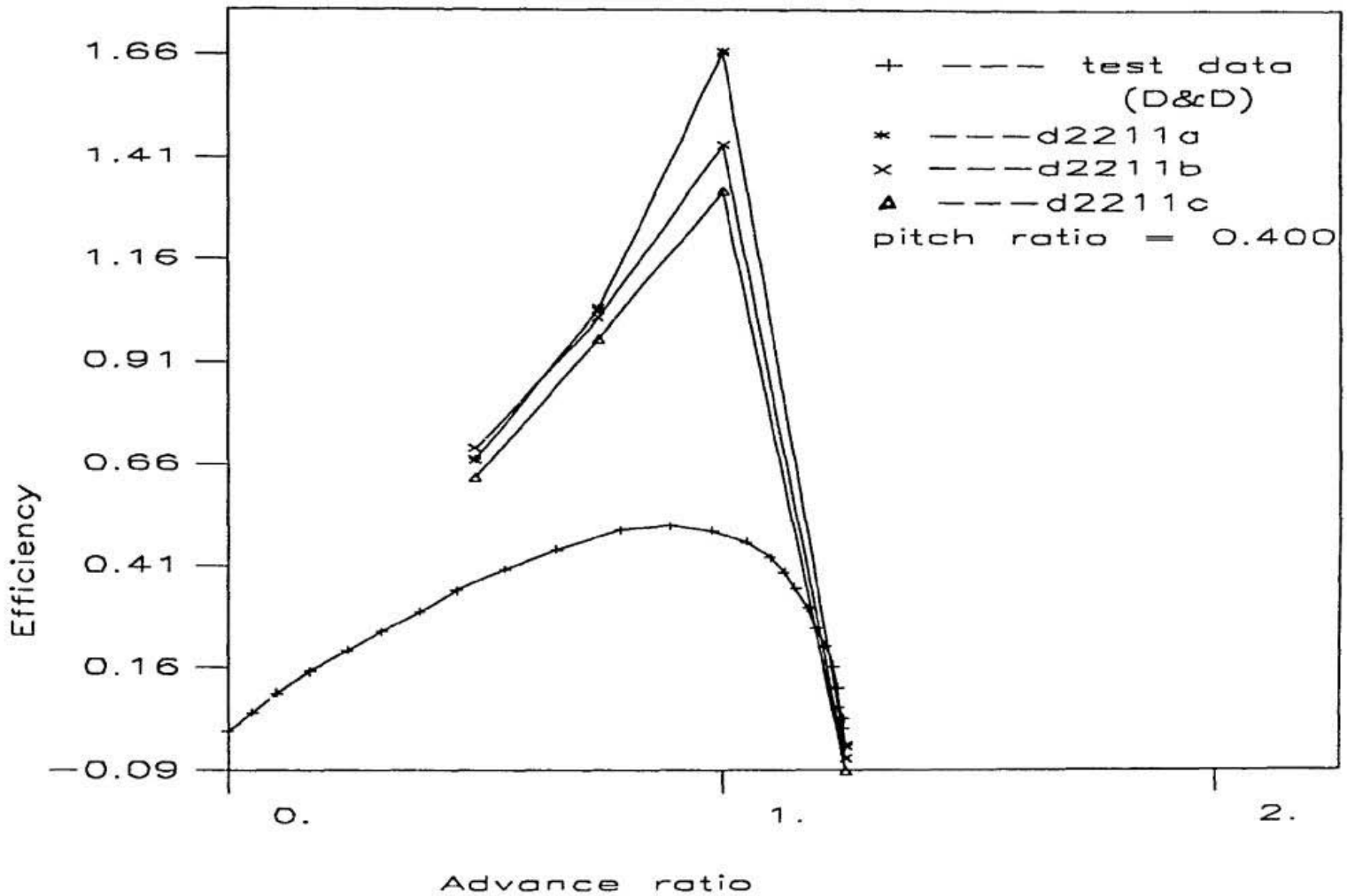


Figure G-23: Comparison of theoretical results with test results — efficiency(pitch ratio=0.4π)

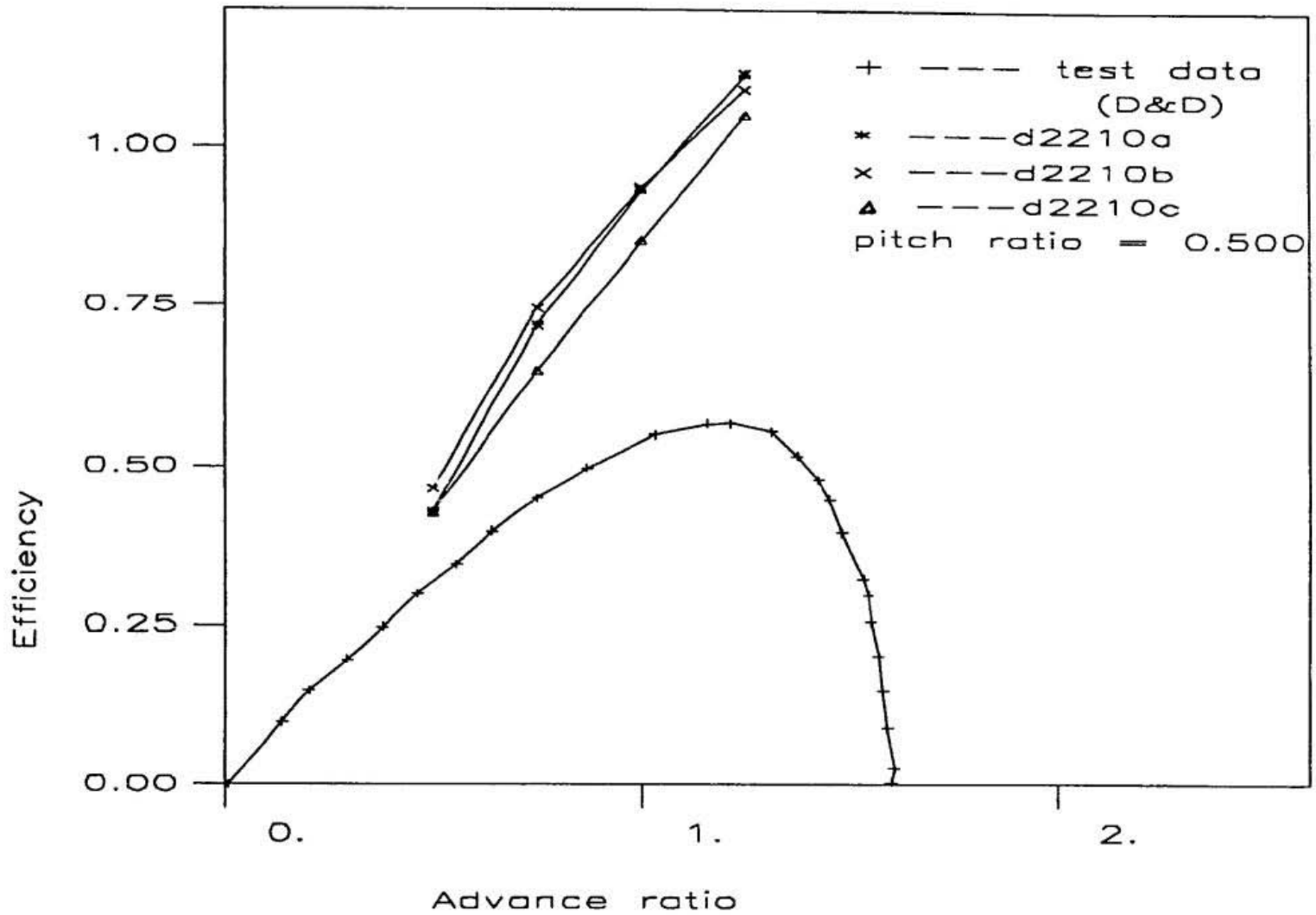


Figure G-24: Comparison of theoretical results with test results — efficiency(pitch ratio=0.5π)

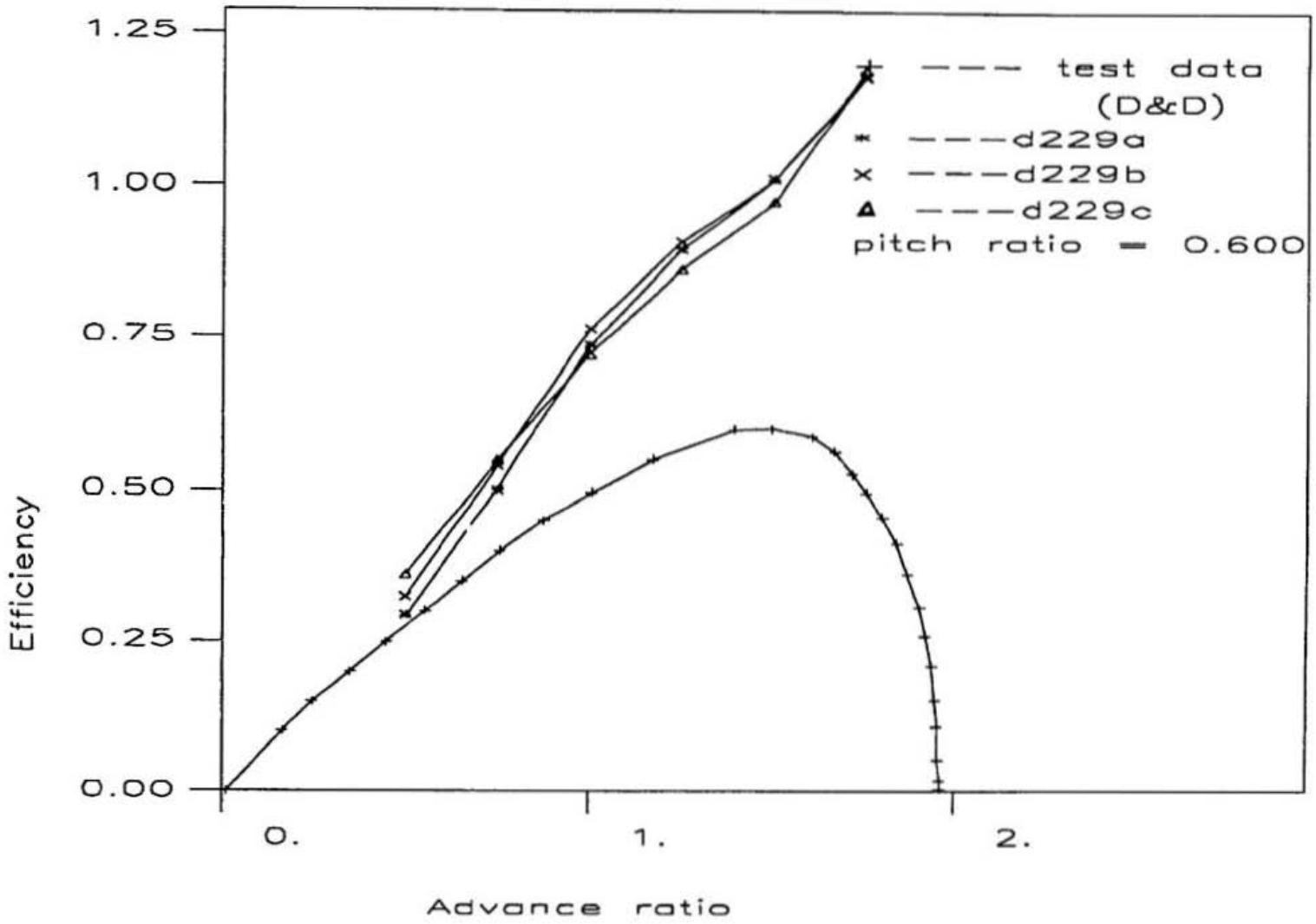


Figure G-25: Comparison of theoretical results with test results — efficiency(pitch ratio=0.6π)

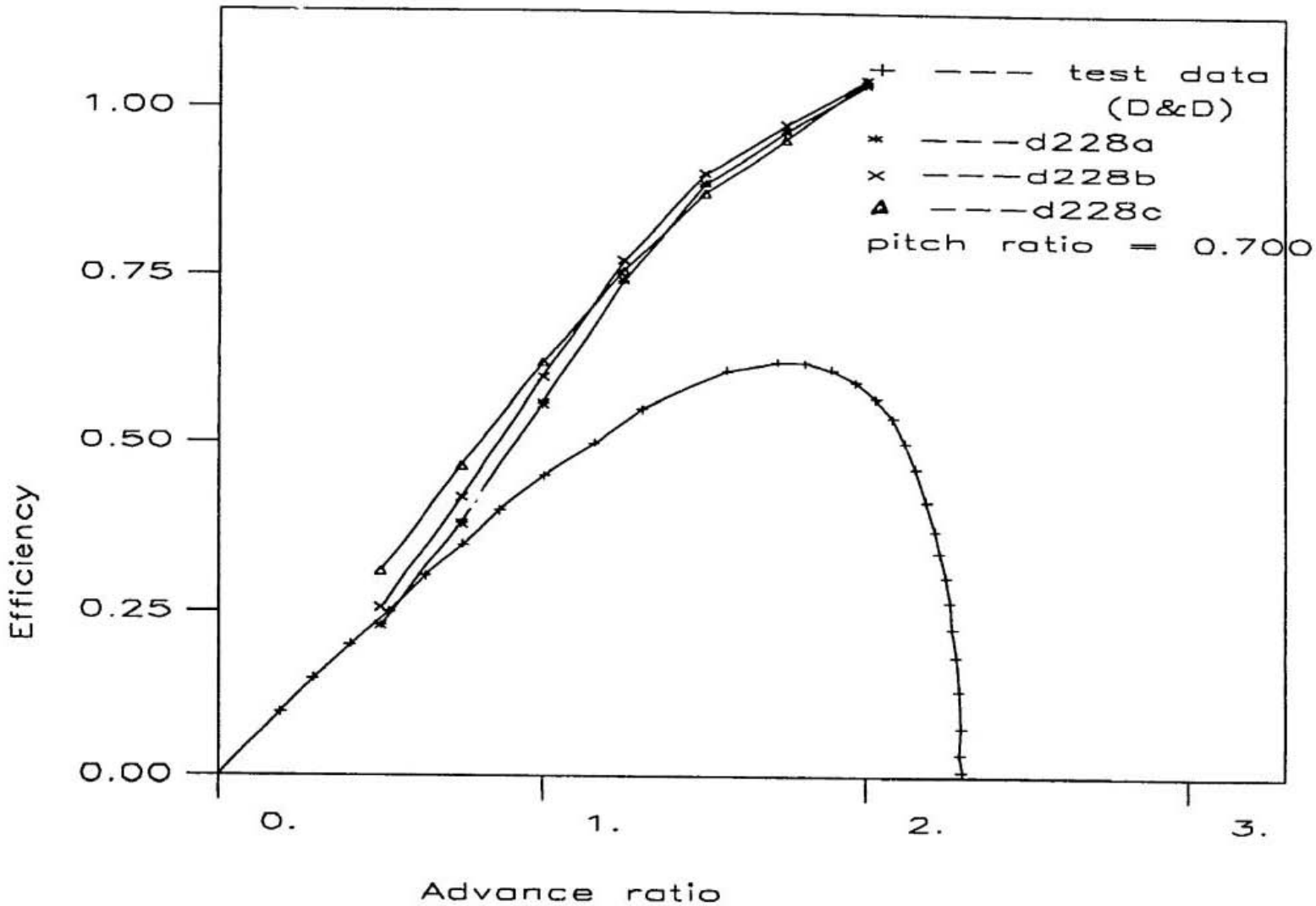


Figure G-26: Comparison of theoretical results with test results — efficiency(pitch ratio=0.7π)

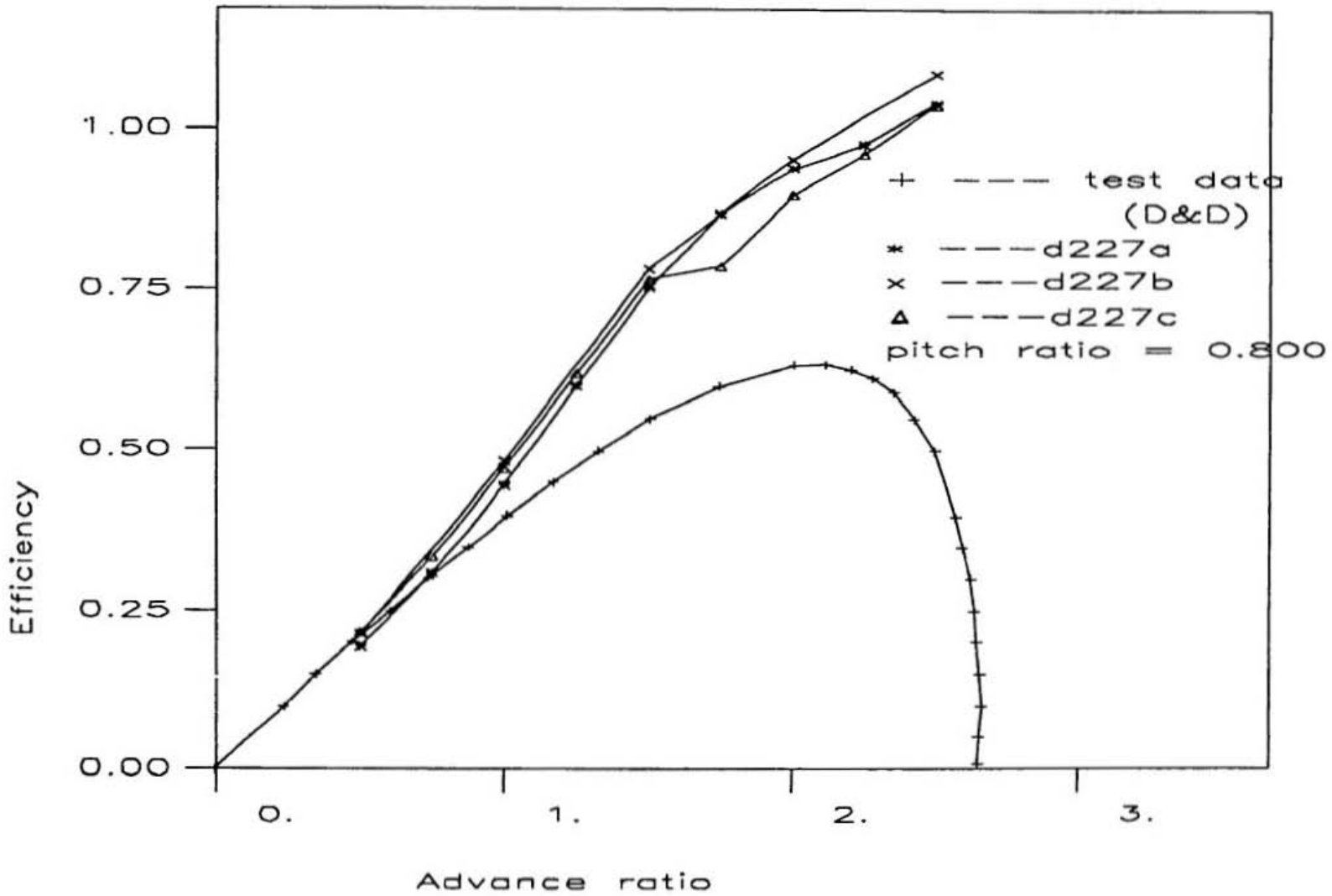


Figure G-27: Comparison of theoretical results with test results — efficiency(pitch ratio=0.8π)

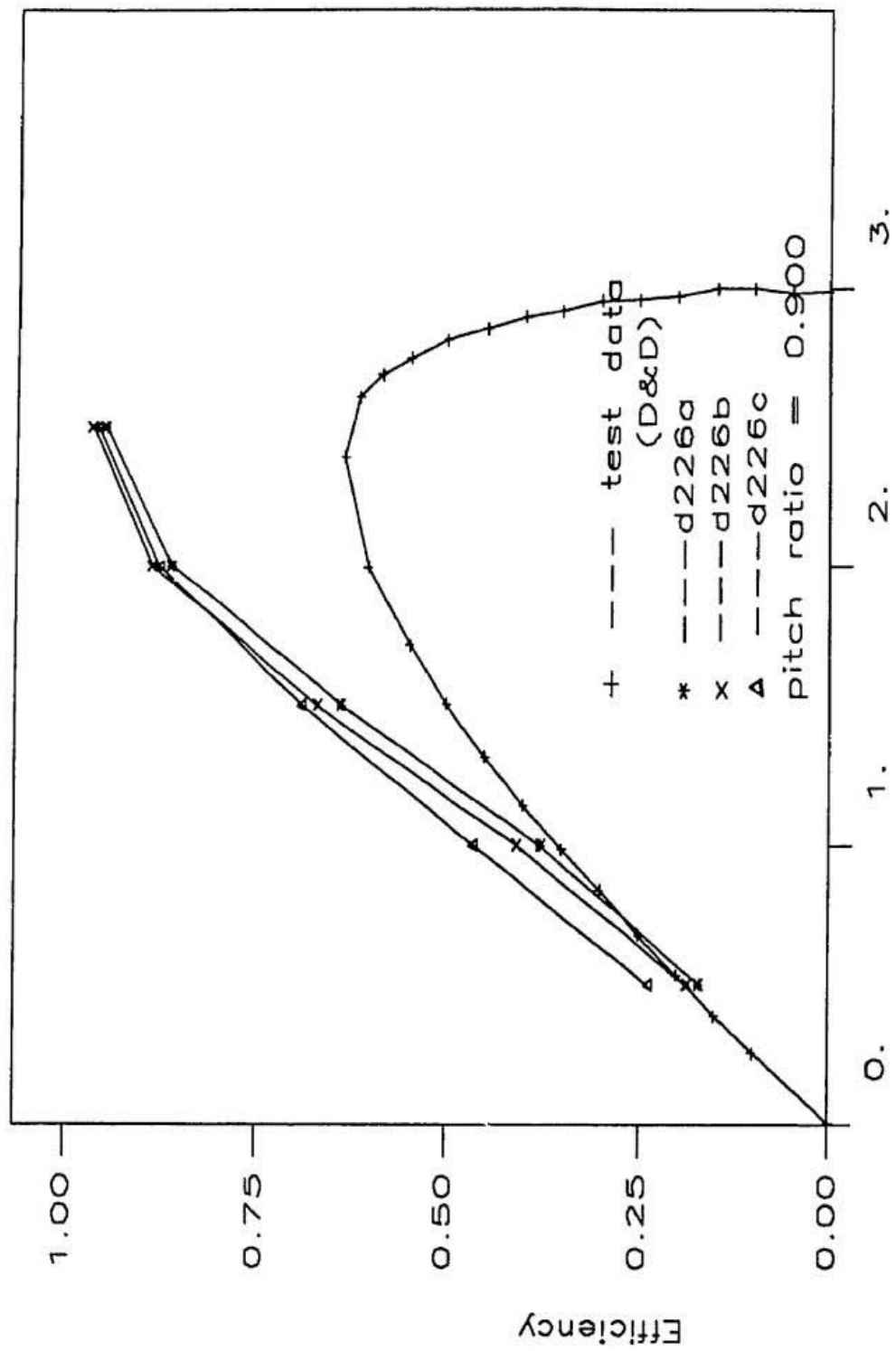


Figure G-28: Comparison of theoretical results with test results — efficiency(pitch ratio=0.9π)

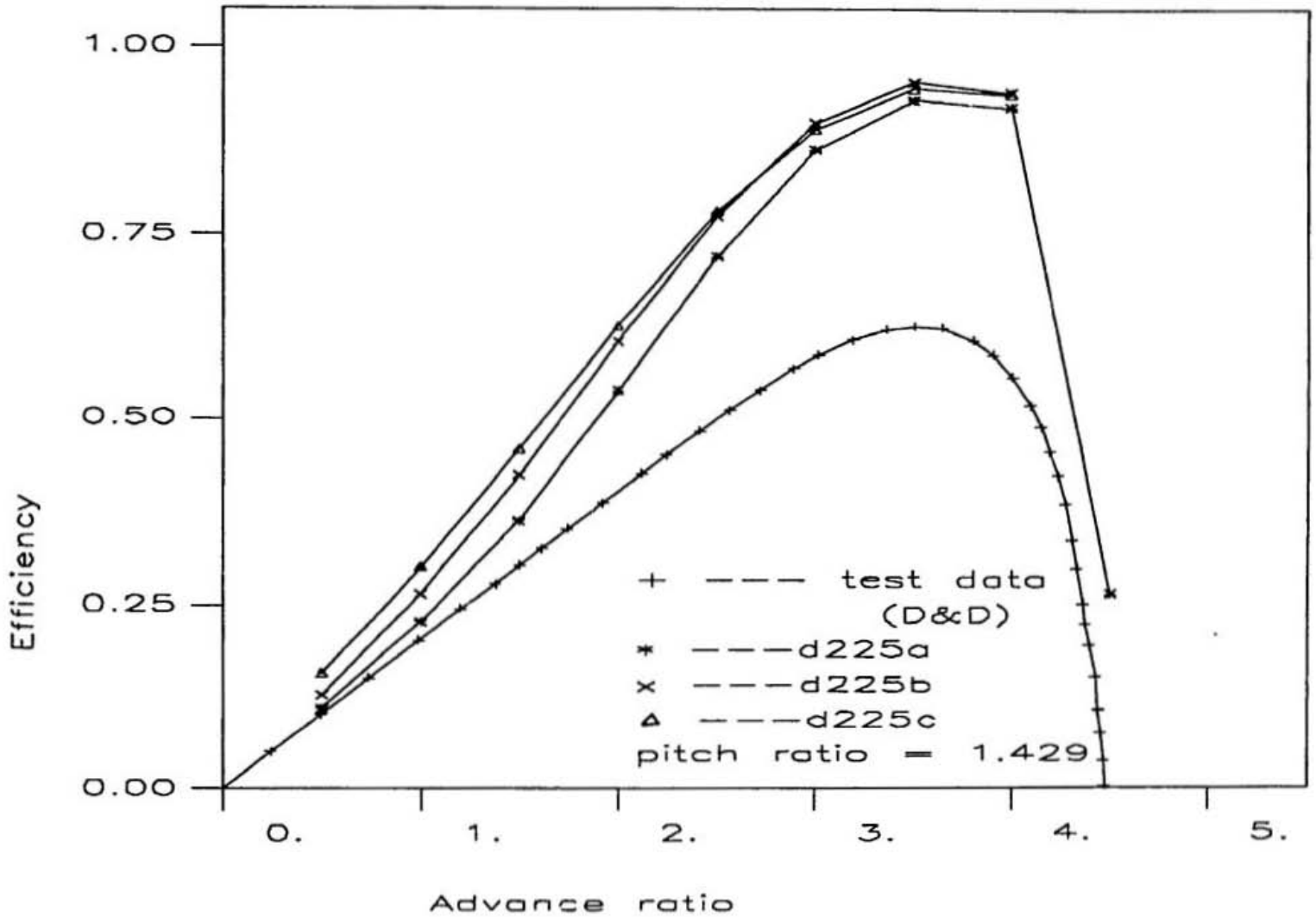


Figure G-29: Comparison of theoretical results with test results — efficiency(pitch ratio=1.429π)

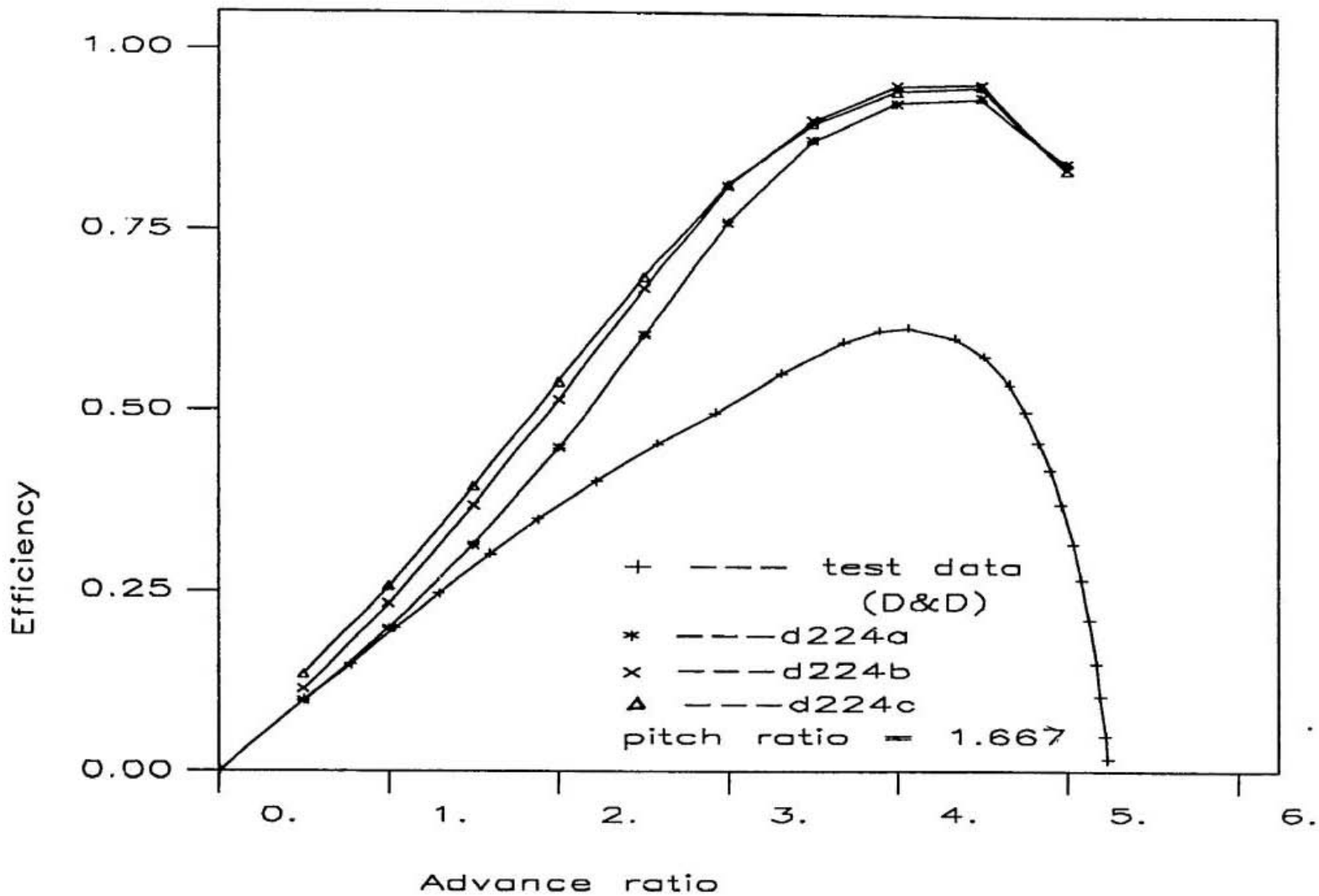


Figure G-30: Comparison of theoretical results with test results — efficiency(pitch ratio=1.667π)

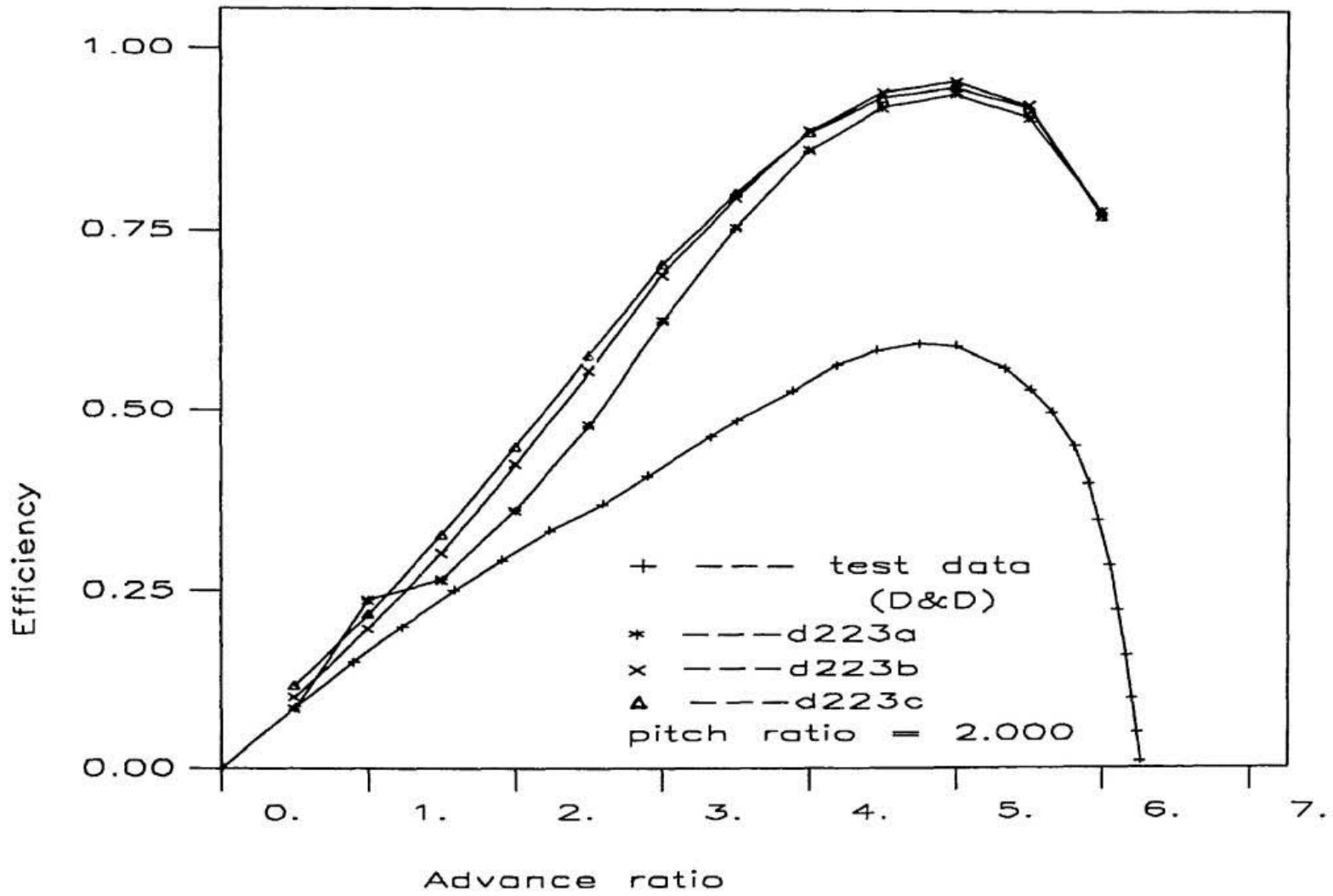


Figure G-31: Comparison of theoretical results with test results — efficiency(pitch ratio=2.000π)

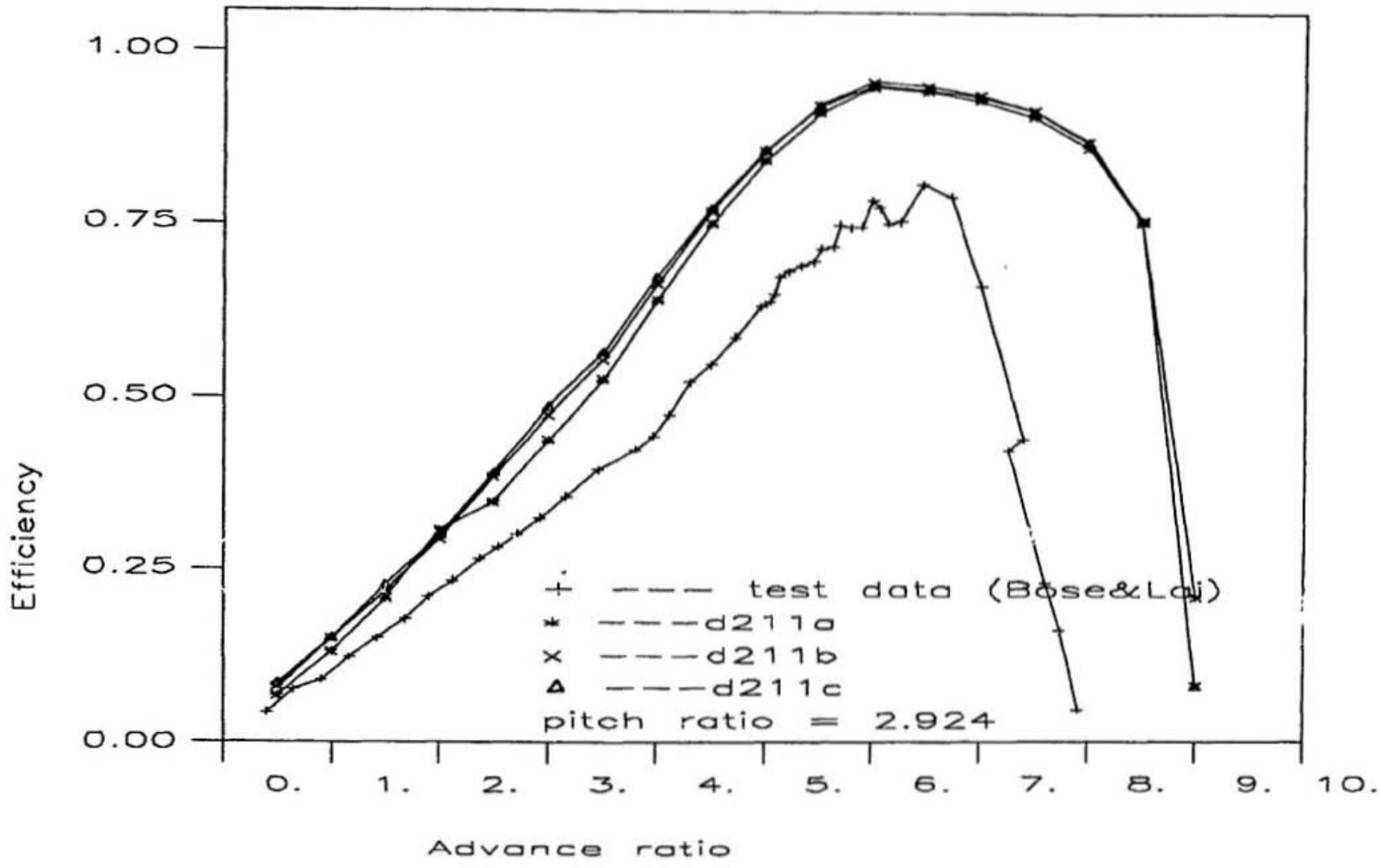


Figure G-33: Comparison of theoretical results with test results — efficiency(pitch ratio=2.924π)

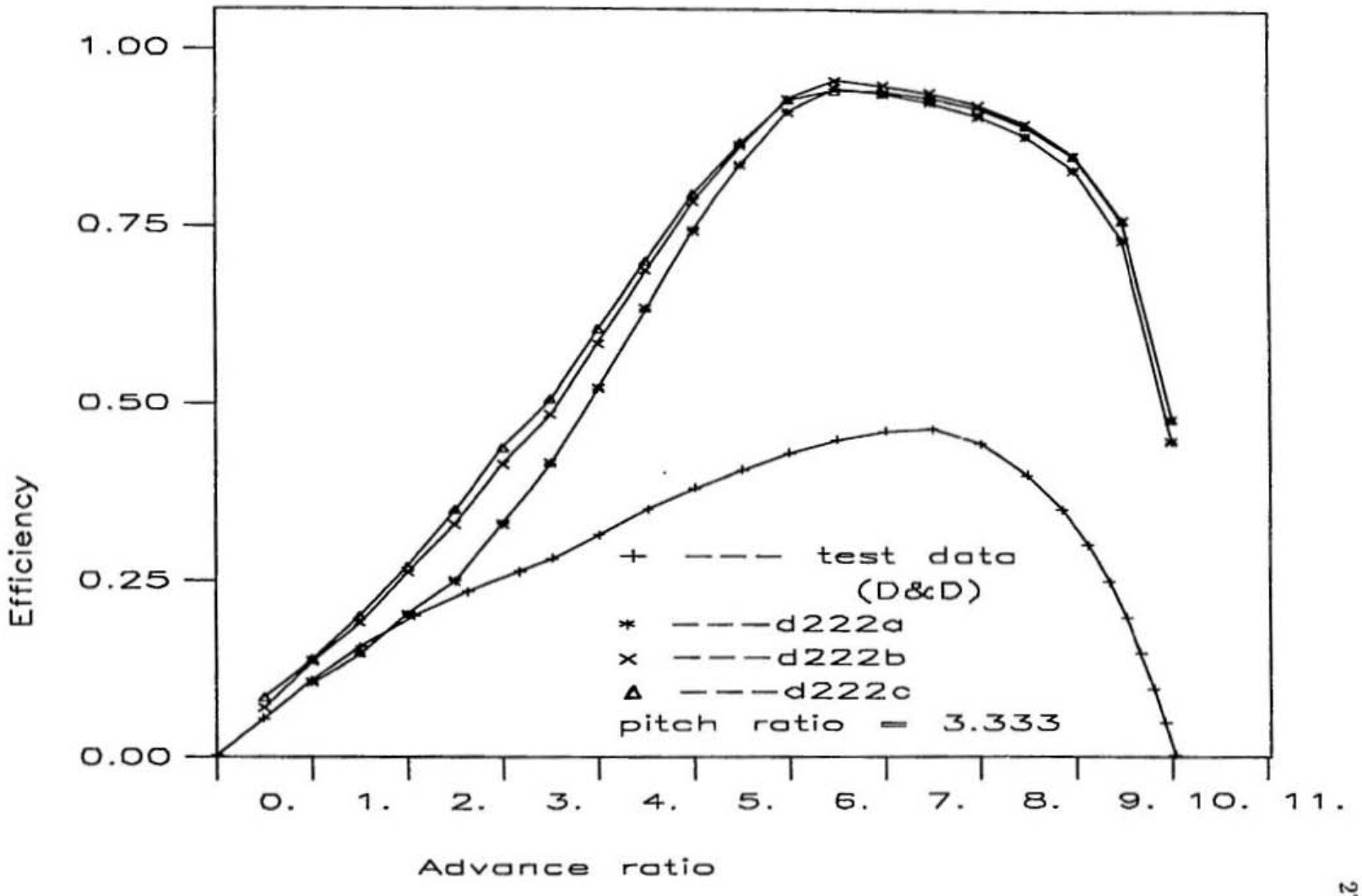


Figure G-32: Comparison of theoretical results with test results — efficiency(pitch ratio=3.333π)